COMBUSTION AND NOISE PHENOMENA IN TURBULENT ALKANE FLAMES

Bram de Jager

De promotiecommissie is als volgt samengesteld:

Voorzitter en secretaris:	
prof.dr. F. Eising	Universiteit Twente
Promotor:	
prof.dr.ir. Th.H. van der Meer	Universiteit Twente
Assistent Promotor:	
dr.ir. J.B.W. Kok	Universiteit Twente
Leden:	
prof.dr.ir. H.W.M. Hoeijmakers	Universiteit Twente
prof.dr.ir. J.A.M. Kuipers	Universiteit Twente
prof.dr. H.B. Levinsky	Rijksuniversiteit Groningen
prof.dr. D.J.E.M. Roekaerts	Technische Universiteit Delft
prof.dr. A.K.M.P. Taylor	Imperial College Londen (GB)

Combustion and noise phenomena in turbulent alkane flames
De Jager, Bram

PhD thesis, University of Twente, Enschede, The Netherlands
March 2007

ISBN 978-90-365-2484-1

Printed by Gildeprint Drukkerijen BV, Enschede, The Netherlands

COMBUSTION AND NOISE PHENOMENA IN TURBULENT ALKANE FLAMES

PROEFSCHRIFT

ter verkrijging van
de graad van doctor aan de Universiteit Twente,
op gezag van de rector magnificus,
prof.dr. W.H.M. Zijm,
volgens besluit van het College voor Promoties
in het openbaar te verdedigen
op donderdag 29 maart 2007 om 13.15 uur

door

Bram de Jager

geboren op 16 maart 1978

te Winschoten

Dit proefschrift is goedgekeurd door de promotor:

prof.dr.ir. Th.H. van der Meer

en de assistent promotor:

dr.ir. J.B.W. Kok

Voor Hannah, Vera, Boaz en Zarah Erin

Abstract

A gas turbine engine is an advanced apparatus for propulsion and power generation that has been developed over the last 60 years. The energy for this production of propulsion and power in a gas turbine is generated by combustion.

It is feasible and relatively easy to solve the governing equations in combustion for one dimensional laminar hydrocarbon combustion with detailed chemistry. This has been done for several hydrocarbon fuels that are representative for liquid fuel combustion. The complex chemistry that is solved completely in a laminar flame is mostly modelled in simulations of turbulent combustion. Essential to this modelling is a correct understanding of the processes that govern the chemistry. Via the route of a numerical perturbation method, the CSP-method, this understanding can be developed. After analysis with CSP, the next step to a model describing turbulent combustion in gas turbines is taken using the CFI combustion model. This model comprises the definition of a reaction progress variable representing the reduced chemistry yielding from CSP, a mixture fraction variable and an enthalpy variable. The thesis presents a version of the CFI combustion model for application in evaporating fuel sprays.

To represent liquid fuel chemistry, often n-heptane and *iso*-octane are chosen as reference fuels. In this thesis a detailed chemical reaction scheme incorporating both fuels is assembled based on literature. This developed mechanism correctly models the oxidation of both fuels. Using this mechanism, the influence of steam on the formation of pollutants of liquid lean premixed prevaporised fuel combustion is assessed. It is found that dilution with steam strongly diminishes the formation of both CO and NO.

Reduction of this mechanism to a global step for various conditions shows that in terms of predicting emissions of CO_2, CO and NO the reduced mechanism produces results equal to the detailed mechanism. This makes the mechanism a suitable candidate for use in turbulent flame modelling, provided a valid reduction method such as CSP is used.

Validation of the CFI combustion model has been carried out using experimental data from a turbulent propane flame. This swirl stabilized flame provided velocity and temperature data. These were used to validate the results obtained by CFD simulations using the CFI combustion model.

Another part of the research carried out in this thesis concerns the development of a combustion noise prediction model for turbulent premixed flames. On the basis of a model for a non-premixed flame a model has been derived for a premixed flame. Using the results of turbulent premixed methane flame sim-

ulations, a sound spectrum was calculated. Comparison to measured sound spectra gave good results. It is shown that the model can be applied to different types of alkane fuels, for example heptane.

In order to take into account the effects of a two-phase flow on combustion, a model is presented that describes a spray on the basis of an Eulerian approach. A presumed distribution function of the fuel droplet radii combined with transport equations for the moments of this distribution function provided a route to the description of a polydisperse spray without the necessity of a spray simulation with particle tracking for each spray droplet. This spray model has been combined with the CFI model in order to model both the chemistry in the gaseous phase and the behaviour of the liquid fuel. Simulation of an experimental methanol spray flame shows that the model is capable of predicting trends in spray flame development.

Samenvatting

Een gas turbine is een geavanceerde machine die toegepast wordt voor opwekking van elektriciteit en kracht. De laatste 60 jaren is het apparaat steeds verder ontwikkeld. De energie benodigd voor elektriciteit en kracht in een gas turbine wordt geleverd door verbranding.

De vergelijkingen die het verbrandingsproces beschrijven kunnen relatief eenvoudig worden opgelost voor één dimensionale laminaire vlammen met volledige chemie. Dit is gedaan voor verscheidene koolwaterstoffen die representatief zijn voor vloeibare brandstoffen. In tegenstelling tot de volledige oplossing van de chemie in laminaire situaties wordt in turbulente verbranding de chemie gemodelleerd. Dan is het belangrijk dat de dominante processen van de chemie goed worden begrepen. Met behulp van een numerieke perturbatie methode, de CSP methode, is dit begrip ontwikkeld. Na een CSP analyse kan de volgende stap in de modellering genomen worden door gebruik te maken van het CFI-verbrandingsmodel. Dit model bestaat uit de definitie van een reactie voortgangsvariabele voor de CSP gereduceerde chemie, een mengingsvariabele en een enthalpie variabele. In dit proefschrift wordt een versie van het CFI verbrandingsmodel gepresenteerd voor toepassing in verdampende brandstof sprays.

Om vloeibare brandstoffen te modelleren worden vaak heptaan en isooctaan gebruikt. Dit proefschrift bevat een gedetailleerd chemisch reactie mechanisme, op basis van recente literatuur, waarin beide brandstoffen zijn opgenomen. Dit ontwikkelde mechanisme modelleert de oxidatie van beide brandstoffen op correcte wijze. Met behulp van dit mechanisme is de invloed van stoom op de vorming van uitlaatgassen in voorgemengde, voorverdampte, vloeibare brandstof verbranding onderzocht. De uitkomst is dat toevoegen van stoom zorgt voor een afname van de vorming van zowel CO als NO.

Reductie van dit mechanisme voor meerdere condities tot een globale stap laat zien dat het gereduceerde mechanisme zich overeenkomstig het gedetailleerde mechanisme gedraagt wat betreft voorspelling van emissies van CO_2, CO en NO. Dit maakt een gereduceerde mechanisme een geschikte kandidaat voor het modelleren van turbulente verbranding, mits een juiste reductie methode is toegepast, in dit geval CSP.

Het CFI verbrandings model is gevalideerd met behulp van experimentele data die verkregen zijn van een turbulente propaan vlam. De data van deze vortex gestabiliseerde vlam bestaande uit temperaturen en snelheidsvelden is gebruikt om de resultaten van CFD berekeningen met het CFI verbrandings

model te valideren.

In dit proefschrift wordt tevens aandacht geschonken aan de ontwikkeling van een model om geluid van turbulente voorgemengde verbranding te voorspellen. Met behulp van een eerder ontwikkeld model voor diffusie vlammen is een model geformuleerd voor voorgemengde vlammen. Met de resultaten van voorgemengde turbulente methaan vlam simulaties zijn geluidsspectra bepaald. Vergelijking met gemeten geluidsspectra laat zien dat het model goede resultaten geeft. Tevens is aangetoond dat het model toegepast kan worden voor verschillende typen van alkaan brandstoffen, zoals heptaan.

Om het effect van een twee-fasen stroming op verbranding in rekening te brengen, wordt een model gepresenteerd dat een spray beschrijft met behulp van een Euleriaanse benadering. Dit is gedaan door een aangenomen distributie functie van de druppel stralen te combineren met transportvergelijkingen voor de statistische momenten van deze distributie functie. Op deze wijze kan een poly-disperse spray beschreven worden zonder het oplossen van een volledig stelsel van bewegingsvergelijkingen voor de afzonderlijke brandstof druppels.

Het spray model is gecombineerd met het CFI verbrandingsmodel om zodoende zowel de chemie van de verbranding als het gedrag van een spray te modelleren. Simulatie van een experimentele methanol spray vlam laat zien dat het model in staat is om trends van de spray vlam te laten zien.

Acknowledgments

The research in this thesis has been carried out in the framework of the EU sponsored project MAST-B-LIQUID.

Table of Contents

1

Introduction

This chapter presents a brief history of the gas turbine and gives a short overview of liquid fuel combustion in gas turbines. The objectives of the research are presented and an overview of the further chapters in this thesis is given.

1.1 A brief history

In 1500, Leonardo da Vinci sketched drawings of a machine that used the energy of hot air flowing up in a chimney from a fireplace to rotate the spit above that fire: the *chimney jack*. This device, as described in the *Codex Atlanticus*, see [3], was the first apparatus that used hot combustion gas for driving a motion. Although simple in its construction, the machine can be considered the first working demonstration of the physical principles applied in a gas turbine. A copy of the original drawing of Da Vinci is shown in figure 1.1.

The first patent granted for a gas turbine adept was registered to John Barber, almost 300 years later in 1791. He constructed a machine consisting of a compressor, combustion chamber and turbine, in search for 'horseless' carriage [4]. About one hundred years later, one of the first working gas turbines is built by Armengaud. This apparatus worked under its own power and further efforts to improve its efficiency were not made. It was not until World War II that the gas turbine had evolved toward a relatively efficient machine for propulsion of high speed aircraft. By that time, logically the gas turbine could produce power with a positive efficiency. Nowadays the gas turbine is not only very important in air and marine propulsion, but also a great percentage of the Western world's electricity is produced by it.

Since the early development or invention of the gas turbine, liquid refined oil products have served as a major source for combustion. The first working gas turbines were designed and equipped for running on liquid fuel. The reason for this was that at start the main application of gas turbines was aircraft propulsion. For transportation, either by air, land or sea, liquid fuel is still preferred due to its easy storage. Yet modern gas turbine technology allows for operating at both liquid and gaseous fuels. The latter has several advantages compared to liquid fuels regarding operation of a gas turbine, but in terms of

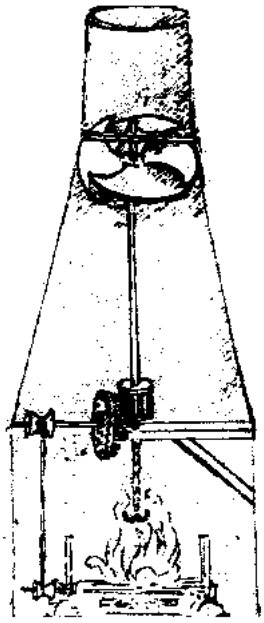

Figure 1.1: A sketch of the *chimney jack* [3].

transportation and storage possibilities, liquid fuel is considered to be a reliable resource. However, one should note that the availability of crude oil is another subject, that is related to geo-political questions which are not the topic of this thesis. Generally speaking, gas turbine manufacturers and users, such as electricity producers, prefer gas turbines to have both gas and liquid fuel firing abilities.

1.2 Working principle of gas turbine engines

From the previous section the very basic working principle of a gas turbine engine can be distilled: a gas that drives a kind of wheel. This very rudimentary description asks for a bit more explanation. Figure 1.2 depicts a cross section view of a simple gas turbine engine with annular combustors. From this picture it is easily deducted that a real gas turbine engine is a complex combination of equipment. In order to gain insight in the working principle, thermodynamic theory is essential. The basic thermodynamic cycle that describes the process in the gas turbine engine is the Joule-Brayton cycle, as seen in figure 1.3. This cycle is shortly described as follows: gas at low or ambient temperature and pressure (1) is compressed to high pressure using a compressor (2). At that elevated pressure heat is added to the gas by means of combustion, reaching a high temperature. The heated gasses are then to expand to atmospheric pressure, (4), in that way driving a turbine. The processes 1-4 from the thermodynamic description are indicated by the numbers on the gas turbine drawing in figure 1.2 as well.

The thermal efficiency η of this simple cycle can be expressed with the ratio of the net work output and the heat entering the cycle. The compressor and turbine in this simple Joule-Brayton cycle are assumed to work without loss of entropy. The actual thermal efficiency of a gas turbine depends on the isentropic efficiencies of the compressor, turbine and combustion, as well as as on temperature and pressure levels.

In order to increase thermal efficiency of a gas turbine, several steps can be taken. Conventionally intercooling, regeneration and reheating are solutions. Steam injection before the combustion process is another option. Next to a positive effect on the thermal efficiency of the process, also emissions will be lower.

1.3 Combustion

The input of heat in the gas turbine cycle by means of combustion is the major topic of the research performed in this thesis. Combustion has a large contribution to the worldwide energy production. About 90% of the power used on this planet is generated by combustion of fossil fuels, i.e. hydrocarbon fuels. According to the online Meriam-Webster dictionary, the definition of combustion reads:

> *A usually rapid chemical process (as oxidation) that produces heat and usually light*

This definition shows that combustion produces heat and light, but it is not mentioned that for any combustion process to occur, there is need for a *fuel* and an *oxidizer*. These two components are essential to the process of combustion, as well as activation energy to start the process. Chemically, for example combustion of a hydrocarbon like n-heptane (a liquid fuel model component) can be written as follows:

$$\mathrm{C_7H_{16}} + 11\,\mathrm{O_2} \longrightarrow 8\,\mathrm{H_2O} + 7\,\mathrm{CO_2}$$

This reaction represents the global conversion from n-heptane and oxygen into water, H_2O, and carbon dioxide, CO_2. The reaction is exothermic, as heat

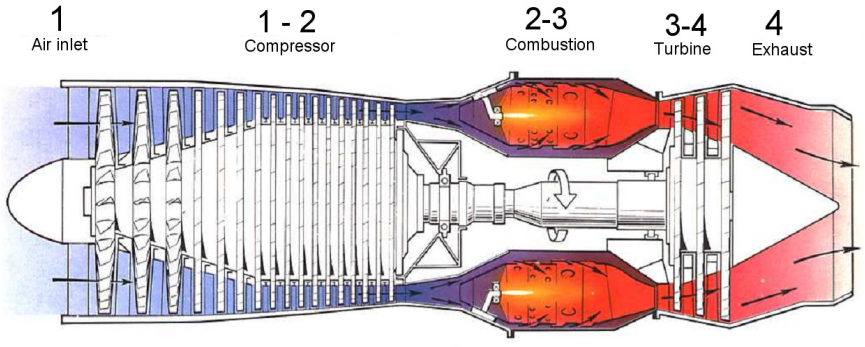

Figure 1.2: A cross sectional view of a gas turbine engine (courtesy of Rolls Royce)

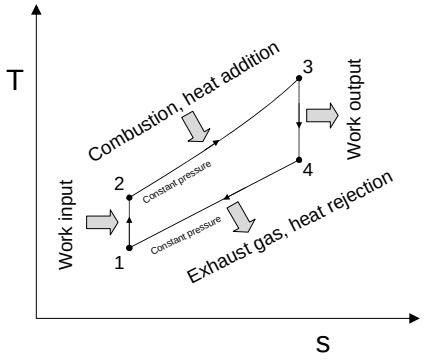

Figure 1.3: Temperature versus entropy diagram for the simple Joule-Brayton cycle.

is released when the bonds between the atoms of the fuel molecule are broken. The inherent production of CO_2 is considered one of the major drawbacks of combustion. An increasing CO_2 concentration in the atmosphere is believed to attribute to a global increase of ambient temperatures [5,6]. Another drawback of combustion, is the formation of pollutants. These pollutants can be soot, unburned fuel, carbon monoxide (CO) or nitric oxides (NOx). All these species are considered poisonous for the habitat of living organisms and have considerable negative health effects on human beings. For this reason, governments have put restrictions on the amount of emissions from (power generation) industry and cars. A lot of effort of the gas turbine industry is aimed at lowering these emissions. As the combustion process itself is the main mechanism in the pollution generation by gas turbines, full understanding of all aspects of this process is needed and has not been achieved yet. The simple reaction given on the previous page does not show the paths that are the route to pollutant formation. To investigate this, detailed kinetic descriptions are needed of the processes that occur in oxidation of a fuel.

1.4 Liquid fuel combustion

Several methods have been developed by science and industry to diminish the emission of pollutants from liquid fuel combustion in gas turbines. Two of these techniques will be subject of research in this thesis.

Lean premixed prevaporised combustion Gaseous combustion has several advantages compared to liquid fuel combustion. These advantages deal both with environmental and operational issues. Gaseous combustion allows for more clean combustion. Operationally, running a gas turbine on liquid fuel tends to need more maintenance on the gas turbine equipment. Next to that, from a thermodynamic point of view, liquid fuel combustion needs heat for vaporisation. This slightly diminishes the thermodynamic efficiency of the cycle as this heat is not directly used for power production. To benefit from relatively clean gaseous combustion and the transportation and availability advantage of liquid fuel, the concept of 'lean premixed prevaporised' (LPP)

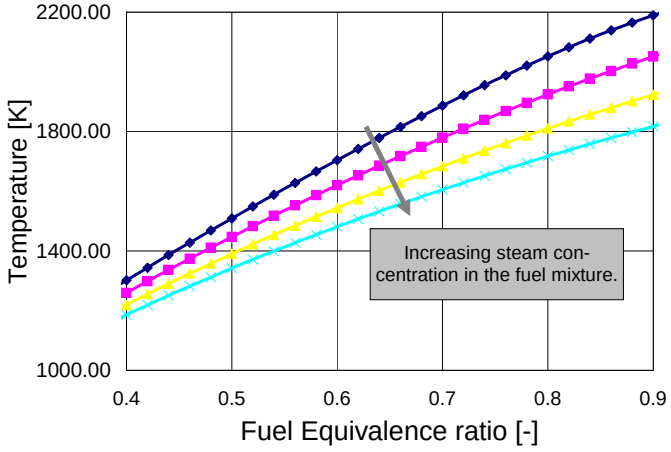

Figure 1.4: Influence of steam load on equilibrium temperatures for *iso*-octane oxidation.

combustion was introduced [7]. This concept allows a gas turbine to run with clean gaseous combustion, but without the necessity of a natural gas supply network. Reported NO_x emissions are lower than 10 ppm in some cases [8].

Several others have reported on the emissions from LPP combustors. ([9, 10]). However, the amount of data in literature is rather scarce. Recently some authors have published on the dynamics of LPP combustion [11]. Modelling of LPP combustion under gas turbine conditions has not gained much attention from research, only some authors have specificly published on LPP combustion modelling [12]. Although LPP combustion is considerably cleaner than direct injection combustion, it is important that the mechanisms of pollutant formation and flame stability are investigated for further lowering of emissions and operation optimisation. With this in mind, LPP combustion modelling is investigated in this thesis.

Steam injection Steam has been applied in the gas turbine cycle since its early development and application. Firstly as the medium to drive the cycle. An example of this is seen in the apparatus designed by John Barber in 1791. Secondly steam served as a cooling agent for combustion gas that entered the turbine stage of the early gas turbine. Armengaud used steam for this objective already in 1905 [13]. The combustion gas at an approximate temperature of 1800°Celsius is diluted with steam to bring the temperature down to below 1000°Celsius. This is the maximum temperature that non-cooled turbine vanes can resist mechanically. Interestingly, steam nowadays is not needed anymore for cooling of the hot gas mixture at the inlet of the turbine. Firstly, thanks to improved compressor efficiency the gas turbine engine produces sufficient dilution air flow. Secondly, material science has offered materials

that can withstand much higher temperatures. Also turbine vane cooling via ingenious internal cooling flows has contributed largely to higher turbine inlet temperatures. For example, with advanced production techniques it is now possible to have turbine blades that can resist gas temperatures of almost 2000 K [14].

In modern gas turbine cycles steam is introduced again, but not only for cooling. It is done for several reasons, which are briefly summarized below:

- Increasing the efficiency of the gas turbine cycle. Injection of steam needs less than 1% of the work for compression, compared to air, but will increase the total mass flow through the turbine, thus increasing the power output of the gas turbine cycle [7, 15].

- Lowering the flame temperature in order to reduce the formation of NO_x, which is mainly temperature dependent [7, 15, 16]. In figure 1.4 this influence of steam is shown by results obtained with chemical equilibrium calculations for *iso*-octane-air oxidation. An increasing concentration of steam in a fuel air mixture lowers the flame temperature, as shown by the decreasing temperature profiles as a function of increasing steam concentration. *Iso*-octane is used here as a model fuel for liquid fuel combustion.

Both effects will have a positive environmental impact. Emission of NO_x is a direct cause for acid rain production. Decreasing its emission will therefore directly decrease acid rain production. Increased efficiency means that less fossil fuels are needed for a constant power production level and less CO_2 is released to the atmosphere. As energy demand on the planet is still increasing and many models [17–19] predict an untimely end to the availability of fossil fuels, it is clear that there is a need for efficient use of fossil fuels . This will stretch the time window that is left for exploration and introduction of new energy production/conversion technologies.

In literature many options are described how to introduce steam or water into the Brayton cycle. For a recent overview, the work of Poullikkas [20] is referred. Derksen [15] has assessed the influence of steam on natural gas combustion, using advanced modelling techniques.

1.5 Combustion noise

To benefit from the lowest possible pollutant emissions, both for liquid and for gaseous fuels, often a flame is operated at fuel lean premixed conditions [7]. Stable operation of a flame is needed for a long life cycle of combustion equipment and constant power output. However, lean premixed combustion is a process that is very sensitive to thermo-acoustic instabilities. The process of sound generation due to heat release, interacting with acoustical waves travelling through the combustor flow domain may result in flame extinction and mechanical failure of gas turbine equipment. Understanding the phenomenon of sound generation in turbulent premixed (prevaporised) flames is of crucial importance in prediction and prevention of thermo-acoustic instabilities.

1.6 Objective of the research

In this thesis turbulent combustion of liquid fuels in gas turbines is the major topic. Following the discussion of liquid fuel combustion chemistry and related phenomena of pollutant emissions and methods to reduce these emissions, this thesis aims at developing and improving models of combustion for liquid fuel.

First of all an efficient combustion model for higher hydrocarbon fuels, characterizing liquid fuel, is introduced. This model is based on a reaction progress variable approach. The model should enable accurate prediction of pollutant emissions in turbulent gas turbine combustion processes. It should be investigated how the model will perform under gas turbine conditions and how the model results will compare to experimental data.

Very often the degree of vaporisation in a combustion chamber is not 100%. This is reason for an investigation into spray combustion models. On the basis of this, a model for description of a spray should be formulated that is compatible with the proposed combustion model.

Acoustic stability is of great importance for good combustor performance. The noise generated by the turbulent flame is a good diagnosis and an indicator for its stability. To gain insight in the sound generation mechanism of a premixed prevaporised turbulent flame, a model should be formulated that can take into account different types of (model)-fuels and it should cooperate with the combustion model.

1.7 Contents of the thesis

The second chapter introduces the CFI reaction progress variable combustion model for large hydrocarbons. Available detailed chemical reaction mechanisms for several fuels are discussed and presented. Based on the theory of the Computational Singular Perturbation (CSP), a method is presented for optimal construction of reduced chemistry for higher hydrocarbon molecules, as typical for liquid fuels. It is shown that this reduction method leads to global steps that are shared by many hydrocarbon fuels.

By using the strategy presented in the second chapter, lean premixed prevaporised combustion of *iso*-octane and n-heptane is investigated under laminar conditions in the third chapter. For this a new detailed kinetic mechanism is assembled that incorporates the combustion chemistry of both n-heptane and *iso*-octane. The influence of steam on *iso*-octane and n-heptane combustion is assessed for formation of NO and CO by means of an examination of equilibrium results of the global step mechanisms.

In order to validate the predictive capabilities of the CFI combustion model, in chapter four the combustion model is applied on a turbulent gaseous propane flame in a lean premixed prevaporised swirl-stabilized combustor. The results are validated against experimental data that consist of temperature fields and velocity fields.

Chapter five proposes an approach to noise emission modelling for turbulent premixed methane or heptane flames, using a simple combustion model from literature and the combustion model from the second chapter. Predicted

sound pressure levels are compared to noise data obtained from an enclosed swirl-stabilized natural gas flame.

General theory of fuel spray modelling in literature is introduced and discussed in the sixth chapter. A model for the behaviour of the statistics of a liquid fuel spray is presented and a relation to the combustion model is given.

By using the spray model from chapter six and the CFI combustion model, a combusting fuel spray of methanol is modelled in the seventh chapter. A comparison with experimental data is used to asses the performance of the combined approach.

2

Theory of combustion, detailed chemistry and the CFI model

In this chapter combustion modelling with the use of the CFI model is presented. First theory of reacting flows is discussed. For laminar premixed prevaporised flames results of detailed chemistry computations are described. A chemistry reduction method is introduced and extended for accurate definition of a reduced chemistry system. For turbulent spray flames the CFI model reaction progress variable model is introduced. It is extended with extra terms for spray-gas interaction.

2.1 Introduction

There has been a lot of research on the prediction turbulent combustion by modelling. The high complexity of the turbulence and the chemistry involved, have pushed research in the direction of general modelling of turbulent flame behaviour. Several models have been developed and applied in research. An overview of recent turbulent combustion modelling approaches is given in the article of Veynante and Vervisch [21].

One very basic model being used in many industrial applications is the 'Eddy-Breakup-Up' (EBU) model [16,21], introduced by Magnussen and Hjertager. This model assumes chemistry time scales are short compared to mixing time scales. The main feature of the model is that under this assumption the rate of chemical reaction is determined by turbulent dissipation, i.e. the break-up of eddies. The chemical source term in the transport equation for a species is then closed with an EBU source term. The model is referred to as turbulent mixing model and finite rates of reactions are not taken into account.

A more sophisticated approach by the use of 'flamelet' modelling has been proposed by several authors. This approach is based upon geometrical visualisation of a flame. For example, there is the BML (bi-modal-limit) model, developed by Bray, Moss and Libby [21]. In this approach a turbulent flame is described by a laminar premixed flame embedded in a turbulent flow field. The main problem of this model is the quantification of the flame speed. Often a reaction progress variable is introduced in this approach. Another formulation in the flamelet description is the use of a 'G-field-equation' [22]. Using a variable 'G' the kinematics of a flame front are described.

The major topic of this thesis is the modelling of turbulent combustion of propane, heptane and octane. In this chapter a model will be proposed to capture essential properties of the chemistry of these fuels in the gas phase. For this the framework of the CFI combustion model with general reaction progress variables is used, according to Derksen [15, 23]. The CFI model is a generalisation of the FIRST model, as developed by Kok and co-workers [24–26] over the past years. Based on first principles, reaction progress variables are used as the means to describe turbulent combustion. This is done using Reynolds Averaged Navier Stokes equations and for that reason a presumed-shape probability density function (PDF) is applied to account for the influence of turbulent fluctuations. The two acronyms CFI and FIRST are both indicating the variables contained by the model. *F* and *I* respectively represent the mixing scalar and enthalpy scalar, while in CFI the *C* stands for a reaction progress variable. Within FIRST, *R*,*S* and *T* are reaction progress variables. From the acronyms the major difference is clear: the definition of the reaction progress variables. CFI uses the Computational Perturbation Method (CSP) to define the reaction progress variables, while FIRST uses manually defined reaction progress variables.

The chapter is started with a presentation of the governing equations for laminar combusting flows. Using these equations some results are presented of laminar simulations of flames with different fuels and detailed reaction mechanisms. Using the Computational Perturbation Method (CSP) of Lam [27] and Goussis [28] global mechanisms can be formulated based on the laminar results. Then for the global mechanism a turbulent combustion model is formulated using the CFI-methodology of Derksen and Kok. The chapter ends with an addition to the CSP algorithm that allows for a physical definition of the low-dimensional manifold on which the chemistry is defined.

2.2 Theory of laminar combusting flows

In this section the general transport equations are given for laminar reacting flows [16]. Combustion is a combination of transport phenomena and chemistry and for that reason both the fluid dynamics and the chemistry are being reviewed. Any reacting flow is instantaneously determined by pressure, concentration of species, temperature and velocity. These properties can change due to transport, either on a molecular scale (diffusion, viscous dissipation) or on a macro scale (convection), chemical reactions or by phase changes. In this section, single phase flows are considered. Overall conservation of mass is described by the continuity equation:

$$\frac{\partial \rho}{\partial t} + \nabla \cdot \rho \boldsymbol{U} = 0 \tag{2.1}$$

Any combusting system contains a number of species N, each with mass fraction Y_i. The sum of the mass fractions of all the species is given by:

$$\sum_{i=1}^{N} Y_i = 1 \tag{2.2}$$

Individual species mass fractions are determined by the transport equation:

$$\frac{\partial Y_i}{\partial t} + \nabla \cdot (Y_i \boldsymbol{U}) + \nabla \cdot \underline{j}_i = \omega_i \text{ with i = 1,...,N} \tag{2.3}$$

The diffusion flux j_i can be replaced with an expression for molecular diffusion, assuming thermal and pressure diffusion do not influence the system. This is formulated in Fick's binary diffusion law [16,21]:

$$j_i = Y_i \boldsymbol{V}_i = \rho D_i \nabla Y_i \tag{2.4}$$

The chemical source term ω_i in equation (2.3) can be expressed using the following equation, which is a combination of the mass action law and the reaction mechanism in Penner notation:

$$\omega_i = M_i \sum_{i=1}^{R} \left(v_i^{''} - v_i^{'} \right) \left[k_{f,j} \prod_{j=1}^{N} Y_j^{v_{ij}^{'}} - k_{b,j} \prod_{j=1}^{N} Y_j^{v_{ij}^{''}} \right] \tag{2.5}$$

The rate constants k in this equation are determined by the Arrhenius equation, which appears as follows:

$$k_i = A_i \exp(-E_a / \Re T) \tag{2.6}$$

The velocity vector $\boldsymbol{U}$ from equation (2.1) describes the motion of the fluid. This is defined by the conservation of momentum, the Navier-Stokes equation. This equation reads as follows:

$$\frac{\partial \rho \boldsymbol{U}}{\partial t} + \nabla \cdot \rho \boldsymbol{U} \otimes \boldsymbol{U} + \nabla \cdot \overline{\overline{p}} = \rho \underline{g} \tag{2.7}$$

The pressure tensor $\overline{\overline{p}}$ is defined with the relation:

$$\overline{\overline{p}} = pI - \mu \left(\nabla \boldsymbol{U} + (\nabla \boldsymbol{U})^T - \frac{2}{3} (\nabla \cdot \boldsymbol{U}) \right) \tag{2.8}$$

In $\overline{\overline{p}}$ the first part (pI) is the hydrostatic part and the second part is the viscous part. I stands for the unity tensor. For a much more in depth discussion of the Navier-Stokes equation see for example Batchelor [29].
Based upon the principles of conservation of energy, the following equation can be derived for the conservation of enthalpy h:

$$\frac{\partial \rho h}{\partial t} + \nabla \cdot (\rho \boldsymbol{U} h) + \nabla \cdot (\rho D \nabla h) = q_{\text{transfer}} \tag{2.9}$$

This enthalpy equation is valid under the following assumptions:

1. Pressure derivatives with respect to time are neglected, the flow is assumed to be isentropic and to have a low Mach number.

2. The Lewis number is unity for all species:

$$Le = \frac{\lambda}{D\rho c_p} = 1 \tag{2.10}$$

In case of a perfect gas, enthalpy is related to temperature by the equation:

$$h_i = \Delta h^0_{f,i} + \int_{T_0}^{T} C_p dT \tag{2.11}$$

The RHS of equation 2.9 refers to processes responsible for dissipation of production of heat. Examples of these processes are viscous dissipation, radiation or evaporation.

Then the total enthalpy of a system is found by a summation over all species:

$$h = \sum_{i=1}^{N} Y_i h_i \tag{2.12}$$

To complete the set of equations mentioned in the paragraphs before, the equation of state is used for a perfect gas:

$$\frac{p}{\rho} = \sum_{j=1}^{N} \frac{Y_i}{M_i} \Re T \tag{2.13}$$

With equation 2.13 the set of equations describing a laminar reacting flow is completed. Equations 2.1-2.13 give the possibility to solve all combustion problems as a function of time and space, both for laminar and turbulent reacting flows, either by use of a numerical procedure or analytically. Unfortunately, only simple problems with low dimensionality and small domains can be solved analytical. When the problem is turbulent, the task will very complex. The variables in such a flow show non-linear variations in all spatial directions and exponential defined reaction rates introduce so-called mathematical stiffness to the problem. In appendix A methods are discussed to model turbulence by using statistical approaches to the problem.

2.3 Laminar flames of heptane and octane

Having discussed the governing equations modelling a laminar reacting flow, in this section results of numerical simulations of some heptane and octane fuelled prevaporised laminar premixed flames will be discussed.

Liquid fuel based on refined products is composed of many different hydrocarbon molecules. As known, the general structure of a hydrocarbon molecule consists of a chain of hydrocarbons, with a set of H-atoms bonded to

	Alkanes	Cyclo-alkanes	Aromatics	Other
Natural gas	99	-	-	1
Middle distillate fuels	50.5	30.9	18.6	-
Gasoline fuels	41	-	26	33

Table 2.1: Average composition of hydrocarbon fuels (masspercentages), sorted on alkane content. [30,31]

them. The number of C-atoms in the molecules can vary considerably, depending on the size of the hydrocarbon molecule. For liquid fuel hydrocarbons such as octane and heptane this number is of the order of 10. For simple alkane molecules this number of C-atoms n determines the number of H-atoms: C_nH_{2n+2}.

Several references [30,31] give an overview of hydrocarbon fuel combustion chemistry, including liquid fuels. Liquid fuels are a result from the refining of crude oil. This oil may be of fossil origin or the product of a biomass pyrolysis process. This refining process essentially is a distillation process at atmospheric pressure that separates crude oil into lighter fractions. Classification of refined products is based on the average molecular weight of the resulting fuel. Three classes are usually distinguished: gasoline fuel, middle distillate fuels (such as diesel and kerosene) and heavy oil. The process of producing any liquid fuel suitable for gas turbine combustion, however is much more complicated than simple distillation of crude oil.

From table 2.1 it is clearly seen that oxidation of alkanes plays a central role in hydrocarbon combustion. The concentration of the alkane components is the highest for all mentioned classes of refinery fuels.

In order to model chemistry of a liquid fuel, the most important factor will be the correct modelling of alkane chemistry. For example, Dagaut [30] shows that combustion of kerosene (a middle distillate fuel) is effectively described using the n-decane molecule as a model fuel. This was shown in jet-stirred reactor experiments as well as in laminar flames. Better agreement was found when detailed kinetic models for cyclo-alkanes (cyclo-hexane) and aromatics (benzene) were added to the detailed model fuel mechanism.

For gasoline fuels, n-heptane and *iso*-octane often are used as reference fuel. With these two alkanes an important mechanism of gasoline combustion can be modelled: early ignition of the fuel as a result of compression (engine-knock). n-Heptane is very sensitive to auto-ignition, while *iso*-octane is highly resistant to auto-ignition. In model fuel calculations blends of these two molecules are often chosen as reference fuel for gasoline calculations [32,33]. In this thesis n-heptane and *iso*-octane have been chosen as model fuels, as they are provided with the largest basis in literature.

Reaction mechanisms As *iso*-octane and n-heptane are widely used as reference fuels for liquid fuel combustion modelling, many detailed chemistry schemes have been developed for use in different applications: freely propagating premixed flames, shock tubes, diffusion flames and flow reactors. For

	Temperature Range (K)	# Species	# Reactions
Curran et al. [35]	550-2000	544	2446
Golovitchev [37]	550-2000	57	290
Williams [38]	550–2000	44	216

Table 2.2: Some n-heptane reaction mechanisms for flame modelling and their characteristics.

n-heptane a recent overview is given in the article of Babushok and Tshang [34]. Several detailed kinetic schemes are discussed in that article. Some of them, the high temperature mechanisms, are used in this thesis and will form the basis for a mechanism that is presented in the third chapter. Basically the reaction mechanisms are split into two parts. A low temperature dependence (550 – $\pm$ 900 K),important for ignition modelling, and a high temperature dependence ($\pm$ 900 – 2600 K), necessary for flame modelling.

According to Curran *et al.* [35, 36] 25 groups of important classes of reactions can be found for higher hydrocarbon atoms. As the low-temperature kinetics are of less importance in this thesis, the high-temperature group of reactions, the (post) flame front reactions, will be shortly discussed below:

1. Unimolecular fuel decomposition. This is a very endothermal step, generating n-heptane radicals and some others. Because of the fact that other reactions also produce radicals, this reaction is not considered as a significant source for radicals.

2. H atom abstraction from the fuel. Occurs at primary and secondary sites of n-heptane, both at low and high temperatures.

3. Alkyl ($C_{2n}H_{2n+1}$) radical decomposition. This so-called β-scission, breaking of the long carbon chain, is considered to be the most active decomposition mechanism. This step occurs at relatively high temperatures.

4. Alkyl radical + O_2 to produce alkenes ($C_{2n}H_{2n}$) + H_2 directly.

5. Alkyl radical isomerization. Transfer of H atoms along the carbon chain.

6. Alkene abstraction reactions. H atom abstraction by radicals.

7. Alkene addition reactions. Addition of $\dot{C}H_3$ and $\dot{H}$ radicals to alkenes

8. Alkenyl radical decomposition. Unimolecular decomposition into alkenes and allyles (a hydrocarbon with a vinyl and methylene group.)

9. Alkene decomposition. Unimolecular decomposition into smaller alkenes.

Mechanisms found in literature to describe the steps mentioned above including low temperature chemistry consist of many elementary reactions and species. In principle, breakup of long hydrocarbon chains has much more degrees of freedom than simple methane oxidation. Of course, oxidation of any hydrocarbon chain will proceed according to thermodynamic laws and

chemical equilibria. For example, for n-heptane it is shown by Xue and Aggarwal [39] that in a partially premixed flame C_2 hydrocarbons are very important.

An essential feature for a mechanism in order to use it as a basis for the reaction progress variable model, to be discussed later on in this chapter, is correct modelling of the high-temperature oxidation reactions, the flame zone reactions. Based on this argument, several mechanisms have been selected from literature that were already tested and validated for flame chemistry. These reaction mechanisms are given in table 2.2 for n-heptane combustion.

The first mechanism considered is constructed by Curran *et al.* [35]. It has been tested against various data from a rapid compression machine, continuously stirred reactor and a turbulent flow reactor. The mechanism incorporates both low- and high temperature oxidation and thus comprises a relatively large amount of species and reactions. A much smaller mechanism, but not so well documented, is the mechanism as proposed by Golovitchev [37]. This mechanism mainly is used for application in direct injection engine modelling and therefore has been optimised to conditions relevant to this type of combustion. The same order of size as the Golovitchev-mechanism is the mechanism as proposed by Williams *et al.* [38]. The basis of this mechanism is given by the general hydrocarbon mechanism from the group of Williams [40,41]. This mechanism has been validated for relevant flame conditions and when looking at the number of species and number of reactions it seems to be the most appropriate mechanism for use in turbulent flame simulations.

Several *iso*-octane detailed chemistry mechanisms are given in table 2.3. As for table 2.2, this list is not complete, as more mechanisms are documented in literature, see for example the work of Bakali [43] and Hasse [44]. From the listed mechanisms the last one from Simon *et al.* [42] is the most detailed mechanism incorporating the largest number of species and reactions. However, this mechanism is less suitable for flame chemistry modelling as validation only took place for chemistry occurring in a jet stirred reactor operating at a constant temperature of 873 K. The mechanism of Curran *et al.* [36] is constructed in the same way as the n-heptane mechanism from the same authors and is validated using the same procedures and apparati. This mechanism is therefore suitable for flame modelling. Golovitchev also proposed a mechanism, that again is not documented very well in literature and has specifically been designed for use in automotive applications. Nevertheless the temperature range and pressure range for which the mechanism has been tested makes it suitable for use in gas turbine combustion modelling.

	Temperature Range (K)	**# Species**	**# Reactions**
Curran *et al.* [36]	550 - 1700	857	3606
Golovitchev [37]	550 - 1700	84	413
Simon *et al.* [42]		473	2411

Table 2.3: Some *iso*-octane reaction mechanisms for flame modelling and their characteristics.

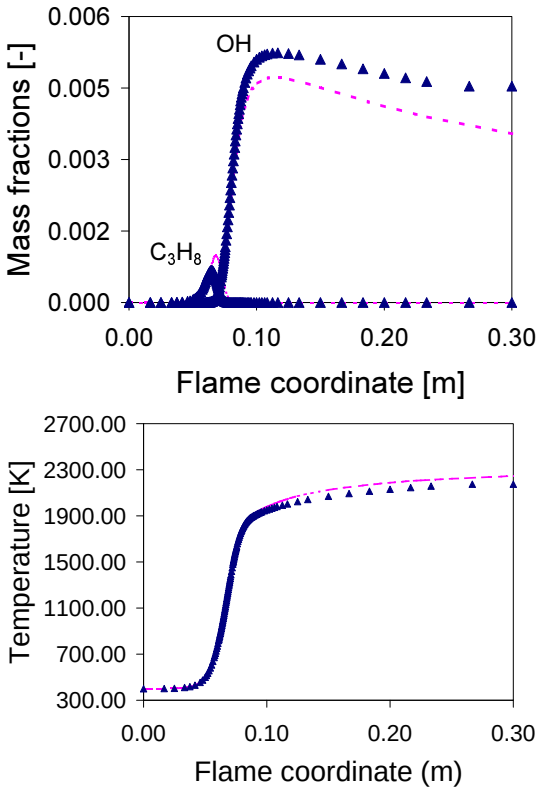

Figure 2.1: Intermediate species (OH and C_3H_8) and temperature profile (△ = Williams, - = Curran).

Some flame results for n-heptane In this section some results will be discussed that are obtained for the simulation of a one dimensional, adiabatic, isobaric, freely propagating flame. For solving the equations involved in this problem, given previously, the widely applied code PREMIX [45] is used. The equations were solved with a mixture averaged diffusion coefficient, assuming unity Lewis numbers. In order to see whether the number of species and reactions influences the outcome of a detailed laminar flame computation, both the mechanisms of Curran and Williams were applied. For the first mechanism the PREMIX code was adapted in terms of data storage capacity, but the general algorithm of the code was kept the same. The inlet conditions of the flame were set to a stoichiometric n-heptane/air mixture at a temperature of 400 K and pressure of 1 atm.

Grid independent solutions were obtained for both mechanisms. Discretisation of the equations is done on an initial grid of 4 points, using an upwind (forward-differencing) scheme. The procedure to find a stable, accurate solution is summarized as follows: When a solution is found, using criteria for the maximum curvature and gradient from gridpoint to gridpoint the mesh is repeatedly refined, until a physical and converged solution is found on a

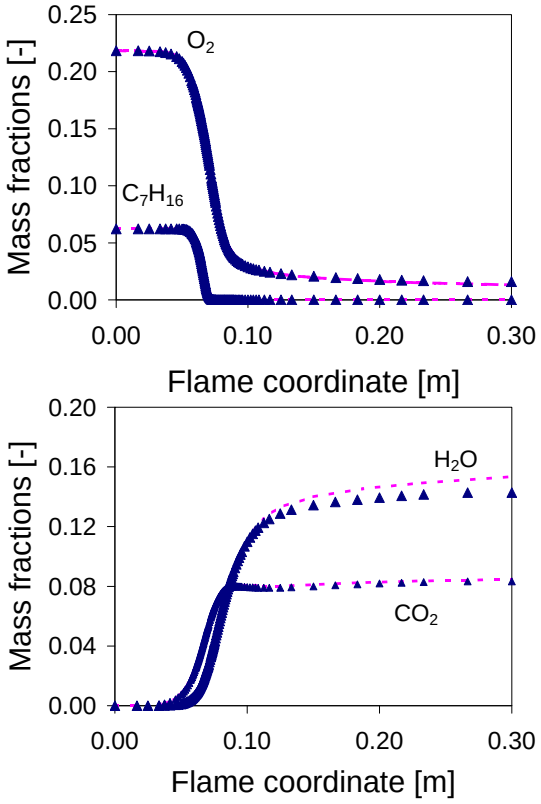

Figure 2.2: Major species involved in n$-C_7H_{16}$ combustion ($\triangle$ = Williams, - = Curran)

sufficiently fine grid. The solution for the Curran mechanism was realized using 211 gridpoints. The Williams mechanism needed 127 gridpoints for a grid independent solution. The difference in gridpoints is explained by the greater amount of tracer species, describing flame front chemistry, in the Curran mechanism. This makes the solution process much more stiff.

Despite the difference in grid size, the converged solutions are very similar in species and temperature profiles. In figure 2.1 the flame temperature as a function of flame length shows hardly any difference comparing the two mechanisms. The only difference between the two mechanisms in term of temperature is a slightly higher exit temperature for the Curran mechanism. That is explained by two effects. Firstly, a minor difference in the polynomial fitting coefficients that were used for the polynomials that take into account the temperature dependence of the system enthalpy and specific heat values occurred. The definition of these well known NASA polynomials can be found in [45]. Secondly the equilibrium of products and temperature differed as the Curran mechanism contains much more species.

The concentration profile of the OH-radical shows, figure 2.1 that the flame front is positioned at the same coordinate for both mechanisms. Nevertheless

the Williams mechanism predicts a higher OH concentration at the flame front and at the exit. The intermediate propane formation is higher with the mechanism of Curran. The differences in the results for the intermediate species are due to the fact that different reaction rate constants in both mechanisms produce different concentrations. Another reason is the fact that the Curran mechanism takes into account more species, having a primarily effect on intermediate species concentrations. However, when the major species are investigated it is seen that the differences are neglectable, see the profiles of species in figure 2.2. The consumption of n-heptane and oxygen are equal, as are the formation of carbondioxide and water.

From a computational point of view it seems attractive to use the detailed mechanism of Williams for further use in this thesis, looking at the equal results obtained for the stoichiometric flame. A smaller detailed mechanism will need lower computational storage capacities and the reduction of the chemistry to a global step will be relatively more easy.

2.4 Turbulent flames: reduced chemistry

Having discussed detailed chemistry mechanisms that can be incorporated directly under laminar conditions, in this section the Computational Singular Perturbation (CSP) algorithm for the construction of a globally reduced mechanism is discussed. Derksen [15] introduced the CSP based reaction progress variables, as proposed by Massias *et al.* for use in laminar flames [28], in a general way. The developed methodology of Derksen is used in this thesis as the basis for the turbulent combustion model.

2.4.1 Construction of a global mechanism

The evolution of the species vector in a chemical reacting flow is determined by equation (2.14). In general notation, separating the linear operations ($\boldsymbol{L}$) of convection and diffusion from the non-linear chemical source term ($\boldsymbol{g}$) this equation can be cast in the following form:

$$\frac{\partial \boldsymbol{Y}}{\partial t} = \mathbf{L}\left(\boldsymbol{Y}\right) + \mathbf{g}(\boldsymbol{Y}) \tag{2.14}$$

This equation can be used to describe the species vector in any type of single phase chemical reacting system. Examples of this can be a premixed laminar flame or a counterflow diffusion flame. In this thesis laminar premixed flames are used for analysis with the CSP algorithm. The aim of the CSP algorithm is to construct a set of S global reactions. This is done by analysis of the Jacobian of the reaction terms in species space. The components of the Jacobian are presented in this relation:

$$J_{ij} = \frac{\partial \omega_i}{\partial Y_i} \tag{2.15}$$

A description of the exact algorithm for construction of a global reduced mechanism can be found in several articles by Goussis, Lam, Massias and Derksen [15,27,28,46]. The major result of application of the global CSP algorithm to the chemical species system in a reacting flow is the definition of a set of basis vectors that defines a steady state space and a slowly developing low-dimensional chemical manifold.

Below the procedure of the reduction method using CSP will be sketched. Assume a chemical system of *N* species and a global system that should consist of *(N-M)* steps. Two sets of orthonormal vectors $\boldsymbol{a}$ and $\boldsymbol{b}$ are defined. Their components can be subdivided as:

$$\begin{aligned} \boldsymbol{a}_r^0 &= \left[a_1^0, a_2^0, ..., a_M^0\right] \\ \boldsymbol{a}_s^0 &= \left[a_{M+1}^0, a_{M+2}^0, ..., a_N^0\right] \\ \text{and } \boldsymbol{b} &= \boldsymbol{a}^{-1} \end{aligned} \tag{2.16}$$

When the numerical solution of the species vector $\boldsymbol{Y}$ is known from laminar flame calculations, from these vectors new sets can be derived using $\boldsymbol{J}$. This yields:

$$\begin{aligned} \boldsymbol{a}_r &= \boldsymbol{J}\boldsymbol{a}_{\boldsymbol{r}}^{\boldsymbol{0}}\tau & \boldsymbol{b}^{\boldsymbol{r}} &= \tau_0 \boldsymbol{b}_{\boldsymbol{0}}^{\boldsymbol{r}} J \\ \boldsymbol{a}_s &= \left[\boldsymbol{I} - \boldsymbol{a}_{\boldsymbol{r}}^{\boldsymbol{0}}\boldsymbol{b}\right]\boldsymbol{a}_{\boldsymbol{s}}^{\boldsymbol{0}} & \boldsymbol{b}^s &= \boldsymbol{b}_0^s\left[\boldsymbol{I} - \boldsymbol{a}_r \boldsymbol{b}^r\right] \end{aligned}$$

$$\text{With } \tau_0 = \left(\boldsymbol{b}_{\boldsymbol{r}}^{\boldsymbol{0}}\boldsymbol{J}\boldsymbol{a}_{\boldsymbol{r}}^{\boldsymbol{0}}\right)^{-1} \qquad \text{and } \tau = \left(\boldsymbol{b}^r \boldsymbol{J}\boldsymbol{a}_{\boldsymbol{r}}^{\boldsymbol{0}}\right) \tag{2.17}$$

After calculating these new vectors, it should be investigated what the M fastest timescales are and how the influence of the species 1 to M on the steady state relations will be. This is indicated by a so-called *local CSP pointer*. Note that 'local' refers to a spatial gridpoint in the numerical solution. The local pointers $\boldsymbol{D}$ are defined as follows:

$$\boldsymbol{D} = \frac{\text{Diag}\left(\boldsymbol{a}_i \boldsymbol{b}^i\right)}{\sum_{i=1,N} b_k^i a_i^k} \tag{2.18}$$

The species with the largest pointer values are assumed to be locally in steady state.

So far, the CSP algorithm has been applied locally. Throughout the numerical solution of a steady-state laminar flame, the values of the local pointers will vary and the ordering of the steady state species will be different. Therefore, in order to construct a mechanism that is globally valid throughout the solution of a laminar flame, the local pointer should be integrated throughout the domain for every species. This integration is obtained by the following relation:

$$I^i = \frac{1}{L}\int_0^L D_i \frac{1}{X^i}\frac{\omega^i}{\omega_{\max}^i} dx \tag{2.19}$$

The definition of the global pointer I_i for a species in this equation is purely on a kinetical basis, as only the reaction rates and local pointers are involved. This could potentially lead to some misjudging of steady state species. Massias *et al.* [28] show this for a premixed methane-air flame, where it is found that N_2O and NO are invariably major species, which is not true for at least N_2O. This can be overcome by adding diffusion effects to the global pointer definition [47]. Applying equation (2.19), the global steady state species can be identified in a laminar reacting flow, according to ordering on the basis of the global pointer value.

When the global steady state species are known, it is possible to define the global reduced mechanism. The global pointer analysis yields a matrix $\widehat{b}_r$ with the steady state relations:

$$\widehat{\boldsymbol{b}}^r = \left[\boldsymbol{I}_{M\times M}, \mathbf{0}_{M\times(N-M)}\right] \tag{2.20}$$

The element conservation relations are constructed additional to the steady state relations, using the molar species element composition. This gives a matrix of size $N \times E$ with E being the number of elements in the system. Finally the global steps are defined, by finding linear independent vectors to the current $(M + E) \times N$ matrix.

$$\widehat{\boldsymbol{b}}^s = \widehat{\boldsymbol{b}}^{s0}\left[\boldsymbol{I}_{N\times N} - \widehat{\boldsymbol{a}}_r\widehat{\boldsymbol{b}}^r\right] \tag{2.21}$$

The corresponding matrix **a** is then found by inverting $\boldsymbol{b}$:

$$\widehat{\boldsymbol{a}} = \begin{bmatrix} \widehat{\boldsymbol{b}}^{\boldsymbol{r}} \\ \widehat{\boldsymbol{b}}^{\boldsymbol{c}} \\ \widehat{\boldsymbol{b}}^{\boldsymbol{s}} \end{bmatrix}^{-1} = \begin{bmatrix} \widehat{\boldsymbol{a}}_{\boldsymbol{r}} & \widehat{\boldsymbol{a}}_{\boldsymbol{c}} & \widehat{\boldsymbol{a}}_{\boldsymbol{s}} \end{bmatrix} \tag{2.22}$$

The given $\widehat{\boldsymbol{a}}$ and $\widehat{\boldsymbol{b}}$ matrix are based on molar concentration. By multiplication with the ratio of the molar weights the matrices can be formulated on mass basis:

$$\widehat{b}_{ij} = \frac{M_j}{M_i} b_{ij} \tag{2.23}$$

Having assembled a reduced mechanism the species vector equation (2.14) can be rewritten:

$$\frac{\partial \boldsymbol{Y}}{\partial t} = \mathbf{L}\left(\boldsymbol{Y}\right) + \boldsymbol{a}_c\boldsymbol{b}^c \cdot \boldsymbol{\omega} + \boldsymbol{a}_r\boldsymbol{b}^r \cdot \boldsymbol{\omega} + \boldsymbol{a}_s\boldsymbol{b}^s \cdot \boldsymbol{\omega} \tag{2.24}$$

Assuming that the chemistry is completely defined by the slow subspace spanned by the vectors $\boldsymbol{a}_s$ and $\boldsymbol{b}^s$, equation (2.24) can be cast in the following form:

$$\begin{aligned} \frac{\partial \boldsymbol{Y}}{\partial t} &\simeq \mathbf{L}\left(\boldsymbol{Y}\right) + \boldsymbol{a}_s\boldsymbol{b}^s \cdot \boldsymbol{\omega} \\ \boldsymbol{a}_c\boldsymbol{b}^c \cdot \boldsymbol{\omega} &= 0 \\ \boldsymbol{a}_r\boldsymbol{b}^r \cdot \boldsymbol{\omega} &\simeq 0 \end{aligned} \tag{2.25}$$

A multiplication of this system with $\boldsymbol{b}$ will lead to a formulation with a composed species definition η and a corresponding rate:

$$\begin{aligned} \frac{\partial \boldsymbol{\eta}^s}{\partial t} &\simeq \mathbf{L}\left(\boldsymbol{\eta}^s\right) + \boldsymbol{b}^s \cdot \boldsymbol{\omega} \\ \frac{\partial \boldsymbol{\eta}^c}{\partial t} &= \mathbf{L}\left(\boldsymbol{\eta}^c\right) \\ \boldsymbol{b}^r \cdot \boldsymbol{\omega} &\simeq 0 \end{aligned} \tag{2.26}$$

This formulation of a global reduced mechanism is only valid when $\boldsymbol{a}$ and $\boldsymbol{b}$ are invariant in space and time, as noted by Derksen on page 21 [15]. This is already implicitly assumed constructing the global pointer.

Regarding the number of steps in a reduced mechanism, there is a difference between laminar and turbulent conditions. Derksen has shown in his work that for turbulent flame modelling, the optimal number of global steps is one $(N - M = 1)$. Increasing the number of steps is only meaningful when the number of global CSP steps will go to an order of 10, this being only feasible to solve under laminar conditions. Massias *et al.* [28] show that 7 steps give a reasonably accurate description of chemistry as defined by the GRI 3.0 mechanism for natural gas combustion.

2.5 An overview of the CFI combustion model

Having explained the theory on the construction of a global reduced chemistry mechanism, this section continues with the description of a combustion model. It was mentioned in the introduction of this chapter that the CFI model and its predecessor FIRST, so far only had been applied to gaseous fuels with small molecules. Examples of this can be found in the articles of Kok, Louis and Derksen [15, 24–26]. Combustion modelling of a spray is a process that differs from gaseous combustion in at least two aspects:

1. Energy loss to the liquid phase due to evaporation: the gaseous combustion is non-adiabatic

2. Mixing of freshly introduced fuel vapor with air and combusted products. Hence the spray introduces local fuel mass sources in the gas phase.

These two aspects can be classified as phase transfer phenomena. Transfer of energy from the gas to the liquid phase and transfer of mass from the liquid phase to the gaseous phase. This can be accounted for by using two variables that already exist in the context of the previous models mentioned. One variable for the description of the mixing process, the well-known mixture fraction f and one for the enthalpy of the gas phase, the i-scalar. These two variables have been introduced in the previous versions of the CFI and FIRST combustion models [15,48] to account for fuel-air mixing in the gaseous phase and for enthalpy losses trough radiation. However, in the context of spray combustion, their contribution to the modelling is even more important.

Chemistry scalar First a reaction progress variable approach is introduced for an efficient description of combustion in the gaseous phase. The reaction progress variables c_i are modeled using the CSP defined composed species mass fractions η_i:

$$c_i = \frac{\eta_i^s - \eta_{i,cold}^s}{\eta_{i,eq}^s - \eta_{i,cold}^s} \text{ with } i = 1, ..., S \tag{2.27}$$

This definition yields that c_i is always larger than 0 and will evolute to its equilibrium value 1. Physically this means that the state of combustion is defined between the unburned or cold conditions and chemical equilibrium conditions. The denominator of equation (2.27) is referred to as the normalisation function W_i. This normalisation function is a function of the local fuel to air ratio, f. In the remainder of this thesis the number of global steps S will be 1, so the subscript i will be omitted from here on.

Derksen [15] described the generalized framework for the formulation of the CFI transport equations. Evaporation of fuel will introduce a mass transfer term in the derivation of the laminar transport equation. This is treated in appendix G. Here the result is presented, a Favre averaged transport equation for the mean of the reaction progress variable $\tilde{c}$:

$$\begin{aligned} \nabla . \left(\bar{\rho} \tilde{\boldsymbol{U}} \tilde{c} \right) - \nabla . \left(\bar{\rho} D_T \right) \nabla \tilde{c} = \\ \tilde{S}_c - \overline{\left(\frac{W_i}{W} \right) c S_i} - \overline{\left(c \frac{W_f}{W} + \frac{\eta_f^u}{W} \right) S_{mt}} + \\ \overline{\left(\frac{W_{ff}}{W} \right)} \tilde{c} \frac{1}{2} \bar{\rho} R_T \frac{\varepsilon}{k} \overline{f''^2} + \\ \widetilde{S_m tc} \end{aligned} \tag{2.28}$$

In this equation the well-known gradient assumption is used for modelling of the fluctuations of c. The RHS of this equation contains several terms that need further explanation. The first term is simply $\frac{\omega_c}{W}$, representing the reaction progress variable source term due to chemical reactions. The second term represents the effect of enthalpy losses in the gaseous phase, and following the discussion in the thesis of Louis, this term can be omitted. Also in the case of a two-phase flow [48]. The third term represents the effect of evaporation through the mixture fraction variable and is considered important. The fourth term is related to the influence of mixing on chemical equilibrium and is shown to be important [15, 48]. The final term on the RHS is the direct influence of liquid to gas mass transfer on the reaction progress variable. The first term and the last term of the RHS will have the largest contribution to the development of the reaction progress variable in reacting flows.

In order to account for turbulent fluctuations, a presumed PDF is used. For the reaction progress variable, averaging is performed over the β-PDF A. A transport equation for the variance of the reaction progress variable is

therefore formulated to be:

$$\nabla.\left(\bar{\rho}\tilde{\boldsymbol{U}}\widetilde{c''^2}\right)-\nabla.\left(\bar{\rho}D_T\nabla\widetilde{c''^2}\right)= 2\frac{\mu_T}{Sc_T}\left(\nabla\tilde{c}\right)^2-2\bar{\rho}\frac{\varepsilon}{k}\widetilde{c''^2}\left(1-\widetilde{f''^2}\left(\frac{\overline{W_{ff}}}{W}-2(\tilde{i}-1)\frac{\overline{V_{ff}}}{V}\frac{W_i}{W}\right)\right)+ 2\overline{\tilde{c}S_c}-2\tilde{c}\overline{S_c}-2\widetilde{c''^2}\frac{\overline{W_i}}{W}\overline{S_{rad,i}} \tag{2.29}$$

It is shown by Kim and Huh [49] that the influence of evaporation is not significant on variances. The development of a variance variable in a turbulent flow is mainly generated by gradients of the mean variable. When the influence of mass transfer is accounted for in the mean variable, this will consequently influence the gradients of these variables in the flow field. Thus the influence of evaporation on the variance is incorporated indirectly via the development of the mean variables.

Mixing scalar As said earlier, an evaporating spray introduces mass into the gas phase. To account for mixing between this fresh vapor and the air, the mixture fraction f is introduced. So far, within the context of the CFI model and its predecessors, this variable accounted for mixing between streams coming from several inlets. In this thesis, the variable not only models this, but also takes into account mixing of fresh vapor and the surrounding gas. However, the mathematical mixture fraction definition remains unchanged:

$$f=\frac{Z_i-Z_i^2}{Z_i^1-Z_i^2}\ \text{with}i=1,...,E \tag{2.30}$$

In this equation Z_i represents the local mass fraction of an element and the superscripts 1 and 2 denote the location of an inlet. The Favre averaged transport equation that has to be solved for f is as follows:

$$\nabla.\left(\bar{\rho}\tilde{\boldsymbol{U}}\tilde{f}\right)-\nabla.\left(\bar{\rho}D_T\nabla\tilde{f}\right)=\tilde{S}_{\text{mt}} \tag{2.31}$$

This equation is seen in several other articles where the mixture fraction is used for the modelling of the fuel concentration in the gaseous phase [50]. The difference with the previous formulations of CFI is the appearance of a source term in the RHS of equation (2.31). This source term is used for the introduction of fuel vapor in the gaseous phase. It is depending on the applied evaporation and spray models, that will be discussed in chapter 6.

A transport equation for the variance of mixture fraction, f''^2 is also solved. This transport equation is similar to the expressions as given by Derksen [15], provided that the effect of source term fluctuations is negligible:

$$\nabla.\left(\bar{\rho}\tilde{\boldsymbol{U}}\widetilde{f''^2}\right)-\nabla.\left(\bar{\rho}D_T\nabla\widetilde{f''^2}\right)=2\frac{\mu_T}{Sc_T}\left(\nabla\tilde{f}\right)^2-\bar{\rho}\frac{\varepsilon}{k}\widetilde{f''^2} \tag{2.32}$$

Here the first RHS term represents the growth of the variance due to a gradient in f. The 2^{nd} RHS term damps all the fluctuations of mixture fraction

to equilibrium. Again the effect of evaporation is neglected. Reveillon and Vervisch [51] discuss the closure of terms in the transport equation for the mixture fraction variance in the case of turbulent spray combustion. Although they do not state explicitly that the effect is negligible, from the presented data it can be seen that the net effect of a turbulent evaporating spray on the production and dissipation of the variance does not change much from the situation in the gaseous phase.

Enthalpy scalar To complete the CFI model for spray combustion the enthalpy loss variable i is introduced. This variable is defined with the following relation between adiabatic enthalpy and the minimal enthalpy of the gaseous mixture:

$$i = \frac{h - h^{\min}}{h^{\mathrm{ad}} - h^{\min}} \tag{2.33}$$

A transport equation for the mean of i has to be solved according to the following formulation. This transport equation is derived in a similar procedure as the reaction progress variable, starting with the laminar transport equation for enthalpy(2.9) and the previous definition. After Favre averaging and modelling steps the following equation is found:

$$\begin{aligned} \nabla.\left(\bar{\rho}\tilde{\boldsymbol{U}}\tilde{i}\right) - \nabla.\left(\bar{\rho}D_T\nabla\tilde{i}\right) = \\ \tilde{S} - \overline{\left(c\frac{V_f}{V} + \frac{h_f^u}{V}\right)S_{mt}} + \left(\tilde{i}-1\right)\overline{\left(\frac{V_{ff}}{V}\right)}\tilde{c}\tfrac{1}{2}\overline{\rho}R_T\frac{\varepsilon}{k}\overline{f''^2} + \widetilde{S_{\mathrm{mt}}i} \end{aligned} \tag{2.34}$$

In this transport equation the effect of the evaporating spray and mixing are accounted for by the last three terms in the RHS. The first term can be used for quantifying radiation losses.

Thermochemical database The formulation of the globally reduced mechanism in section 2.4 was basically performed to remove the stiffness from the governing equations of combustion. Having formulated a globally reduced mechanism and introduced the governing variables of the combustion model it is possible to model a turbulent flow. However, real time calculation of the instantaneous value of variables as a function of the globally reduced mechanism as formulated in equation (2.26) is not feasible in numerical simulations as it is numerically expensive. In order to reduce the numerical effort, the globally reduced mechanism is first solved on a mesh of the coordinates c, f and i. The exact procedure is discussed in Derksen [15] and will not be repeated here. The result of the procedure is a laminar database in which all variables of interest are stored as a function of c, f and i.

This laminar database can be prepared for turbulent simulations by averaging all quantities over presumed PDF's. This will yield all variables as function of the mean and variance values:

2.6 Physical definition of a global mechanism, b^s

Before application and further validation of the combustion model, in this section attention is given to the definition of η. In paragraph 2.4 it was introduced as the composed species that defines the global behaviour of a reduced mechanism. Derksen states that this variable should vary monotonically between its bounds of unburned and burned values. The CSP-S-STEP algorithm does not check for this. The behaviour of η depends on the definition of $\boldsymbol{b}^s$.

The definition of $\boldsymbol{b}^s$ is the last step in the CSP algorithm. Multiple vectors will allow for a mathematical correct solution for the definition of this $\boldsymbol{b}^s$, but it is found that not all of these matrices will behave correctly in physical space. This is seen when η is calculated as post-processing step of a laminar flame calculation, using a CSP generated globally reduced mechanism.

For example, the $\boldsymbol{b}^s$ tensor can be constructed in such a way that the composed species definition (equation (2.26)) behaves non-monotonic in the spatial domain of a laminar flame solution. This implies that the global reaction rate definition is defined non-unique when projected on the definition of the composed species. Figure 2.3 shows this phenomenon for a C_8H_{18}-air flame. The global reaction rate is depicted as a function of the reaction progress variable. It can be observed that multiple values exist for the global reaction at one value of the reaction progress variable. This despite the fact that the composed species is defined unique as a function of the reaction progress variable. A non-unique solution for the global reaction rate as a function of composed species will yield problems when a global reduced mechanism is used for the construction of a thermochemistry database.

When the steady state space $\boldsymbol{b}^r$ is formed and element conservation relations $\boldsymbol{b}^c$ are added to that, the next step is to choose a unity vector that is linearly independent to the formed matrix of steady state species and element conservation:

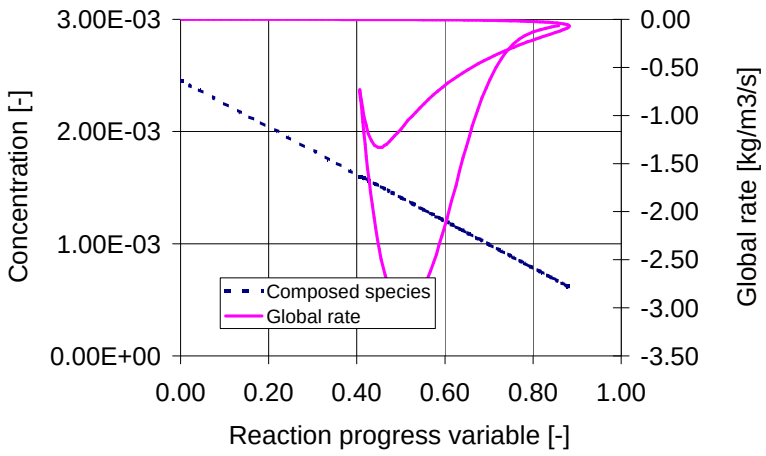

Figure 2.3: Definition of the composed species and global reaction rate as a function of the normalised composed species for a stoichiometric C_8H_{18}-air flame.

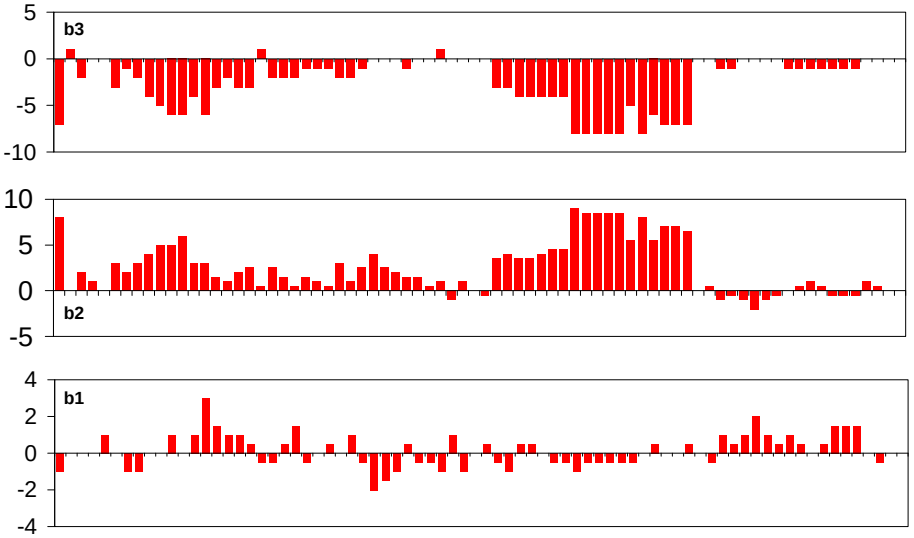

Figure 2.4: The definition of the global reaction rate for three different definitions of $\boldsymbol{b}^s$ in a stoichiometric C_8H_{18} flame.

$$\boldsymbol{e}_k \text{ with } k = 1, ..., N \tag{2.35}$$

The original CSP S-STEP [28] algorithm tests unity vectors until an independent vector $\boldsymbol{e}_{k=x}$ is found. However, there are N unity vectors to test and the default CSP implementation stops after finding the first possible vector that completes the b-matrix. Although a linear independent matrix is formed that defines N equations for the N unknowns, the solution of this set of equations does not necessarily ensure physical behaviour of a global mechanism.

The solution to this problem is rather straightforward. The original CSP-S-STEP algorithm is modified in such a way that *all* possible definitions of the slow system are generated, by simply testing linear independence for *all* N unity vectors (equation (2.35)). From this a set of reduced mechanisms is generated. The generated set of reduced mechanisms is then tested for a unique definition of the global reaction rate.

Verification The method described above is applied using two different laminar flame solutions. One in which the fuel is *iso*-octane and one fuelled with propane. The detailed mechanisms were respectively taken from chapter 4 and from Petrova [40]. Both flames are stoichiometric and at atmospheric pressure. Analysis of the flames with the proposed algorithm produces interesting results.

Figure 2.4 shows three different definitions of $\boldsymbol{b}^s$ that are mathematically valid for a reduced mechanism of a stoichiometric C_8H_{18}-air flame. The figures show histograms of the coefficients of $\boldsymbol{b}^s$ for all N species involved in

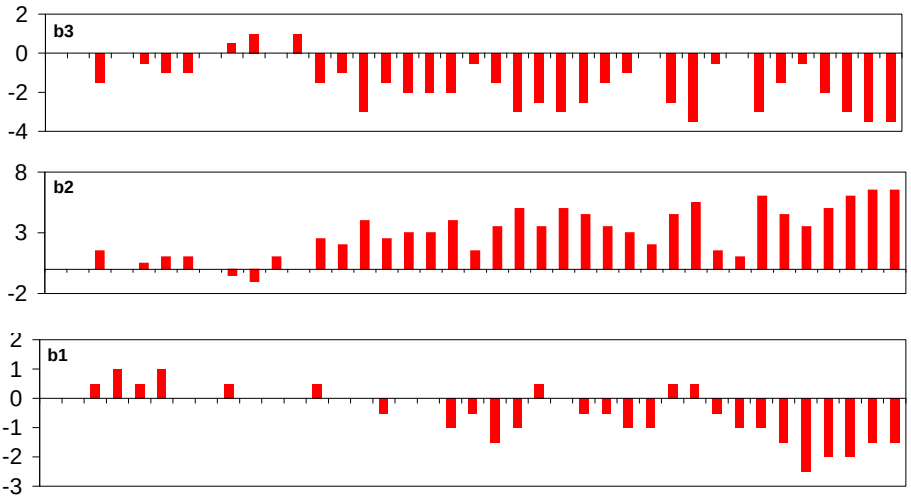

Figure 2.5: Different CSP definitions for the slow chemical manifold in a stoichiometric C_3H_8-air flame, represented by the coefficient value of b_{ij} for every species

the mechanism. The two upper histograms show a clear difference compared to the lowest histogram. The latter shows a balanced division of coefficients, leading to an average of 0.13 for b_{ij}, while the two histograms above have averages of 2.14 and -2.5 respectively. The effect of the definition of $\boldsymbol{b}^s$ on the definition of the global reaction rate is depicted in figure 2.6. The figure shows the value of the global reaction rate as a function of the reaction progress variable. The first and second definition $\boldsymbol{b}^s$ are not consistent with how a rate definition should apply. For system one, the source term is active already at $c = 0$, while the second definition gives a non-unique solution of the global reaction rate. The third system shows behaviour as should be expected from a chemical conversion rate: ignition occurring at a value of around $c = 0.5$ and a no non-unique definition. Note that the third system has the lowest averaged coefficient value b_{ij}

By looking at a stoichiometric C_3H_8-air flame this is further investigated. Again three mathematical valid solutions are found for the global system as is shown in figure 2.5. The same balancing effect is seen for the three mathematical valid definition. This balancing effect seems less pronounced compared to the C_8H_{18}-chemistry, but is still present. When the average value of b_{ij} is calculated, again there is a clear difference between the first two and the last histograms. While the latter are both relatively far from zero, the last average lies relatively closer to zero, as presented in table 2.4.

From this case and the previous case, a trend is easily observed and it can be concluded: the average coefficient value of b_{ij} has to go to zero for a physical global reaction rate definition.

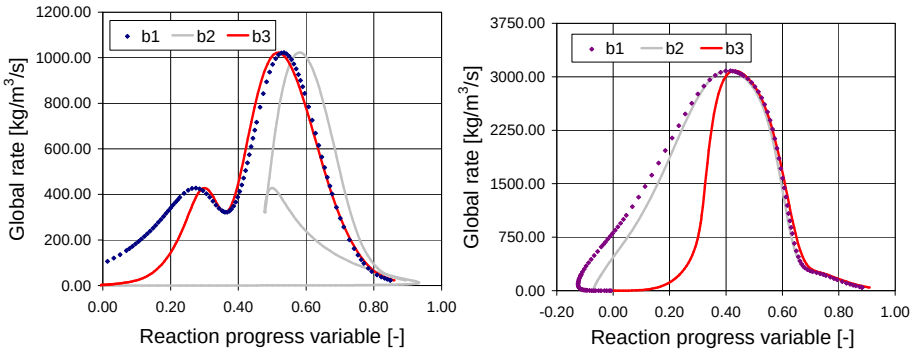

(a) C_8H_{18} (b) C_3H_8

(2.36)

Figure 2.6: The definition of the global reaction rate for three different definitions of $\boldsymbol{b}^s$ as found in an a C_3H_8 flame.

2.7 Reduction to one global step

In literature large hydrocarbon combustion chemistry only has been analysed using Intrinsic Low Dimensional Manifold (ILDM) methods [52]. In this thesis CSP is the tool for mechanism reduction.

In this section the reduction method is applied to numerical results of a number of premixed, prevaporised laminar flame simulations of different hydrocarbons fuels, varying from methane to decane. In table 2.5 an overview is given of the applied mechanisms and fuel molecules. The PREMIX-package has been used in obtaining the numerical solution. The applied solution method was the same as discussed earlier in paragraph 2.3.

The results of the various flame simulations have been analysed with the CSP-S-STEP-package by reduction to one global reaction step. When constructing this single step for all flames as given in table 2.5, one trend is very clear. The major species found by the CSP-algorithm in a premixed flame are always CO_2, H_2O and O_2. This is found for all the stoichiometric premixed flames of the hydrocarbon fuels from table 2.5. Using the global CSP-pointer (equation 2.19) definition as an indication for the division of species into major and steady state species, an interesting trend is observed. A higher global CSP-pointer value represents a lower contribution of the species to the low-

Fuel	**C_8H_{18}**	**C_3H_{18}**
$\overline{b_{ij}}$	-2.42	-1.26
$\overline{b_{ij}}$	2.44	2.71
$\overline{b_{ij}}$	0.13	-0.36

Table 2.4: Average b_{ij} values

dimensional manifold that governs the combustion chemistry.

In figure 2.7 the values of the global CSP-pointers are plotted for the species involved in the applied detailed mechanisms. The logaritmic vertical axis represents the global pointer value. The horizontal axis in the figure does not has a significant meaning, it only indicates the number of species in the mechanisms. The left parts of the graphs in this figure, where the global CSP-pointers have low values, is constructed with all the major species in the chemical systems. For all tested hydrocarbon mechanisms, combustion products CO_2 and H_2O as well as the oxidiser O_2 are identified as major species by the global CSP pointer. The plateau of global CSP-pointer values with the lower slope that follows after the major species, is mainly dictated by the fuel species and radicals that have a relative high concentration in hydrocarbon flames, such as H_2 and OH. Species with a very high global CSP-pointer value follow after this plateau. Depending on the size of the mechanism and the number of inert or very small tracer species, the graphs increase exponentially.

Fuel	# species / # reactions	Reference
Methane CH_4	53/325	[53]
Propane C_3H_8	39/175	[40]
n-Heptane C_7H_{16}	44/210	[38]
iso-Octane C_8H_{18}	76/477	[54]
n-Decane $C_{10}H_{22}$	85/325	[55]
Methanol CH_3OH	46/235	[38]

Table 2.5: The tested mechanisms for reduction to one global step

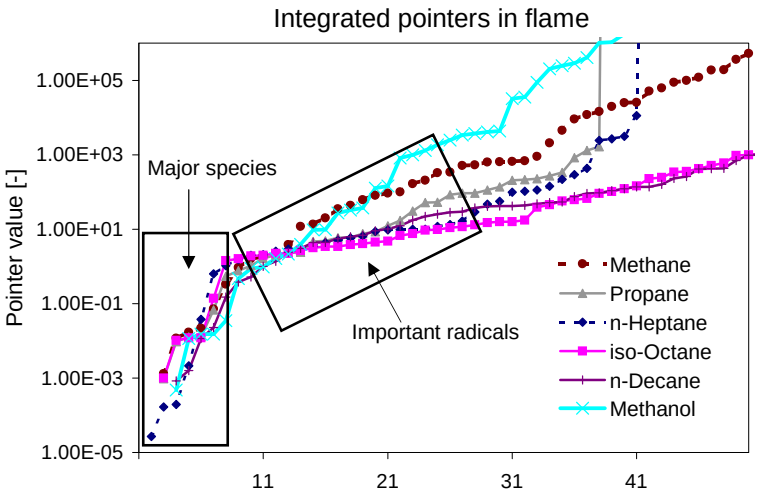

Figure 2.7: Integrated pointers calculated for atmospheric stoichiometric fuel conditions, according to equation (2.19).

2.8 Conclusions

This chapter ends with a paragraph summarizing the major conclusions of the previous paragraphs.

Laminar flame simulations A wide range of different detailed chemistry mechanisms is available from literature. When selecting such a mechanism for use in combustion modelling, size of the mechanism is an important parameter. It has been shown that for laminar flame simulations there is not a specific gain in applying the largest and most detailed mechanism available. Of much more importance is the experimental background of the detailed mechanism: a detailed mechanism should represent flame chemistry accurately.

The CFI combustion model A two-phase formulation of the CFI model has been adopted. The major change to the CFI equation is due to the transfer of mass from the liquid phase to the gaseous phase via the mechanism of evaporation. An essential step in the modelling will now be the definition of a correct mass transfer rate. This will be discussed in chapters 6 and 7.

Construction of physical valid reduced global mechanisms When the CSP methodology is used for the reduction of a complex reaction mechanism, it does not automatically define a proper physical manifold for the chemistry. This is found and shown empirically in this thesis for hydrocarbon combustion. There always exists a set of mathematical correct solutions for the reduced system, but physical behaviour of the manifold is not guaranteed. In order to establish a global reaction step mechanism using CSP, analysis of the physical implication of the definition of the reaction progress variable is needed. This chapter provides a route for obtaining the proper manifold. Presumably there is a theoretical reason for the fact that there are correct mathematical solutions to the reduction problem of which not all solutions adhere to physical behaviour of the global step mechanism. The existence of a mathematical assumption or operation in the CSP algorithm could be the cause for this. It will be useful for further development and application of this reduction method to investigate this.

Reduction of hydrocarbon combustion chemistry Combustion of hydrocarbon fuels, as discussed in this chapter, can be characterized by a global reaction step that is equal for many types of hydrocarbon molecules. This is shown by application of the CSP-algorithm to methane, methanol, *iso*-propane, n-heptane, *iso*-octane and n-decane. The major species are always CO_2, H_2O and O_2.

3

The effect of steam addition on *iso*-octane and *n*-heptane flames*

ABSTRACT *Lean Premixed Prevaporised (LPP) combustion of liquid fuels with steam dilution and under high pressure conditions is numerically assessed. A detailed chemical kinetic mechanism for* n*-heptane and* iso*-octane combustion is assembled on the basis of existing detailed mechanisms and validated against experimental data from laminar premixed flames. A Computational Singular Perturbation (CSP) method is then used to analyse and reduce the mechanism to one global step. This reduced mechanism forms the basis for the reaction progress variable (RPV) approach from the CFI combustion model. The obtained one-step combustion mechanism is validated by comparing the CFI model results, stored in a thermochemical database as a function of the RPV, with detailed laminar flame solutions in reaction progress variable space. The single step global mechanism is then used to assess, under LPP gas turbine operating conditions, the influence of dilution and fuel equivalence ratio on* iso*-octane and n-heptane combustion. The above formulation is shown to accurately capture NO and CO emission trends.*

KEYWORDS: LPP Combustion, Emissions, Detailed Kinetics, Single-step reduction, Flame modelling.

3.1 Introduction

Lean premixed prevaporised (LPP) combustion constitutes a very promising means for NOx emissions reduction from land based gas turbine engines e.g. [7]. Moreover, LPP MAST (Mixed Air-Steam Turbine) technology is particularly attractive since air humidification results in additional power, provided by the increased mass flow of steam and the enhanced thermal capacity of the mixture, with improved efficiency, since no additional compression work is

*B. de Jager, J.B.W. Kok and G. Skevis. Effects of water addition on pollutant formation from LPP gas turbine combustors. *Proceedings of the Combustion Institute*, 31, 2006

required, e.g. [56, 57]. Steam addition to the combustion air is also beneficial to the reduction of NOx emissions from gas turbines, operating both in the premixed and non-premixed modes e.g. [58]. This is mainly associated with a reduction in flame temperature.

The influence of moisture on NO_x emissions has been a subject of several investigations with early work reviewed by Dryer [59]. Miyauchi *et al.* [60] showed that NO levels in premixed methane-air flames were reduced by steam addition even when the peak flame temperature was kept constant. Bhargava *et al.* [61] studied the effects of humidity in premixed flames at a pressure of 14 bar and concluded that the reduction in NOx was mainly due to the reduction in temperature with chemical effects also being important through O atom suppression. Furthermore, thermal NOx was found to be dominant even at high humidity levels. Dlugogorski *et al.* [62] studied the propagation of laminar flames in wet premixed natural gas air mixtures and showed that burning velocities decrease significantly with the addition of even small amounts of humidity. Recently, Landman *et al.* [63] experimentally studied the effects of combustion air dilution, by either nitrogen or water vapor, in a premixed turbulent natural gas flame under constant adiabatic flame temperature. It was shown that NO reduction in water-diluted flames was larger than the corresponding reduction in nitrogen diluted flames and thus was concluded that chemical effects should be important.

The effect of steam dilution on molecular growth and eventually soot formation is currently unclear. There is experimental and theoretical evidence suggesting, for example, that CO_2 addition to hydrocarbon flames reduces their sooting propensity [64]. On the other hand, it is well known that NO reduction in gas turbines under humid combustion conditions is accompanied by CO level increases [58]. There has been no systematic investigation of the influence of steam dilution on soot precursor and soot emissions from combustion systems, although there is evidence to suggest that reductions in soot levels may be expected [65, 66].

Computations of industrial-scaled turbulent combustion processes, such as LPP MAST gas turbine combustion, using full detailed chemistry, require computational times and storage that outranges current computer capacities. However, systematic chemistry reduction and coupling of the reduced chemistry with a combustion model allows for reliable industrial turbulent combustion calculations. To this end, several workers, e.g. [67–69] have proposed the use of flamelets to model turbulent combustion, thus allowing for the incorporation of detailed chemistry in turbulent flame simulations. Kok *et al.* [24, 26] successfully used reaction progress variables with reduced chemistry for the calculation of a turbulent syngas flame. Derksen [15] extended this method for turbulent natural gas combustion by using a systematically reduced global mechanism on the basis of the Computational Singular Perturbation (CSP) methodology as formulated by Massias *et al.* [28].

The objective of the present work is to provide a reduced model of the high temperature combustion chemistry of liquid fuels at high temperature and high humidity conditions. Such a model can be directly incorporated into CFD codes for quantitative predictions of heat release and pollutant emissions

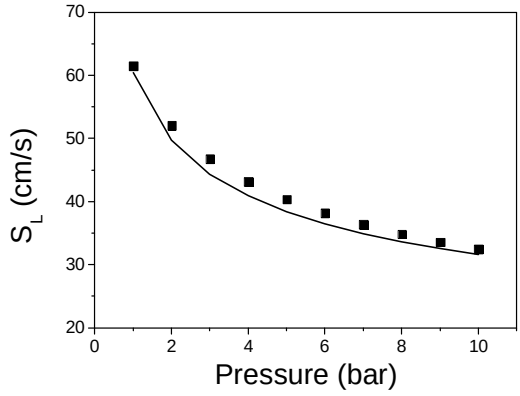

Figure 3.1: Comparison between computed (line) and experimentally determined (symbols) laminar flame speeds of atmospheric n-heptane-air mixtures. Experimental data are from Davis and Law [70]

from gas turbines. At the same time the reduction methodology can be utilised to systematically quantify the chemical and physical effects of steam dilution to hydrocarbon flames.

The structure of the paper is as follows. A comprehensive detailed kinetic mechanism is assembled and validated against experimental data for n-heptane and *iso*-octane flames. The reaction mechanism is subsequently mapped into a single dimensionless reaction progress variable, using the CSP methodology. The resulting thermochemical database is assessed against detailed computations from adiabatic laminar premixed *iso*-octane flames. The developed reduced model is subsequently used to quantify the effects of steam dilution on the thermal NO pathway and CO emissions for selected operating conditions in adiabatic n-heptane and *iso*-octane flames.

3.2 Detailed mechanism formulation and validation

There are several detailed mechanisms for the high temperature combustion of n-heptane, e.g. [71,72], comprehensively reviewed by Babushok and Tsang [34]. The mechanism of Held *et al.* [72] is particularly appealing as a starting point for the present work since, it is relatively compact while retaining enough detail for chemistry simulations. The Held mechanism has been validated against flow reactor, stirred reactor and shock tube data, successfully reproducing the experimentally determined laminar flame speeds of atmospheric n-heptane-air mixtures of Davis and Law [70]. Naha and Aggarwal [66] have further demonstrated the ability of the mechanism to accurately predict basic features of n-heptane partially premixed flame structures.

Detailed kinetic mechanisms for *iso*-octane are mostly geared toward low and intermediate temperature oxidation and auto-ignition, e.g. [36,73,74]. A detailed kinetic mechanism for n-heptane/*iso*-octane mixtures, focusing on low and intermediate temperatures, has been proposed by Slavinskaya and Haidn [75],. Detailed kinetic mechanisms for *iso*-octane combustion in flames have been developed by Pitsch *et al.* [76], as a basis for the asymptotic analysis

of premixed *iso*-octane-air flames, and by Hasse *et al.* [44] for the quenching of laminar premixed *iso*-octane flames at cold walls. The latter mechanism has been successfully validated by the authors against high pressure burning velocity data of Bradley *et al.* [77] and has also been shown [32] to favourable agree with the atmospheric pressure burning velocity data of Davis and Law [70].

In the present study the n-heptane mechanism of Held *et al.* [72] has been combined with the *iso*-octane oxidation chemistry - up to and including the C_4H_8 isomers formation reactions from Hasse *et al.* (Mechanism A in [44]). These have also been coupled with the NO chemistry of the GRI3.0 mechanism [53], an approach used successfully in earlier related work, e.g. [66,70]. The resulting mechanism consists of 76 species and 477 elementary reactions. The constituent parts of the mechanism, including the nitrogen chemistry, have been extensively validated, as also discussed in the previous section. Here, additional validation is provided for conditions relevant to the present

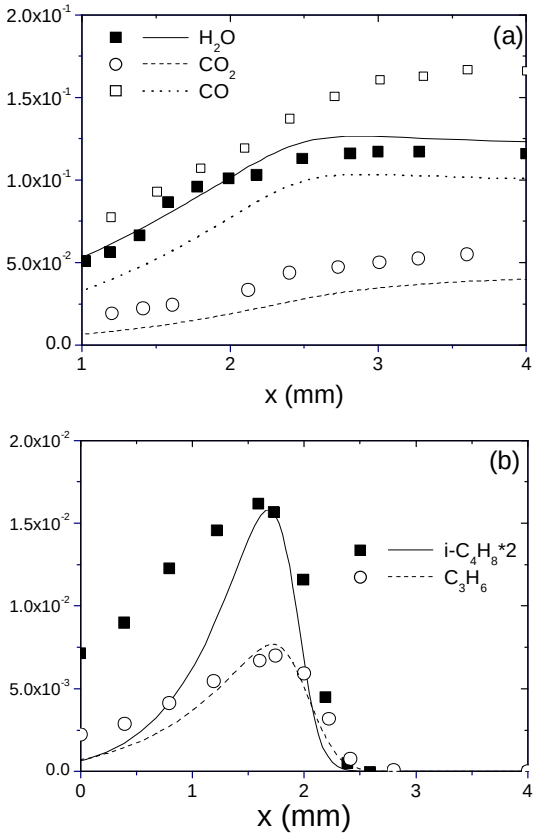

Figure 3.2: Comparison between computed (line) and measured (symbols) [43] mole fraction profiles in an atmospheric, rich (ϕ = 1.9), burner-stabilised $C_8H_{18}/O_2/N_2$ flame: (top) H_2O, CO_2, CO and (bottom) C_4H_8 and C_3H_6.

work. The proposed mechanism accurately predicts laminar flame speeds for atmospheric n-heptane-air and *iso*-octane-air mixtures and high-pressure *iso*-octane-air mixtures, shown in figure 3.1.

Mechanism validation has also been performed against measured species profiles in the atmospheric, rich (ϕ = 1.9), burner-stabilised $C_8H_{18}/O_2/N_2$ flame of Bakali *et al.* [43]. Generally, the agreement between computed and experimental major species profiles is very satisfactory as shown in figure 3.2. Further, as shown in figure 3.2, the mechanism successfully predicts the levels of the crucial *iso*-butene and propene intermediates.

3.3 Reduced mechanism development

A CSP-based algorithm is employed in order to map the detailed chemical kinetic mechanism into a single dimensionless scalar (RPV). The algorithm considers a 1D laminar adiabatic freely propagating flame problem, described by a detailed chemical kinetic mechanism consisting of N species, E elements and K elementary reactions. The species and energy conservation equations can be cast as follows:

$$\begin{aligned} &\text{(a) } \frac{\partial \mathbf{Y}}{\partial t} = \mathbf{L}\left(\mathbf{Y}\right) + \mathbf{g}\left(\mathbf{Y}\right) \\ &\text{(b) } \frac{\partial E}{\partial t} = L\left(E\right) + S\left(E\right) \end{aligned} \tag{3.1}$$

The left hand side (lhs) of equation 3.1 is the time dependent N-dimensional species vector, $\mathbf{Y}$, or the energy scalar, E. In the right hand side (rhs) $\mathbf{g}$ is a vector function describing the non-linear chemical kinetics source term and L is the linear convective and diffusive operator. The source term $\mathbf{g}$ can be written as $\mathbf{WS}(\mathbf{Y})$, where $\mathbf{W}$ is an N x N matrix containing in the diagonal the molecular weight of the species divided by the total mass density, $\mathbf{S}$ is the N x K stoichiometric matrix composed of K stoichiometric vectors, S_i representing the participation of the N^{th} species in K^{th} reaction and is a vector containing the K elementary rates i.

Based on eigenvalues of the Jacobian matrix of each species' reaction rate and chemical time scales in a 1D laminar flame, it is possible to split the rhs of equation 3.1 into a fast domain and slow domain, selecting M slow (major) species and N-M fast (steady-state) species:

$$\frac{\partial \mathbf{Y}}{\partial t} = \mathbf{a}\mathbf{b}^r\mathbf{L} + \mathbf{a}_r\mathbf{b}^r\mathbf{g} + \mathbf{a}_s\mathbf{b}^s\mathbf{L} + \mathbf{a}_s\mathbf{b}^s\mathbf{g} \tag{3.2}$$

In equation 3.2 the a's are column basis vectors of respectively N-M and M elements. The fast domain, indicated by the subscript r, is driven by the slow domain, subscript s. In other words, the slow domain defines the manifold on which the chemical system moves:

$$\frac{\partial \mathbf{Y}}{\partial t} \approx \mathbf{a}_s\mathbf{b}^s\mathbf{L} + \mathbf{a}_s\mathbf{b}^s\mathbf{g} \tag{3.3}$$

The fast domain is assembled of assumed steady state species ($\mathbf{g_0}$), having relatively fast rates and only being present for a fraction of the total domain.

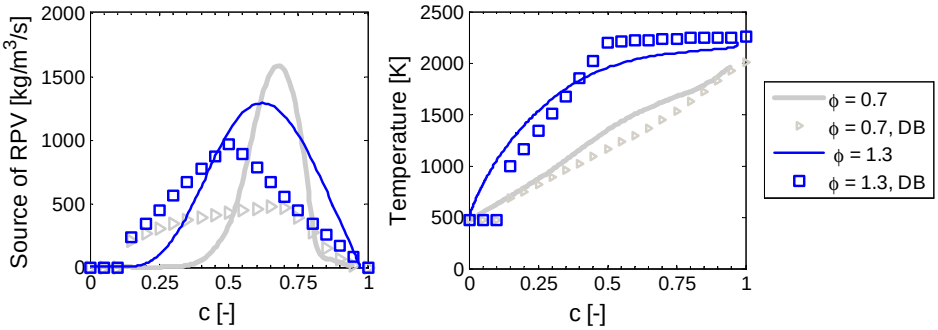

Figure 3.3: Comparison between detailed PREMIX solution (lines, solid bold ϕ = 0.7, solid) and database solution (symbols) for the (left) source term of the global rate and (right) temperature at p = 1 bar.

The slow species are thus the 'rate determining' species in the chemical system. A detailed outline of the method can be found in [28].

The separation of the chemical modes into fast and slow parts, as defined by $\mathbf{b}_r$ and $\mathbf{b}_s$, allows the definition of a composed species with a global rate:

$$\begin{aligned} &\text{(a) } \eta_i^s = \sum_{j=1}^{N} b_{ij}^s Y_j \\ &\text{(b) } \omega_{\eta_i} = \sum_{j=1}^{N} b_{ij}^s \omega_j \end{aligned} \tag{3.4}$$

By normalization with the equilibrium value of η_i and inlet conditions, a RPV (c_i) is defined between inlet conditions (c_i = 0) and full equilibrium conditions (c_i = 1). Combination of the normalized version of 3.4 with the steady state relations from 3.2 and element conservation defines the CFI combustion model equations:

$$\begin{aligned} \mathbf{c} - \mathbf{c}^0 = 0 &: \quad \text{RPV's} \\ \mathbf{b}^r \cdot \omega = \mathbf{0} &: \quad \text{steady state relations} \\ \mathbf{E}^c - \mathbf{E}^{c,in}\left(\mathbf{Y}^0\right) = \mathbf{0} &: \quad \text{element conservation relations} \end{aligned} \tag{3.5}$$

This set of equations is solved with the CFI-code [15] and provides a database in which the density, temperature and the species vector are stored as a function of the RPV(s).

3.4 Database assessment

The performance of the CFI database against detailed computations in laminar premixed methane-air flames has been already assessed by Derksen [15]. It was shown that a single step mechanism was adequate to describe the, near-equilibrium, conditions prevailing in the combustor exit. Extending the formulation to a two-step mechanism did not improve the performance of the chemical database. This may appear counterintuitive given the fact that a two

RPV formulation have been shown to accurately reproduce laminar premixed CO/H_2 flames [52]. However, methane flames are significantly more complex and it has been shown [28] that at least seven RPVs are required for a satisfactory representation of their features, including NO chemistry. In the present study the performance of the database is further assessed against freely propagating *iso*-octane flames. These include lean (ϕ = 0.7), stoichiometric and rich (ϕ = 1.3) atmospheric pressure flames, a high pressure (p = 2 bar) stoichiometric flame and a water diluted (ω = 2.6) stoichiometric and atmospheric pressure flame. The parameter ω is defined as the mass fraction of water vapor over the mass fraction of the fuel. All computations have been performed for an initial temperature of 473 K. The comparison methodology is as follows. Laminar flame solutions obtained with thePREMIX code [45] are analysed with the CSP-based CSP-S-STEP code [28] and the resulting global mechanisms are used to construct thermochemical databases, using the CFI method. By mapping the global rate definition as given by equation 4b on the laminar flame solution, the accuracy of the database can be assessed in the RPV domain. At a gas turbine combustor exhaust is the majority of the chemical processes assumed to be at equilibrium, c = 1, and the level of agreement between the PREMIX solution and the database will determine the extent at which the lat-

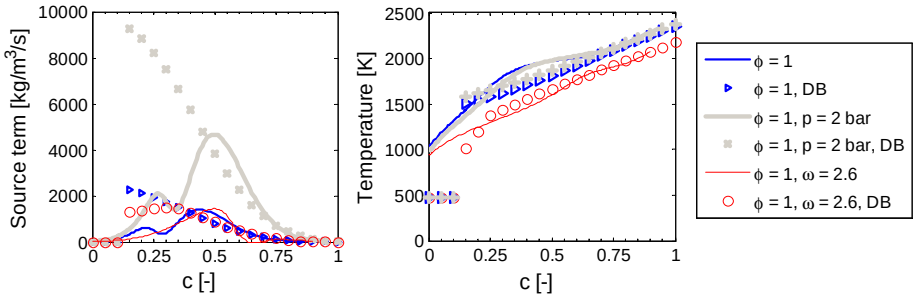

Figure 3.4: Comparison between detailed PREMIX solution (solid lines) and the database solution (symbols) for the (left) source term of the global rate and (right) temperature at p = 1 bar, p = 2 bar and with ω = 2.6, ϕ = 1

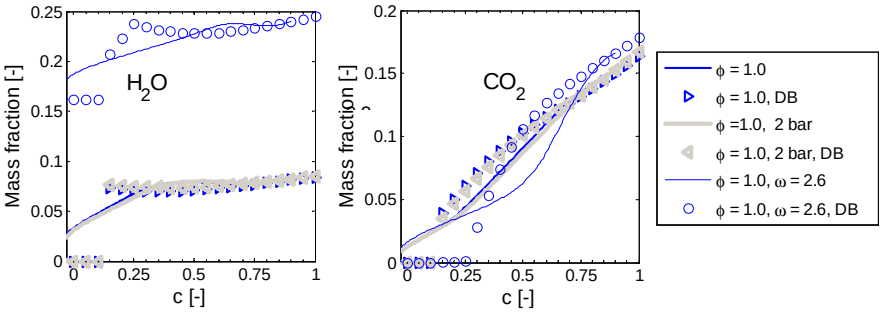

Figure 3.5: Effect of steam dilution and pressure on (left) H_2O and (right) CO_2 in PREMIX solutions (solid lines) and database solutions (symbols)

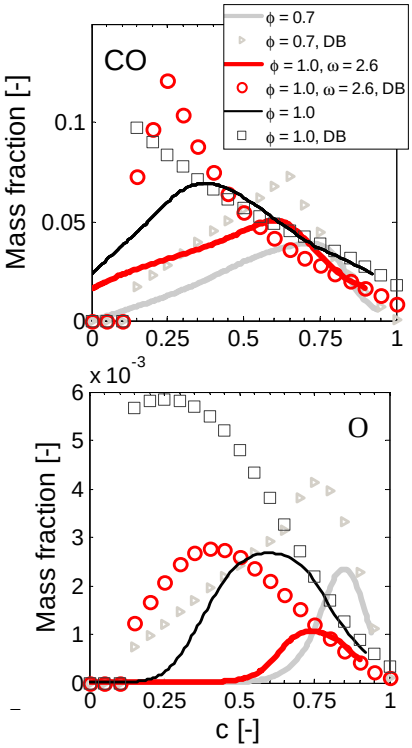

Figure 3.6: Effect of steam dilution and pressure on (top) CO and (bottom) O in PREMIX solutions (solid lines) and database (symbols).

ter will correctly predict exhaust concentrations of major species and of most intermediates. Such an equilibrium assumption is clearly not valid for the NO chemistry. However, it can safely be assumed that at the high temperature conditions prevailing at the combustor exit, the Zeldovich mechanism is dominant so that the NO exhaust concentration can be calculated as follows:

$$\frac{\partial Y_{\mathrm{NO}}}{\partial t} = 2M_{\mathrm{NO}}\rho^2 k_f \frac{Y_{\mathrm{O}}}{M_{\mathrm{O}}}\frac{Y_{\mathrm{N_2}}}{M_{\mathrm{N_2}}} \tag{3.6}$$

In equation 3.6 M_i denotes the molar mass of species i, ρ is the mixture density and the rate constant k_f is set equal to $1.8108e^{-38369/T}$ $[m^3/mol/s]$ [15]. Hence, NO levels are linearly dependent on the O and N_2 concentrations obtained from the database.

The projection of the global mechanisms on the PREMIX solution and the database predictions accurately reproduces the effects of equivalence ratio variation on the source term of the global rate, as shown in Figs. 3.4 and 3.4., The thermochemical database does not account for convection and diffusion, as naturally opposed to the PREMIX formulation, resulting in wider source terms compared to those obtained by PREMIX. The agreement is generally very good for RPV values greater than about 0.5, where chemical reactions

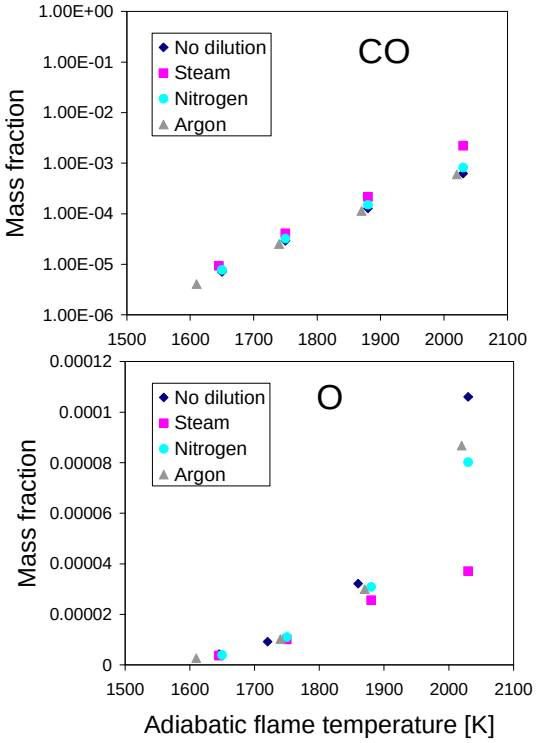

Figure 3.7: Effect of dilution on (top) CO and (bottom) O concentrations as a function of adiabatic flame temperature at equilibrium for C_8H_{18} databases with a preheat temperature of 473 K and pressure of 1 atm.

are generally slower and the majority of the species can safely be assumed to be in steady state. For higher pressures and high humidity ratios, Figs. 3.4 and 3.4, the applicability of the single step approximation appears to extend to RPV values of 0.25. This is because of the fact that steam addition lowers flame temperatures and high pressure reduces the overall radical levels so that a larger portion of the flame domain approaches steady state, in both cases.

The agreement between the database and the PREMIX solution is generally very good for the evolution of the temperature profile, figures 3.4 and 3.4, and the major CO_2 and H_2O species for all stoichiometries, shown in figure 3.4. Further, figure 3.6, CO and O radical concentrations as a function of RPV match well with the laminar flame solutions, especially near equilibrium conditions. The agreement is generally better for lean flames. The reason is that in lean flames the fuel oxidation chemistry is significantly simpler due to the absence of molecular growth processes so that a reduced single step description is expected to provide a more accurate description of the 'real' chemistry.

3.5 Flame and database computations

Computations are performed using the previously assessed method in order to reproduce the experimentally determined NO emission trends as a function

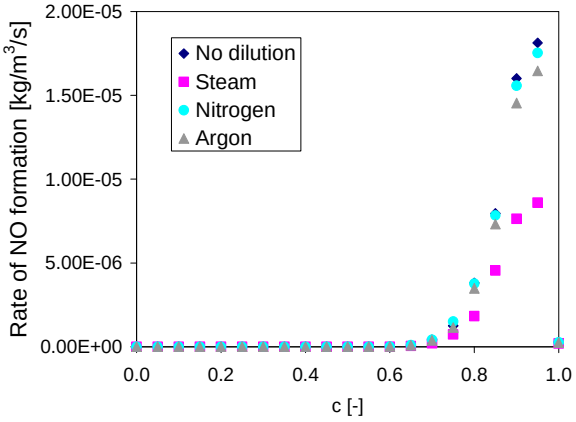

Figure 3.8: Effect of dilution on the rate of NO formation as a function of the RPV in a lean (ϕ = 0.5) C_7H_{16} database with a preheat temperature of 473 K and pressure of 1 atm.

of combustion temperature and flame dilution of Landman *et al.* [63] and to quantify fuel, humidity and pressure effects on NO and CO emissions. Flames are computed on a dry basis (ω = 0) and at constant dilution levels (ω= 2.6). In the latter case the diluents are water, nitrogen and argon. Argon dilution eliminates the possible effects of the increased nitrogen levels to NO emissions and thus makes the results directly comparable to the dry and steam-diluted cases. An additional constraint imposed is that the adiabatic flame temperature is kept constant for both dry and diluted flames. This will naturally result in differences in stoichiometry (C/O ratio) between the dry and each diluted case. A comprehensive investigation would also need to explicitly quantify the effects of changes in the flame stoichiometry. Such computations will involve the opposite procedure whereas the mixture stoichiometry is fixed and the flame temperature is allowed to vary. It is well known however that most pollutants emissions, and particularly NO, are highly sensitive even to small temperature changes. Accordingly, the current methodology, where both temperature and level of dilution are kept constant, can provide very useful insight into the chemical effects of steam dilution to NO and CO emissions from flames of practical fuels.

The methodology is as follows. First, a PREMIX solution is obtained for a dry flame with a given equivalence ratio. Then, an equilibrium code is utilised to obtain the required air concentration to keep the flame temperature to its 'dry' value for all three 'diluted' flames. Computations have been performed for a set of lean atmospheric n-heptane and *iso*-octane flames (ϕ = 0.5, 0.556, 0.625 and 0.714 for dry octane mixtures) at an initial temperature of 473 K. The resulting flames are analysed with S-STEP, constructing single step RPV mechanisms and CFI databases for every fuel and pressure condition.

The effect of adiabatic flame temperature and dilution on O and CO concentrations at c = 1 is shown in figure 3.7 for C_8H_{18}. Results for C_7H_{16} are of the same order. Clearly, the O radical levels generally increase with temperature

thus leading to a correspondingly increased NO formation rate, figure 3.8. Steam dilution significantly reduces O levels, and consequently the NO formation rate, for adiabatic flame temperatures higher than approximately 1800 K. On the other hand, N_2 and Ar dilution has a small but appreciable effect on O concentrations at temperatures higher than 2000 K. Interestingly enough, figure 3.8, nitrogen dilution has no effect on NO formation rates since the decrease in O levels is counterbalanced by an increase in N_2 levels, see equation 3.6. The same trend is observed by Landman *et al.* [63] for turbulent premixed methane combustion. It can thus be argued that steam addition, under lean flame conditions, does not have any appreciable chemical effect on NO levels at temperatures below 1800 K. At higher temperatures the situation is reversed and chemical effects appear to dominate. The CO concentration increases with increasing adiabatic flame temperature as an effect of increasing C/O ratio, therefore the databases follows the trends measured by Correa [58]. Further, there appears to be a small but important chemical effect from steam dilution on CO levels and at temperatures higher than 2000 K.

3.6 Conclusions and further work

The present work provides a quantitative evaluation of the effects of steam addition on major pollutants emissions, under conditions representative for LPP gas turbine combustion, using a single progress variable approach. A detailed chemical kinetic mechanism for n-heptane and *iso*-octane combustion is assembled on the basis of existing detailed mechanisms and validated against experimental data from laminar premixed flames. Results obtained with the CFI combustion model methodology, incorporating analytical mechanism reduction and chemistry description by a single RPV, clearly show that the database computations capture the substantial NO reductions and the corresponding moderate rise in CO, under high humidity conditions. There is no significant effect under diluting with N_2 or Ar.

The present work demonstrates that the CFI combustion model, coupled with a single RPV description, is a very promising tool for describing essential chemistry features, such as NO and CO emissions in practical combustors. Further work is required in validating both the detailed and reduced kinetic mechanisms under higher pressure and temperatures. Another step to be taken, will be the assessment of NO and emission of other pollutants, such as soot, from flames of multicomponent fuels, constituting of mixtures of *iso*-octane, n-heptane and other hydrocarbons.

Acknowledgments
The authors are grateful to the EU for financial support through the MAST-B-LIQUID project.

4

Turbulent combustion of propane*

ABSTRACT *In this paper combustion of propane under gas turbine conditions is investigated with a focus on the chemistry and chemical kinetics in turbulent flames. The work is aimed at efficient and accurate modeling of the chemistry of heavy hydrocarbons, ie. hydrocarbons with more than one carbon atom, as occurring in liquid fuels for gas turbine application. On the basis of one dimensional laminar flame simulations with detailed chemistry, weight factors are determined for optimal projection of species concentrations on one or several composed concentrations, using the Computational Singular Perturbation (CSP) method. This way the species concentration space of the detailed mechanism is projected on a one dimensional space spanned by the reaction progress variable for use in a turbulent simulation. In the projection process a thermochemical database is used to relate with the detailed chemistry of the laminar flame simulations. Transport equations are formulated in a RaNS code for the mean and variance of the reaction progress variable. The turbulent chemical reaction source term is calculated by presumed shape probability density function averaging of the laminar source term in the thermochemical database. The combined model is demonstrated and validated in a simulation of a turbulent premixed prevaporised swirling propane/air flame at atmospheric pressure. Experimental data are available for the temperature field, the velocity field and the unburnt hydrocarbon concentrations. The trends predicted by CFI compare well to the experiments.*

4.1 Introduction

A modern approach for efficient and clean combustion of liquid fuel is the lean premixed prevaporised (LPP) technique. This should lower emissions as the flame is not influenced by spray effects [78, 79]. The combustion process takes place in the gaseous phase. In contrast to most gaseous fuels, chemistry is dominated by hydrocarbons chains consisting of more than one C-atom.

*B. de Jager and J.B.W. Kok, Modelling of turbulent combustion of lean premixed prevaporised propane using the CFI combustion model, *Proceedings of GT2006*, Barcelona, paper no. GT2006-90565 2006

For correct modelling of the flame structure, an efficient model of chemistry therefore is necessary. This model should take into account the presence of the larger hydrocarbon molecules in the fuel. Full modelling of the chemical kinetics would be the most accurate solution to this. However, modelling a turbulent flame with a detailed chemistry mechanism would involve enormous computational times and storage capacities. In order to overcome this, it is common practice to reduce chemical mechanisms, either analytical or by hand.

In this article a model will be proposed that reduces the detailed chemistry of propane down to 1 reaction that can be used in a turbulent simulation. Previous studies for natural gas and syngas have shown that the approach is useful under gasturbine conditions [23,24,26]. Experimental data from [80] is being used for validation of the turbulent flame computations.

4.2 Theory

The modelling approach consists of several steps. It starts with detailed chemistry computations in a laminar flame. These detailed calculations are being analysed with the CSP method and the outcome of this reduction is projected on one reaction progress variable. The reaction progress variable serves as input for the thermochemical database construction that can be used in a turbulent flow.

4.2.1 Laminar chemistry and CSP reduction

Detailed chemistry calculations have been carried out using PREMIX [45]. This code was setup to calculate a laminar, freely propagating 1-dimensional adiabatic flame. The code solves transport equations for the species vector $\mathbf{Y}$ and energy E which are given in a transient form below:

$$\begin{aligned} &\text{(a) } \frac{\partial \mathbf{Y}}{\partial t} = \mathbf{L}\left(\mathbf{Y}\right) + \mathbf{g}\left(\mathbf{Y}\right) \\ &\text{(b) } \frac{\partial E}{\partial t} = L(E) + S_E \end{aligned} \tag{4.1}$$

The PREMIX solutions are analysed using the CSP-S-STEP code [28,46]. This code indicates the fast and slow modes within the chemical system based on Jacobian analysis and global integrated pointers. A detailed outline of the method can be found in [28]. A short overview is presented here: The conservation equations for a reacting flow existing of N species and K reactions are given by the same set as for the PREMIX code: part (a) of equation 4.1. The left hand side (LHS) is the N-dimensional species vector. The right hand side (RHS) of this equation, $\mathbf{g}$ is a vector function describing the non-linear chemical kinetics and $\mathbf{L}$ is the linear operator for convection and diffusion. The non-linear function $\mathbf{g}$ can be written as $\mathbf{WS}\omega(\mathbf{y})$, in which $\mathbf{W}$ is an $N \times N$ matrix with the molecular weight of the species divided by the total mass density. $\mathbf{S}$ is the stoichiometric matrix that is composed of K stoichiometric vectors $S_i$representing participation of the N species in K reactions. ω is a vector containing the K elementary rates ω_i.

Based on analysis of the Jacobian of each species' reaction rate and chemical time scales for every gridpoint of the PREMIX solution from the previous paragraph, it is possible to split the RHS of equation 4.1(a) into a fast domain and slow domain, selecting M slow species and $N - M$ steady-state species:

$$\frac{\partial \mathbf{Y}}{\partial t} = \mathbf{a}_\mathrm{r}\mathbf{b}^r\mathbf{L}+\mathbf{a}_\mathrm{r}\mathbf{b}^r\mathbf{g} + \mathbf{a}_\mathrm{s}\mathbf{b}^s\mathbf{L} + \mathbf{a}_\mathrm{s}\mathbf{b}^s\mathbf{g} \tag{4.2}$$

Looking at equation (4.2), the **a**'s are column basis vectors of respectively $N - M$ and M elements. The fast domain, indicated with subscript r, is driven by the slow domain, subscript s. In other words, the slow domain defines the manifold on which the chemical system moves:

$$\frac{\partial \mathbf{Y}}{\partial t} \approx \mathbf{a}_\mathrm{s}\mathbf{b}^s\mathbf{L}+\mathbf{a}_\mathrm{s}\mathbf{b}^s\mathbf{g} \tag{4.3}$$

The fast domain is assembled of assumed steady state species ($\mathbf{g}\approx 0$), species which have relatively fast rates and are only present for a fraction of the total domain. In contrast, the slow domain, describing the whole chemical system, is filled with the relatively slow species. The slow species are 'rate determining' species in the chemical system.

4.2.2 CFI combustion model and thermochemical database analysis

The separation of the chemical modes into fast and slow parts as defined by $\mathbf{b}^r$ and $\mathbf{b}^s$ allows to define a composed species with a global rate. This is done according to the methodology of the CFI combustion model. In the term CFI, C stands for the chemistry defined by the reaction progress variable. F symbolizes mixing by means of a mixture fraction. For non-adiabatic combustion, I comes in as a normalized enthalpy scalar. In this article, only a reaction progress variable is applied, using the composed species definition as a basis:

$$\eta^s = \sum_{j=1}^{N} b_{ij}^s Y_j \tag{4.4}$$

By normalization with the equilibrium value of η and inlet conditions a reaction progress variable (c) is defined between cold conditions (c = 0) and full equilibrium conditions (c = 1):

$$c = \frac{\eta^s - \eta^s_{unburnt}}{\eta^s_{burnt} - \eta^s_{unburnt}} \tag{4.5}$$

Combination of equation (4.5) with the steady state relations as seen in (4.2) and element conservation defines the CFI combustion model equations:

$$\begin{aligned} c - c^0 &= 0 \\ \mathbf{b}^r \cdot \omega &= \mathbf{0} \\ \mathbf{E}^c - \mathbf{E}^{c,in}\left(f^0\right) &= \mathbf{0} \end{aligned} \tag{4.6}$$

In equation (4.6), the 0 superscript indicates an initial or inlet value of the mentioned variable. This set of equations is solved with the CFI-code [15] and the results of that are Favre averaged presuming a β-probability density function:

$$\tilde{\phi} = \frac{1}{\overline{\rho}} \int_0^1 \rho\phi\beta \left(\tilde{c}, \widetilde{c''^2}\right) dc \tag{4.7}$$

The complete combustion model for calculation of a turbulent flame now consists of Favre averaged transport equations for conservation of mass, momentum, reaction progress variable and accompanying variance and turbulence quantities (either the Reynolds stresses and a dissipation component or the turbulent kinetic energy and a dissipation component) and a turbulent thermochemical database containing all the species from the detailed mechanism, temperature and density.

For 1 reaction progress variable and variance, the transport equations for a steady state type of flow are given below:

$$\nabla \cdot (\overline{\rho}\widetilde{\mathbf{u}}\widetilde{c}) - \nabla \cdot (\overline{\rho} D_T \nabla \widetilde{c}) = \widetilde{S}_{\widetilde{c}} \tag{4.8}$$

$$\begin{aligned} &\nabla \cdot \left(\overline{\rho}\tilde{\mathbf{u}}\widetilde{c''^2}\right) - \nabla \cdot \left(\overline{\rho} D_T \nabla \widetilde{c''^2}\right) = \\ &2\tfrac{\mu_T}{Sc_T} \left(\nabla \widetilde{c}\right)^2 - \overline{\rho}\tfrac{\varepsilon}{k}\widetilde{c''^2} + 2\widetilde{cS}_{\widetilde{c}} - 2\widetilde{c}\widetilde{S}_{\widetilde{c}} \end{aligned} \tag{4.9}$$

These equations can either be combined with a Reynolds Stress model or a k-ε model for the turbulence, see for example [81] for an overview of these models. A turbulent Schmidt number of 0.9 is assumed.

4.3 Results and discussion

4.3.1 Laminar flame and database

The chemical mechanism used in this calculation is the most recent San Diego propane mechanism from [40]. This mechanism has been tested for several flame conditions showing good agreement regarding laminar burning velocities and ignition delay times. The mechanism consists of 39 species and 175 reactions. Calculations have been performed for a freely propagating laminar premixed flame. Conditions examined were two fuel equivalence ratios, ϕ = 0.5 and ϕ = 1.0 at atmospheric pressure with an inlet temperature of 573 K, both adiabatic. The first fuel equivalence ratio as well as the inlet temperature and pressure resemble the experimental turbulent flame. In figure 4.1 part of the solution for this condition is shown. This solution was obtained on 201 grid points. The profiles of the major species show that the flame front is located in the interval x = [0.005,0.015]. This is indicated by the consumption of $O_2$and C_3H_8 and the formation of CO (note that CO is plotted on the scale of the major species axis) and OH. The adiabatic temperature of the flame is 1729 K.

The next step is to use the CSP-S-Step code to investigate how chemical modes can be separated into steady state and domain governing species. The obtained solutions for both stoichiometries serve as input for the analysis of

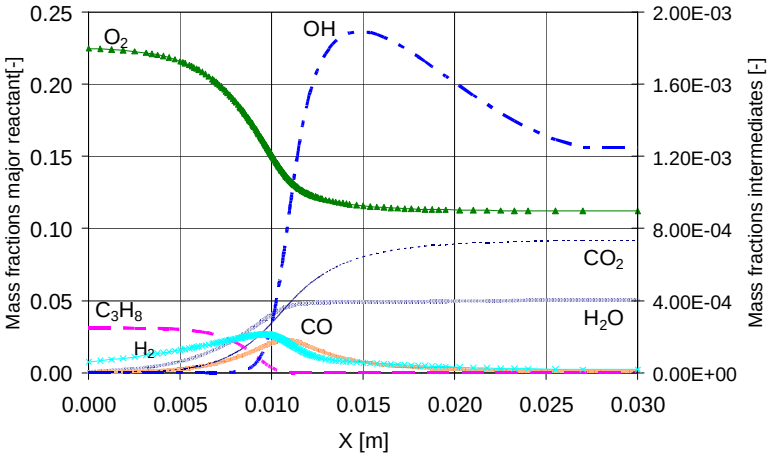

Figure 4.1: Premix solution for ϕ = 0.5, T_{Inlet} = 573 K and p = p_{atm}

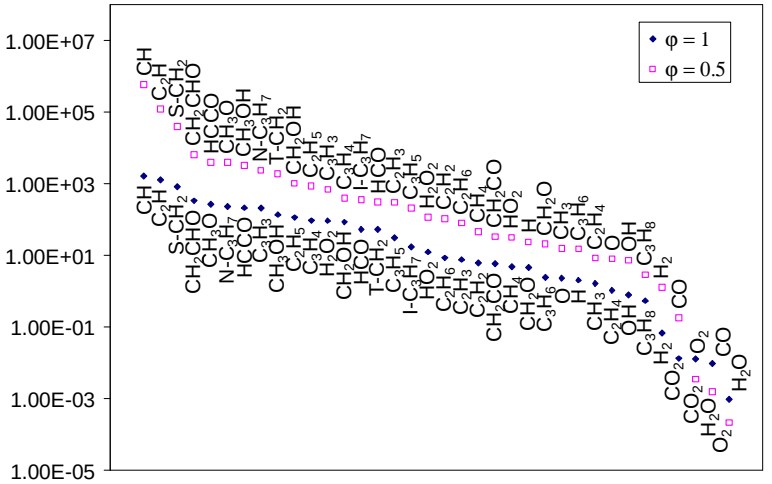

Figure 4.2: Pointer comparison for ϕ = 0.5 and ϕ = 1.0

CSP-S-STEP. Local pointers in one-dimensional space are calculated and by integration over space and weighting with the molar reaction rates the global CSP pointers are calculated. These global pointers are applied in the construction of the reduced mechanism. Figure 4.2 shows the global CSP pointers. A high pointer value means that a species has very little presence in the domain and high reaction rates, allowing the species to be in steady state. The lower the pointer value, the more significant is the presence in the domain and the more slowly the concentration changes throughout the domain. It can be seen that going to leaner conditions slightly changes the ordering of the slow species. Lean combustion introduces an excess amount of air and a lower concentration of the fuel. This is seen in the global pointers: for lean

combustion O_2 gets the lowest pointer value and C_3H_8 gets a higher pointer value, indicating it is less dominant in the domain compared to stoichiometric combustion.

Oxidation of propane is represented by the following reactions, according to the CSP reduction, of which the first step is in partial equilibrium and the second step will be rate determining :

$$\begin{aligned} C_3H_8 + 3.5\,O_2 &\rightarrow 3\,CO + 4\,H_2O \\ CO + 0.5\,O_2 &\rightarrow CO_2 \end{aligned} \tag{4.10}$$

The last step of reaction (4.10) is the same for both equivalence ratios, however, the global reaction rate (based on equation (4.4)) is defined different. This can be seen in figure 4.3 where these differences of the b_{ij}-coefficients are plotted. The differences are calculated by subtraction of the stoichiometric coefficients from the global rate definition for ϕ= 1.0 and ϕ = 0.5. The largest differences come from the intermediates in the oxidation process of propane combustion such as C_3H_7,C_3H_6,C_3h_4,C_2h_4. Propane itself is having a lower stoichiometric coefficient for the lean case, for O_2 however there is no difference. The global rate definition in this way, does account for the dominance of O_2 under lean combustion conditions, as it decreases the contribution of the fuel C_3H_8 and the first intermediates formed from it.

The construction of a global 1 step mechanism allows the projection on a reaction progress variable. This is done according to the CFI methodology. Solving the CFI equations gives a solution of the chemical system as function of the reaction progress variable: a laminar thermochemical database.

Next to the species concentrations, temperature, density and a source term for the global step are calculated. Using the detailed PREMIX solution mapped

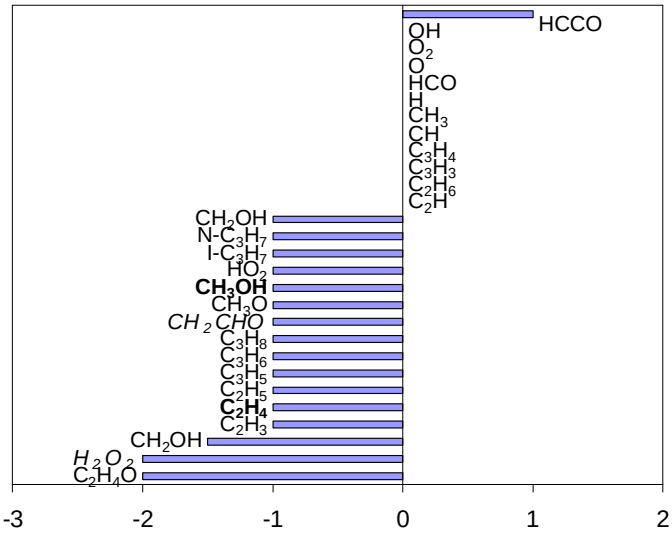

Figure 4.3: Differences in the b_{ij}^s**m**atrices for both stoichiometries

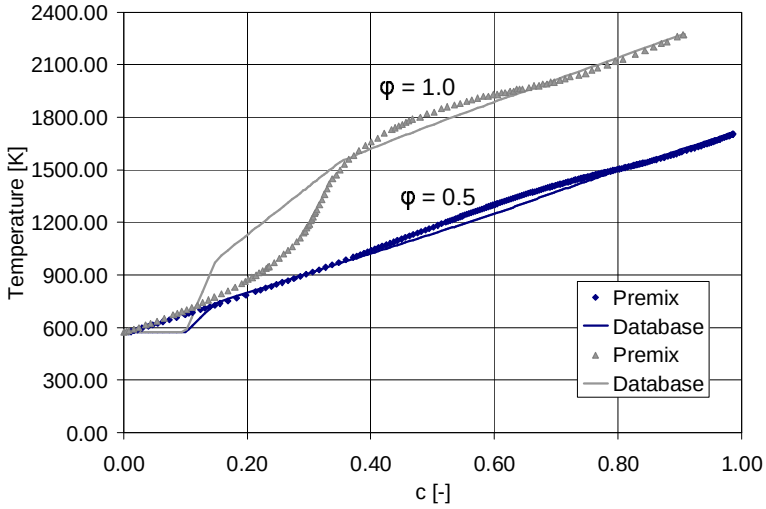

Figure 4.4: Laminar database comparison of temperature with PREMIX solution for ϕ = 0.5 and 1.0

on the reaction progress variable it is possible to assess the accuracy of the laminar thermochemical database. For the temperature of the flame, the database gives very good agreement as is seen in figure 4.4. At both cold (c = 0) and equilibrium conditions (c = 1) the PREMIX solution and the database solution are matching. Largest differences are seen in the interval c = [0.1, 0.3]. This is where ignition is important and the steady state species are the most active. However, for the lean flame, the differences are relatively small. Looking at the fit of the species with the PREMIX solution in figure 4.5, differences are

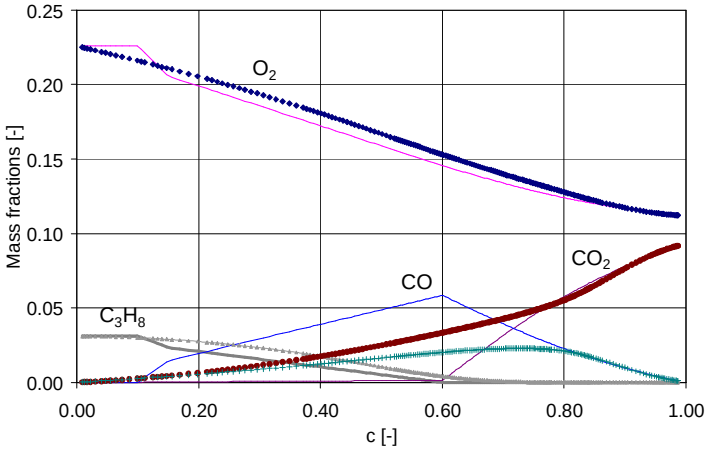

Figure 4.5: Laminar database comparison of species with PREMIX solution for ϕ = 0.5 (solid = Database, dotted = PREMIX).

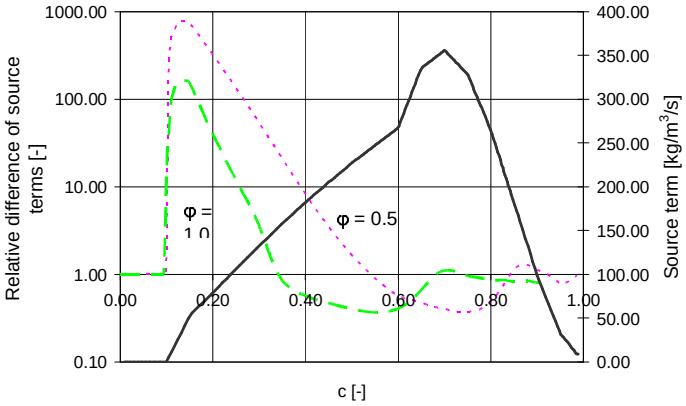

Figure 4.6: Laminar database comparison of c source term with PREMIX solution for ϕ = 0.5 and ϕ = 1.0 (solid = database source term at ϕ = 0.5, dashed - $\frac{S_{c,\text{Database}}}{S_{c,\text{PREMIX}}}$ for ϕ = 1.0)

larger, but still at cold and equilibrium conditions the match of the database with the PREMIX solution is very good. The largest differences in comparing the database solution with the laminar flame are seen for the source term defining the global step. This is seen in figure 4.6, where the relative difference of the source term in the database and the PREMIX solution is plotted. For ϕ = 1.0 the match is rather bad, having peaks for different values of c and having a factor of 2 difference for the magnitude of the source term. Looking at the situation with ϕ = 0.5 the source terms has its peak at a single c value, but again the magnitude is differing a factor of 2. Next to that, it should be mentioned

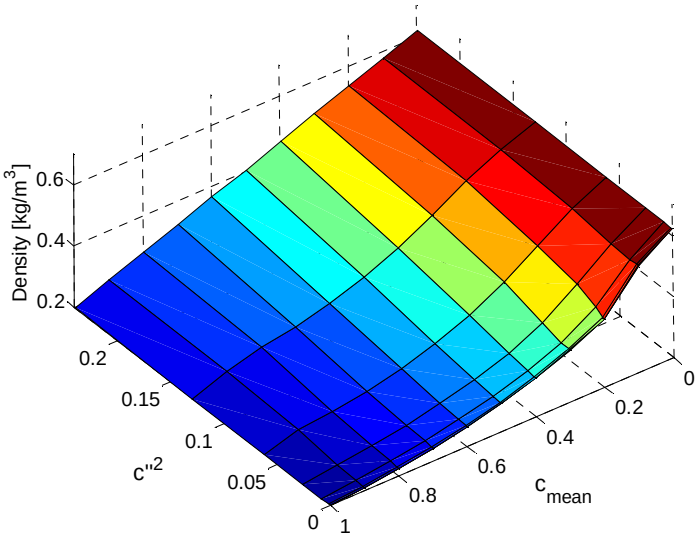

Figure 4.7: Density of the mixture as a function of the mean and variance of c

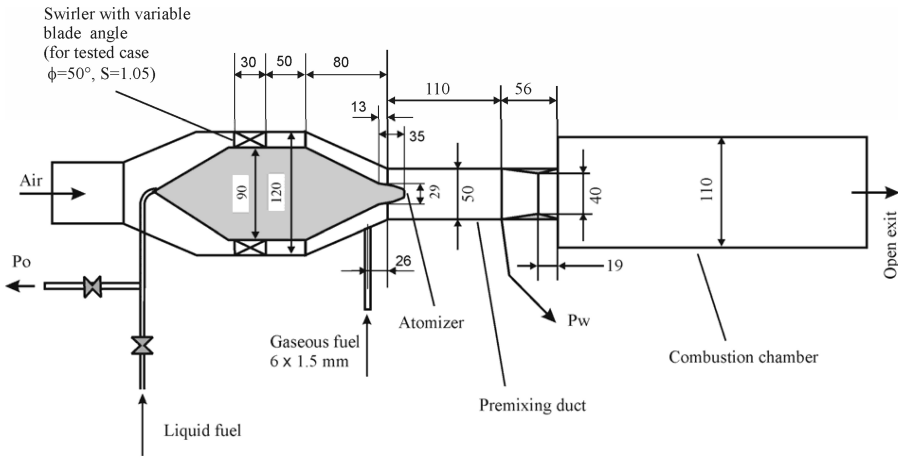

Figure 4.8: Experimental setup

that the order of magnitude of the source term comparing both stoichiometries is different. For the stoichiometric database and PREMIX solution the size of the source term is of the order of several thousands while for the lean conditions the order is of several hundreds. This indicates that the global step clearly responds as expected going from stoichiometric to lean conditions, in other words going from high burning velocity to lower burning velocity.

As is seen with the species and temperatures, the database has the largest deviations for conditions at intermediate values of c. Knowing that the source term is just a summation of individual species' rates according to the definition of the global rate, this explains the large difference for the stoichiometric case, as the source term is active in this region where the database has the least matching fit.

From the analysis it is clear that the laminar database for the condition of ϕ = 0.5, has the best fit with the laminar solution mapped on the reaction progress variable definition.

The next step in the CFI model, is the averaging procedure of the laminar database. With this step the temperature, density, source term and species concentrations are known as a function of the Favre averaged reaction progress variable, c, and its variance,c''^2. In figure 4.7 this is shown for the density. The averaging over the β-pdf has a smearing effect on the database, that represents turbulent fluctuations.

4.4 Combustor simulations

For validation of the work described in the paragraphs above it is essential to compare to relevant experimental data. In this article the lean premixed prevaporised experiments data from Anacleto *et al.* [80] are used as a reference for the modelling work. The setup consists of a swirling device connected to a prevaporizing and premixing chamber ending with a combustion chamber,

as can be seen in figure 4.8. The combusting flow of propane gas (no liquid) has a swirl number of 1.05 and is operated atmospheric pressure.

This combustion chamber has a radius of 55 mm and a length of 300 mm. The flame in the combustion chamber is stabilized by a recirculation zone as a result of the swirling flow and the sudden increase of the radius at the inlet of the combustion chamber.

Boundary conditions for the velocities and turbulence at the inlet of this combustor have been obtained by measurements, providing mean velocities and the RMS's of the velocity fluctuations in axial, radial and tangential directions.

For computational efficiency only a slice of the combustor is modeled and axial symmetry is expected in view of the 10^o section and the cylindrical geometry, which is calculated for a steady state situation. Next to this, the measured inlet boundary conditions provide velocities and velocity fluctuations only as a function of the radius, starting around the axis of the combustor until the wall of the premixing duct. Further it is assumed that the mixture enters the combustor perfectly premixed.

4.4.1 Comparison to experimental data

Simulations have been performed using the finite volume solver ANSYS--CFX combined with the CFI combustion model. The flow, turbulence and reaction progress variable transport equations are solved by the ANSYS-CFX solver, while the source terms for the reaction progress variable and its variance (the right hand side of equations (4.8) and (4.9)) are calculated by CFI and fed back to the CFD solver. The calculations have been performed using steady state equations. A grid of 1,152,166 elements is used to diminish effects of grid dependency. Both the k-ε turbulence model and the Reynolds Stress turbulence model have been used in the simulations.

The inlet velocity boundary conditions given by the measurement data are compared with the obtained results in figure 4.9. It is seen that the RS model has the best fit. At the centerline there is a discrepancy for the radial velocity and the tangential velocity. This is caused by enforcing zero tangential velocity at the centerline. For unknown reasons this is not the case in the measured data at 0 mm. At larger radius there is axial symmetry in the measurements.

For the location just behind the inlet at z = 9 mm (figure 4.9(b,d,f)), the RS model again gives a good fit with the data. The tangential velocity component gives the least accurate fit. One reason for this could be that the number of cells in the tangential direction is too small, as only a slice of 10 degrees of the domain is modeled, the other reason is the assumption of axi-symmetry as stated before.

The velocity in axial direction at z = 245 (figure 4.10mm is reasonably captured by the RS model but not by the k-ε model. The tangential measurement data at the same location suggest that there is still a strongly rotating structure present in the flow, however, the prediction by both turbulence models are not matching this behaviour.

In figure 4.12 contour plots of the temperature field are presented. From

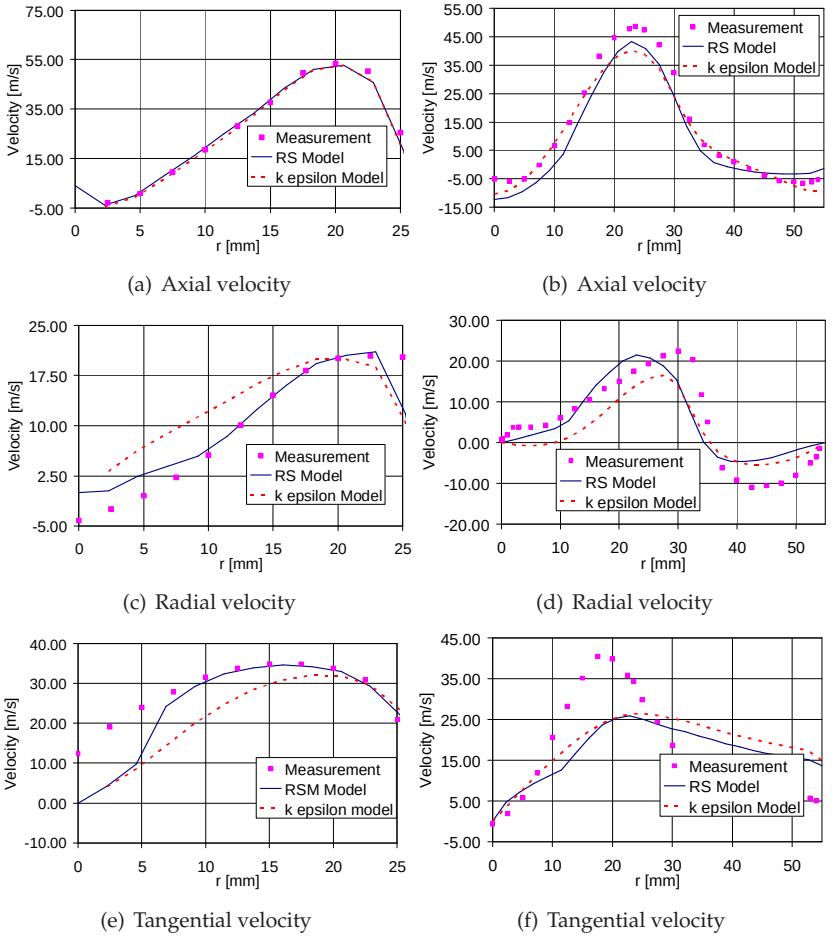

(a) Axial velocity (b) Axial velocity

(c) Radial velocity (d) Radial velocity

(e) Tangential velocity (f) Tangential velocity

Figure 4.9: Comparison of velocities at z = 0 mm (a,c,e) and z = 9 mm (b,d,f)

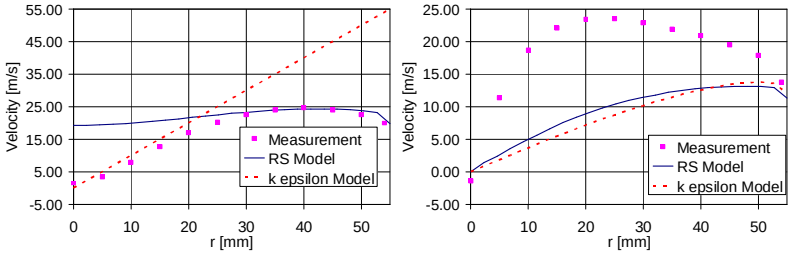

(a) Axial velocity (b) Tangential velocity

Figure 4.10: Comparison of velocities at z = 245 mm

this figure it is seen that the position of the flame and the length of the flame zone are nicely captured.

However the measurement data show a cold spot at the location of r = 40 mm and z = +/- 50 mm that is not captured by both models. Regarding the two turbulence models applied, it seems that the RS model performs slightly better, when comparing the penetration lengths of the cold mixture. It should be noted that the model assumes an adiabatic flame, which results in an over prediction of the exit temperature of $\pm$ 100 K.

The unburned hydrocarbon fraction is calculated as a post processing step by summing all the mass fractions containing hydrocarbons using the thermochemical database. Results are presented in figure 4.13. For the UHC fraction, again the same trends are observed as for temperature. However the measurements show a larger area of presence of UHC, while this area is smaller for the model computations. The concentration of UHC is overpredicted by a factor of 2. This is due to the assumption of adiabatic combustion and it is expected that accounting for heat loss will improve the results.

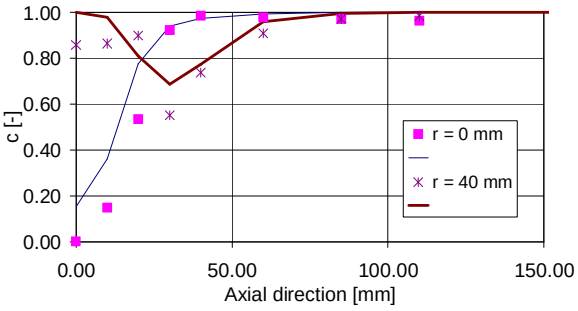

Figure 4.11: Reaction progress variable *c* at several radial positions

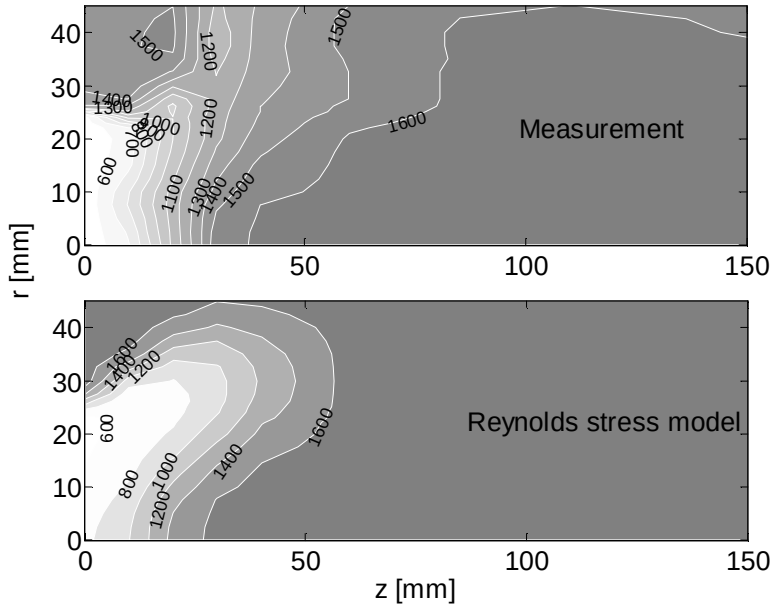

Figure 4.12: Temperature field [K]

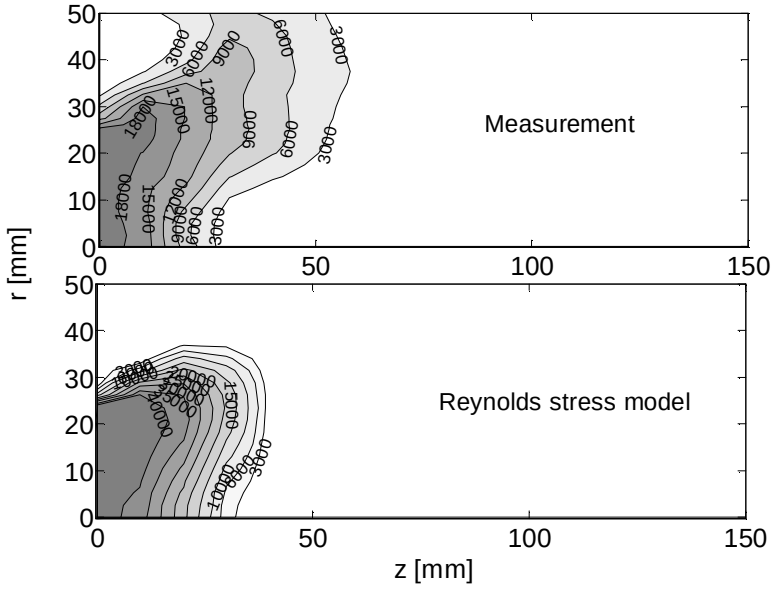

Figure 4.13: UHC contour plot [ppm]

4.5 Conclusions

Using CSP reduction and analysis is it shown that for different equivalence ratios, the global rate definition for the oxidation of propane will change. The reduced single step mechanism for an equivalence ratio of $\phi = 0.5$ gives the best comparison with a laminar PREMIX solution.

From the laminar database assessment it can be seen that a single step mechanism will have difficulties with capturing laminar ignition. Improvement of database quality in comparison with a laminar PREMIX solution is seen for lean conditions.

Using a single RPV gives acceptable results, comparing to the measured reaction progress indicated by temperature. The CFI model gives a reasonable prediction of the development of the mean temperature field in a turbulent flame and is also able to predict the trend of the UHC fraction field. The prediction of temperature and UHC does not depend heavily on the turbulence model used. However, it is clear the that RS model predicts the velocities better, and therefore the central recirculation zone, making it a more suitable model for swirl stabilized flames.

Further work will be the inclusion of heat loss in the model. This supposedly will have a positive effect on UHC burnout (chemical kinetics) and will improve the prediction of temperature. Next to that it will be interesting to apply the methodology described in this article to larger hydrocarbon molecules and mixtures of different components, more accurately representing commercially used liquid fuel.

Acknowledgments The work is partially funded by the EU 5^{th} Framework programme Mast-B-Liquid. Dr. S.I.Shtork and Dr. E.C Fernandes from Instituto Superior Técnico (Lisbon, Portugal) are gratefully acknowledged for making available the experimental data.

5

Combustion noise generated by turbulent premixed flames*

ABSTRACT *In regular operation all gas turbine combustors have a significant noise level induced by the turbulent high power flame. This noise is characteristic for the operation as it is the result of the interaction between turbulence and combustion. Pressure fluctuations may also be generated by thermoacoustic instabilities induced by amplification by the flame of the acoustic field in the combustor. This paper focuses on prediction of the former process of the noise generation in a premixed natural gas combustor. In order to predict noise generated by turbulent combustion, a model is proposed to calculate the power spectrum of combustion noise in a turbulent premixed natural gas flame on the basis of a steady state RaNS CFD analysis. The instantaneous propagation of acoustic pressure fluctuations is described by the Lighthill wave equation, with the combustion heat release acting as a monopole source term. For a semi infinite tube the solution can be written as a volume integral over the acoustic domain using a Green's function. The source term is written as a function of a reaction progress variable for combustion. Finite chemical kinetics is taken into account by using the TFC model, and turbulence is described by the k-ε model. Subsequently the volume integral for the noise field is evaluated for the turbulent situation on basis of the calculated steady state combustion solution and presumed shape probability density function weighting. The k- ε model provides the parameters for the presumed spectrum shape. Experiments have been performed in a 100 kW preheated premixed natural gas combustor. Comparison of predicted sound spectra with experimental results shows that the model is capable of prediction of the Sound Pressure Level. The modeled spectrum agrees well with the trends observed in the measured spectra.*

*B. de Jager and J.B.W.Kok, Modelling of combustion noise in turbulent premixed flames, *Proceedings of GT2006*, Barcelona, paper no. GT2006-90567, 2006

5.1 Introduction on combustion roar

Acoustic effects can dramatically influence the lifetime and combustion performance in a gas turbine combustor. An important side effect of a turbulent combustion process is the radiation of a sound field from the reaction zone. This is called combustion roar and occurs in all turbulent combustion processes. The flame is a source of sound and thus influences the acoustic behaviour of the combustor and its related components. Apart from radiating sound, a flame also acts as an amplifier of sound [82, 83]. However, this role of the flame will not be considered in the present work. Roar spontaneously generated by turbulent combustion shows a broad band noise spectrum. Currently two main sources are identified as the main sources of combustion roar: the turbulent flow and the release of heat due to the chemical reactions. The latter gives the greatest contribution to the noise spectrum radiated. Fortunately only a small part of the thermal power of a flame is converted into acoustic energy with efficiencies between 10^{-3} and 10^{-8} for the conversion of chemical energy input to acoustic energy [84]. But as the thermal power is of the scale of MW, the acoustic power generated can still be extremely high.

Noise modelling efforts for non-premixed turbulent combustion have been undertaken by Klein and Kok [82]. Their results show good agreement with experimental data. Boineau and Gervais [85] modeled noise generation of turbulent non-premixed flames in a similar way and also obtained good results. For turbulent premixed combustion no recent work on noise generation was found.

5.2 Theory

In a flame multiple chemical species are mixed and chemically reacting. Noise can be generated by several processes, like fluctuations in chemical reaction or heat addition. The chemical reactions cause density changes of over a factor 5, and this acts like a monopole acoustic source term when the process is unsteady. By combining the equations of continuity and momentum the following propagation equation for fluctuations of the pressure in a flame can be derived, as shown first by Sir James Lighthill [86]:

$$\frac{\partial}{\partial t}[\frac{1}{a^2}\frac{\partial p}{\partial t}] - \nabla^2 p = -\frac{\partial}{\partial t}[\frac{\gamma-1}{a^2}\rho\sum_{i=1}^{n}\frac{\mu_i}{M_i}\frac{Dy_i}{Dt}] \tag{5.1}$$

Here is used that for an ideal gas:

$$\frac{\alpha}{c_p} = \frac{\gamma-1}{a^2} \tag{5.2}$$

At combustion interfaces the differences between the Gibbs potentials of reactants and products are large, and hence in a flame there is a significant source term driving pressure fluctuations in case of fluctuating combustion. In a turbulent flame the rate of production of a product species, and associated heat release, has a strong spatial dependence and is temporally fluctuating due to

turbulence. These fluctuations are the origin of the thermo-acoustic noise production, but are not easily calculated. Strahle [87,88] presented a good analysis but the correlations presented for the noise level did not fit well with experimental data. The modelling of the transient and averaged monopole source term in equation 5.1, which is local in the flame field, has to be performed with the use of Computational Fluid Dynamics in order to predict acoustic effects. Processes that have to be described are mixing, turbulence and chemical reaction delay times. The instantaneous transport of each species mass fraction is described by:

$$\rho \frac{Dy_i}{Dt} + \nabla . \underline{J}_i = \omega_i \tag{5.3}$$

In many flame applications the species mass fractions all depend on a small number of independent variables and the species concentrations evolve with time in a low dimensional chemical variable space. The simplest approximation for a flame where chemical reaction kinetics and fuel/air mixing can be important, is a situation where the species mass fractions depend on the mixture fraction variable f and a reaction progress variable c [25]:

$$y_i = y_i(f(t), c(t)) \tag{5.4}$$

Hence the material derivative of each species mass fraction can be written as:

$$\rho \frac{Dy_i(f,c)}{Dt} = \rho \left. \frac{\partial y_i}{\partial f} \right|_{c_j} \frac{Df}{Dt} + \rho \left. \frac{\partial y_i}{\partial c} \right|_{f} \frac{Dc}{Dt} \tag{5.5}$$

The scalar f is a conserved variable and transported according to:

$$\rho \frac{Df}{Dt} - \nabla \cdot (\rho D \nabla f) = 0 \tag{5.6}$$

and the scalar c according to the transport equation:

$$\begin{array}{l} \rho \frac{Dc}{Dt} - \nabla \cdot (\rho D \nabla c) = S_c(f,c) + \\ \rho D \left(\frac{1}{W} \frac{\partial^2 W}{\partial f^2} \right) \mathrm{c} + 2\rho D \left(\frac{1}{W} \frac{\partial W}{\partial f} \right) \nabla f \nabla c \end{array} \tag{5.7}$$

With: $W = y_{burnt} - y_{unburnt}$ By combining equations 5.5, 5.6 and 5.7 the following can be stated now for the material derivative for a species mass fraction in a flame:

$$\begin{array}{l} \rho \frac{Dy_i(f,c)}{Dt} = \left. \frac{\partial y_i}{\partial f} \right|_{c} \nabla \cdot (\rho D \nabla f) + \\ \left. \frac{\partial y_i}{\partial c} \right|_{f} \left(\begin{array}{l} S_c(f,c) + \nabla \cdot (\rho D \nabla c) + \rho D \left(\frac{1}{W} \frac{\partial^2 W}{\partial f^2} \right) c \\ +2\rho D \left(\frac{1}{W} \frac{\partial W}{\partial f} \right) \nabla f \nabla c \end{array} \right) \end{array} \tag{5.8}$$

Hence in a low mach number, *premixed* flame, where gradients for mixture fraction vanish and neglecting fluctuations of gradients in reaction progress compared to the chemical reaction source term, equation 5.8 simplifies to:

$$\rho \frac{Dy_i(f,c)}{Dt} = \left. \frac{\partial y_i}{\partial c} \right|_{f} S_c(f,c) \tag{5.9}$$

The acoustic wave equation 5.1 in this case reads as:

$$\begin{aligned} &\tfrac{\partial}{\partial t}[\tfrac{1}{a^2}\tfrac{\partial p}{\partial t}] - \nabla^2 \cdot p = \\ &-\tfrac{\partial}{\partial t}[\tfrac{\gamma-1}{a^2} \sum_{i=1}^{n} \tfrac{\mu_i}{M_i} \tfrac{\partial y_i}{\partial c}\Big|_f S_c\Big|_f] \end{aligned} \tag{5.10}$$

The reaction progress variable c is computed with the use of a composed mass fraction y defined by a weighted sum over all mass fractions:

$$y = \sum_{i=1}^{n} b_i y_i \tag{5.11}$$

The weight factors are optimized to describe chemical kinetics accurately [24] . The reaction progress variable c is then defined by:

$$c = \frac{y - y_{unburnt}}{y_{burnt} - y_{unburnt}} \tag{5.12}$$

It can be calculated from equations 5.11,5.12 that:

$$\frac{\partial y_i}{\partial c} = \frac{y_{burnt} - y_{unburnt}}{b_i} \tag{5.13}$$

The thermo acoustic source term will then be calculated as:

$$-\frac{\partial}{\partial t}\left(\frac{\gamma-1}{a^2}\sum_{i=1}^{n}\frac{\mu_i}{b_i W_i}\left(y_{burnt} - y_{unburnt}\right).S_c\right) \tag{5.14}$$

For a premixed flame, the gas mixture composition can be divided in a type 'unburned' and a type 'burned' mixture. The summation of Gibbs energy in equation 5.14 is then calculated from the net release of thermal energy, assuming a constant value of the specific heat:

$$\sum_{i=1}^{n}\frac{\mu_i}{b_i W_i} = c_p(T_{burnt} - T_{unburnt}) \tag{5.15}$$

This gives for the thermo acoustic source term of equation 5.14:

$$-\frac{\partial}{\partial t}\left(\frac{\gamma-1}{a^2}(T_{burnt} - T_{unburnt})\left(y_{burnt} - y_{unburnt}\right).S_c\right) \tag{5.16}$$

Application of the TFC combustion model [89] will yield the following term for the source term S_c:

$$S_c = \rho_{unburnt} C_f u'^{3/4} S_L^{1/2} \chi^{-1/4} l_t^{1/4} \left|\nabla c\right| \tag{5.17}$$

In this term C_f is a constant equal to 0.52, u' is the mean turbulent velocity fluctuation, $S_L$is the laminar flame speed depending on the relevant combustion conditions, χ is the thermal diffusivity of the mixture, l_t is the turbulent length scale.

5.2.1 Solving the wave equation for combustion noise

Assuming the characteristic turbulent length scales in the flame (Gibson scales) to be small compared to the acoustic wave length and the source term to vanish in the far field, the following solution can be derived for equation 5.1. A Green's function is used for a 1D acoustical situation in a semi-infinite pipe (differs a factor 2 from an infinite pipe), which is:

$$G(x_0, t|\, x, t') = \frac{a_0}{O} H\left(t - t' - \frac{|x_0 - \underline{x}|}{a_0}\right) \tag{5.18}$$

The solution for the acoustic pressure can be written as follows then:

$$p'(x_0, t) = \frac{a_0}{O} \int\int\int A S_c d\underline{x} \tag{5.19}$$

with:

$$A = \frac{(\gamma - 1)\, c_p}{a^2} \left(T_{burnt} - T_{unburnt}\right)\left(y_{burnt} - y_{unburnt}\right) \tag{5.20}$$

As this is applicable to a semi-infinite pipe, reflections and eigenfrequencies resulting from the finite situation in the experiments will not be seen.

5.2.2 Spectrum of the acoustic pressure

Mean spectra of the acoustic pressure fluctuations are determined by applying a Fourier-transform in time space to the space time correlation function (cross covariance) of equation 5.19, giving:

$$pp(x_0, \omega) = \left[\frac{a_0}{O}\right]^2 \int_{\Delta t} \left[\int_V A S_c|_{\underline{x}} dV\right] \cdot \left[\int_{\Delta V} A S_c|_{\underline{x}+\Delta\underline{x}, \Delta t}\right] \mathrm{e}^{i\omega\Delta t} d\Delta t \tag{5.21}$$

Now it is assumed that A is constant over the turbulent correlation length. The term is mainly determined by large scale mixing of hot and cold flows. Klein and Kok [82, 83] introduce the following variable for the time, thus splitting and introducing a combined time scale of turbulence and acoustic propagation (one dimensional):

$$\Delta t^* = \Delta t + \frac{\Delta x}{a_0} \tag{5.22}$$

The second double integral in equation 5.21 is replaced (at position x_2 by an integral over Δx (at x_2, $x_2 = x_1 + \Delta x$). This because for the far field only the 1 dimensional coordinate is of importance. Therefore Δ t is substituted with Δt^* and the exponential-function is split, thus leaving a Fourier-transform in space and time of the fluctuating heat release:

$$\begin{aligned} pp(x_0, \omega) &= \left[\tfrac{a_0}{O}\right]^2 \cdot \int_V A^2 \\ &\int_{\Delta t^*} \int_{\Delta\underline{x}} \overline{S_c S_c}\,(\underline{x}; \Delta\underline{x}, \Delta t^*) e^{i\omega\Delta t^*} e^{-i\frac{\omega}{a_0}\Delta\underline{x}} d\Delta\underline{x} d\Delta t^* dV \end{aligned} \tag{5.23}$$

And transformed to frequency space:

$$\begin{aligned} &pp(x_0,\omega) = \left[\tfrac{a_0}{O}\right]^2 \cdot \int_V \\ &A^2 F^{\omega,\underline{k}} \left[\overline{S_c S_c}\left(\underline{x};\Delta\underline{x},\Delta t^*\right)\right].(\underline{x};\omega,\underline{k}=(-\omega/a_0,0,0))dV \end{aligned} \tag{5.24}$$

The product of the source terms in equation 5.24 will be Reynolds averaged now, this gives:

$$\begin{aligned} &\overline{S_c|_{y_1,y_2,y_3} \cdot S_c|_{\Delta y_1,\Delta y_2,\Delta y_3,\Delta t^*}} = \\ &\overline{S_c}_{y_1,y_2,y_3}\overline{S_c}_{y_1+\Delta y_1,y_2+\Delta y_2,y_3+\Delta y_3,\Delta t^*} + \\ &\overline{S_C{}'_{y_1,y_2,y_3} S_C{}'_{y_1+\Delta y_1,y_2+\Delta y_2,y_3+\Delta y_3,\Delta t^*}} \end{aligned} \tag{5.25}$$

Both terms on the RHS of equation 5.25 will contribute to the sound spectrum, because both terms are correlations of $\underline{\Delta x}$. Noted should be that the terms are linear. It is expected that the contribution of the fluctuating term to the spectrum is negligible. Then equation 5.24 simplifies to:

$$\begin{aligned} &pp(x_0,\omega) = \\ &\left[\tfrac{a_0}{O}\right]^2 \int_V A^2 F^{\omega,\underline{k}} \Omega(\underline{x};\omega,\underline{k}=(-\omega/c_0,0,0))dV \end{aligned} \tag{5.26}$$

With:

$$\Omega = \overline{S_c}_{x_1,x_2,x_3}\overline{S_c}_{x_1+\Delta x_1,x_2+\Delta x_2,x_3+\Delta x_3,\Delta t^*} \tag{5.27}$$

Now a Fourier transform needs to be calculated of

$$F^{\omega,\underline{k}} \Omega(\underline{x};\omega,\underline{k}) \tag{5.28}$$

Using the fact that the acoustic wave number ω/a is much smaller than the typical turbulent wave numbers for low Mach number flows, then the acoustic wave number can be set to 0. Also assumed is symmetry of turbulence in wave number space. First, the problem is made one dimensional by introducing a correlation length scale for the other two spatial directions. Then a Fourier transformation for Δt and Δx and factorization in a wave number part and wave number-time part are performed:

$$\begin{aligned} &F^{\omega,\underline{k}}\left[\overline{S_c}\cdot\overline{S_c}\big|_{\Delta t^*,\underline{\Delta x}}\right] = l_{cor}^2 F^{\omega,k}\left[\overline{S_c}\cdot\overline{S_c}\big|_{\Delta t^*,\Delta x}\right] = \\ &l_{cor}^2 \int_{\Delta x}\int_{\Delta t^*} F\left[\overline{S_c}\cdot\overline{S_c}\big|_{\Delta t^*,\Delta x}\right] e^{i\omega\Delta t^*} e^{-i\frac{\omega}{c_0}\Delta x} d\Delta t^* d\Delta x = \\ &\tfrac{l_{cor}^2}{2\pi}\int_{\lambda}\int_{\Delta t^*} F^k\left[\overline{S_c}\cdot\overline{S_c}\big|_{\Delta x}\right](\Delta t^*,-\lambda) e^{i\omega\Delta t^*} d\Delta t^* d\lambda = \\ &\tfrac{l_{cor}^2}{2\pi}\int_{\lambda}\int_{\Delta t^*} F^k\left[\overline{S_c}\cdot\overline{S_c}\big|_{\Delta y}\right](\lambda) r(\lambda,\Delta t^*) e^{i\omega\Delta t^*} d\Delta t^* d\lambda = \\ &\tfrac{l_{cor}^2}{2\pi}\int_{\lambda} F^k\left[\overline{S_c}\cdot\overline{S_c}\big|_{\Delta y}\right](\lambda) r(\lambda,\omega) d\lambda \end{aligned} \tag{5.29}$$

Applying a correlation function in the frequency/wave number domain as based on the sweeping hypothesis by Rubinstein and Zhou [90] or also known

as Taylor hypothesis [91], fluctuations in time can be correlated to spatial fluctuations:

$$r(\lambda,\omega) = \frac{2\pi}{U}\delta\left(\lambda - \frac{\omega}{U}\right) \tag{5.30}$$

Combining equations 5.29 and 5.30 gives:

$$\begin{aligned} &\tfrac{1}{2\pi}\int_{\lambda} F^k\left[\overline{S_c}\cdot\overline{S_c}\big|_{\Delta y}\right](\lambda) r(\lambda,\omega)d\lambda = \\ &\tfrac{1}{2\pi}\int_{\lambda} F^k\left[\overline{S_c}\cdot\overline{S_c}\big|_{\Delta y}\right](\lambda)\tfrac{2\pi}{U}\delta\left(\lambda - \tfrac{\omega}{U}\right)d\lambda = \\ &\tfrac{1}{U}F^k\left[\overline{S_c}\cdot\overline{S_c}\big|_{\Delta y}\right](\tfrac{\omega}{U}) \end{aligned} \tag{5.31}$$

5.2.3 Turbulence spectrum coupling to the thermo acoustic source term spectrum

The spectrum of the fluctuations of the thermo acoustic source term from the final RHS of equation 5.30 is presumed to scale with the Kolmogorov spectrum of isotropic turbulence, as the flow has a high Reynolds number (Obukov's Law, assuming that it is also valid for reactive scalars [91]:

$$S_c(k) \propto k^{-5/3} \tag{5.32}$$

For high Reynolds number flows the following relations are valid, K being the total turbulent kinetic energy and ε its dissipation rate:

$$\int_0^\infty E(k)dk = K \tag{5.33}$$

$$2\upsilon\int_0^\infty k^2 E(k)dk = \varepsilon \tag{5.34}$$

The shape of the three-dimensional energy spectrum of turbulence can be defined as a function of wave-number space with the 'modified' Von Karman spectrum, [92, 93]

$$E(k) = C\frac{{}^2\!/_3 K}{k_{int}}\frac{\left(\frac{k}{k_{int}}\right)^4}{\left(1+\left(\frac{k}{k_{int}}\right)^{17/6}\right)}e^{-2\left(\frac{k}{k_{kol}}\right)^2} \tag{5.35}$$

In this expression k_{int} and k_{kol} can be calculated from a steady state RANS CFD calculation. The three-dimensional spectrum is related to the one-dimensional spectrum with the following relation:

$$E^{1D}(k_1) = \int_{k_1}^\infty \frac{E(k)}{k}dk \tag{5.36}$$

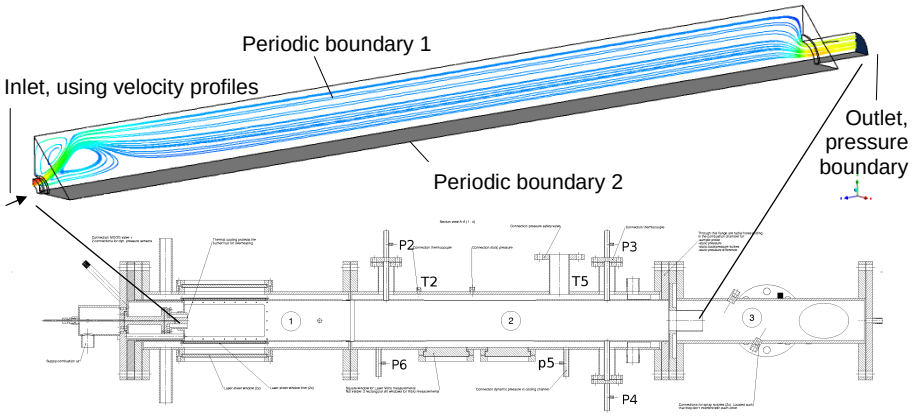

Figure 5.1: The computational domain and combustor setup, with sensor locations P2-P6.

The Fourier transform from equation 5.30 can now be coupled to the one-dimensional spectrum, introducing B as a scaling factor.

$$\begin{aligned} F^k\left[\overline{S_c}\cdot\overline{S_c}\big|_{\Delta x}\right](k) &= F^k\left[\overline{\overline{S_c}\cdot\overline{S_c}\big|_{\Delta x}}\right](k) \\ &= B\int_{\Delta x}\overline{\overline{S_c}\cdot\overline{S_c}\big|_{\Delta x}}e^{ik\Delta x}d\Delta y \\ &= BE^{1D}_{S_c\cdot S_c}(k) \end{aligned} \tag{5.37}$$

It is assumed that the one-dimensional turbulence spectrum of the combustion source term scales with the combustion scalar dissipation, therefore using Parsevals theorem gives a relation to calculate B:

$$B\int_0^\infty E^{1D}_{S_c\cdot S_c}(k)dk = D_{thermal}\nabla\tilde{c}\nabla\tilde{c} \tag{5.38}$$

Finally this leads to the following calculable expression for the spontaneous noise spontaneously generated by turbulent combustion:

$$pp(\omega) = \left[\frac{a_0}{O}\right]^2\int_V\frac{1}{U}A^2l_{cor}^2BE^{1D}_{S_c\cdot S_c}(k)\,dV \tag{5.39}$$

5.3 Results and discussion

Preliminary results of the modelling work in the previous chapters are presented here. The results are obtained using CFX 5.6 with the TFC combustion model [89,94] for perfectly premixed mixtures. With user defined subroutines all data necessary with respect to equation 5.39 were retrieved from the steady state simulation solution. Subsequently the noise in the combustor was computed in a post processing code on basis of equation 5.39. The geometry for this study is a generic swirl combustor in a 100 mm x100 mm square cross

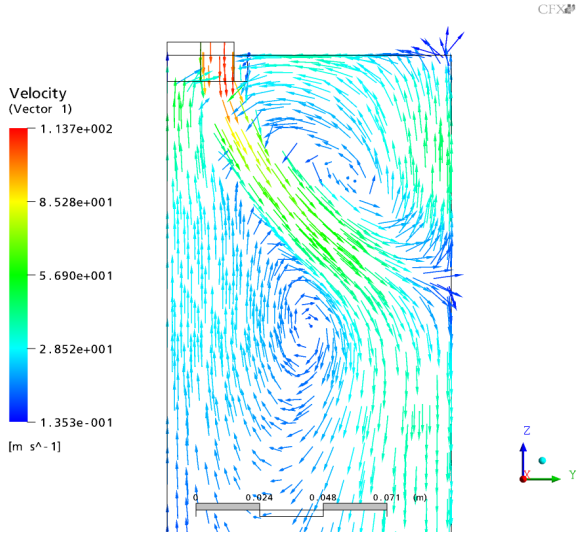

Figure 5.2: Vector plot of the predicted velocity field.

section and a combustor length of 1800 mm, used in an experimental setup at our laboratory, see [95] for a detailed description of the setup. The combustor is operated with air preheated to 300°C and mixed prior to combustor entry with natural gas. The air factor was 1.8. The pressure is atmospheric and the thermal power is 100 kW. The Reynolds number of this setup is around 45,000. The experimental set up is sketched in figure 5.1.

The CFD calculations were set up using the k-ε turbulence model, taking into account a quarter of the burner meshed with 527,018 elements, using pe-

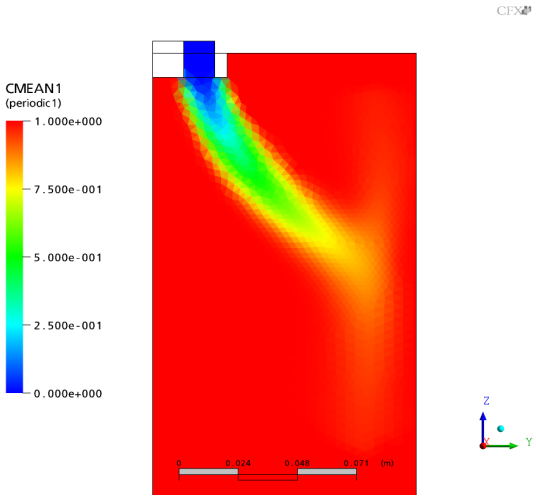

Figure 5.3: The predicted field of the reaction progress variable.

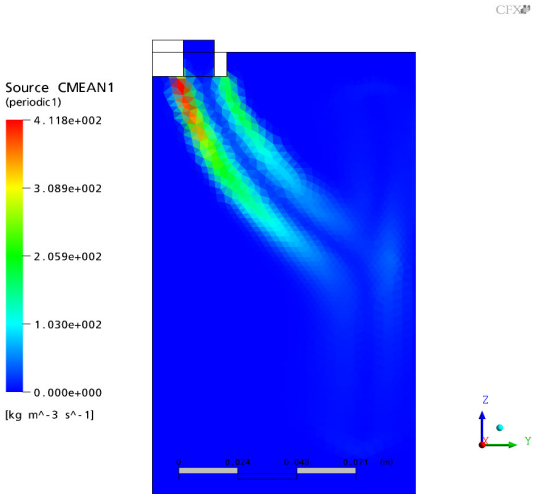

Figure 5.4: The predicted field of the source term of the reaction progress variable.

riodic boundary conditions.

The predicted velocity field is presented in figure 5.2 by a vector plot. Clearly it can be observed that the premixed gas/air flow emerging from the burner at the top RHS of the figure, develops a central recirculation area and a minor area of recirculation in the corner of the combustor.

In figure 5.3 the predicted field of the reaction progress variable c is presented. The reaction progress variable increases from zero at the burner inlet to a transition zone of about 0.5 to 0.7 at the flame front at the edge of the recirculation area. Subsequently the reaction progress variable approaches 1 for

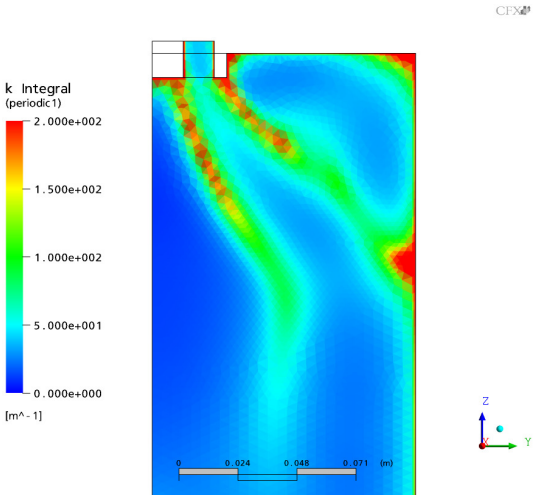

Figure 5.5: The field of the predicted integral wave number.

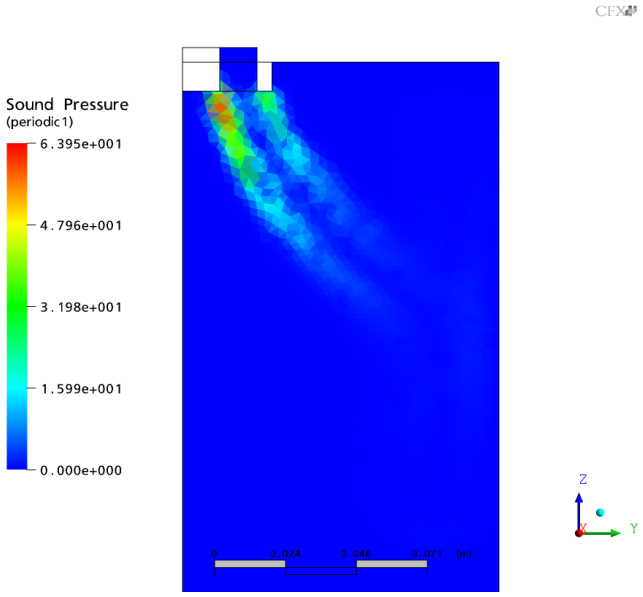

Figure 5.6: The field of the predicted sound pressure.

the burnt situation.

The predicted field of the source term of the reaction progress variable is depicted in figure 5.4. The source term can be observed to be zero in the burner inlet flow and to be large at the two combustion interfaces, at the side in contact with the inner and at the side in contact with the outer recirculation area. The computed integral wave number of the turbulent flow field is shown in figure 5.5. This is high at the exit of the burner, both near the axis and at the burner edge, where there is a high shear with the fluid in the combustor. The predicted field of the sound pressure on basis of equation 5.39 is shown in figure 5.3. The sound pressure is very high, about 100 Pa, at the areas where combustion occurs, and is also at a considerable level in a large area downstream the flame front, where the reaction progress variable develops slowly to the burnt equilibrium situation.

The predicted power spectra of the noise at locations P2 and P3 (see figure 5.1) in the combustor, plotted against measured data are given in figure 5.7(a) and (b) respectively. The power spectra are predicted on basis of the CFX simulation data using equation 5.39.

At both locations P2 and P3 the sound pressure level is observed and predicted to be at a maximum at low frequencies, approximately 140 dB. The sound level decreases, with exception of a few eigenfrequency points, smoothly to 85 dB at 2,000 Hz. The measured data show some eigenfrequencies, for example 400, 600, 800, 1000 Hz. Here the sound pressure level rises with about 10 dB. This can not be predicted by the present model as the solution method does not take into account reflections in the combustor.

5.4 Further validation of the model (this thesis)

In this section further validation steps have been taken. First, the model is tested for a different thermal power. Next to that the model has been used to predict the sound spectrum of an LPP flame, with n-heptane as a model fuel. This shows that the model in potential can be applied to any type of hydrocarbon combustion.

5.4.1 Result for a 200 kW flame

Following the modelling approach, the level of sound should be dependent on the thermal power of the flame. This is implicated by the equation of Lighthill (equation (5.1)), where the RHS is a function of the heat release rate. An increase in power of a flame should yield an increase in SPL as well. In the model this relation is given by the scaling with the mean of the global reaction rate S_c.

The flame used for testing the dependence on thermal power, is chosen from the same experimental data set as the earlier presented simulation data. This allows to use the same grid and numerical models developed. The only difference to the 100 kW flame from the earlier sections, is an increase of operating pressure. This yield a doubling of the thermal power to 200 kW. Velocity profiles and temperature at the inlet were kept the same.

In figure 5.4.1 it is shown that this coupling between the thermal power exists and that the increase in sound generation is modelled well. The SPL as produced by the 100 kW flame is slightly lower than the SPL produced by the 200 kW flame. This difference is seen in the measurement data as well as in the model results. The fall-off of the SPL with frequency does not change for both measured data sets, indicating that the turbulence spectrum of the flow is not changed significantly. This agrees to what would be expected, as only the operating pressure has been changed.

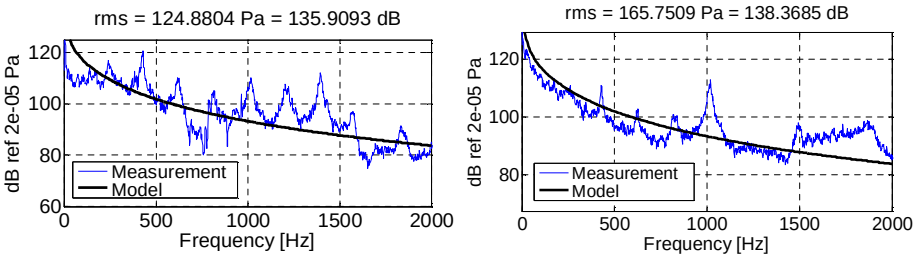

(a) Microphone P2 (b) Microphone P3

Figure 5.7: The sound pressure measured and predicted at location P2 (a) & P3 (b).

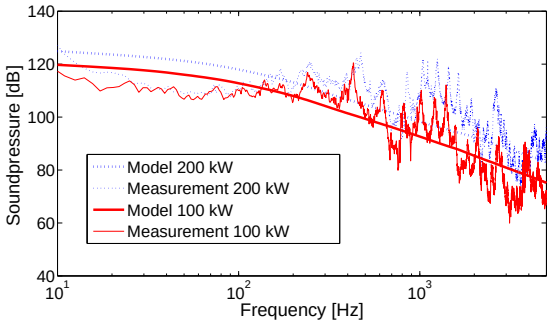

Figure 5.8: Comparison of sound generation in the DESIRE flame at two operating powers.

5.4.2 Results for LPP heptane combustion

The major topic of the research in this thesis is liquid fuel combustion modelling. LPP combustion conceptually can be regarded as a process similar to natural gas combustion. The model as presented in the previous paragraphs should easily be adapted to model flames operating on a different fuel. The description of the reaction progress variable (equation (5.11) and the corresponding rate in equation (5.16)) is such, that any type of fuel can be used, as long as a globally reduced mechanism is available or an expression for the laminar flame speed is known to calculate the global rate (equation (5.17)).

A stoichiometric, atmospheric n-heptane flame has been modelled using the detailed mechanism of Williams as a basis for the CFI combustion model (see chapter 2). A detailed outline of these calculations can be found in a conference paper by the author of this thesis [96]. The resulting calculations of the SPL are plotted in figure 5.4.2. For reference the sound produced by a 100 kW methane flame as discussed earlier in this chapter is plotted as well. Comparison between the two lines is difficult as conditions for the two flames are not equal: the inlet temperature and fuel to air ratio are different. As expected due to the presumed shape of the turbulence spectrum, the fall-off with frequency is equal to the results obtained for natural gas. The spectrum is shifted to the right. This could indicate that n-heptane combustion inherently produces more noise. However, as the fuel to air ratio is stoichiometric for this flame it is more logical to explain the phenomenon to an increased power of the flame. The low frequency part is overlapping with the natural gas flame. This can be explained by the fact that the low frequencies are a result of geometry mainly and are therefore not influenced much by the type of fuel.

5.5 Conclusions

The model is capable of predicting the fall-off and amplitude of the sound spectrum with good agreement with measured data. This is done without taking into account the fluctuating term of the Reynolds averaged source term. Apparently it was correct to neglect this term.

It seems that the one dimensional semi-infinite tube assumption is valid

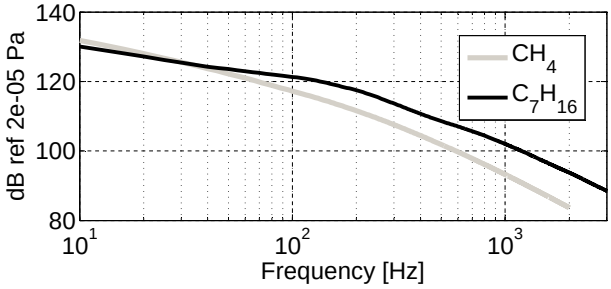

Figure 5.9: Sound produced by a stoichiometric heptane flame (black line) compared to a natural gas flame spectrum (grey line).

and that sound mainly is generated by turbulence at the mixing interface of hot products and cold mixture within the combustor.

Eigenfrequencies of the combustion chamber as seen in the measurement data, are not observed in the model spectrum. This is due to the one dimensional semi-infinite tube assumption, where reflections, and hence feed back phenomena are not taken into account.

Further work performed to validate the model at other operating conditions, pressure and power levels, has been conducted and shows that the model in principle correctly grasps different thermal power levels of flames. Next to that it has been shown that the model is generally valid for modelling noise emissions from turbulent premixed hydrocarbon flames. A correct description of the global chemical rate in the flame is the main contributor to this result.

The current mathematical assumption of an infinite tube does not hold for finite length combustion chambers. When a closed tube is taken into account in the analytical solution to the acoustic wave equation, a different solution will be found. This will also enhance insight in the interaction of the sound produced by a turbulent premixed flame and the thermo-acoustic instabilities. Reflection from the predicted sound will presumably result in eigenfrequencies in the model spectra.

An interesting extension to the model would be the inclusion of two-phase effects in the theoretical derivation of the acoustic wave equation.

Acknowledgments
The authors appreciate the financial support by Siemens Industrial Turbo Machinery in Lincoln (UK) and the valuable discussions with dr. Khawar Syed. dr. Ian P. Jones of ANSYS-CFX is thanked for his support to implement our noise code into the CFD software package.

6

Theory of spray modelling

In this chapter a model for the description of a liquid spray is presented and discussed. The first section describes basic theory of two-phase flows. Then a statistical theory is presented that will be used in describing the spray evolution.

6.1 Introduction

Modelling and simulation of combusting sprays have been subject of research for several decennia. As spray combustion has wide application, varying from land based gas turbines to direct inject engines for automotive applications, many models are available in literature, giving a broad spectrum of application for liquid spray combustion. In this introduction several aspects related to sprays will be discussed.

6.2 Liquid spray concepts

The aim of this section is to discuss the fundamental properties of sprays on a macroscopic scale and how the underlying microstructure of a spray is described by using statistical techniques. Next to that, the concept of spray combustion is introduced via the *Chiu*-diagram.

6.2.1 Generation of a liquid spray; the macro-structure

Creation of a cloud of droplets from a liquid is called atomization. One of the simplest ways to generate a droplet cloud or spray of liquid fuel, is by injecting a liquid turbulent jet from a small nozzle into an open chamber. Many sprays are generated with such a device, belonging to the category of so called pressure atomizers. Other types of atomizers can be categorised as gaseous, mechanical, acoustic of ultrasonic atomizers. These categories are related to the method of kinetic energy transfer to the liquid sprayed with the atomizer. A pneumatic atomizer is an example of a gaseous atomizer, while a rotary atomizer is an example of a mechanical atomizer. The choice of a certain type of atomizer depends on the application and desired shape of the spray.

Atomization itself can be described by liquid break up into drops by acting forces. This process is facilitated better when the liquid is in a form that

is more susceptible to disintegration. Therefor a sheet or jet of liquid often is used as the basis for atomization, as these forms have the highest surface energy and therefore are prone to the greatest instability. To introduce some dimensionless numbers of atomization, the process of a liquid jet breakup will be roughly sketched.

Inside a liquid jet, turbulence, caused by the high shear stresses of the injector, forces the jet to break up in strands or sheets, that then again will break up into single droplets. The driving force behind the decay of the jet into a cloud of droplets is the amount of energy contained by the jet. The minimum amount of energy is found when the jet is completely broken up into single droplets.

Several authors have published on the phenomena of disintegration of liquid into a spray. The first one to present an analytical solution for disintegrating liquid was Rayleigh [97]. He obtained a solution for disintegration by forcing small disturbances with increasing magnitude on a liquid jet in a vacuum, using the forces of surface tension as variable. Weber, extended the modelling by adding the use of aerodynamical forces to the model. He introduced the *Weber number* We: a measure for the ratio of aerodynamical forces and surface tension:

$$We_l = \frac{\rho_L V_L^2 D_0}{\sigma} \tag{6.1}$$

The aerodynamical forces are taken into account via the liquid density, ρ_l, injection velocity of the liquid, V_l and the initial droplet diameter, d_0. σ is the surface tension. Using equation 6.1 together with the theory from Rayleigh a formula is derived, giving the possibility to calculate a critical diameter D_c for which a jet will be unstable:

$$\frac{D_c}{D_0} = 1.436 \left(1 + 3\frac{We_l^{0.5}}{Re}\right)^{1/6} \tag{6.2}$$

The ratio of $We_l^{0.5}/Re$ is called the *Ohnesorge number* Z, which is a measure for the relative importance of aerodynamical forces and viscous forces acting on the liquid jet. In equation 6.2 Re is the Reynolds particle number, which will be introduced in the next section.

In many cases the atomization conditions are such that one can neglect the viscosity of the liquid and the environment. Neglecting these variables, analytical solutions can be obtained for a disintegrating liquid jet. These then give a relation that allows to calculate an average drop diameter. For completely developed turbulence during axisymmetric jet disintegration the following relation is found [98]:

$$\frac{L_c}{D_0} = 11.5We^{0.31} \tag{6.3}$$

In this equation L_c is the critical length of the jet after which break-up of the jet starts. The diameter of this jet is given by the geometry of the atomization apparatus. Unfortunately, this simple relation and the other aspects discussed,

are not sufficient to describe the shape of the spray and the final spectrum of droplet diameters. In order to accurately calculate the full atomization process from liquid to dispersed droplet spray, many variables have to be taken into account and difficulties are spread over a wide range of physical phenomena. As modelling of atomization is not the aim of this thesis, in the remainder of the thesis the atomization process is not further discussed. For an in depth overview of liquid atomization and related theory: see for example the book of Bayvel and Orzechowski [98].

Micro-structure of a spray

Although presuming completed atomization allows for a much simpler spray evolution model, still a description of the droplet cloud is needed for correct description of the fluid dynamics of a combusting fuel spray. In literature this is referred to as the micro-structure of the spray. As mentioned, the resulting droplet cloud is spread over a range of droplet sizes. By measuring this droplet size distribution a probability density function over the droplet diameters can be obtained. Theoretical prediction of this probability density function is a difficult task. Several methods are described in literature, a good overview can be found in the article of Babinksi and Soyka [99]. Methods used for obtaining a droplet size distribution function are either empirical or theoretical. The first basically comes down to a curve fitted through a set of experimental data. The theoretical path involves two methods:

- The maximum entropy(ME) method.
- The discrete probability function(DPF) method.

Naturally the theoretical methods are interesting for engineering and design purposes, as no experimental work is needed for constitution of a droplet size distribution function. However, the theoretical methods do need verification with experimental data, as is clearly shown by Babinsky [99]. Depending on the breakup mechanism either the ME method or DPF method will give the best results. When secondary breakup is the determining factor in the atomization process, the ME method will give the best results, due to the highly stochastic nature of the phenomenon. When primary breakup will determine the shape of the droplet size distribution function, the DPF method is a good candidate. However, as an extra input condition for the calculation, the probability density function of the fluctuating inlet conditions of the atomizer is needed. This makes the DPF model difficult to verify. This thesis will not further focus on the derivation of the droplet size distribution function, but a presumed shape of this function will be applied that is based on empirical data.

Before empirical droplet size functions will be discussed, some attention is given to the statistics that are the basis of these functions. Every spray has a certain amount of droplets N. These droplets vary in diameter as a result of the atomization process, evaporation rates and droplet interaction processes. Due to this, droplets can be divided into diameter ranges, giving the possibility to use statistical description techniques. The total amount of droplets is

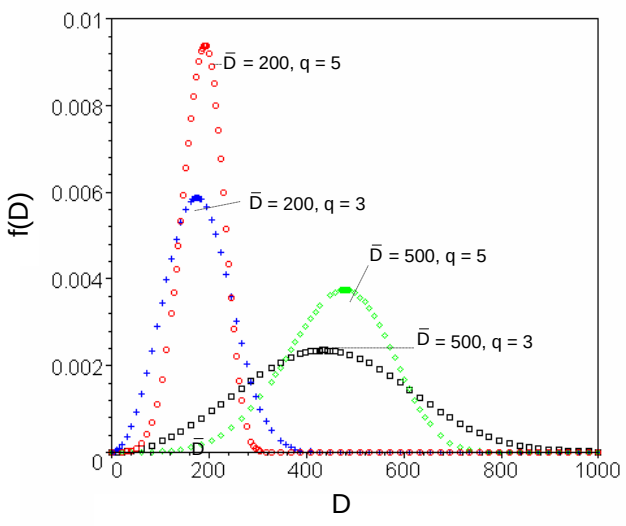

Figure 6.1: The Rosin-Rammler volume distribution function plotted for several values of parameters q [-] and $\overline{D}[\mu\text{m}]$.

given by the following relation:

$$N = \sum_{i=1}^{\text{no.classes}} n_i \tag{6.4}$$

This can be related to a number fraction as follows:

$$\overline{n}_i = \frac{n_i}{N} \tag{6.5}$$

By treating the droplet diameter as a continuous variable and weighting with an infinitesimale droplet size interval, a continuous number distribution function f_n is found:

$$f_n\left(D\right) = \frac{d\overline{n}}{dD} \tag{6.6}$$

Integration of this function from a zero diameter to infinity will yield unity. This droplet number distribution function is proportional to a droplet volume distribution function. For application in combustion processes, the Rosin--Rammler volume distribution function is found to give a good description of the volume distribution of the mass [7, 98]. The distribution is defined according to the following relation:

$$f\left(D\right) = \frac{q}{\overline{D}^q} D^{q-1} \exp\left[-\left(\frac{D}{\overline{D}}\right)^q\right] \tag{6.7}$$

In this equation D is the diameter, q is a parameter depending on the atomization conditions and $\overline{D}$ is a size parameter, characteristic for a spray. An example for some values of q and $\overline{D}$ is shown in figure 6.1. The Rosin-Rammler distribution was used first for pulverized coal particle size distributions [100].

Another volume distribution regularly referred to in literature is the log-normal distribution:

$$f(y) = \frac{h}{\sqrt{\pi}} \exp\left(-h^2 y^2\right) \tag{6.8}$$

This equation defines y which is the log-normal of $D/\overline{D}$, with h as mean standard deviation of y and $\overline{D}$ being the mean drop diameter.

For accurate description of the droplet number distribution, the Nukiyama Tanasawa equation is applied often:

$$f(D) = BD^2 \exp\left(-bd^q\right)$$

Generally, this distribution gives a better fit for experimental data than the first two distributions, due to the number tuning parameters B,b and q. The higher the number of tuning parameters, the better a distribution will be able to fit to a certain experimental data set [101].

Combustion of a liquid fuel spray

When the microstructure of a spray is known, attention can be given to the process of combustion. Literature [16, 102, 103] indicates the following parameters to be relevant to spray combustion:

1. The number of droplets N.
2. The droplet diameter D.
3. The droplet spacing distance S.

The group combustion number G characterizes the spray on basis of these variables as follows:

$$G = 3\left(1 + 0.276\mathrm{Re}^{\frac{1}{2}}\mathrm{Sc}^{\frac{1}{3}}\right)\mathrm{Le}N^{\frac{2}{3}}\frac{D}{2S} \tag{6.9}$$

Based on investigation of these parameters in experiments Chiu*et al.* [103] constructed a diagram characterizing the different types of regimes of droplet combustion that occur in real applications. This diagram is given in figure 6.2. In this diagram typical spray flame regimes are defined as a function of the mentioned parameters. When these parameters are known locally in the flame, an estimation of the droplet density is possible and the relevant combustion regime can be indicated. The given modes in the diagram vary from single droplet combustion to external sheath combustion. When G $\gg 1$, group combustion is the most important mechanism, while for G $\ll 1$, single droplet combustion will occur. Most turbulent spray flames have values of N of $\sim$ o(10^{10}). Together with small droplet radii, very often below 10 μm and small distances between droplets, turbulent spray combustion mainly is located in

the regime of 'external sheath combustion'. Depending on evaporation rates and mixing of oxidizer with the spray, 'external' or 'internal' group combustion is also a possibility in a turbulent spray flame. The difference between the last two possibilities depends on the position of the flame front: respectively outside the spray boundaries or within the boundaries of the spray.

For modelling of turbulent spray combustion, it is not necessary to model the process occurring at single droplet scale. However, a short overview of the process of combustion of a single droplet in a spray flame is discussed.

1. When a fuel droplet gets closer to the flame zone, first its temperature increases because of the surrounding hot gas. Resulting from convection some mass has evaporated.

2. The droplet starts evaporating at a high rate as its temperature approaches boiling temperature. Fuel is transferred into the gaseous phase. Obviously the droplet diameter decreases.

3. The evaporated fuel (mixed with air) ignites and starts to combust. Now depending on the kinetical rates of the chemistry a partially premixed flame is formed around the droplet, that decreases in size.

As detailed modelling of single droplet combustion is a topic that is related to many issues that are beyond the scope of this thesis, it is not discussed in further detail in the thesis. For the work in this thesis modelling of the 'external sheath' and 'external group' combustion regimes are the most relevant.

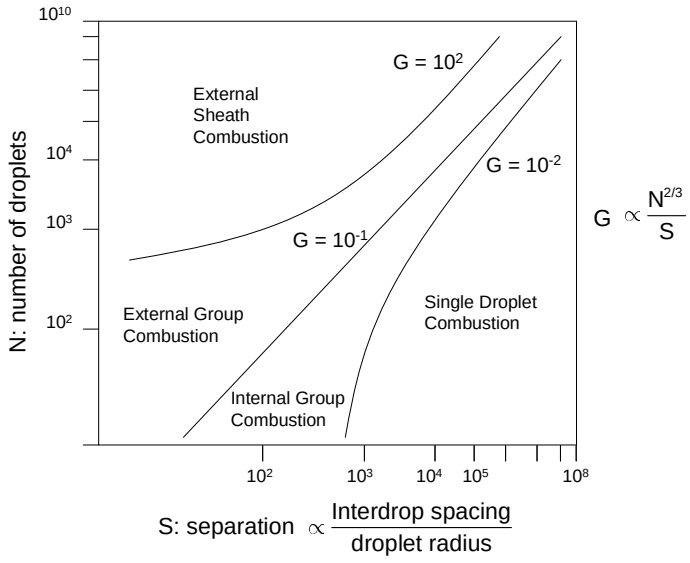

Figure 6.2: Characterisation of spray combustion

6.3 Modelling

In this section the mathematical basis for two-phase flow modelling will be discussed. It starts from basic principles and ends with an overview of how a liquid phase and gaseous phase flow are described and coupled.

6.3.1 Mathematical basis for phase description

The mathematical models for description of a fluid flow fall into two categories: either an Eulerian or a Lagrangian flow description. Shortly, an Eulerian description is given by quantities, such as velocity and density, representing the flow of a fixed volume or parcel of fluid:

$$\boldsymbol{U}_{\text{volume}}\left(\mathbf{x},t\right),\rho_{\text{volume}}\left(\mathbf{x},t\right),\ \text{etc.} \tag{6.10}$$

The Lagrangian formulation describes the changing quantities of a fluid parcel only as a function of time, moving with the flow:

$$\mathbf{x}_{\text{volume}}\left(t\right),\boldsymbol{U}_{\text{volume}}\left(t\right) \tag{6.11}$$

The spatial position vector of a fluid parcel has become a property of the fluid parcel, in contrast to the Eulerian formulation where a fixed coordinate frame is applied.

A two-phase flow model should be a combination of these two approaches. For spray modelling applications, it is most natural to model the gas phase as a continuum and therefore the Eulerian description is used most often. A fully atomized liquid spray however consists of discrete droplets, intuitively hinting the Lagrangian approach as most suitable.

Depending on the applied theory, these droplets are either seen as an independent droplet or as a droplet representing a number of droplets with similar properties. In the latter case, statistical sampling techniques are applied to calculate averaged information for exchange with the gaseous phase. Most spray models for liquid fuel combustion apply the Eulerian formulation for the gas phase and the Lagrangian formulation for spray description. Examples of these models are can be found in many articles [104–107].

A complete direct description of an industrial turbulent fuel spray would involve individual droplet tracking of millions of droplets. Despite the simple equation of motion that has to be solved for a single particle, for millions of particles this will be very costly in terms computational power. Hence, it is attractive to replace this discrete description by a continuous description, an Eulerian description (see for example [108, 109]).

In the Eulerian description the spray phase is seen as a continuum interacting and interpenetrating with the gas phase continuum. To model the spray as a continuum, equations should be derived by averaging over a certain volume, consisting of gas and liquid. The book of Sirignano [105] gives a good overview and derivation of continuity and momentum equations for two-phase flows, based on this volume averaging principle. This so-called

two-continua description of a flow can be extended to multi-continua methods when the dispersed phase is divided in classes, such as initial size or velocity [110]. Based on more stringent statistical averaging methods, Zhang and Prosperetti [111, 112] present a similar theoretical basis for the two-continua approach. Several other authors have published on two-continua methods [113, 114].

The advantage of an Eulerian description is that both phases can be described with the standard transport equations and source/sink terms can account for interaction between the liquid and the gas. Computational times required for solving a turbulent spray problem are much lower than for a Lagrangian approach. However, in order to describe the poly-disperse nature of fuel sprays, modelling is needed. Next to that, effects of turbulence-particle interactions, particle-particle interactions need to be modelled as well. In a Lagrangian context these phenomena can be taken into account more straightforward. A recent article of Loth [115] discusses the various possibilities either application of Euler/Euler models or Euler/Lagrange models.

Another possibility for the calculation of a turbulent spray is via the route of a probability density function (PDF). This is based on a probabilistic formulation that adheres to the stochastic nature of turbulent sprays. The basis of most of the work published on the prediction a PDF for a spray is the work done by Williams [116]. He proposes a *spray equation* that defines a probable number of droplets f_j as in a certain diameter range as a function of space, time, velocity and diameter. The full function for the development of f can be reconstructed using particle methods. A good example and theoretical outline of this method is given in the thesis of Naud [117].

6.3.2 Timescales and phasic interaction

Depending on the nature of the spray and gas phase, a certain amount of coupling between the spray and the carrier gas is needed for correct modelling. When one phase is completely determined by what happens in the other phase, so-called *one-way* coupling is sufficient for modelling the interaction between the phases: the flow field of the dependent phase is a direct result of the flow field for the dominant phase. This level of coupling is sufficient when the volume fraction of the liquid is very small ($\theta_p < 10^{-6}$)

When two phases do have mutual influence, eg. the liquid phase has a higher volume fraction ($10^{-6} < \theta_p < 10^{-3}$) or turbulence created by particles has an influence on the flow field of the surrounding gas, two-way coupling should be applied. That way the effects of the two phases on each other are taken into account.

Four-way coupling is desired when particles directly influence behaviour of neighbouring particles, (eg. collisions, coalescence, secondary breakup) and in this manner influence the surrounding phase. Modelling four-way coupling effects is especially important when the spray is dense ($\theta_p > 10^{-3}$), for example in the region nearby the fuel injection nozzle. An overview of the mutual dependence of the phases in the case of a turbulent dispersed flow is given in figure 6.3.

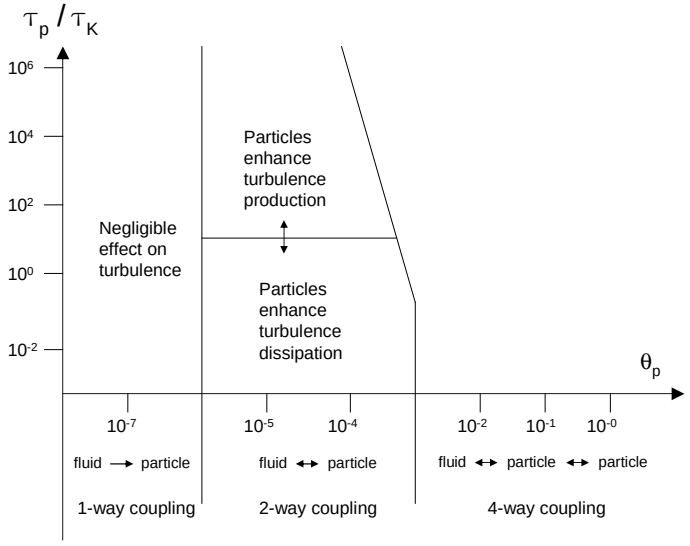

Figure 6.3: Coupling between a spray and gas as a function of the particle relaxation time, turbulence time scale and volume fraction of the spray [114]

.

In a turbulent fuel spray, where $\rho_g \ll \rho_l$, the drag exerted on a particle by the fluid is the most important mechanism for phasic interaction. Other effects, such as the so-called 'jet-propulsion' effect due to evaporating fuel at the surface of the droplet are neglected in this thesis [105].

To study the phasic interaction for impulse, the Stokes number St is introduced as a measure for the influence of the spray on the gaseous flow and vice versa. This number can either be defined on a macroscopic scale or on a microscopic scale, the scale of the smallest turbulent eddies. In the first case, the number indicates how much a particle is influenced by the mean flow. The latter case is a measure for the influence of smallest turbulent eddies on the dispersion of the particles. The Stokes number is defined by:

$$\mathrm{St}_{int} = \frac{\tau_p}{\tau_{int}} \tag{6.12}$$

In equation 6.12, τ_p is the particle relaxation time and τ_{int} is the integral time scale of turbulence. The Stokes number with the Reynolds particle number allow the interaction of the continuous phase and liquid phase to be described:

$$\mathrm{Re} = \frac{\rho_g \left| \boldsymbol{U}_g - \boldsymbol{U}_l \right| D}{\mu_g} \tag{6.13}$$

When $\mathrm{Re} \rightarrow 0$, the flow around the particle is considered to be creeping and the particle relaxation time is defined as follows:

$$\tau_p = \frac{\rho_p D^2}{18 \mu_g} \tag{6.14}$$

This timescale is a measure for the time needed for a particle to respond to a change in the instantaneous velocity field of the gaseous phase by the acting forces resulting from Stokesian drag. Relevant parameters in this equation are the density ρ_p of the particle and its diameter D, the dynamic viscosity of the gas μ_g. When Re is higher, a correction factor f is introduced. This correction factor is defined as:

$$f = \frac{C_D \mathrm{Re}_p}{24} \tag{6.15}$$

Now for a Stokes number smaller than unity the particle will act as a passive tracer and follows instantaneous fluctuations readily. When St $\gg 1$, the particle will follow the mean gaseous fluid convection much better.

6.4 Combusting fuel spray models in literature

This section gives a short overview of recently developed combusting spray models. Schmehl [118] proposes a hybrid approach between a simple Eulerian spray model and a Lagrangian model, where the Eulerian description is used to precondition the Lagrangian equations. This combined approach shortens computational times, but still benefits from the Lagrangian amount of detail. Results obtained look promising. Klose [119] uses this approach and combines it with a Joint-PDF combustion model.

In contrast to the previous authors, Guo et al. [120] use a simple Eulerian description for the fuel spray and combine it with a simple mixing rate dependent combustion model. For the spray number density and bulk density transport equations are solved. The predictions of a experimental combusting kerosene spray are reasonable. The authors mentioned previously, all consider steady state evaporating and combusting sprays, using relatively simple turbulence models, such as the k-ϵ-model.

Sankaran and Menon [109] used Large Eddy Simulation (LES) for the description of a non-stationary turbulent combusting turbulent spray under gas turbine conditions. Together with a Lagrangian technique for the description of the liquid phase and a simple combustion model, they investigated the effects of swirl intensity and heat release on the droplet dispersion and the flow pattern.

Evaporation of the fuel spray is modeled with classical single droplet evaporation models in all cases. These are either Ranz-Marshall [121] correlations or the D^2-law as formulated by Spalding [122]. Several fundamental aspects of droplet evaporation will be discussed in detail further on in the chapter.

6.5 The Beck & Watkins spray model

Based on the work of Beck and Watkins [123–125], in this thesis a spray model is proposed that uses statistical properties of sprays to describe the liquid and gas phase both in an Eulerian way. The key idea of this model is that it is possible to describe a polydisperse spray by the use of moments of a droplet size or number distribution function. Instead of calculating huge amounts of individual droplet tracks to solve a polydisperse spray or to divide the spray into classes, only Eulerian transport equations for the statistical moments of this droplet size or number distribution function need to be solved. Together

with a presumed shape of the distribution function, a complete description can be given of a real spray. The major assumption of the model is that the spray is statistically stationary.

Statistical moments As said earlier, a volume distribution function is proportional to the droplet number distribution function $n(r)$, describing the distribution of a number of droplets over a range of droplet diameters. When this function is integrated over all droplets (integration over all possible radii) and weighted, the total number of droplets per unit volume is obtained:

$$Q_0 = \int_0^\infty n(r)dr \tag{6.16}$$

The ith moment of the distribution is given by:

$$Q_i = \int_0^\infty r^i n\left(r\right) dr \tag{6.17}$$

The moments as defined by equation 6.17 can be used to classify spray properties by use of characteristic diameters. Often typical diameters are used to characterize different aspects of sprays:

$$D_{pq} = 2^{p-q}\frac{Q_q}{Q_p} \tag{6.18}$$

A frequently used diameter that can be calculated using the liquid surface area and the liquid volume, is the Sauter Mean Diameter:

$$D_{32} = \frac{Q_3}{Q_2} \tag{6.19}$$

It was demonstrated by Chin and Lefebvre [98] that the Sauter Mean Diameter is the most accurate parameter for representation of a combusting liquid fuel. Other useful moments that can be calculated are given by:

- i = 1, the total sum of radii is obtained per unit volume.
- i = 2, the total surface is given, if Q_2 is multiplied with 4π.
- i = 3 and multiplication with $^4/_3\pi$ will give the total volume of the droplets per unit volume.

In a finite volume description, this third moment is related to the liquid volume fraction via the following relation:

$$\frac{V_{liquid}}{V_{cell}} = \frac{4}{3}\pi Q_3 = 1 - \theta \tag{6.20}$$

In equation 6.20 a new variable θ appears: the gas volume fraction. This volume fraction is determined by the fourth moment of the normalized spray distribution function and the local volumes V of the gas and liquid.

6.5.1 Averaged equations for the liquid phase

In this section the liquid volume fraction $1-\theta$ as defined by 6.16 will be related to an Eulerian transport equation. This constitutes the basis for the Eulerian formulation of the other spray properties. The general idea is that there exists a moment average quantity Φ:

$$\Phi_i = \frac{1}{Q_i} \int_0^\infty r^i n(r) \Phi dr \tag{6.21}$$

The moment averaged quantity can be a mass-average velocity for example, when knowledge of the development of net convection of liquid mass is desired. Beck & Watkins [123–125] show that a transport equation for the fourth droplet moment resembles a liquid-phase continuity equation. Their approach is to start from a multi-size Eulerian treatment transport equation for a droplet group k with a certain number of droplets. Extending this equation to a formulation in which the droplet number distribution function is incorporated, effectively a transport equation is found for liquid-phase continuity:

$$\nabla \cdot (\rho_l \boldsymbol{U}_l (1-\theta)) = -S_m \tag{6.22}$$

In this equation the RHS is governed by interfacial mass transfer due to evaporation. Using a similar procedure the mass-average liquid momentum transport equation is derived:

$$\nabla \cdot (\rho_l (1-\theta) \boldsymbol{U}_l \otimes \boldsymbol{U}_l) - \nabla \cdot (\rho_l (1-\theta) \sigma_v D_{T,gas} \nabla \boldsymbol{U}_l) = -S_U - S_m \boldsymbol{U}_l \tag{6.23}$$

The RHS of this equation describes the influence of both momentum transfer by drag force and loss of momentum due to evaporation, but of course other effects (lift force, gravity etc.) also could be taken into account in this term.

Using equations 6.22, 6.23 it is a simple step to an Eulerian description of the two-phase flow system of a spray: having θ as a multiplier for the gaseous phase equations and $1-\theta$ for the liquid phase transport equations, a system with a total volume fraction equaling 1 is described.

The general moment transport equation for Q_i is given by Beck & Watkins as well:

$$\nabla \cdot (Q_i \boldsymbol{U}_i) = S_{Q_i} \tag{6.24}$$

Liquid surface-area A surprising element in equation 6.24 is the moment-average velocity $\boldsymbol{U}_i$, as it was already found for the mass-average momentum transport equations 6.23. For the transport equation of the average surface-area this will give a surface-area average convection velocity. Beck & Watkins state that similar to net mass convection, also this surface-area average convection velocity is important. These different liquid phase velocities do not necessarily have to be the same: larger droplets (more mass) experience less drag and have higher velocities than smaller droplets. This gives a higher

mass-average velocity compared to the surface-area-average velocity. Not only this is valid for moment-average velocities but also for other moment-average quantities, such as energy: for example small droplets heat up faster than large droplets. However, regarding the work done in this thesis, the mass-average convection velocity is used for transport of the surface-area Q_2:

$$\nabla \cdot (\rho_l \boldsymbol{U}_l (1-\theta) Q_2) - \nabla \cdot (\rho_l (1-\theta) \sigma_v D_{T,gas} \nabla Q_2) = S_{Q_2} \tag{6.25}$$

Independent transport of liquid-surface-area average momentum gives the development of the spray an extra degree of freedom: it is now possible for the presumed size distribution function to change as function of the solution to the net liquid mass and liquid surface area average, in that way taking account of poly-disperse spray effects.

Liquid enthalpy Assuming that the temperature of the droplets is independent of the size of the droplets and that the enthalpy is convected at mass average velocity, the transport equation for the enthalpy of the spray is defined as follows:

$$\nabla \cdot \rho_l \boldsymbol{U}_l (1-\theta) h_l - \nabla \left(\rho_l (1-\theta) \sigma_v D_{T,gas} \nabla h_l\right) = -S_{h_l} - h_l S_m \tag{6.26}$$

The RHS describes the effects of evaporation and heat up of the liquid spray due to heat transfer.

Turbulence All transport equations given so far are valid for a stationary spray and are Reynolds averaged. Turbulent dispersion of droplets and turbulent diffusion of the liquid is modelled using a so-called zero equation turbulence model, based on the modelling of turbulence in the gaseous phase. From the gaseous phase an eddy viscosity should be obtained and multiplied with a turbulence dampening coefficient σ_v of 0.7, giving the eddy viscosity of the liquid phase [126, 127].

6.5.2 Favre averaged equations for the gas phase

The transport equations for the gaseous phase yield the same form as the standard Reynolds averaged Navier-Stokes (RaNS) equations for gaseous flows, but all variables are multiplied with the volume fraction θ of the gaseous phase. Gas phase continuity should therefore be obtained by :

$$\nabla \cdot (\rho_g \theta \boldsymbol{U}_g) = S_m \tag{6.27}$$

The RHS of this equation is given by the interfacial mass transfer due to evaporation. Transport of momentum in the gaseous phase is given by the equation:

$$\nabla \cdot (\rho_g \theta \boldsymbol{U}_g \otimes \boldsymbol{U}_g) - \nabla \cdot \left(\rho_g \theta D_T \left(\nabla \boldsymbol{U}_g + \nabla \boldsymbol{U}_g^T\right)\right) = S_U + S_m \boldsymbol{U}_l \tag{6.28}$$

Momentum transfer between the phases due to the drag force is taken into account by S_U. Mass transfer due to the increase of momentum by vaporisation

of liquid, having the liquid velocity, is taken into account with the secondary fluxes yields $S_m \boldsymbol{U}_l$.

In this thesis a standard two-equation k-ϵ turbulence model is applied [128]. This model employs two scalars to calculate a turbulent viscosity. The first variable is the total turbulent kinetic energy of the flow k, transported by the vapour phase according to:

$$\nabla \cdot (\rho_g \theta \boldsymbol{U}_g k) - \nabla \cdot (\rho_g \theta D_T \nabla k) = \theta G_k - \theta \rho \varepsilon \tag{6.29}$$

The 2^{nd} variable is the dissipation of turbulent energy ϵ according to:

$$\nabla \cdot (\rho_g \theta \boldsymbol{U}_g \varepsilon) - \nabla \cdot (\rho_g \theta D_T \nabla \varepsilon) = \theta \left(C_1 G_k - C_2 \rho \varepsilon\right) \frac{\varepsilon}{k} + \theta C_{\varepsilon 3} \rho_g \varepsilon \nabla \cdot \boldsymbol{U}_g \tag{6.30}$$

The RHS of equations 6.29 and 6.30 contain the turbulent kinetic energy production rate G_k that is given by the next relation:

$$G_k = \rho_g C_\mu \frac{k^2}{\varepsilon} \nabla \boldsymbol{U} \cdot \left(\nabla \boldsymbol{U} + \nabla \boldsymbol{U}^T\right) \tag{6.31}$$

The turbulent kinetic energy and dissipation are used to calculate an effective eddy viscosity μ_T for the gas phase. This eddy viscosity is used in the closure for the turbulent fluxes. The well-known gradient diffusion hypothesis is applied for this turbulent fluxes, given in a general form for a transported variable ϕ:

$$\nabla \cdot \left(\overline{\rho_g \boldsymbol{u}' \phi'}\right) = \nabla \cdot \left(\rho_g \frac{\mu_T}{\mathrm{Pr}_T} \nabla \phi\right) \text{ with } \mu_T = C_v \frac{k^2}{\varepsilon} \tag{6.32}$$

In this equation Pr_T is the turbulent Prandtl number that is defined as a constant throughout this thesis.

In chapter 2 the transport equations for the (normalised) enthalpy and the fuel vapour (mixture) fraction were already presented and discussed. Also the reaction progress variable transport equation was given in that chapter. Combination with the spray model will not alter the definition of these equations.

6.5.3 Spray-gas interaction

Knowing the mean properties of the spray and the gas phase, it is possible to calculate moment averaged phase interaction by integration over the presumed shape of the droplet number distribution function. Source terms for the interaction between the two phases are calculated per unit volume according to the following general relation for a variable ϕ:

$$S_\phi = \int n(r) \frac{D\phi}{Dt} dr \tag{6.33}$$

Momentum The dispersed phase is exchanging momentum with the gas phase mainly due to drag. Assuming spherical particles, the force acting on a single droplet can be described as follows:

$$\frac{D\boldsymbol{U}}{Dt} = \frac{3}{8} \frac{\rho_g}{\rho_l} \frac{|\boldsymbol{U}_{relative}|}{r} C_d \boldsymbol{U}_{relative} \tag{6.34}$$

For the drag coefficient C_d several models exist in literature. From these models the correlation of Wallis [129]is used here:

$$C_d = 0.424 \quad Re_{particle} > 1000 \tag{6.35}$$

$$C_d = 24\left(\frac{1}{Re} + 0.15Re^{-0.313}\right) \quad Re_{particle} < 1000 \tag{6.36}$$

The particle Reynolds number is defined according to equation 6.13. This number is proportional to the relative velocity and the droplet radius. Other mechanisms of momentum exchange (like added mass, lift force, gravity) between the phases are considered negligible compared to drag. Integration of equation (6.34) using equation (6.33) the source term for the dispersed phase momentum yields:

$$S_{\boldsymbol{U}_l} = 6\pi\mu_g \boldsymbol{U}_{rel} Q_1 + 1.8\pi \left(\rho_g \left|\boldsymbol{U}_{rel}\right| Q_2\right)^{0.687} \left(\frac{\mu_g Q_1}{2}\right)^{0.313} \boldsymbol{U}_{rel,j} \tag{6.37}$$

Mass Starting with the well-known model by Spalding [122] droplet evaporation can be calculated from:

$$d^2(t) \quad = \quad d_0^2 - Kt \qquad \text{with } K \equiv \frac{8\lambda_g}{\rho_l c_{p,g}} \ln[1+B] \tag{6.38}$$

This formulation is often referred to as the D^2 law and is valid when equal Lewis numbers are assumed and the thermal conductivity λ, specific heat c_p and ρ_l are independent of the interior droplet temperature. In the above equation, B is the Spalding mass transfer number. This number accounts for mass transfer effects related to combustion and evaporation in the film between the liquid phase and the gaseous free field. For evaporating droplets, B is defined as follows:

$$B = \frac{Y_{surface} - Y_\infty}{1 - Y_{surface}} \tag{6.39}$$

From equation 6.38 an evaporation rate can be formulated easily, this mass flow is given by:

$$\dot{m} \quad = \quad \frac{2\pi\lambda_g d}{c_{p,g}} \ln[1+B] \tag{6.40}$$

This equation shows that the evaporation rate is strongly dependent on the properties of the surrounding gas and the diameter of the droplet. Fuel parameters only have a minor influence on this rate via the Spalding number. Convective and turbulence effects from the surrounding flow on droplet evaporation are not taken into account by this equation. In spray combustion this can be done by the use of dimensionless numbers that can be found in literature*.

*A well-known example of these corrective correlations are the Ranz-Marshall correlations that were derived for evaporating water drops in a turbulent flow [121].

Therefore in a more general form the mass flow rate can be expressed using the Sherwood number Sh, that may incorporate convective effects on the evaporation rate:

$$\dot{m} = \pi d \left(\frac{\lambda}{c_{p,g}} \right) Sh \tag{6.41}$$

Depending on the situation correlations for the Sherwood number Sh can be used. For example, when droplets are non-moving and the flow is considered quiescent, Sh equals 2. However, in a turbulent spray this is not true. A model to account for this is based on the Spalding mass transfer number:

$$\mathrm{Sh} = 1 + \ln(1 + B) \tag{6.42}$$

This correlation has proved to be successful for the calculation of evaporating sprays in the context of the described spray model [124] and will therefore be used in this thesis[†].

Knowing an expression for Dm_l/Dt the droplet number distribution integrated source term is given by:

$$S_m = 4\pi \left(\frac{\lambda}{c_p} \right)_g Q_1 \ln(1 + B) \tag{6.43}$$

The given equations were determined for single component evaporation. When looking at oil combustion, this is clearly not the case, as refined liquid products often contain several components that all have different evaporation temperatures. This should be accounted for with a multi-component fuel evaporation model. Note that the Spalding model does not contain specific fuel properties and therefore can easily be used for a multicomponent fuel spray. Some authors have tried to model this with the use of 'representative' single fuel [130]. With this single fuel model, the most important characteristics of the multicomponent fuel are taken into account. Catoire *et al.* however showed that it is also possible to implement a multi-component fuel evaporation model, performing more physical than the 'representative' fuel model, by allowing differentiation in evaporation rates.

Energy Energy transfer between the phases is defined by a simple balance. This balance is defined by the heat needed for evaporation and heat-up of droplets and the heat loss from the gas phase. For a single droplet the following relation can be stated:

$$Q_{heatup} - Q_{evaporation} = 2\pi r \lambda_g \left[Nu(T_g - T_l) - Sh \frac{L}{c_{pg}} \right] \tag{6.44}$$

[†]Use of the Ranz Marshall correlations will yield the following equations:

$$Sh = 2(1 + 0.3 Re^{\frac{1}{2}} Sc^{\frac{1}{3}})$$

This correlation is proposed by Ranz and Marshall with the turbulent Schmidt number defined as follows:

$$Sc = (\frac{\mu}{\rho D_{km}})_{gas}$$

.

Similar to the mass transfer models discussed, there is an expression needed for the definition of the Sherwood number and the Nusselt number. The Nusselt number can be defined as a function of the Spalding number as follows[‡]

$$\mathrm{Nu} = 2\frac{\ln(1+B)}{B} \tag{6.45}$$

Assuming a quasi-steady state and using equation 6.33, the integrated enthalpy source term for spray heat-up and evaporation reads as follows:

$$S_h = -4\pi\lambda_g \left(T_g - T_l - \frac{L}{c_p}\right) Q_1 \ln(1+B) \tag{6.46}$$

This expression for the energy exchange between te spray and the gas phase is valid only when the droplets are not at their boiling point.

Liquid-surface area The change in liquid-surface area is a function of both spray kinetics and evaporation. In this thesis only evaporation is considered. The change in liquid-surface area can be related to the flux of mass $\dot{m}$ via the radius of a droplet:

$$\delta m = \rho_l 4\pi r^2 \delta r \tag{6.47}$$

The change in the square of the radius is calculated as:

$$\delta r^2 = 2r\delta r \tag{6.48}$$

Combining these two equations and substituting equation 6.41 and 6.42 yields:

$$\frac{\partial(r^2)}{\partial t} = \frac{2}{\rho_l}\left(\frac{\lambda}{c_p}\right)(\ln(1+B)) \tag{6.49}$$

Change of surface area is now governed by the following source term, found after integration of equation 6.49 according to the above given definition of equation 6.33:

$$S_{Q_2} = \frac{2\lambda}{\rho_l c_p}\ln(1+B)Q_0 \tag{6.50}$$

6.5.4 Kinetic spray effects

The model of Beck & Watkins allows to take into account changing spray properties due to effects such as secondary breakup and collision of droplets. This will effectively give a change in the liquid-surface area. Modelling of these effects have been described in the work of Beck & Watkins [123]. Both the secondary breakup model and the collision model take into account the various possibilities of the effects, such as bag breakup, surface wave breakup and stripping breakup, coalescence, bouncing droplets and separation.

[‡] Again it is also possible to use Ranz-Marshall correlations giving:

$$\mathrm{Nu} = 2(1 + 0.3Re^{\frac{1}{2}}\mathrm{Pr}^{\frac{1}{3}})$$

6.6 Modelling of a simple jet spray

The discussed theory and the presented equations from the last sections have been implemented in the CFD code ANSYS CFX. The next chapter will discuss this implementation more precisely. The results of a simple jet spray simulation are briefly discussed. This simulation was performed to test and validate the possibility of the suggested modelling. Results are presented in appendix D. The results obtained with implementation of the spray model are compared with the results obtained with a Lagrangian description of the spray. From these results it can be concluded that the approach gives good results and is suitable for use with a commercial CFD package. Comparison with the CPU time consuming Lagrangian method is rather good. Further validation against experimental data in swirled sprays will be beneficial for reliability.

6.7 Conclusions

After a general overview of theory for turbulent two-phase flows, a simple Eulerian model has been suggested for the description of the statistics of a dilute turbulent spray. The model should be capable of incorporating the effect of a distribution of droplet diameters over a certain range. This is done via a presumed shape of the droplet size distribution function. Application of the model to a simple non-reacting, non-evaporating jet spray shows that the model is capable of simulating essential features of a spray, such as the Sauter Mean Diameter and liquid velocities.

7

Simulation of a combusting methanol spray

Applying a combination of the models of chapters 2 and 6, a combusting methanol spray is simulated. Results from the simulations are compared to experimental data.

7.1 Introduction

In the previous chapter a model has been presented that is able to describe the development of a spray in a stationary flow. This model is coupled to the combustion model as presented in chapter 2. With this combination a combusting spray can be simulated. This chapter is divided in three parts. First an experimental setup used by Widmann *et al.* [1, 2] will be introduced and explained. Then an overview is presented of the work on the combined models from chapters 2 and 6. As a start an isothermal spray is simulated. The results of this are compared to measured non-reacting spray data. This is followed by the description of the CFI combustion model database, that is generated for non-premixed, non-adiabatic methanol combustion. With this database the reacting spray is simulated. After a discussion of the results, the chapter ends with conclusions.

7.2 Experimental setup

A spray flame in literature is found in the work of Widmann *et al.* [1, 2]. The spray flame presented in their work is meant to be a benchmark for combustion modelling efforts. In their papers measurement data of a simple enclosed methanol spray is presented. Figure 7.1 shows a photographic impression of the flame. In these photographs the shape of the flame is seen clearly: a hollow cone spray flame.

Methanol is directly injected into a combustion chamber, where swirling air enters through a co flowing channel. The injection of methanol is done with a simple pressure jet atomizer operating at an injection pressure of 690 kPa. The atomized methanol forms a hollow cone spray with a nominal angle of 60°. The nominal methanol mass flow was set to 3 kg/hr. The swirling air enters the combustion chamber by means of a radial swirler with 12 adjustable vanes. In total 56.7 m^3/hr of air is fed to the system. The pressure

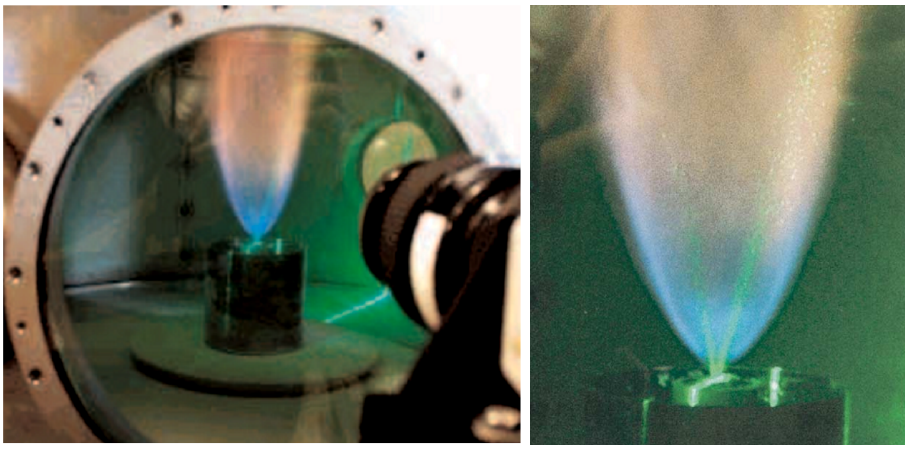

(a) From behind the window (b) Close up of the flame

Figure 7.1: Photographs of the burning methanol spray, from [1]

in the combustion chamber is equal to ambient pressure. Altogether, this constitutes a non-premixed, prevaporized spray flame operating at atmospheric conditions.

The flame is operated in a combustion chamber with a height of 1245 mm and a diameter of 813 mm. For optical access two windows have been constructed in the chamber. The exhaust gases leave the combustion chamber via a radially mounted tube with a diameter of 407 mm.

The measurement data available can be separated into two parts: a set with non-reacting data and a set with reacting data. These data were obtained using laser diagnostic tools. For the fuel spray measurements a Phase Doppler interferometry (PDI) system was used. The velocity field of the gaseous phase was analysed using Particle Image Velocimetry (PIV) techniques. At the exhaust, species concentrations were measured with a Fourier transform infrared spectroscopy analyser, using an air cooled probe. The temperature at the exhaust was measured using thermocouples.

7.3 Modelling overview

In this chapter the modelling approach for combustion as presented and applied in the previous chapters 2-4 is combined with the spray model from chapter 6. This gives a set of equations that provides a framework for the modelling of combusting sprays. The variables that govern the solution of a combusting spray with the adopted formulation are presented in table 7.1. The commercial CFD package ANSYS CFX is used for the solution process of the governing transport equations. Several important properties of both the gaseous and liquid phase are calculated using the CFI thermochemistry database and the spray model. An overview of these properties is listed in table 7.2. Figure 7.3 presents a diagram in which the two models and the re-

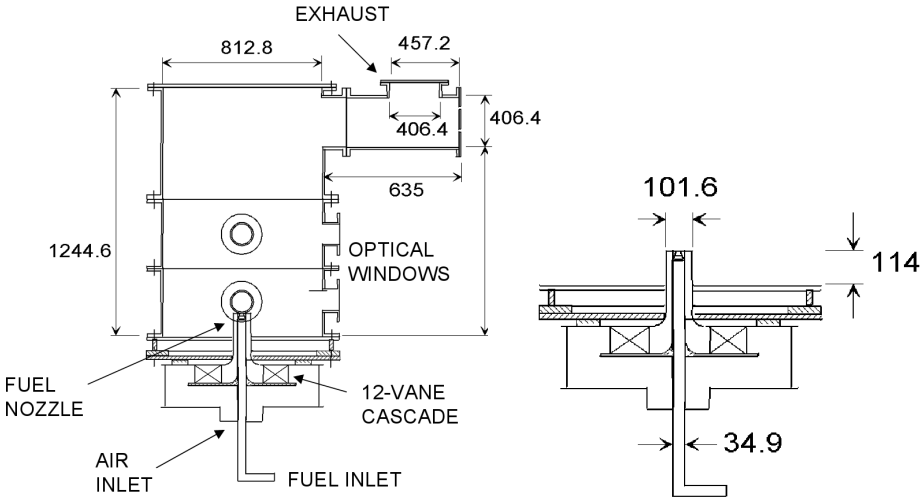

(a) The combustion chamber (b) The burner

Figure 7.2: Drawing of the experimental setup [1], dimensions in mm

Gas	
Velocity	$\boldsymbol{U}_g$
Volume fraction	θ
Pressure	p
Reaction progress (and variance)	c, c''^2
Mixture fraction (and variance)	f, f''^2
Enthalpy Scalar	i
Turbulent Kinetic Energy	k
Dissipation of k	ε
Spray	
Velocity	$\boldsymbol{U}_l$,
Volume fraction	$(1-\theta)$
Number averaged spray surface	Q_2
Enthalpy	h

Table 7.1: Variables in the combined model for which the CFD solver is used.

lations are presented. The interaction arrows between the gaseous phase and the liquid phase indicate whether the process is described by user defined routines or that ANSYS CFX provides the interface. Heat and mass transfer between the two phases is calculated with in-house FORTRAN 77 developed routines, according to the transfer models presented in chapter 6. Momentum exchange is calculated by ANSYS CFX, with the provision of the interfacial area by the spray model. The turbulence of the gas phase is modelled with the standard version of k–ε, as implemented in ANSYS CFX.

7.3.1 Computational domain

The computational domain is chosen to be an axial slice of 10°, assuming that the flow is axial symmetric and that the influence of the exhaust is minor on the axial symmetry. A mesh of 938,851 tetrahedral elements was constructed. The regions close to the nozzle and the inlet contain the smallest elements, with a grid size of 0.5 mm. Gradually the element size is enlarged toward grid sizes of 0.1 m. Figure 7.4 shows the mesh at one side of the fluid domain. On this unstructured mesh all transport equations are solved with a so-called 'high resolution' discretization scheme. This scheme switches between the second order central differencing scheme and the first order upwind scheme depending on the local Courant number.

7.3.2 Inlet conditions

Air The combustion air inlet conditions have been set to the measured velocity profiles as given in [1]. Provided are two sets of profiles: one observed without a flame and one set observed with a flame.

Methanol The nozzle is modelled as a hole with a radius of 0.1 mm. This radius was obtained using a simple mass conservation relation [98]:

$$\dot{m} = \mu_{\text{discharge}} A_0 \sqrt{2\rho\Delta P} \tag{7.1}$$

Using the atomizer pressure of 689 kPa, the density of methanol, an assumed discharge coefficient for the atomizer of 0.5 and the specified methanol mass flow of 8.33 10^{-4} kg/s, this yields a nozzle diameter 0.1 mm. For methanol this is a reasonable diameter, as the viscosity of methanol is low. The applied relation yields an inlet velocity of 26.7 m/s for the spray. This velocity corresponds to the velocities as measured just downstream the nozzle. Using the available experimental inlet data for the spray, tables are generated for the actual inlet velocities of the spray.

Gas	
Temperature	T_g
Specific heat	$c_{p,l}$
Thermal conductivity	λ_l
Density	ρ_l
Spray	
Temperature	T_l
Specific heat	$c_{p,l}$
Thermal conductivity	λ_l
Density	ρ_l
Average number of droplets	Q_0
Average droplet radius	Q_1

Table 7.2: Variables in the combined model that are solved via algebraic relations or tabulated.

7.3.3 Near nozzle modelling

As known, the flow just after the fuel injector is very complex and many phenomena occur that need addressing in models. One essential problem is a correct prediction of the drag force between spray droplets and the gas flow. In the proposed model simple drag coefficient relations (6.36) are used that are valid for a single droplet or a dilute spray. However in the region near the nozzle, the model is likely to fail and preliminary simulations have shown this. In the region where the atomized liquid just enters the combustor, many processes occur that cannot be described by assuming a dilute spray. The liquid is still mainly in the form of a thin sheet [98]. When this is the case, the outer surface of the spray is not defined by the sum of individual droplet surfaces. However, the spray model in present formulation does assume single droplets and does not account for the actual topology of the spray. For the work done in this chapter, a method is used to fill this gap in the model. The method is based on the local volume fraction of the spray. When the local

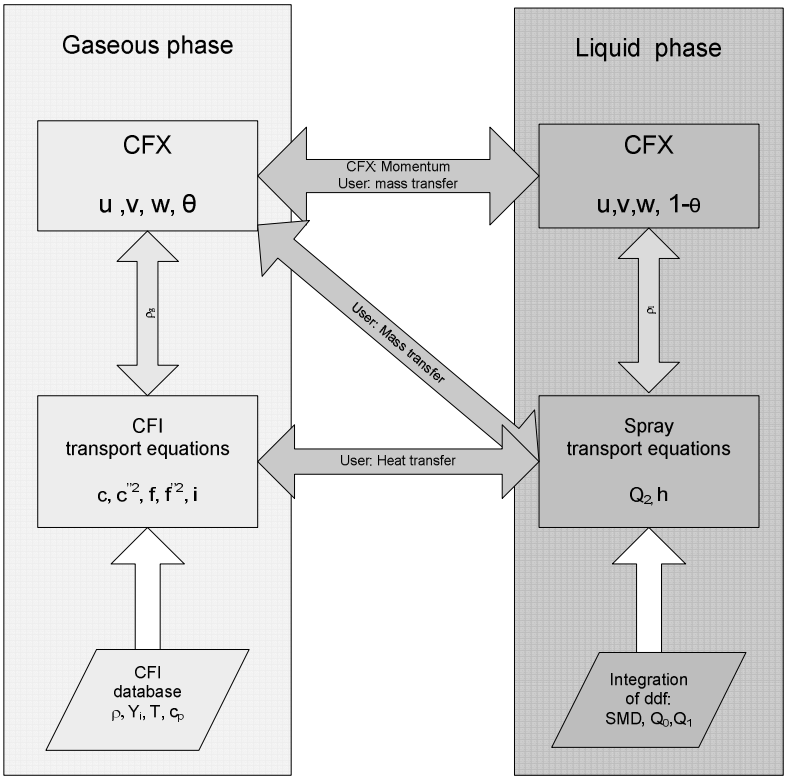

Figure 7.3: Schematic representation of the implementation of the combined spray combustion model.

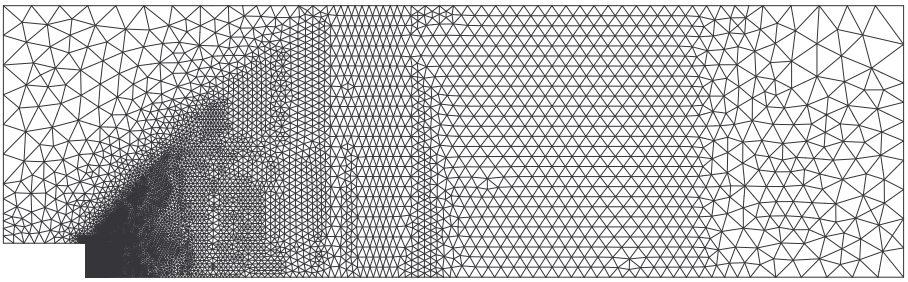

Figure 7.4: Sideview of the unstructured mesh, 10°slice modelled.

volume fraction is high and the corresponding mass load of the spray is high:

$$\eta_{ml} = (1 - \theta)\,\frac{\rho_l}{\rho_g} \tag{7.2}$$

the spray is assumed to have the form of a thin sheet that has not been fully atomized yet. Assuming the spray to be a thin sheet reduces the available interfacial area for the exchange of momentum.

7.4 Iso-thermal simulation

Results obtained for the non-evaporating spray are presented in this section. The experimental data is split into gaseous phase measurements and spray measurements. From the gaseous phase the available data consists of radial mean velocity fields at two axial locations. For the liquid phase, the mean axial and radial velocities are measured at several axial locations.

7.4.1 The gaseous phase

A comparison between the velocities of the combustion air as calculated by the model and as measured is shown in figures 7.5-7.7. In these figures the velocities along radial traverses at two axial locations are plotted. Overall the comparison between the measurement data and the model results is good. However, at small radii, close the center of the combustor, the comparison is not very accurate. The model overpredicts the axial and radial velocity for the combustion air at small radii. It is expected that combustion air is entrained slightly in regions close to the fuel nozzle and resulting in an acceleration of the combustion air. In this case the measurements do not show an acceleration of the combustion air and the measured profiles give the impression that there is no spray present at all. A reason for this can be the fact that it is a difficult task to measure velocities of a gaseous phase in a region where a dispersed phase is present in high concentration. Although not plotted in the figures, the measurement uncertainty is not so large according to the experimentators. This suggests that there were no difficulties in measuring the right velocity data of the gaseous phase. However, the measurement data violate conservations of mass, while the computational model conserves mass. This indicates an error in these data near the axis. When the turbulent kinetic energy

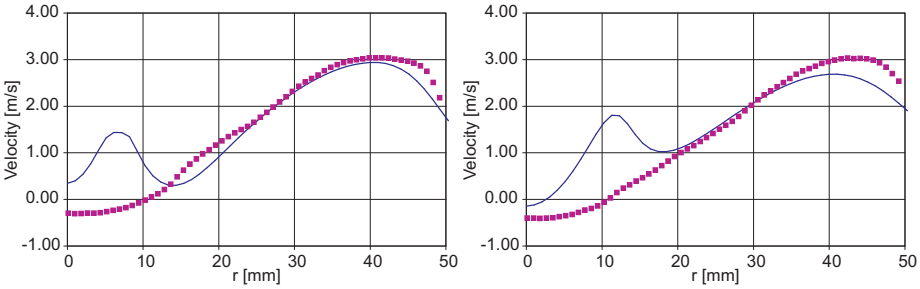

(a) z = 9.5 mm (b) z = 17.5 mm

Figure 7.5: Cold flow, axial velocities of the combustion air. (Lines: model, dots: experiment)

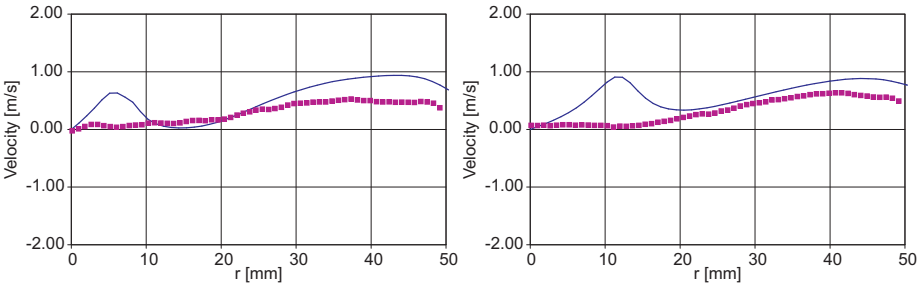

(a) z = 9.5 mm (b) z = 17.5 mm

Figure 7.6: Cold flow, mean radial velocities of the combustion air. (Lines: model, dots: experiment)

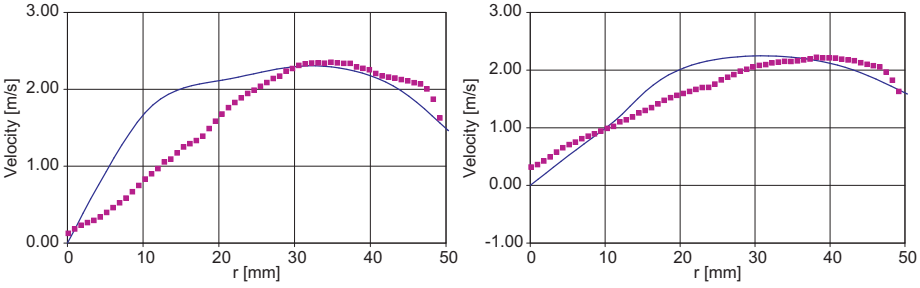

(a) z = 9.5 mm (b) z = 17.5 mm

Figure 7.7: Cold flow, mean tangential velocities of the combustion air. (Lines: model, dots: experiment)

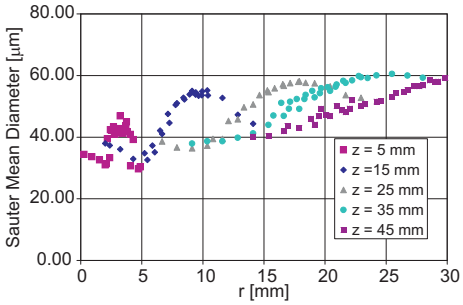

Figure 7.8: The Sauter Mean Diameter of the spray at several axial positions.

is calculated according to a summation and quadratation of the fluctuating components, it is found that the model agrees well with the measured turbulent kinetic energy. This is shown in figure 7.9. The small saddle points and peaks in the measurements are not seen in the model data. The slight overprediction of the turbulent kinetic energy of the flow at the lower radii is due to the fact that the influence of the spray on the gas velocities is overpredicted, as was seen in the comparison of the velocities.

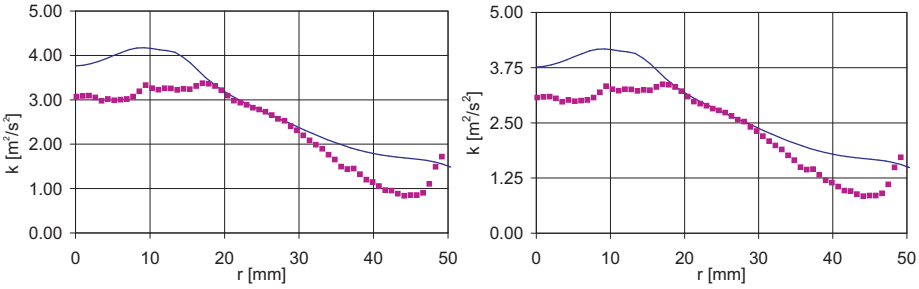

(a) z = 9.5 mm (b) z = 17.5 mm

Figure 7.9: Cold flow, mean turbulent kinetic energy (Lines: model, dots: experiment)

7.4.2 The spray

The measured velocity data of the methanol spray consists of several radial traverses. Again a comparison is given for the radial and axial velocities as measured and as calculated with the model. Figures 7.10–7.11 show the measured axial and radial velocities of the methanol spray. For the axial positions z = 5 mm and z = 15 mm the agreement is very good. Further downstream the modelling results show that the spray is relaxing to the gaseous phase velocities faster than the measurements indicate. Using the observed SMD of the spray, see figure 7.8, this phenomenon can be explained. The SMD of the spray is increasing as a function of axial position. The SMD in the model is constant as the ratio of volume fraction to surface stays constant in this model, yielding a constant SMD as specified by the inlet conditions. As the measured data indicates larger droplets, and thus larger relaxation times, this can explain the lowering velocities of the model. The first moment of the droplet size distribution function, the droplet number density is plotted in figure 7.12. This variable is available both from the measurements and the model. It is seen that close to the inlet and at z = 35 mm, the agreement between the model results and the measurement data is good. At z = 15 mm and z = 25 mm the model underpredicts the droplet number density. When the radial spread of the spray is taken into account, one expects that the droplet number density should decrease at conditions further downstream. The measured spray does

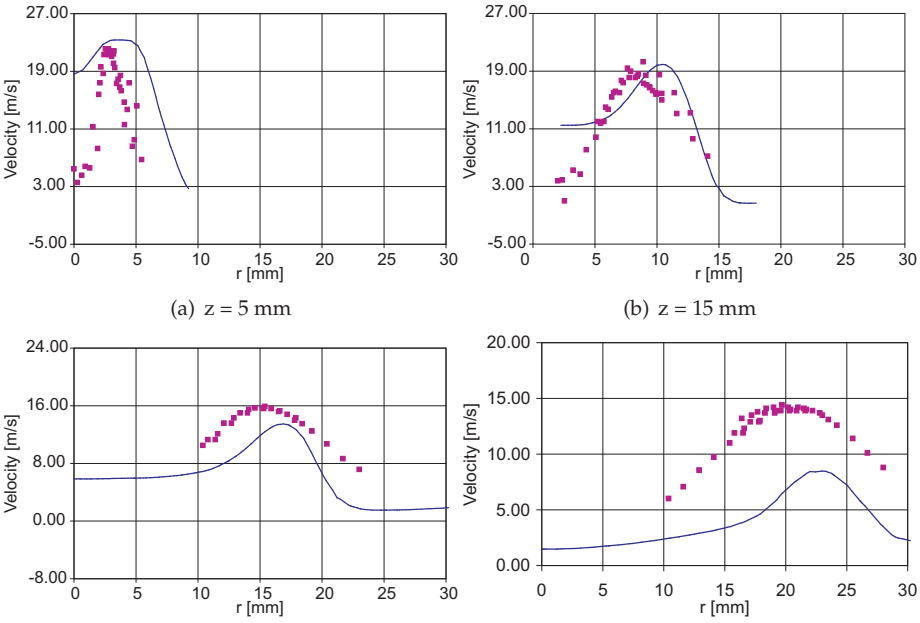

Figure 7.10: Cold flow, mean axial velocities of the methanol spray. (Lines: model, dots: experiment)

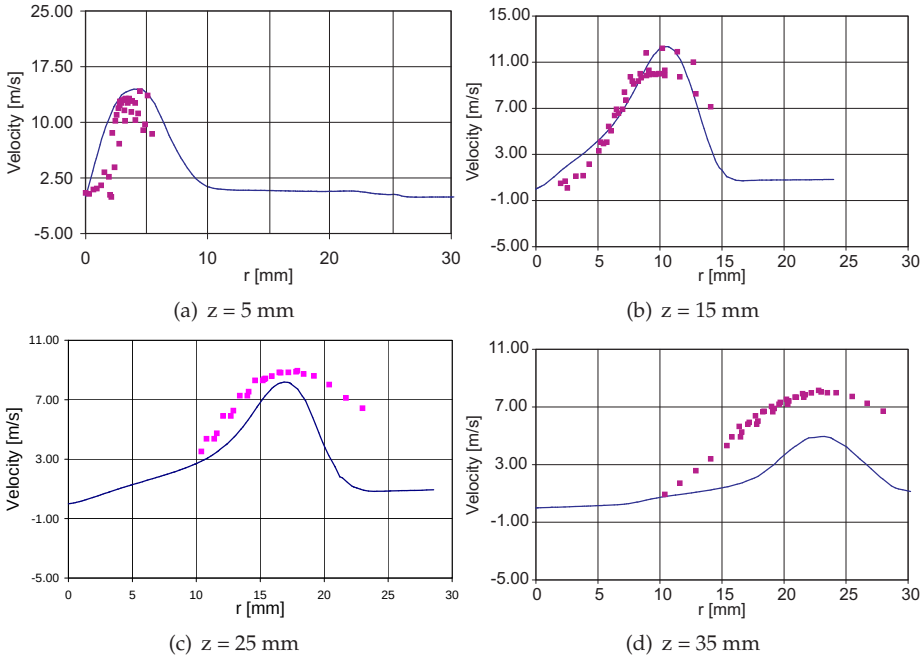

Figure 7.11: Cold flow, mean radial velocities of the methanol spray. (Lines: model, dots: experiment)

behave according to this expectation, in contrast to the model. The model predicts a faster decay of the droplet number density, but at z = 35 mm the model and the measurement data show a good match again.

7.5 The CFI methanol database

In this section the preparation of the CFI model for a methanol diffusion flame is discussed. The detailed mechanism, the reduction and the resulting database are presented. Next to that, some insight in the approach of CFI in the case of diffusion flames is discussed.

7.5.1 Detailed mechanism

As discussed shortly in chapter 2 many mechanisms are available for hydrocarbon combustion simulations. For methanol one mechanism is discussed and reduction results were presented in that chapter. It could then already be concluded that methanol chemistry is described by the same major species as other hydrocarbon fuels.

The detailed mechanism that is used for the modelling work of this chapter is equal to the previous discussed mechanism. The mechanism is built on the basis of the San Diego hydrocarbon combustion chemistry mechanism and is completed with the oxidation steps for methanol [38]. This mechanism has

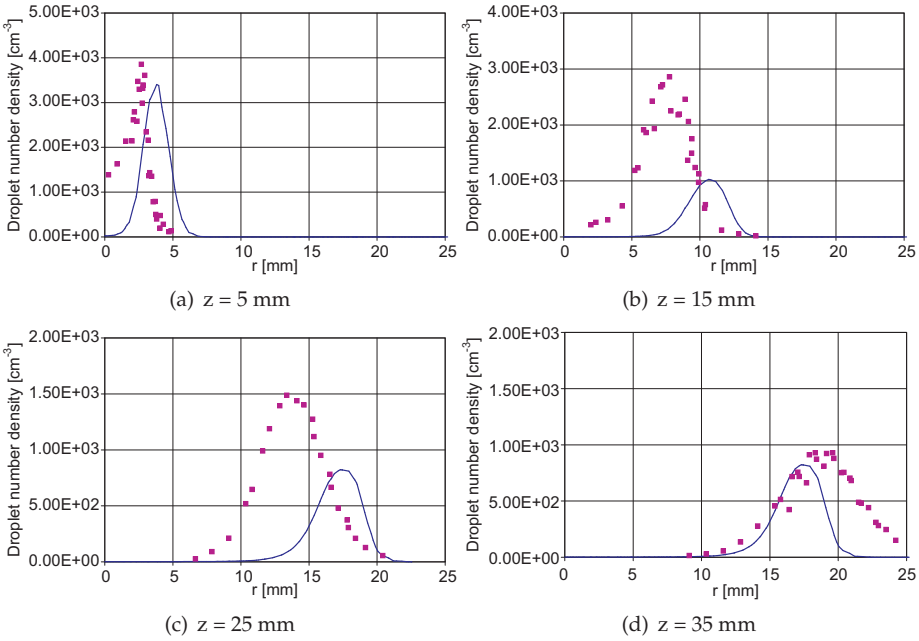

Figure 7.12: Cold flow, droplet number density (Lines: model, dots: experiment)

been validated in a laminar two-stage methanol air flame. The number of species in this mechanism is 46, with 235 reactions accounting for kinetics.

Using the PREMIX-code a laminar flame has been calculated, relevant to the pressure and inlet temperature of the experimental setup. This pressure is 1 atm. and the temperature of the methanol is 293 K. This laminar flame served as the basis for the reduction to one global step using CSP. The CFI database that has been constructed is based on the solution of the full set of equations:

$$\begin{aligned} \mathbf{c} - \mathbf{c}^0 = 0 &: \quad \text{RPV} \\ \mathbf{f} - \mathbf{f}^0 = 0 &: \quad \text{Mixture fraction} \\ \mathbf{i} - \mathbf{i}^0 = 0 &: \quad \text{Enthalpy} \\ \mathbf{b}^r \cdot \omega = \mathbf{0} &: \quad \text{Steady state relations} \\ \mathbf{E}^c - \mathbf{E}^{c,in}\left(\mathbf{Y}^0\right) = \mathbf{0} &: \quad \text{Element conservation relations} \end{aligned} \tag{7.3}$$

The solution to equation 7.3 provides the database of the chemistry, of which some results are discussed. One of the major variables in the simulation, the temperature of the gas phase is plotted in figure 7.13. In this series of figures, the temperature of the gas phase is plotted as a function of the reaction progress variable c and the mixing variable f . The plots are conditioned on the value of the enthalpy scalar. It is clear that for total heat loss, the temperature of the mixture equals the inlet temperature. As the enthalpy scalar i increases, the overall temperature of the mixture increases. For the adiabatic case, $i = 1$, the maximum temperature equals the adiabatic flame temperature

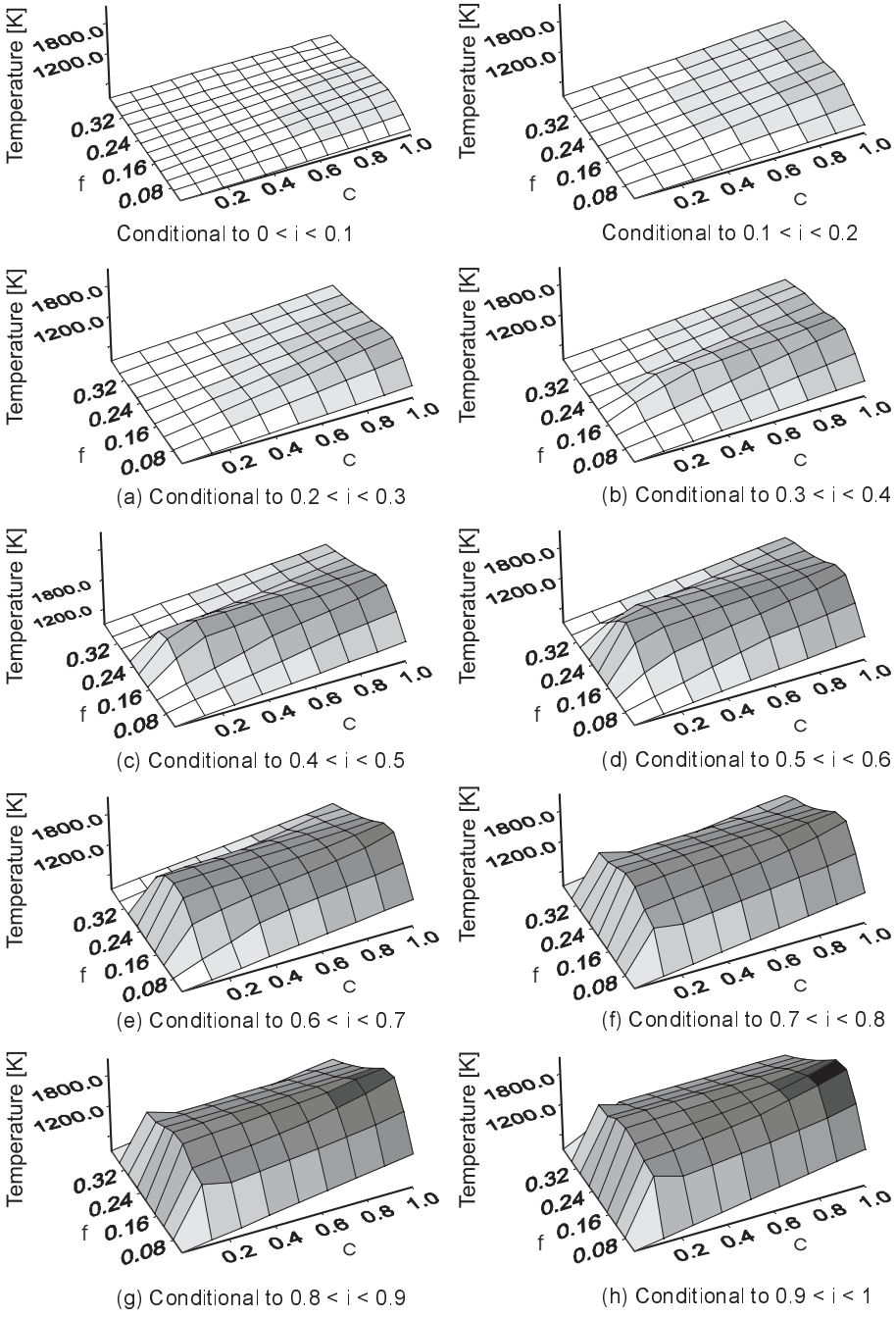

Figure 7.13: Temperatures of the gas phase as a function of the reaction progress variable c and mixture fraction f, conditional to the enthalpy scalar i.

at chemical equilibrium. In appendix E other important output variables of the database, such as the major species and the global chemical reaction rate are plotted. For the simulations of the reacting spray flame, the database is integrated over the β-pdf for c and f. For the enthalpy scalar i, the δ-pdf is used.

7.5.2 Some words on chemical equilibrium

The use of a reaction progress variable description in the context of a diffusive combustion system is contra-intuitive. The reaction progress variable using a CSP defined composed species is not just an indicator for the explicit progress of the chemical reactions. However, the rates of the reactions are connected to this variable, based on the position of the CSP defined composed species relative to chemical equilibrium. For a 1 step mechanism some considerations are made. The CSP composed species η is specified by a matrix $\boldsymbol{b}^s$. To obtain a reaction progress variable definition, normalisation is needed. For this the function W is used, using the chemical equilibrium value of the mixture and the unburned value of the stoichiometric mixture composition of fuel and air. When only fuel is present in the mixture, the actual value of η equals:

$$\eta = b_i^s Y_i \text{ with } i \text{ indicating the fuel composition} \tag{7.4}$$

The mixture fraction f equals 1 at this point. The normalisation function W was defined as follows in chapter 2:

$$W = \eta_{f=1}^{eq} - \eta_{f=\text{stoich.}}^{cold} \tag{7.5}$$

At the point where $f = 1$, the equilibrium value of the composed species equals equation (7.4). When the definition of the reaction progress variable is

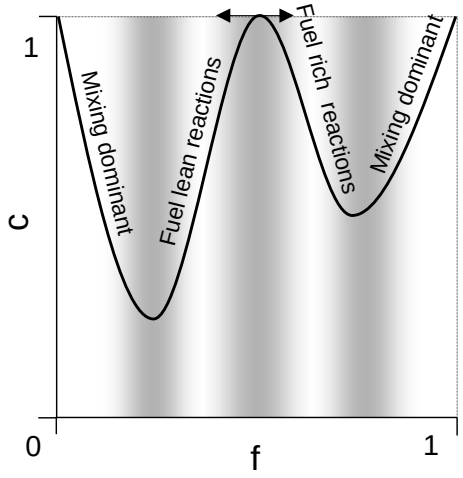

Figure 7.14: The relation between the reaction progress variable and the mixture fraction in non-premixed combustion.

applied, this will give:

$$c_{\text{fuel inlet}} = \frac{b_i^s Y_{i=\text{fuel}} - \eta^{cold}_{f=\text{stoich.}}}{b_i^s Y_{i=\text{fuel}} - \eta^{cold}_{f=\text{stoich.}}} = 1 \tag{7.6}$$

At the air inlet, the same procedure can be applied, with the mixture fraction $f = 0$ and the composed species definition yielding:

$$\eta = \boldsymbol{b}_i^s Y_i \text{ with } i \text{ indicating the air components} \tag{7.7}$$

When $f = 0$, the equilibrium concentration of η will equal the cold concentration (7.7). Now calculations of c again will give a value of 1:

$$c_{\text{air inlet}} = \frac{b_i^s Y_{i=\text{air}} - \eta^{cold}_{f=\text{stoich.}}}{b_i^s Y_{i=\text{air}} - \eta^{cold}_{f=\text{stoich.}}} = 1 \tag{7.8}$$

Chemical equilibrium is thus indicated for both the fuel and air inlet of the problem.

Now suppose the state of the system has changed due to downstream mixing and f will have a certain value x, but has not reached complete mixing. Regarding chemistry, two options are open: (a) either no chemical reaction occurred (yet) or (b) there have been chemical reactions. For the first situation η is defined according to the mass fractions following from $f = x$. Therefore the equilibrium value of η for $f = x$ will have a value that is different from the actual concentrations. Both fuel and air are available for reactions. The unburned value of η still corresponds to the stoichiometric mixture composition of fuel and air. When normalisation is applied now this will give a derivation from chemical equilibrium:

$$c_{\text{downstream}} = \frac{b_i^s Y_{i \text{ following from } f=x} - \eta^{cold}_{f=\text{stoich.}}}{b_i^s Y_{i=\text{eq. } f=x} - \eta^{cold}_{f=\text{stoich.}}} \neq 1 \tag{7.9}$$

The second situation with reactions taking place will bring c closer to equilibrium, changing again the composed species' actual concentration until chemical equilibrium is reached. Mixing has an influence on this via the composed species definition and the normalisation function, but clearly mixing alone is not enough to describe the state of the system.

To illustrate the above reasoning, the relation between c and f is sketched in figure 7.14. In this figure the horizontal axis is defined by the mixture fraction and the vertical axis corresponds to the reaction progress variable. The left part of the figure represents logically the air side in a flame, the right part of the figure the fuel side. The influence of mixing is shown by a deviation from equilibrium at both the fuel lean and fuel rich side. The largest deviation from equilibrium depends on the definition of W. The second derivative of this function W in mixture fraction space drives the system away from equilibrium both at the fuel and air side, see transport equation (G.3). The two saddle points in the figure correspond to the largest deviations from equilibrium. Note that these two saddle points do not need to have the same actual value

of the reaction progress variable. Chemical reactions will drive the system back to equilibrium, the maximum plotted in the middle. The corresponding mixture fraction of this equilibrium depends on the actual mass flows in the system.

7.6 Reacting simulation

The obtained database for the chemistry of methanol is used for the simulation of an evaporating and chemically reacting simulation of the spray. As an estimate to start this simulation the results of the iso-thermal simulation are taken. Inlet boundary conditions for both the spray and the combustion air are again taken from the experimental data.

7.6.1 The gaseous phase

When the velocity field of the evaporating and reacting spray simulation is compared to the measured velocity profiles of the combusting spray in figures 7.15-7.17, the same deviations are found as for the iso-thermal case. The size of the deviations is much larger though. Due to the predicted fast evaporation of the spray, a lot of momentum enters the gaseous phase. This significantly increases the velocities near to the centerline of the combustor. The measurements do show an increase of the axial velocities at low radii, but not as large as predicted by the model. This gives the impression that the high evaporation rates that are predicted by the model are not encountered in the actual spray flame. When the increase of the velocity of the gas phase is taken as a measure for the evaporation rate, the actual evaporation rate in the spray flame is much lower than predicted.

The contour plots of the combustion variables of the gaseous phase are plotted in figures 7.18–7.19. These figures do not show the complete solution domain. Only the area where changes in the variables are seen are plotted. This is mostly in the zone were the flame is stabilizing and the spray is injected. When the reaction progress variable is observed (figure 7.18(a)), the initial values specified at the boundary indicating full equilibrium, are rapidly going down in the region close the injection and evaporation of the spray. In this region the mixture fraction variable has a rather high value (figure 7.18(b)), indicating that almost a pure vapor of methanol is present at the center of the domain, close the the nozzle. Immediately, about 2 mm's after the spray injection nozzle, almost all liquid has evaporated. This is due to the high evaporation rates resulting from the simple mass transfer correlation model as specified in chapter 6.

7.7 Conclusions and recommendations

In this chapter the combination of the spray and combustion model has been demonstrated to provide results. The validation of the spray model under iso-thermal conditions yields quantatively good results. The predicted mean velocities of the spray and the combustion air comply with the measurement data. The interaction of the spray with the gas phase in the flame needs more

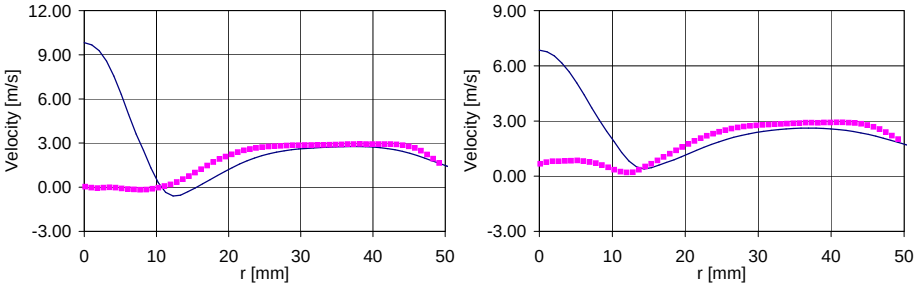

(a) z = 9.5 mm (b) z = 17.5 mm

Figure 7.15: Reacting flow, axial velocities of the combustion air. (Lines: model, dots: experiment)

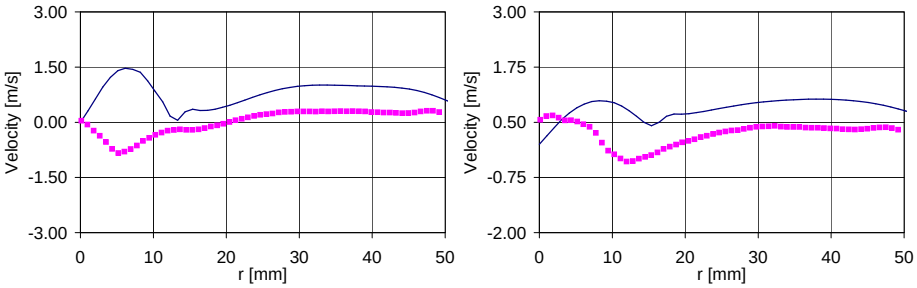

(a) z = 9.5 mm (b) z = 17.5 mm

Figure 7.16: Reacting flow, mean radial velocities of the combustion air. (Lines: model, dots: experiment)

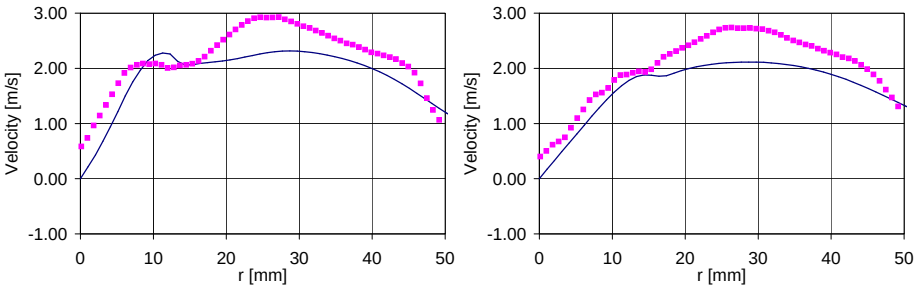

(a) z = 9.5 mm (b) z = 17.5 mm

Figure 7.17: Reacting flow, mean tangential velocities of the combustion air. (Lines: model, dots: experiment)

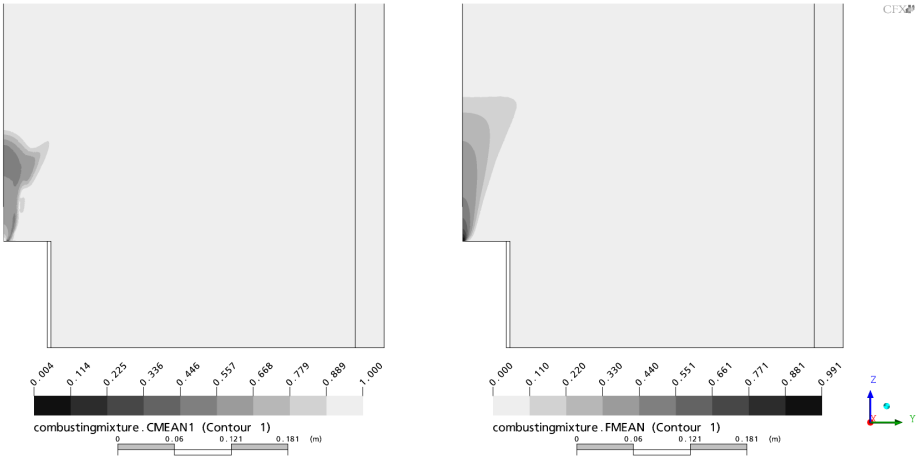

(a) Reaction progress c (b) Mixing f

Figure 7.18: Reaction progress variable and mixture fraction contour plots for the reacting flow.

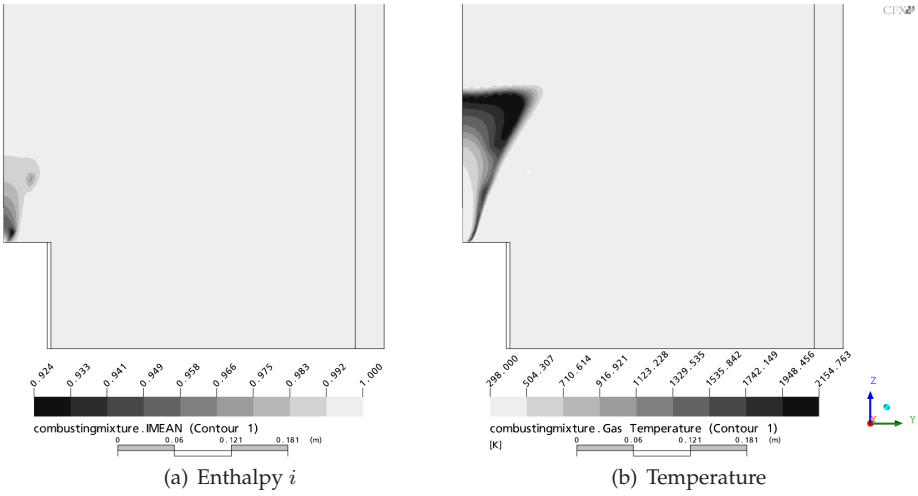

(a) Enthalpy i (b) Temperature

Figure 7.19: Temperature and enthalpy scalar contour plots for the reacting flow.

attention, as the current model tends to overpredict the local combustion air velocity.

As said, the spray model as proposed in this thesis is able to capture some features of iso-thermal sprays. For a spray flame however, the model clearly has difficulties in predicting the mean flow field. Nevertheless the simulations of the reacting flow field do give an impression corresponding to the topology of a spray flame. The developing flame sheet around the spray is observed, as well as a widening flame brush as seen often in spray flames.

Regarding further validation of the reacting spray, more experimental data is needed. The used data of the methanol spray did not contain concentrations of major reactants and products throughout the flow field, neither were temperatures measured in the flame zone.

The proposed spray model in its current form is limited and needs further improvement. The interaction between the spray and the combustion air needs more attention, especially in the near nozzle region. Turbulence is modelled poorly using the k-ε model. The influence of the spray on the gas phase turbulence is significant, but not seen in the model results.

The final recommendation is related to the topology of the spray. For the model it will be beneficial to implement spray effects. These additions should model the effect of coalescence and secondary break-up, resulting in a more correct description of the Sauter Mean Diameter. This extension is a possibility using the current formulation as a basis and has been shown to work adequately for iso-thermal diesel sprays [123].

Nomenclature

Greek

α	Coefficient of thermal expansion	[m^3/K]
δ	Delta function	
η_{th}	Thermodynamic efficiency	[–]
ϵ	Dissipation of turbulent kinetic energy	[m^3/s^-1]
ϵ	Dissipation of turbulent kinetic energy	[m^2/s^3]
η	Composed species mass fraction	
Φ	Fuel equivalence ratio	[-]
ϕ	Moment average spray quantity	
γ	Ratio of specific heats	[-]
λ	Wave length	[m]
μ	Molecular viscosity	[Pa s]
μ_i	Gibbs potential	[kJ/kg]
ω_i	Reaction rate of species i	[$kg/m^3/s$]
ρ	Density	[kg/m^3]
σ	Turbulent Prandtl number	[-]
σ_v	Turbulence dampening constant	[-]
τ	Vector of timescales corresponding to eigenvalues	
$\tau_i nt$	Integral timescale of turbulence	[1/s]
τ_p	Particle relaxation time	[1/s]
θ	Volume fraction of gas	[-]
ω	Frequency	[rad/s]
χ	Thermal diffusivity	[m^2/s]
k	Wave number	[1/m]
l_{cor}	Correlation length scale	[m]
l_t	Length scale of turbulence	[m]

Roman

$\boldsymbol{a}$	Left eigenvector matrix	
A	Pre-exponential factor	[1/s]
A	Sound generation constant	
a	Velocity of sound	[m/s]
$\boldsymbol{b}$	Right eigenvector matrix	
B	Spectrum amplitude constant	
c	Reaction progress variable	
C_D	Drag coefficient	[-]
C_f	TFC model constant	
c_p	Specific heat capacity at constant pressure	[J/kg/K]
$\boldsymbol{D}$	Vector of local CSP pointers	
$\overline{D}$	Rosin-Rammler size parameter	[m]
D	Droplet diameter	[m]
D_c	Critical droplet diameter	[m]
D_{ij}	Binary diffusion coefficient	[m^2/s]
D	Droplet diameter	[m]
E	Number of elements	[-]
E_a	Activation energy	[J/mol]
e_k	Unity vector	[-]
f	Mixture fraction	[-]
$\boldsymbol{g}$	Vector of chemical rates	
g	Gravity	[m^2/s]
H	Heaviside function	[-]
h	Enthalpy	[J/kg]
$\boldsymbol{I}$	Vector of global CSP pointers	
I	Unity tensor	[–]
i	Normalised enthalpy scalar	[-]
J_{ij}	Jacobian	
j_i	Diffusion flux	[kg/m^2/s]
k	Kinetic energy of turbulence	[m^2]
k	Turbulent kinetic energy	[m^2/s^2]
k_f or k_b	Forward resp. backward rate of reaction	[mol/s]
k_{int}	Integral wave number of turbulence	[1/m]

k_{Kol}	Kolmogorov wave number of turbulence	[1/m]
$\boldsymbol{L}$	Linear operator describing convection and diffusion	
L	Length of domain	[m]
L_c	Critical jet length	[m]
M	Number of steady state species	[–]
M_i	Molar mass	[kg/mol]
N	Number of droplets	[-]
n_i	Number of droplets in class i	[-]
N	Number of species	[–]
O	Area	[m^2]
O	Surface	[m^2]
p	Pressure	[Pa]
q	Atomization parameter	[-]
Q_0	Total number of droplets	[-]
Q_1	Sum of spray radii	[m^-2]
Q_2	Total spray surface	[m^-1]
Q_3	Total spray volume	[-]
$\Re$	Universal gas constant	[J/molK]
R	Number of reactions	[–]
r	Correlation function	
r	Droplet radius	[m]
R_T	Turbulence proportionality constant	[-]
S	Source term	[kg/m^3/s]
S_L	Laminar burning velocity	[m/s]
T	Temperature	[K]
t	Time	[s]
$\boldsymbol{U}$	Velocity vector	[m/s]
u'	Turbulent velocity fluctuation	[m/s]
$\boldsymbol{V}_i$	Diffusion velocity	[kg/m/s]
V	CFI defined normalisation function	[-]
V	Volume	[m^3]
v_i	Stoichiometric coefficient	[–]
W	CFI defined normalisation function	[-]
x	Spatial coordinates	[m]
Y_i	Mass fraction of species i	[–]
Z_i	Element mass fration	[-]
u	Instantaneous velocity vector	[m/s]

Bibliography

[1] J.F. Widmann and C. Presser. A benchmark experimental database for multiphase combustion model input and validation. *Combustion and Flame*, 129(1):47–86, 2002.

[2] J.F. Widmann, C. Presser, and G. Papadopolous. Benchmark Database for Input and Validation of Spray Combustion Models: Inlet Air Characterization. *39th Aerospace Sciences Meeting & Exhibit, Paper AIAA2001-1116, Reno, NV, Jan*, pages 8–11, 2001.

[3] C.H. Gibbs-Smith and G. Rees. *The inventions of Leonardo da Vinci*. Phaidon, 1978.

[4] J. Barber. A method for rising inflammable air for the purposes of producing motion and facilitating metallurgical operations. British patent, no. 1833, 1791.

[5] WC Wang, YL Yung, AA Lacis, T. Mo, and JE Hansen. Greenhouse Effects due to Man-Made Perturbations of Trace Gases. *Science*, 194(4266):685–690, 1976.

[6] S. Manabe and R.T. Wetherald. The effects of doubling the co_2 concentration on the climate of a general circulation model. *Journal of the Atmospheric Sciences*, 32(1):3–15, 1975.

[7] Arthur H. Lefebvre. *Gas turbine combustion*. Taylor and Francis, 1999.

[8] G. Poeschl, W. Ruhkamp, and H. Pfost. Combustion with low pollutant emissions of liquid fuels in gas turbines by premixing and prevaporization. In *ASME Paper 94–GT–443*, 1994.

[9] D.A. Santavicca, R.L. Steinberger, K.A. Gibbons, J.V. Citeno, and S. Mills. The effect of incomplete fuel-air mixing on the lean limit and emissions characteristics of a lean prevaporized premixed(lpp) combustor. *AGARD, Fuels and Combustion Technology for Advanced Aircraft Engines 12 p(SEE N 94-29246 08-25)*, 1993.

[10] NA Røkke and AJW Wilson. Experimental and theoretical studies of a novel venturi lean premixed prevaporized (lpp) combustor. *Journal of Engineering for Gas Turbines and Power*, 123:567, 2001.

[11] C.A. Armitage, R.S. Cant, A.P. Dowling, and T.P. Hynes. Linearised theory for lpp combustion dynamics. *ASME Paper GT2003-38670*, 2003.

[12] B. Zuo and E.V.D. Bulck. The modeling, scale and no_x characteristics of prevaporized, premixed fuel oil burner combustions. *Combustion science and technology*, 137(1-6):149–169, 1998.

[13] W. Dunham. *Journey through genius : the great theorems of mathematics*. Wiley, 1990.

[14] K. Kobayashi, Y. Waku, N. Nakagawa, and S. Yokoi. Technology research on high efficiency gas turbines utilizing melt-growth composite ceramics. *Proceedings of the International Gas Turbine Congress*, 2:4, 2003.

[15] M.A.F. Derksen. *On the influence of steam on combustion*. PhD thesis, University of Twente, 2005.

[16] J. Warnatz, U. Maas, and R.W. Dibble. *Combustion*. Springer Verlag Berlin Germany, 2000.

[17] H.H. Rogner. An assessment of world hydrocarbon resources. *Annual Review of Energy and the Environment*, 22(1):217–262, 1997.

[18] P.M. Vitousek, H.A. Mooney, J. Lubchenco, and J.M. Melillo. Human Domination of Earth's Ecosystems. *Science*, 277(5325):494–499, 1997.

[19] R. Guseo and A. Dalla Valle. Oil and gas depletion: Diffusion models and forecasting under strategic intervention. *Statistical Methods and Applications*, 14(3):375–387, December 2005.

[20] A. Poullikkas. An overview of current and future sustainable gas turbine technologies. *Renewable & sustainable energy review*, 9(5):409–443, 2005.

[21] D. Veynante and L. Vervisch. Turbulent combustion modeling. *Prog. Energy Comb. Sci.*, 28:193, 2002.

[22] N. Peters. *Fifteen lectures on laminar and turbulent combustion*. RWTH Aachen Ercoftac Summer School, 1992.

[23] M.A.F. Derksen, J.B.W. Kok, and T.H. van der Meer. Modelling of turbulent combustion with reaction progress variables and csp. *Proc. ECM*, 2003.

[24] J.B.W. Kok and J.J.J. Louis. Modeling turbulent combustion in a CO/H_2 diffusion flame using reaction progress variables. *Combust. Sci. and Tech.*, 131:225–249, 1998.

[25] J.B.W. Kok and C.G.J. De Hoon. *Modeling turbulent premixed CH_4 flames with flow recirculation using reaction progress variables*. Nova Science Publishers, New York, USA, 2006.

[26] J. J. J. Louis, J.B.W. Kok, and S.A. Klein. Modeling and measurements of a 16-kw turbulent nonadiabatic syngas diffusion flame in a cooled cylindrical combustion chamber. *Combustion and Flame*, 125(1-2):1012–1031, April 2001.

[27] S.H. Lam and D.A. Goussis. The csp method for simplifying kinetics. *International Journal of Chemeical Kinetics*, 26:461–486, 1994.

[28] A. Massias, D. Diamantis, E. Mastorakos, and D.A. Goussis. An algorithm for the construction of global reduced mechanisms with csp data. *Combustion and Flame*, 117:685–708, 1999.

[29] G.K. Batchelor. *An Introduction to Fluid Dynamics*. Cambridge University Press, 2000.

[30] P. Dagaut. On the kinetics of hydrocarbons oxidation from natural gas to kerosene and diesel fuel. *Phys. Chem. Chem. Phys*, 4(11):2079–2094, 2002.

[31] IR Kaplan, Y. Galperin, S.T. Lu, and R.P. Lee. Forensic environmental geochemistry: differentiation of fuel-types, their sources and release time. *Organic Geochemistry*, 27(5):289–317, 1997.

[32] Y. Huang, CJ Sung, and JA Eng. Laminar flame speeds of primary reference fuels and reformer gas mixtures. *Combustion and Flame*, 139(3):239–251, 2004.

[33] A.T. Ingemarsson, J.R. Pedersen, and J.O. Olsson. Oxidation of n-heptane in a premixed laminar flame. *J. Phys. Chem. A*, 103(41):8222–8230, 1999.

[34] V.I. Babushok and W. Tsang. Kinetic modeling of heptane combustion and pah formation. *Journal of Propulsion and Power*, 20(3):403–414, 2004.

[35] H.J. Curran, P. Gaffuri, W.J. Pitz, and C.K. Westbrook. A comprehensive modeling study of n-heptane oxidation. *Combustion and Flame*, 114:149–177, 1998.

[36] H.J. Curran, P. Gaffuri, W.J. Pitz, and C.K. Westbrook. A comprehensive modeling study of iso-octane oxidation. *Combustion and Flame*, 129(3):253–280, 2002.

[37] V. Golovitchev. http://www.tfd.chalmers.se/ valeri/mech.html. Technical report, Chalmers University of Technology, 2000.

[38] F.A. Williams. http://maemail.ucsd.edu/combustion/cermech/. Technical report, University of California, 2005.

[39] H. Xue and S.K. Aggarwal. emissions in n-heptane/air partially premixed flames. *Combustion and Flame*, 132:723–741, 2003.

[40] M. Petrova and F.A. Williams. A small detailed chemical-kinetic mechanism for hydrocarbon combustion. *Combustion and Flame*, 144(3), 2006.

[41] S.C. Li, B. Varatharajan, and F.A. Williams. The chemistry of jp-10 ignition. *AIAA Journal*, 39(12):2351–2356, 2001.

[42] Y. Simon, G. Scacchi, and F. Baronnet. Études des réactions d'oxydation du n-heptane et de l'isooctane. *Can. J. Chem./Rev. can. chim*, 74(7):1391–1402, 1996.

[43] A. El Bakali, J.L. Delfau, and C. Vovelle. Experimental study of 1 atmosphere, rich, premixed n-heptane and iso-octane flames. *Combust Sci Technol*, pages 69–91, 1998.

[44] C. Hasse, M. Bollig, N. Peters, et al. Quenching of laminar iso-octane flames at cold walls. *Combustion and Flame*, 122(1):117–129, 2000.

[45] R.J. Kee, J.F. Grcar, M.D. Smooke, and J.A. Miller. A fortran computer program for modeling steady laminar one-dimensional premixed flames. *Sandia National Laboratories Report, SAND85-8240*, 1991.

[46] D.A. Goussis. On the construction and use of reduced chemical kinetic mechanisms produced on the basis of given algebraic relations. *Journal of Computational Physics*, 128:261–273, 1996.

[47] G. Skevis. Alternative pointer definitions. private communication, 2005.

[48] J.J.J. Louis. *On Turbulent Combustion of Coal Gas*. University of Twente, 1997.

[49] W.T. Kim and K.Y. Huh. Numerical simulation of spray autoignition by the first-order conditional moment closure model. *Proceedings of the Combustion Institute*, 29:569–576, 2002.

[50] F.X. Demoulin and R. Borghi. Modeling of turbulent spray combustion with application to diesel like experiment. *Combustion and Flame*, 129(3):281–293, 2002.

[51] J. Reveillon and L. Vervisch. Accounting for spray vaporization in turbulent combustion modeling. In *Center for Turbulence Research*, volume 10, page 2, 1998.

[52] U. Maas and S.B. Pope. Twenty-fifth symposium (international) on combustion. *The Combustion Institute, Pittsburgh*, pages 1349–1356, 1994.

[53] G.P. Smith, D.M. Golden, M. Frenklach, N.W. Moriarty, B. Eiteneer, M. Goldenberg, C.T. Bowman, R.K. Hanson, S. Song, W.C. Gardiner Jr, et al. Gri mech 3.0 mechanism. *Berkeley University, USA*, 1999.

[54] B. De Jager, J. B.W. Kok, and G. Skevis. The effect of water addition in lpp gas turbine combustors. *Proceedings of the Combustion Institute*, 31, 2006.

[55] Z. Zhao, J. Li, A. Kazakov, F.L. Dryer, and S.P. Zeppieri. Burning velocities and a high-temperature skeletal kinetic model for n-decane. *Combustion Science and Technology*, 177(1):89–106, 2005.

[56] E. Macchi, S. Consonni, G. Lozza, and P. Chiesa. An assessment of the thermodynamic performance of mixed gas-steam cycles. part a: Intercooled and steam-injected cycles. *Journal of Engineering for Gas Turbines and Power*, 117(3), 1995.

[57] J.H. Horlock. Evaporative gas turbine[egt] cycle. *Journal of Engineering for gas turbine and power*, 120(2):336–343, 1998.

[58] S.M. Correa. Power generation and aeropropulsion gas turbines: From combustion science to combustion technology. *Proceedings of the Combustion Institute*, 27:1793–1807, 1998.

[59] F.L. Dryer. *Proceedings of the Combustion Institute*, 16:279–295, 1976.

[60] T. Miyauchi, Y. Mori, and T. Yamaguchi. Effect of steam addition on no formation. *Symposium/International/ on Combustion, 18 th, Waterloo, Ontario, Canada*, 1981.

[61] A. Bhargava, M. Colket, W. Sowa, K. Castleton, and D. Maloney. An experimental and modeling study of humid air premixed flames. *Journal of Engineering for Gas Turbines and Power*, 122:405, 2000.

[62] B.Z. Dlugogorski, R.K. Hichens, E.M. Kennedy, and J.W. Bozzelli. Propagation of laminar flames in wet premixed natural gas- air mixtures. *Process Safety and Environmental Protection*, 76:81–9, 1998.

[63] M.J. Landman, M.A.F. Derksen, and J.B.W. Kok. Effect of combustion air dilution by wator vapor or nitrogen on nox emission in a premixed turbulent natural gas flame: an experimental study. *Combustion Science and Technology*, 178(4):623–634, 2006.

[64] F. Liu, H. Guo, G.J. Smallwood, and O.L. Gulder. The chemical effects of carbon dioxide as an additive in an ethylene diffusion flame- implications for soot and no (x) formation. *Combustion and Flame*, 125(1):778–787, 2001.

[65] J. Richard, J.P. Garo, J.M. Souil, J.P. Vantelon, and V.G. Knorre. Chemical and physical effects of water vapor addition on diffusion flames. *Fire Safety Journal*, 38(6):569–587, 2003.

[66] S. Naha and S.K. Aggarwal. Fuel effects on nox emissions in partially premixed flames. *Combustion and Flame*, 139(1):90–105, 2004.

[67] N. Peters. Laminar flamelet concepts in turbulent combustion. *Symposium(International) on Combustion, 21 st, Munich, Federal Republic of Germany*, pages 1231–1250, 1988.

[68] R.W. Bilger. *Turbulent reactive flows*, chapter Turbulent flows with non-premixed reactants. Springer, 1980.

[69] J.A. van Oijen, G.R.A. Groot, R.J.M. Bastiaans, and L.P.H. de Goey. A flamelet analysis of the burning velocity of premixed turbulent expanding flames. *Proc. Combust. Inst*, 30(1):657–664, 2005.

[70] S.G. Davis and C.K. Law. Laminar flame speeds and oxidation kinetics of iso-octane-air and n-heptane-air flames. *Proceedings of the Combustion Institute*, 27:521–527, 1998.

[71] R.P. Lindstedt and L.Q. Maurice. Detailed kinetic modelling of n-heptane combustion. *Combustion Science and Technology*, 107(4):317–353, 1995.

[72] T.J. Held, A.J. Marchese, and F.L. Dryer. A semi-empirical reaction mechanism for n-heptane oxidation and pyrolysis combust. *Combustion Science and Technology*, 123:107–46, 1997.

[73] E. Ranzi, T. Faravelli, P. Gaffuri, A. Sogaro, A. D'Anna, and A. Ciajolo. A wide-range modeling study of iso-octane oxidation. *Combustion and Flame*, 108(1):24–42, 1997.

[74] E.I. Axelsson, K. Brezinsky, F.L. Dryer, W.J. Pitz, and C.K. Westbrook. Chemical kinetic modeling of the oxidation of large alkane fuels: n-octane and iso-octane. *Proceedings of the Combustion Institute*, 21, 1986.

[75] N.A. Slavinskaya and O.J. Haidn. Modeling of n-heptane and iso-octane oxidation in air. *Journal of Propulsion and Power*, 19(6):1200–1216, 2003.

[76] H. Pitsch, N. Peters, and K. Seshadri. Numerical and asymptotic studies of the structure of premixed iso-octane flames. *Proceedings of the Combustion Institute*, pages 763–71, 1996.

[77] D. Bradley, R.A. Hicks, M. Lawes, C.G.W. Sheppard, and R. Woolley. The measurement of laminar burning velocities and markstein numbers for iso-octane-air and iso-octane-n-heptane-air mixtures at elevated temperatures and pressures in an explosion bomb. *Combustion and Flame*, 115(1):126–144, 1998.

[78] A.H. Lefebvre. The role of fuel preparation in low-emission combustion. *Journal of engineering for gas turbines and power*, 117(4):617–654, 1995.

[79] S.M. Correa. A review of nox formation in gas turbine combustion. *Combustion science and technology*, 87(1):329–362, 1993.

[80] P.M.S. Anacleto, E.C.S. Fernandes, M.V.S. Heitor, and S.I.S. Shtork. Swirl flow structure and flame characteristic in a model lean premixed combustor. *Combustion Science and Technology*, 175(8):1369–1388, 2003.

[81] S.B. Pope. *Turbulent Flows*. Cambridge University Press, 2000.

[82] J.B.W. Kok and S.A. Klein. Sound generation by turbulent non-premixed flames. *Proceedings of the International Congress on Sound and Vibration*, pages 338–5, 1999.

[83] S.A. Klein. *On the acoustics of turbulent non-premixed flames*. PhD thesis, Universitity of Twente, 2000.

[84] A. Putnam and L. Faulkner. An overview of combustion noise. *Journal of Energy*, 7, no 6.:458–469, 1983.

[85] P. Boineau and Y. Gervais. Determination du spectre de puissance acoustique is par une flammeturbulente. *CR.Acad. Sci. Paris*, 326:747–754, 1998.

[86] D.G. Crighton et al. *Modern methods in analytical acoustics*. Springer New York, 1992.

[87] W.C. Strahle. On combustion generated noise. *Journal of Fluid Mechanics*, 49, part 2:399–414, 1971.

[88] W.C. Strahle. Some results in combustion generated noise. *Journal of Sound and Vibration*, 23, part 1:pp. 113–125, 1972.

[89] V.L. Zimont. Theory of turbulent combustion of a homogeneous fuel mixture at high reynolds numbers. *Combustion, Explosions and Shock Waves*, 15:305–311, 1979.

[90] R. Rubinstein and Y. Zhou. The dissipation rate transport equation and subgrid-scale models in rotating turbulence. *ICASE Report No*, pages 97–63, 1997.

[91] J.O. Hinze. *Turbulence*. McGraw-Hill New York, 1975.

[92] W. Becharam, P. Lafon, and C. Bailly. Application of a k-ϵ-turbulence model to the prediction of noise for simple an coaxial free jets". *Journal of the Acoustical Society of America*, 97(6):3518–3530, June 1995.

[93] W. Bechara, C. Bailly, and P. Lafon. Stochastic approach to noise modeling for free turbulent flows. *AIAA Journal*, 32(3):455–463, 1994.

[94] V.L. Zimont, F. Biagioli, and K.J. Syed. Modelling turbulent premixed combustion in the intermediate steadypropagation regime. *Progress in Computational Fluid Dynamics*, 1 Nos. 1/2/3:14–28, 2001.

[95] Jaap van Kampen. *Acoustic pressure oscillations induced by confined turbulent premixed natural gas flames*. PhD thesis, Ph. D. Thesis, University of Twente, 2006.

[96] B. De Jager, Kok J.B.W., and Th.H. Van der Meer. Development of reduced chemistry with csp for application in turbulent n-heptane flames. In *Proceedings of the European Congress on Computational Methods in Applied Sciences and Engineering (ECCOMAS)*, 2004.

[97] J.W.S. Rayleigh. On the capillary phenomena of jets. *Proceedings of the Royal Society of London*, 29:71–97, 1879.

[98] L. Bayvel and Z. Orzechowksi. *Liquid Atomization*. Taylor & Francis, 1993.

[99] E. Babinsky and P.E. Sojka. Modeling drop size distributions. *Progress in energy and combustion science*, 28:303–329, 2002.

[100] P. Rosin and E. Rammler. The laws governing the fineness of powdered coal. *Journal of Inst. Fuel*, pages 29–36, 1933.

[101] T. Paloposki. Drop size distributions in liquid sprays. *Acta Polytechnica Scandinavia*, Mechanical Engineering Series:114–, 1994.

[102] H.H. Chiu. Advances and challenges in droplet and spray combustion. i. towards a unified theory of droplet aerothermochemistry. *Progress in Energy and Combustion Science*, 26:381 – 416, 2000.

[103] *Accounting for spray vaporization in turbulent combustion modeling*. Center for turbulence research, 1998.

[104] S.K. Aggarwal and W.A. Sirignano. Unsteady spray flame propagation in a closed volume. *Combustion and Flame*, 62:69–84, 1985.

[105] W.A. Sirignano. *Fluid Dynamics and Transport of Droplets and Sprays*. Cambridge University Press, 1999.

[106] G. Gouesbet and A. Berlemont. Eulerian and lagrangian approaches for predicting the behaviour of discrete particles in turbulent flows. *Progress in Energy and Combustion Science*, 25:133–159, 1999.

[107] T. Furuhata, S. Tanno, T. Miura, Y. Ikeda, and T. Nakajima. Performance of numerical spray combustion simulation. *Energy Conversion and Management*, 38:1111–1122, 1997.

[108] D.H. Caraeni, C.H. Bergström, and L.H. Fuchs. Modeling of liquid fuel injection, evaporation and mixing in a gas turbine burner using large eddy simulations. *Flow, Turbulence and Combustion*, 65(2):223–244, 2000.

[109] V.M. Sankaran and S.M. Menon. Les of spray combustion in swirling flows. *Journal of Turbulence*, 3(11):1–23, 2002.

[110] J.K. Dukowicz. A particle-fluid numerical model for liquid sprays. *Journal of Computational Physics*, 35:229–253, 1980.

[111] D.Z. Zhang and A. Prosperetti. Momentum and energy equations for disperse two-phase flows and their closure for dilute suspensions. *International Journal of Multiphase Flow*, 23(3):425–453, 1997.

[112] D.Z. Zhang and A. Prosperetti. Ensemble phase-averaged equations for bubbly flows. *Physics of Fluids*, 6:2956, 1994.

[113] R. Aliod and C. Dopazo. A statistically conditioned averaging formalism for deriving two-phase flow equations. *Particle and Particle Systems Characterization*, 7(1-4):191–202, 1990.

[114] S.E. Elghobashi and T.W. Abou-Arab. A two-equation turbulence model for two-phase flows. *Physics of Fluids*, 26:931, 1983.

[115] E. Loth. Numerical approaches for motion of dispersed particles, droplets and bubbles. *Progress in Energy and Combustion Science*, 26(3):161–223, 2000.

[116] F.A. Williams. Spray Combustion and Atomization. *Physics of Fluids*, 1:541, 1958.

[117] B. Naud. *PDF modeling of turbulent sprays and flames using a particle stochastic approach*. PhD thesis, Ph. D. Thesis, Delft University of Technology, 2003.

[118] R. Schmehl, G. Klose, G. Maier, and S. Wittig. Efficient numerical calculation of evaporating sprays in combustion chamber flows. *92nd Symp. on Gas Turbine Combustion, Emissions and Alternative Fuels, RTO Meeting Proceedings*, 14, 1998.

[119] *Evaluation of advanced two-phase flow and combustion models for predicting low emission combustors*, 2000.

[120] Y. C. Guo, C. K. Chan, and K. S. Lau. A pure eulerian model for simulating dilute spray combustion. *Fuel*, 81(16):2131–2144, November 2002.

[121] W.E. Ranz and W..R Marshall. Evaporation from drops. *Chem. Eng. Prog*, 48(3):141–146, 1952.

[122] D.B. Spalding. The combustion of liquid fuels. *Fourth Symposium (International) on Combustion*, pages 847–864, 1952.

[123] J.C. Beck and A.P. Watkins. On the development of spray submodels based on droplet size moments. *Journal of Computational Physics*, 182(2):586–621, 2002.

[124] J.C. Beck and A.P. Watkins. The droplet number moments approach to spray modelling: The development of heat and mass transfer sub-models. *International Journal of Heat and Fluid Flow*, 24(2):242–259, 2003.

[125] J.C. Beck. On the development of a spray model based on drop-size moments. *Proceedings: Mathematical, Physical and Engineering Sciences*, 459(2034):1365–1394, 2003.

[126] W.K. Melville and K.N.C. Bray. A model of the two-phase turbulent jet. *International Journal of Heat and Mass Transfer*, 22:647–656, 1979.

[127] A.A. Mostafa and H.C. Mongia. On the modeling of turbulent evaporating sprays-Eulerian versus Lagrangian approach. *International Journal of Heat and Mass Transfer*, 30:2583–2593, 1987.

[128] B.E. Launder and D.B. Spalding. The numerical computation of turbulent flow. *Computer Methods in Applied Mechanics and Engineering*, 3:269–289, 1974.

[129] G.B. Wallis. *One-dimensional two-phase flow*. McGraw-Hill New York, 1969.

[130] F. Catoire, J.E.D. Gautier, M.F. Bardon, and A. Benaissa. Quasi-steady state evaporation model for real multi-component fueldroplets. Technical report, Royal Military College of Canada, Kingston, Ontario, 2001.

A

Turbulent reacting flow modelling

This appendix gives a short introduction of the applied turbulence modelling used in this thesis. The book of Pope [81] is referred to as an excellent start for the interested reader.
Turbulence is characterised by continuous fluctuations of the variables describing a flow: the velocities. This influences scalars like temperature, density and pressure. Vortices, generated by shear in the flow, are the cause of these fluctuations. These vortices grow as a result of a competition between a (non-linear) generation process and a destruction process caused by viscous dissipation. A useful number to describe whether a flow is turbulent or laminar is the Reynolds number. The Reynolds number is the ratio of a destabilising momentum term and a stabilising viscous effect. When the generation term is much stronger than the viscous damping term, the Reynolds number exceeds a critical value, and the flow is turbulent. In that case the Reynolds number will be large (> 2300).

A.1 Typical turbulence scales

The size of the smallest vortices or structures in turbulent flows is characterised by the Kolmogorov length scale η, equation A.1 . The geometrical dimensions of a flow system determine the largest length scales that occur in turbulence, the integral length scale l_t. The turbulent Reynolds number describes the degree of turbulence and is expressed in equation A.2.

$$\eta = \left(\frac{\nu^3}{\varepsilon}\right)^{1/4} \tag{A.1}$$

$$R_l = \frac{\rho l_t \sqrt{2k}}{\mu} \tag{A.2}$$

A relation between the Kolmogorov length scale and the turbulent Reynolds number is given by equation A.3. This relation makes it clear that the turbulent Reynolds number is a measure for the ratio between the integral length scale and the Kolmogorov length scale η.

$$R_l = \left(\frac{l_t}{\eta}\right)^{4/3} \tag{A.3}$$

Two other numbers used in determining the governing turbulent combustion regime are the turbulent Karlovitz and the turbulent Damkohler number. The Karlovitz number (Ka) denotes the ratio between the time scale τ_l of the laminar flame and the Kolmogorov time scale τ_k:

$$Ka = \frac{\tau_l}{\tau_k} \text{ with } \tau_k = \sqrt{\frac{\nu}{\varepsilon}} \tag{A.4}$$

The Damkohler number (Da) is the ratio between the macroscopic time (mixing time) and the chemical time:

$$Da = \frac{\tau_{turb}}{\tau_c} \tag{A.5}$$

The size of eddies that interact with the flamefront is determined by the Gibson scale:

$$l_G = \frac{u_L^3}{\varepsilon} \tag{A.6}$$

Peters [22] defines the Gibson scale as the size of the burned pockets that move into the unburned mixture. A diagram that shows the different regimes in premixed turbulent combustion and their relation to R_l, Ka and Da is presented in Figure C.1. This is the well-known Borghi-diagram.

The regimes appearing in this diagram are:

It must be said that distinction between these regimes is not always as clear as shown in Figure C.1. Turbulence is mostly inhomogeneous and the dissipation of energy ε is not constant throughout the flow.

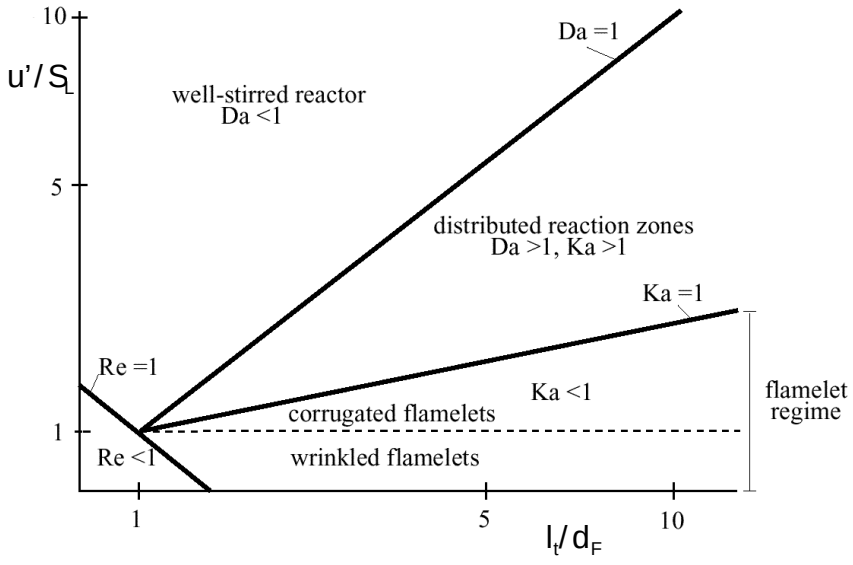

Figure A.1: The Borghi diagram.

				Regimes
$R_l > 1$	$Da < 1$	$Ka > 1$		'Well-mixed reactor' The velocity of the chemical reactions, the chemical time, is that large that turbulent eddies nearly all embed in the reacting zone, therefor there is no 'flame-front'.
$Da > 1$		$Ka > 1$		'Distributed reaction zones' Due to the fast chemistry Da is high and thin reaction zones are generated locally. The forming and destruction of these zones is an equilibrium process, driven by flame stretch. Smaller eddies will broaden the flamefront, since l_k is smaller than the laminar flame thickness.
		$Ka < 1$	$\eta < l_G < l_0$	'Corrugated flamelets' Large eddies with a velocity greater than the burning velocity will push the flamefront around, producing convolution.
		$Ka < 1$		'Wrinkled flamelets' The laminar burning velocity is larger than the turbulent velocity fluctuation and the flamefront will be wrinkled by the largest eddies.
$R_l < 1$				'Laminar plane flame fronts' When there is no turbulence, the flames will be laminar.

A.2 Solving methods

There are several methods that provide solutions for the Navier-Stokes equations in case of turbulent flows:

1. Direct Numerical Simulations (DNS). With this method the Navier Stokes equations are solved by direct time dependent simulation of the flow. However, it's clearly seen that this will take a lot of computational time even for a small domain. A very fine grid is necessary to take into the account the smallest vortices that occur.

2. Large Eddie Simulations (LES). This method also uses direct numerical simulations but without simulating the small eddies, as the name of the method already says. The subscale structures are modelled as isotropic turbulence using any of the available turbulence models. Although LES methods need less computational time, it is still only useful for simple geometries and problems.

3. Reynolds Averaged Navier Stokes equations (RaNS). Often there is only interest in the mean properties of a flow. In this case the Navier Stokes

equations are solved for mean values of the variables by averaging the equations for time. Modelling relations for the fluctuations capture the effect of turbulence. The RaNS method makes it possible to deal with more complex problems on less numerical expense.

In industrial CFD codes and in literature there is a trend of merging LES models with RaNS models. Roughly, the LES model is used for the bulk of the flow, whilst the RaNS model is the tool for modelling the processes close to the wall. These hybrid approaches are referred to as DES (Detached Eddy Simulation). As mentioned, spatial and temporal scales in turbulence cover a wide spectrum and solving the governing equations with DNS or LES is not possible within reasonable time and use of computers. Therefore, to solve turbulence problems, the RaNS method is the most useful. This means that less detailed levels are subjected to research. A consequence of this is loss of eventual important data. Another implication is that these simplifications introduce new unknowns that need modelling in order to close the system of equations. This problem is being referred to as the 'closure' problem.

A.3 Statistical averaging

Averaged equations are a useful way to determine turbulent reacting flow properties. The time-average of a function u can be described as:

$$\overline{u(\underline{x})} = \lim_{\Delta t \to \infty} \frac{1}{\Delta t} \int_0^{\Delta t} u(x,t)dt \tag{A.7}$$

Equation A.7 is only valid when the time-average is constant in the interval [0, Δt]. The value of any variable can be seen as the sum of its mean value and its fluctuation:

$$u = \overline{u} + u' \tag{A.8}$$

An inherent result of time-averaging is that the mean of the fluctuations is zero:

$$\overline{u'} = 0 \tag{A.9}$$

In combustion processes large density variations are typical and thus it is usefull to take this into account by use of density weighted averaging, or Favre-averaging. Given any arbitrary property q, the Favre-average yields:

$$\tilde{q} = \frac{\overline{\rho q}}{\overline{\rho}} \tag{A.10}$$

This property q can also be split into its mean value and its fluctuation:

$$q = \tilde{q} + q'' \tag{A.11}$$

Again there is an important result, namely the average of the Favre-fluctuation equals zero:

$$\overline{q''} = 0 \tag{A.12}$$

It can be shown [16] that Favre-averaging gives a compact formulation of equations with fewer unknown relations than just time-averaging.

Methods based on averaging of equations are often referred to as 'moment methods', because averages are the first moments of a probability distribution function. Averaging the Navier-Stokes equations will introduce not only first moments, but also second moments that need modelling to solve the closure problem. Equations can be derived for these second moments, but then again higher moments are introduced and the problem will not be closed. Therefore, in order to solve the averaged equation a modelling assumption needs to be done for the introduced unknowns.

A.3.1 The k-ε model

A very broad used model to close the Reynolds Averaged Navier Stokes equations is the k-ε model (Launder and Spalding, 1972). The RaNS-equation for an arbitrary scalar looks as follows:

$$\frac{\partial \tilde{\phi}}{\partial t} + \nabla \cdot (\tilde{\phi}\tilde{\boldsymbol{U}} + \phi'' \underline{u}'') = D\nabla^2 \tilde{\phi} + \omega_\phi \tag{A.13}$$

Equation A.13 has a new unknown; the fluctuation of the Favre average: u''. The so called 'gradient assumption' is used to model this fluctuation:

$$\phi'' \underline{u}'' = -\Gamma_T \nabla \tilde{\phi} \tag{A.14}$$

This assumption states that the fluctuation of u is proportional to the gradient of the mean value of u multiplied with a new unknown: the 'turbulent diffusion coefficient' Γ_T. The turbulent diffusion coefficient can be expressed as:

$$\Gamma_T = \frac{\nu_T}{\mathrm{Pr}_t} \text{ with } \nu_T = c_\mu \frac{k^2}{\varepsilon} \tag{A.15}$$

The other variables k and ε are introduced earlier as the turbulent energy resp. the energy dissipation. Two differential equations need to be solved for k and ε:

$$\frac{\partial \overline{\rho}\tilde{k}}{\partial t} + \nabla \cdot (\overline{\rho}\tilde{\boldsymbol{U}}\tilde{k}) - \nabla \cdot (\overline{\rho}\nu_T \nabla \tilde{k}) = -\overline{\rho \underline{u}'' \underline{u}''} : \nabla \tilde{\boldsymbol{U}} - \overline{\rho}\tilde{\varepsilon} \tag{A.16}$$

$$\frac{\partial \overline{\rho}\tilde{\varepsilon}}{\partial t} + \nabla \cdot (\overline{\rho}\tilde{\boldsymbol{U}}\tilde{\varepsilon}) - \nabla \cdot (\overline{\rho}\nu_T \nabla \tilde{\varepsilon}) = (-c_1(\overline{\rho \underline{u}'' \underline{u}''} : \nabla \tilde{\boldsymbol{U}} + \overline{\rho}\tilde{\varepsilon}) - c_2 \overline{\rho}\tilde{\varepsilon}) \frac{\tilde{\varepsilon}}{\tilde{k}} \tag{A.17}$$

A.3.2 Probability density functions

In this paragraph a look is taken on statistical methods, which can be used in turbulent reacting flow modelling. One way to look at turbulent flows is assuming them to be a random, chaotic process that can be described by its statistics. The values that certain variables can have at certain moments are

called stochastic. These stochastic values can be defined by a Probability Density Function (PDF). The probability that a variable has a certain value is represented by this function. The statistical moment of any order n for a variable ϕ is given by:

$$\overline{\phi^n}(\underline{x},t) = \int_{\Phi} \phi^n PDF(\phi;\underline{x},t)d\phi \tag{A.18}$$

Φ : interval that contains all possible values of ϕ The statistical average of an arbitrary dependent quantity $f(\phi)$ is given in the next equation:

$$\overline{\phi^n}(\underline{x},t) = \int_{\Phi} \phi^n PDF(\phi;\underline{x},t)d\phi \tag{A.19}$$

When a quantity is dependent on more variables a joint PDF can be applied. The form of a joint PDF for n variables can look as follows:

$$\overline{f(\phi)} = PDF(\phi_1,\phi_2,...,\phi_n;\underline{x},t) \tag{A.20}$$

which in case of statistical independence of the variables is written as:

$$\overline{f(\phi)} = PDF(\phi_1;\underline{x},t)(\phi_2;\underline{x},t)...PDF(\phi_n;\underline{x},t) \tag{A.21}$$

For the joint PDF(ψ,ξ;$\underline{x}$,t) the following relation is valid, Bayes theorem:

$$P(\psi|\,\xi) = P_{\psi|\xi}(\psi|\,\xi)P_{\xi}(\xi) = P_{\xi|\psi}(\xi|\,\psi)P_{\psi}(\psi) \tag{A.22}$$

If all PDFs that describe a system are independent of time or space, it is said that turbulence is respectively steady or homogeneous.

β-function distributions A very common distribution used in combustion modelling is the β-distribution. This is a two-parameter distribution, describing the probability of a certain parameter to have a certain value. The PDF-functions based on a β-distribution are calculated with the following equations:

$$PDF(f) = \frac{f^{r-1}(1-f)^{s-1}}{\int_0^1 f^{r-1}(1-f)^{s-1}df} \tag{A.23}$$

with

$$r = \bar{f}\left(\bar{f}\frac{1-\bar{f}}{\bar{f}''^2} - 1\right) \text{ and } s = r\left(\frac{1-\bar{f}}{\bar{f}}\right) \tag{A.24}$$

These equations show that a β-distribution PDF indeed is a function of only two parameters, named r and s in this case, based on the mean value of a scalar and its variance.

A.3.3 Chemistry

Chemistry plays an important role in turbulent reacting flows and needs to be modelled in an appropriate way. Temperatures fluctuate heavily in turbulent reacting flows. One way of dealing with these temperature fluctuations is to decompose the temperature T in its Favre average and fluctuation and derive a power series for the exponential function of the reaction rate constant k_r:

$$k_r = A \exp\left(\frac{-T_a}{\tilde{T}}\right)\left(1 + \left(\frac{T_a}{\tilde{T}^2}\right)T'' + \left(\frac{T_a^2}{2\tilde{T}^4} - \frac{T_a}{\tilde{T}^3}\right)T''^2 + \mathcal{O}\right)(T) \quad \text{(A.25)}$$

Experiments have shown that the 20^{th} order Taylor expansion is needed in order to correctly predict k_r. This is not practical for the calculation of a solution. Instead, as it is mentioned before, PDF modelling can be used, yielding good results with respect to chemistry.

B

Detailed octane/heptane mechanism

The following table contains the detailed reaction mechanism assembled from several well validated seperate mechanisms for n-heptane and iso-octane combustion as described in chapter 3. The mechanism contains 76 species and 477 reactions. The basis of the mechanism is given by n-heptane mechanism of Held *et al.* [72] and the iso-octane mechanism from Hasse *et al.* [72].

Reaction	A (cm-moles-sec-K)	n	E (cal/mole)
$H + O_2 \rightleftharpoons O + OH$	1.915E+14	0.00	1.644E+04
$O + H_2 \rightleftharpoons H + OH$	5.080E+04	2.67	6.290E+03
$H_2 + OH \rightleftharpoons H_2O + H$	2.160E+08	1.51	3.430E+03
$O + H_2O \rightleftharpoons OH + OH$	2.970E+06	2.02	1.340E+04
$H_2 + M \rightleftharpoons H + H + M$	4.577E+19	-1.40	1.044E+05
Enhanced Collision Efficiencies:			
H_2=2.5, H_2O=12, CO=1.9, CO_2=3.8			
Enhanced Collision Efficiencies:			
AR=0			
$H_2 + AR \rightleftharpoons H + H + AR$	5.840E+18	-1.10	1.044E+05
$O + O + M \rightleftharpoons O_2 + M$	6.165E+15	-0.50	0.000E+00
Enhanced Collision Efficiencies:			
H_2=2.5, H_2O=12, CO=1.9, CO_2=3.8			
Enhanced Collision Efficiencies:			
AR=0.			
$O + O + AR \rightleftharpoons O_2 + AR$	1.886E+13	0.00	-1.788E+03
$O + H + M \rightleftharpoons OH + M$	4.714E+18	-1.00	0.000E+00
Enhanced Collision Efficiencies:			
H_2=2.5, H_2O=12, CO=1.9, CO_2=3.8			
Enhanced Collision Efficiencies:			
AR=0.75			
$H + OH + M \rightleftharpoons H_2O + M$	2.212E+22	-2.00	0.000E+00
Enhanced Collision Efficiencies:			
H_2=2.5, H_2O=6.3, CO=1.9, CO_2=3.8			
Enhanced Collision Efficiencies:			
AR=0.38			
$H + O_2(+M) \rightleftharpoons HO_2(+M)$	4.517E+13	0.00	0.000E+00
Low pressure limit	6.700E+19	-1.42	0.000E+00
Enhanced Collision Efficiencies:			

Reaction	A (cm-moles-sec-K)	n	E (cal/mole)
H_2=2.5, H_2O=12, CO=1.9, CO_2=3.8			
Enhanced Collision Efficiencies:			
AR=0.0			
$H + O_2(+AR) \rightleftharpoons HO_2(+AR)$	4.517E+13	0.00	0.000E+00
Low pressure limit	6.167E+17	-0.80	0.000E+00
Troe parameters: a=0.5, T***=1E-30, T*=1E+30			
$HO_2 + H \rightleftharpoons H_2 + O_2$	6.630E+13	0.00	2.130E+03
$HO_2 + H \rightleftharpoons OH + OH$	1.690E+14	0.00	8.740E+02
$HO_2 + O \rightleftharpoons O_2 + OH$	1.810E+13	0.00	-3.970E+02
$HO_2 + OH \rightleftharpoons H_2O + O_2$	1.900E+16	-1.00	0.000E+00
$HO_2 + HO_2 \rightleftharpoons H_2O_2 + O_2$	4.200E+14	0.00	1.198E+04
Duplicate Reaction			
$HO_2 + HO_2 \rightleftharpoons H_2O_2 + O_2$	1.300E+11	0.00	-1.629E+03
Duplicate Reaction			
$H_2O_2(+M) \rightleftharpoons OH + OH(+M)$	2.951E+14	0.00	4.843E+04
Low pressure limit	1.202E+17	0.00	4.550E+04
Troe parameters: a=0.5, T***=1E+30, T*=1E-30			
Enhanced Collision Efficiencies:			
H_2=2.5, H_2O=12, CO=1.9, CO_2=3.8			
Enhanced Collision Efficiencies:			
AR=0.0			
$H_2O_2(+AR) \rightleftharpoons OH + OH(+AR)$	2.951E+14	0.00	4.843E+04
Low pressure limit	1.904E+16	0.00	4.300E+04
Troe parameters: a=0.5, T***=1E+30, T*=1E-30			
$H_2O_2 + H \rightleftharpoons H_2O + OH$	1.000E+13	0.00	3.590E+03
$H_2O_2 + H \rightleftharpoons HO_2 + H_2$	4.820E+13	0.00	7.950E+03
$H_2O_2 + O \rightleftharpoons OH + HO_2$	9.550E+06	2.00	3.970E+03
$H_2O_2 + OH \rightleftharpoons HO_2 + H_2O$	1.000E+12	0.00	0.000E+00
Duplicate Reaction			
$H_2O_2 + OH \rightleftharpoons HO_2 + H_2O$	5.800E+14	0.00	9.557E+03
Duplicate Reaction			
$CO + O + M \rightleftharpoons CO_2 + M$	2.510E+13	0.00	-4.540E+03
Enhanced Collision Efficiencies:			
H_2=2.5, H_2O=12, CO=1.9, CO_2=3.8			
Enhanced Collision Efficiencies:			
AR=0.87			
$CO + O_2 \rightleftharpoons CO_2 + O$	2.530E+12	0.00	4.770E+04
$CO + OH \rightleftharpoons CO_2 + H$	1.500E+07	1.30	-7.650E+02
$CO + HO_2 \rightleftharpoons CO_2 + OH$	6.020E+13	0.00	2.300E+04
$HCO + M \rightleftharpoons H + CO + M$	1.860E+17	-1.00	1.700E+04
Enhanced Collision Efficiencies:			
H_2=2.5, H_2O=12, CO=1.9, CO_2=3.8			
$HCO + O_2 \rightleftharpoons CO + HO_2$	7.580E+12	0.00	4.100E+02
$HCO + H \rightleftharpoons CO + H_2$	7.230E+13	0.00	0.000E+00
$HCO + O \rightleftharpoons CO + OH$	3.020E+13	0.00	0.000E+00
$HCO + O \rightleftharpoons CO_2 + H$	3.000E+13	0.00	0.000E+00
$HCO + OH \rightleftharpoons CO + H_2O$	3.020E+13	0.00	0.000E+00
$HCO + HO_2 \rightleftharpoons CO_2 + OH + H$	3.000E+13	0.00	0.000E+00
$HCO + CH_3 \rightleftharpoons CO + CH_4$	1.200E+14	0.00	0.000E+00
$HCO + HCO \rightleftharpoons CH_2O + CO$	1.800E+13	0.00	0.000E+00
$HCO + HCO \rightleftharpoons H_2 + CO + CO$	3.000E+12	0.00	0.000E+00
$CH_2O + M \rightleftharpoons HCO + H + M$	4.000E+23	-1.66	9.147E+04

Reaction	A (cm-moles-sec-K)	n	E (cal/mole)
$CH_2O + M \rightleftharpoons CO + H_2 + M$	8.250E+15	0.00	6.954E+04
$CH_2O + H \rightleftharpoons HCO + H_2$	1.140E+08	1.66	1.834E+03
$CH_2O + O \rightleftharpoons HCO + OH$	1.810E+13	0.00	3.080E+03
$CH_2O + OH \rightleftharpoons HCO + H_2O$	4.800E+09	1.18	-4.470E+02
$CH_2O + O_2 \rightleftharpoons HCO + HO_2$	2.000E+13	0.00	3.900E+04
$CH_2O + HO_2 \rightleftharpoons HCO + H_2O_2$	1.500E+13	0.00	1.520E+04
$CH_2O + CH_3 \rightleftharpoons HCO + CH_4$	5.540E+03	2.81	5.862E+03
$CH_2O + C_3H_5 \rightleftharpoons HCO + C_3H_6$	1.445E+08	1.80	1.818E+04
$CH_3O + M \rightleftharpoons CH_2O + H + M$	8.300E+17	-1.20	1.550E+04
$CH_3O + H \rightleftharpoons CH_2O + H_2$	2.000E+13	0.00	0.000E+00
$CH_3O + O \rightleftharpoons CH_2O + OH$	6.000E+12	0.00	0.000E+00
$CH_3O + OH \rightleftharpoons CH_2O + H_2O$	1.800E+13	0.00	0.000E+00
$CH_3O + O_2 \rightleftharpoons CH_2O + HO_2$	9.033E+13	0.00	1.198E+04
Duplicate Reaction			
$CH_3O + O_2 \rightleftharpoons CH_2O + HO_2$	2.200E+10	0.00	1.748E+03
Duplicate Reaction			
$CH_3O + HO_2 \rightleftharpoons CH_2O + H_2O_2$	3.000E+11	0.00	0.000E+00
$CH_3O + CO \rightleftharpoons CH_3 + CO_2$	1.600E+13	0.00	1.180E+04
$CH + O_2 \rightleftharpoons HCO + O$	1.000E+13	0.00	0.000E+00
$CH_2 + H \rightleftharpoons CH + H_2$	9.640E+13	0.00	0.000E+00
$CH_2 + O \rightleftharpoons CO + H + H$	1.050E+13	0.00	0.000E+00
$CH_2 + O \rightleftharpoons CO + H_2$	1.050E+13	0.00	0.000E+00
$CH_2 + O_2 \rightleftharpoons CO + OH + H$	1.130E+13	0.00	0.000E+00
$CH_2 + O_2 \rightleftharpoons CO + H_2O$	4.820E+12	0.00	0.000E+00
$CH_3 + O \rightleftharpoons CH_2O + H$	8.430E+13	0.00	0.000E+00
$CH_3 + OH \rightleftharpoons CH_2 + H_2O$	1.500E+13	0.00	5.000E+03
$CH_3 + O_2 \rightleftharpoons CH_3O + O$	1.990E+18	-1.57	2.923E+04
$CH_3 + HO_2 \rightleftharpoons CH_3O + OH$	2.000E+13	0.00	1.076E+03
$CH_3 + CH_3(+M) \rightleftharpoons C_2H_6(+M)$	9.030E+16	-1.18	6.540E+02
Low pressure limit	3.180E+41	-7.03	2.762E+03
Troe parameters: a=6.190E-01, T***=73.2, T*=1180.0			
$CH_3 + CH_3 \rightleftharpoons C_2H_4 + H_2$	1.000E+16	0.00	3.201E+04
$CH_3 + CH_3 \rightleftharpoons C_2H_5 + H$	8.000E+15	0.00	2.651E+04
$CH_4(+M) \rightleftharpoons CH_3 + H(+M)$	3.700E+15	0.00	1.038E+05
Low pressure limit	7.210E+30	-3.49	1.059E+05
$CH_4 + H \rightleftharpoons CH_3 + H_2$	5.470E+07	1.97	1.121E+04
$CH_4 + O \rightleftharpoons CH_3 + OH$	6.930E+08	1.56	8.484E+03
$CH_4 + OH \rightleftharpoons CH_3 + H_2O$	5.720E+06	1.96	2.639E+03
$CH_4 + O_2 \rightleftharpoons CH_3 + HO_2$	4.000E+13	0.00	5.691E+04
$CH_4 + HO_2 \rightleftharpoons CH_3 + H_2O_2$	1.810E+11	0.00	1.858E+04
$C_2H + O \rightleftharpoons CO + CH$	1.810E+13	0.00	0.000E+00
$C_2H + O_2 \rightleftharpoons HCCO + O$	6.020E+11	0.00	0.000E+00
$C_2H + O_2 \rightleftharpoons CO + HCO$	2.410E+12	0.00	0.000E+00
$HCCO + H \rightleftharpoons CH_2 + CO$	3.000E+13	0.00	0.000E+00
$HCCO + O \rightleftharpoons H + CO + CO$	1.200E+12	0.00	0.000E+00
$HCCO + O_2 \rightleftharpoons CO + CO + OH$	1.460E+12	0.00	2.500E+03
$C_2H_2 + M \rightleftharpoons C_2H + H + M$	7.460E+30	-3.70	1.271E+05
$C_2H_2 + H \rightleftharpoons C_2H + H_2$	6.020E+13	0.00	2.225E+04
$C_2H_2 + O \rightleftharpoons CH_2 + CO$	1.450E+06	2.09	1.560E+03

Reaction	A (cm-moles-sec-K)	n	E (cal/mole)
$C_2H_2 + O \rightleftharpoons HCCO + H$	5.780E+06	2.09	1.560E+03
$C_2H_2 + OH \rightleftharpoons C_2H + H_2O$	3.380E+07	2.00	1.400E+04
$C_2H_2 + O_2 \rightleftharpoons C_2H + HO_2$	1.200E+13	0.00	7.451E+04
$C_2H_2 + HO_2 \rightleftharpoons CH_2CO + OH$	6.030E+09	0.00	7.950E+03
$C_2H_3(+M) \rightleftharpoons C_2H_2 + H(+M)$	1.260E+32	-5.91	4.680E+04
Low pressure limit	4.170E+41	-7.49	4.550E+04
$C_2H_3 + H \rightleftharpoons C_2H_2 + H_2$	3.000E+13	0.00	0.000E+00
$C_2H_3 + O \rightleftharpoons CH_2CO + H$	9.600E+13	0.00	0.000E+00
$C_2H_3 + OH \rightleftharpoons C_2H_2 + H_2O$	3.000E+13	0.00	0.000E+00
$C_2H_3 + OH \rightleftharpoons CH_3CHO$	3.000E+13	0.00	0.000E+00
$C_2H_3 + O_2 \rightleftharpoons CH_2O + HCO$	4.480E+26	-4.55	5.480E+03
Duplicate Reaction			
$C_2H_3 + O_2 \rightleftharpoons CH_2O + HCO$	1.050E+38	-8.22	7.030E+03
Duplicate Reaction			
$C_2H_3 + O_2 \rightleftharpoons 2\,HCO + H$	3.270E+23	-3.94	5.010E+03
$C_2H_3 + HO_2 \rightleftharpoons CH_2CO + OH + H$	3.000E+13	0.00	0.000E+00
$C_2H_3 + CH_3 \rightleftharpoons C_2H_2 + CH_4$	3.900E+11	0.00	0.000E+00
$C_2H_3 + C_2H_3 \rightleftharpoons C_2H_4 + C_2H_2$	9.600E+11	0.00	0.000E+00
$C_2H_4(+M) \rightleftharpoons C_2H_2 + H_2(+M)$	7.940E+12	0.44	8.876E+04
Low pressure limit	6.100E+06	2.88	6.720E+04
$C_2H_3 + H(+M) \rightleftharpoons C_2H_4(+M)$	6.080E+12	0.27	2.800E+02
Low pressure limit	1.400E+30	-3.86	3.320E+03
Troe parameters: a=0.7820, T***=207.50, T*=2663.00, T**=6095.00			
Enhanced Collision Efficiencies:			
H_2=2, H_2O=6, CH_4=2, CO=1.5, CO_2=2, C_2H_6=3			
Enhanced Collision Efficiencies:			
AR=0.7			
$C_2H_4 + H \rightleftharpoons C_2H_3 + H_2$	1.320E+06	2.53	1.224E+04
$C_2H_4 + O \rightleftharpoons CH_3 + HCO$	1.320E+08	1.55	4.272E+02
$C_2H_4 + OH \rightleftharpoons C_2H_3 + H_2O$	2.020E+13	0.00	5.955E+03
$C_2H_4 + O_2 \rightleftharpoons C_2H_3 + HO_2$	4.215E+13	0.00	5.760E+04
$C_2H_4 + CH_3 \rightleftharpoons C_2H_3 + CH_4$	6.620E+00	3.70	9.500E+03
$C_2H_5(+M) \rightleftharpoons C_2H_4 + H(+M)$	4.900E+09	1.19	3.720E+04
Low pressure limit	5.10E+64	-13.96	6.010E+04
$C_2H_5 + O \rightleftharpoons CH_3CHO + H$	9.600E+14	0.00	0.000E+00
$C_2H_5 + OH \rightleftharpoons C_2H_4 + H_2O$	2.400E+13	0.00	0.000E+00
$C_2H_5 + OH \rightleftharpoons CH_3 + H + CH_2O$	2.400E+13	0.00	0.000E+00
$C_2H_5 + O_2 \rightleftharpoons C_2H_4 + HO_2$	8.430E+11	0.00	3.874E+03
$C_2H_5 + HO_2 \longrightarrow CH_3 + CH_2O + OH$	2.400E+13	0.00	0.000E+00
$C_2H_5 + HO_2 \rightleftharpoons C_2H_4 + H_2O_2$	3.000E+11	0.00	0.000E+00
$C_2H_5 + C_2H_5 \rightleftharpoons C_2H_4 + C_2H_6$	1.400E+12	0.00	0.000E+00
$C_2H_6 \rightleftharpoons C_2H_5 + H$	2.080E+38	-7.08	1.065E+05
$C_2H_6 + H \rightleftharpoons C_2H_5 + H_2$	5.420E+02	3.50	5.166E+03
$C_2H_6 + O \rightleftharpoons C_2H_5 + OH$	1.200E+12	0.60	7.311E+03
$C_2H_6 + OH \rightleftharpoons C_2H_5 + H_2O$	5.130E+06	2.06	8.544E+02
$C_2H_6 + O_2 \rightleftharpoons C_2H_5 + HO_2$	4.000E+13	0.00	5.090E+04
$C_2H_6 + HO_2 \rightleftharpoons C_2H_5 + H_2O_2$	2.940E+11	0.00	1.494E+04
$C_2H_6 + CH_3 \rightleftharpoons C_2H_5 + CH_4$	5.480E-01	4.00	8.284E+03
$C_2H_6 + C_2H_3 \rightleftharpoons C_2H_5 + C_2H_4$	6.000E+02	3.30	1.050E+04
$C_2H_6 + C_3H_5 \rightleftharpoons C_2H_5 + C_3H_6$	2.349E+02	3.30	1.983E+04

Reaction	A (cm-moles-sec-K)	n	E (cal/mole)
$CH_2CO + M \rightleftharpoons CH_2 + CO + M$	3.600E+15	0.00	5.927E+04
$CH_2CO + H \rightleftharpoons CH_3 + CO$	7.000E+12	0.00	3.000E+03
$CH_2CO + O \rightleftharpoons HCO + HCO$	2.000E+13	0.00	2.294E+03
$CH_2CO + OH \rightleftharpoons CH_2O + HCO$	1.000E+13	0.00	0.000E+00
$CH_3CO(+M) \rightleftharpoons CH_3 + CO(+M)$	1.200E+22	-3.04	1.880E+04
Low pressure limit	8.730E+42	-8.62	2.240E+04
$CH_3CO + H \rightleftharpoons CH_3 + HCO$	9.600E+13	0.00	0.000E+00
$CH_3CO + O \rightleftharpoons CH_3 + CO_2$	9.600E+12	0.00	0.000E+00
$CH_3CO + OH \rightleftharpoons CH_2CO + H_2O$	1.200E+13	0.00	0.000E+00
$CH_3CO + OH \longrightarrow CH_3 + CO + OH$	3.000E+13	0.00	0.000E+00
$CH_3CO + HO_2 \longrightarrow CH_3 + CO_2 + OH$	3.000E+13	0.00	0.000E+00
$CH_3CHO \rightleftharpoons CH_3 + HCO$	7.079E+15	0.00	8.176E+04
$CH_3CHO + H \rightleftharpoons CH_3CO + H_2$	4.000E+13	0.00	4.207E+03
$CH_3CHO + O \rightleftharpoons CH_3CO + OH$	5.000E+12	0.00	1.793E+03
$CH_3CHO + OH \rightleftharpoons CH_3CO + H_2O$	1.000E+13	0.00	0.000E+00
$CH_3CHO + O_2 \rightleftharpoons CH_3CO + HO_2$	2.000E+13	0.50	4.220E+04
$CH_3CHO + HO_2 \rightleftharpoons CH_3CO + H_2O_2$	1.700E+12	0.00	1.070E+04
$CH_3CHO + CH_3 \rightleftharpoons CH_3CO + CH_4$	1.740E+12	0.00	8.440E+03
$C_3H_3 + O \rightleftharpoons CH_2O + C_2H$	2.000E+13	0.00	0.000E+00
$C_3H_3 + O_2 \rightleftharpoons CH_2CO + HCO$	3.010E+10	0.00	2.870E+03
$C_3H_3 + CH_3 \rightleftharpoons C_2H_5 + C_2H$	1.000E+13	0.00	3.750E+04
$C_3H_3 + CH_3 \longrightarrow C_4H_6$	5.000E+12	0.00	0.000E+00
$2\,C_3H_3 \rightleftharpoons C_6H_6$	3.000E+11	0.00	0.000E+00
$2\,C_3H_3 \rightleftharpoons 3\,C_2H_2$	5.000E+11	0.00	0.000E+00
$C_3H_4 + M \rightleftharpoons C_3H_3 + H + M$	1.000E+17	0.00	7.000E+04
Enhanced Collision Efficiencies: H_2=2.5, H_2O=12.0, CO=1.9, CO_2=3.8, CH_4=12.0			
$C_3H_4 + H \rightleftharpoons C_3H_3 + H_2$	1.000E+12	0.00	1.500E+03
$C_3H_4 + O \rightleftharpoons CH_2O + C_2H_2$	3.000E-03	4.61	-4.243E+03
$C_3H_4 + O \rightleftharpoons CO + C_2H_4$	9.000E-03	4.61	-4.243E+03
$C_3H_4 + OH \rightleftharpoons C_3H_3 + H_2O$	1.450E+13	0.00	4.170E+03
$C_3H_4 + OH \rightleftharpoons CH_2CO + CH_3$	3.120E+12	0.00	-3.970E+02
$C_3H_4 + O_2 \rightleftharpoons C_3H_3 + HO_2$	4.000E+13	0.00	6.150E+04
$C_3H_4 + HO_2 \longrightarrow CH_2CO + CH_2 + OH$	4.000E+12	0.00	1.900E+04
$C_3H_4 + CH_3 \rightleftharpoons C_3H_3 + CH_4$	2.000E+12	0.00	7.700E+03
$C_3H_4 + C_3H_3 \rightleftharpoons C_6H_6 + H$	2.200E+11	0.00	2.000E+03
$C_3H_4O + H \longrightarrow C_2H_3 + CO + H_2$	4.000E+09	1.16	2.400E+03
$C_3H_4O + O \longrightarrow C_2H_3 + CO + OH$	6.000E+12	0.00	1.900E+03
$C_3H_4O + OH \longrightarrow C_2H_3 + CO + H_2O$	8.000E+12	0.00	0.000E+00
$C_3H_5 \rightleftharpoons C_3H_4 + H$	1.500E+11	0.84	5.981E+04
$C_3H_5 + H \rightleftharpoons C_3H_4 + H_2$	1.800E+13	0.00	0.000E+00
$C_3H_5 + O \rightleftharpoons C_3H_4O + H$	6.020E+13	0.00	0.000E+00
$C_3H_5 + OH \rightleftharpoons C_3H_4 + H_2O$	6.020E+12	0.00	0.000E+00
$C_3H_5 + O_2 \rightleftharpoons C_3H_4 + HO_2$	1.325E+07	0.00	0.000E+00
$C_3H_5 + HO_2 \longrightarrow C_2H_3 + CH_2O + OH$	6.720E+11	0.00	0.000E+00
$C_3H_5 + HCO \rightleftharpoons C_3H_6 + CO$	6.000E+13	0.00	0.000E+00
$C_3H_5 + CH_3 \rightleftharpoons C_3H_4 + CH_4$	3.000E+12	-0.32	-2.620E+02
$C_3H_5 + C_2H_3 \rightleftharpoons C_3H_6 + C_2H_2$	4.800E+12	0.00	0.000E+00
$C_3H_5 + C_2H_3 \rightleftharpoons C_3H_4 + C_2H_4$	2.400E+12	0.00	0.000E+00
$C_3H_5 + C_2H_5 \rightleftharpoons C_3H_6 + C_2H_4$	2.600E+12	0.00	-1.310E+02

Reaction	A (cm-moles-sec-K)	n	E (cal/mole)
$C_3H_5 + C_2H_5 \rightleftharpoons C_3H_4 + C_2H_6$	9.600E+11	0.00	-1.310E+02
$2\,C_3H_5 \rightleftharpoons C_3H_4 + C_3H_6$	8.430E+10	0.00	-2.630E+02
$2\,C_3H_5 \rightleftharpoons C_6H_{10}$	1.020E+13	0.00	-2.630E+02
Duplicate Reaction			
$C_3H_6 \rightleftharpoons C_2H_3 + CH_3$	1.100E+21	-1.20	9.771E+04
$C_3H_6 \rightleftharpoons C_3H_5 + H$	2.500E+15	0.00	8.758E+04
$C_3H_6 + H \rightleftharpoons C_3H_5 + H_2$	1.730E+05	2.50	2.490E+03
$C_3H_6 + H \rightleftharpoons C_2H_4 + CH_3$	1.325E+13	0.00	3.261E+03
$C_3H_6 + O \longrightarrow CH_2CO + CH_3 + H$	7.700E+07	1.66	6.337E+02
$C_3H_6 + O \rightleftharpoons C_2H_5 + HCO$	3.431E+07	1.66	-1.928E+02
$C_3H_6 + O \rightleftharpoons C_3H_5 + OH$	1.750E+11	0.70	5.883E+03
$C_3H_6 + OH \rightleftharpoons C_3H_5 + H_2O$	3.120E+06	2.00	-2.980E+02
$C_3H_6 + O_2 \rightleftharpoons C_3H_5 + HO_2$	6.020E+13	0.00	4.760E+04
$C_3H_6 + HO_2 \rightleftharpoons C_3H_5 + H_2O_2$	9.635E+03	2.60	1.390E+04
$C_3H_6 + CH_3 \rightleftharpoons C_3H_5 + CH_4$	2.220E+00	3.50	5.675E+03
$C_3H_6 + C_2H_3 \rightleftharpoons C_3H_5 + C_2H_4$	2.216E+00	3.50	4.679E+03
$C_4H_6 \longrightarrow C_2H_2 + C_2H_3 + H$	1.580E+16	0.00	1.100E+05
$C_4H_6 \rightleftharpoons C_2H_3 + C_2H_3$	1.800E+13	0.00	8.500E+04
$C_4H_6 + H \rightleftharpoons C_2H_3 + C_2H_4$	5.000E+11	0.00	0.000E+00
$C_4H_6 + H \longrightarrow H_2 + C_2H_2 + C_2H_3$	6.300E+10	0.70	6.000E+03
$C_4H_6 + OH \longrightarrow HCO + H + C_3H_5$	5.000E+12	0.00	0.000E+00
$C_4H_6 + OH \longrightarrow C_3H_4O + CH_3$	5.000E+12	0.00	0.000E+00
$C_4H_6 + CH_3 \longrightarrow CH_4 + C_2H_2 + C_2H_3$	7.000E+13	0.00	1.850E+04
$C_4H_8 \longrightarrow C_3H_5 + CH_3$	1.000E+16	0.00	7.300E+04
Duplicate Reaction			
$C_3H_5 + CH_3 \longrightarrow C_4H_8$	1.000E+16	0.00	7.300E+04
Duplicate Reaction			
$C_4H_8 + H \rightleftharpoons C_2H_4 + C_2H_5$	7.230E+12	0.00	1.302E+03
$C_4H_8 + H \rightleftharpoons C_3H_6 + CH_3$	7.230E+12	0.00	1.302E+03
$C_4H_8 + H \longrightarrow H_2 + C_4H_6 + H$	1.150E+05	2.50	2.490E+03
$C_4H_8 + H \longrightarrow H_2 + C_2H_3 + C_2H_4$	6.600E+05	2.54	6.760E+03
$C_4H_8 + O \longrightarrow OH + C_4H_6 + H$	1.160E+11	0.70	5.880E+03
$C_4H_8 + O \longrightarrow OH + C_2H_3 + C_2H_4$	9.600E+04	2.68	3.720E+03
$C_4H_8 + OH \longrightarrow H_2O + C_4H_6 + H$	2.080E+06	2.00	-2.980E+02
$C_4H_8 + OH \longrightarrow H_2O + C_2H_3 + C_2H_4$	1.580E+07	1.80	9.300E+02
$C_4H_8 + CH_3 \longrightarrow CH_4 + C_4H_6 + H$	1.480E+00	3.50	5.670E+03
$C_5H_{10} \rightleftharpoons C_3H_5 + C_2H_5$	1.000E+16	0.00	7.134E+04
$C_5H_{10} \rightleftharpoons C_3H_6 + C_2H_4$	3.160E+12	0.00	5.704E+04
$C_5H_{10} + H \longrightarrow 2\,C_2H_4 + CH_3$	7.230E+12	0.00	1.302E+03
$C_5H_{10} + H \rightleftharpoons C_3H_6 + C_2H_5$	7.230E+12	0.00	1.302E+03
$C_5H_{10} + H \longrightarrow H_2 + C_4H_6 + CH_3$	1.150E+05	2.50	2.490E+03
$C_5H_{10} + H \longrightarrow H_2 + C_2H_4 + C_3H_5$	6.600E+05	2.54	6.760E+03
$C_5H_{10} + H \longrightarrow H_2 + C_3H_6 + C_2H_3$	1.300E+06	2.40	4.470E+03
$C_5H_{10} + O \longrightarrow OH + C_4H_6 + CH_3$	1.160E+11	0.70	5.880E+03
$C_5H_{10} + O \longrightarrow OH + C_2H_4 + C_3H_5$	9.600E+04	2.68	3.720E+03
$C_5H_{10} + O \longrightarrow OH + C_3H_6 + C_2H_3$	4.760E+04	2.71	2.110E+03
$C_5H_{10} + OH \longrightarrow H_2O + C_4H_6 + CH_3$	2.080E+06	2.00	-2.980E+02
$C_5H_{10} + OH \longrightarrow H_2O + C_2H_4 + C_3H_5$	1.580E+07	1.80	9.300E+02
$C_5H_{10} + OH \longrightarrow H_2O + C_3H_6 + C_2H_3$	7.080E+06	1.90	1.600E+02
$C_5H_{10} + CH_3 \longrightarrow CH_4 + C_4H_6 + CH_3$	1.480E+00	3.50	5.670E+03
$C_6H_{12} \rightleftharpoons 2\,C_3H_6$	3.980E+12	0.00	5.743E+04
$C_6H_{12} \longrightarrow C_3H_5 + C_2H_4 + CH_3$	7.940E+15	0.00	7.074E+04
$C_6H_{12} + H \longrightarrow C_3H_6 + C_2H_4 + CH_3$	7.230E+12	0.00	1.302E+03

Reaction	A (cm-moles-sec-K)	n	E (cal/mole)
$C_6H_{12} + H \longrightarrow 2C_2H_4 + C_2H_5$	7.230E+12	0.00	1.302E+03
$C_6H_{12} + H \longrightarrow H_2 + C_4H_6 + C_2H_5$	1.150E+05	2.50	2.490E+03
$C_6H_{12} + H \longrightarrow H_2 + 2C_2H_4 + C_2H_3$	6.600E+05	2.54	6.760E+03
$C_6H_{12} + H \longrightarrow H_2 + C_3H_6 + C_3H_5$	1.300E+06	2.40	4.470E+03
$C_6H_{12} + H \longrightarrow H_2 + C_2H_3 + C_4H_8$	1.300E+06	2.40	4.470E+03
$C_6H_{12} + O \longrightarrow OH + C_4H_6 + C_2H_5$	1.160E+11	0.70	5.880E+03
$C_6H_{12} + O \longrightarrow OH + 2C_2H_4 + C_2H_3$	9.600E+04	2.68	3.720E+03
$C_6H_{12} + O \longrightarrow OH + C_3H_6 + C_3H_5$	4.760E+04	2.71	2.110E+03
$C_6H_{12} + O \longrightarrow OH + C_2H_3 + C_4H_8$	4.760E+04	2.71	2.110E+03
$C_6H_{12} + OH \longrightarrow H_2O + C_4H_6 + C_2H_5$	2.080E+06	2.00	-2.980E+02
$C_6H_{12} + OH \longrightarrow H_2O + 2C_2H_4 + C_2H_3$	1.580E+07	1.80	9.300E+02
$C_6H_{12} + OH \longrightarrow H_2O + C_3H_6 + C_3H_5$	7.080E+06	1.90	1.600E+02
$C_6H_{12} + OH \longrightarrow H_2O + C_2H_3 + C_4H_8$	7.080E+06	1.90	1.600E+02
$C_6H_{12} + CH_3 \longrightarrow CH_4 + C_4H_6 + C_2H_5$	1.480E+00	3.50	5.670E+03
$C_7H_{16} \longrightarrow H + 3C_2H_4 + CH_3$	1.800E+16	0.00	1.006E+05
$C_7H_{16} \longrightarrow H + C_3H_6 + C_2H_4 + C_2H_5$	1.200E+16	0.00	9.809E+04
$C_7H_{16} \longrightarrow H + C_4H_8 + C_2H_4 + CH_3$	1.200E+16	0.00	9.809E+04
$C_7H_{16} \longrightarrow H + C_5H_{10} + C_2H_5$	6.000E+15	0.00	9.809E+04
$C_7H_{16} \longrightarrow CH_3 + 2C_2H_4 + C_2H_5$ Duplicate Reaction	4.000E+17	0.00	8.730E+04
$C_7H_{16} \longrightarrow CH_3 + 2C_2H_4 + C_2H_5$ Duplicate Reaction	4.000E+17	0.00	8.540E+04
$C_7H_{16} \longrightarrow CH_3 + 2C_2H_4 + C_2H_5$ Duplicate Reaction	2.000E+17	0.00	8.490E+04
$C_7H_{16} + H \longrightarrow H_2 + 3C_2H_4 + CH_3$	1.320E+06	2.54	6.760E+03
$C_7H_{16} + O \longrightarrow OH + 3C_2H_4 + CH_3$	2.880E+06	2.40	5.505E+03
$C_7H_{16} + OH \longrightarrow H_2O + 3C_2H_4 + CH_3$	1.740E+07	1.80	9.740E+02
$C_7H_{16} + O_2 \longrightarrow HO_2 + 3C_2H_4 + CH_3$	3.970E+13	0.00	5.090E+04
$C_7H_{16} + HO_2 \longrightarrow H_2O_2 + 3C_2H_4 + CH_3$	4.760E+04	2.55	1.650E+04
$C_7H_{16} + CH_3 \longrightarrow CH_4 + 3C_2H_4 + CH_3$	9.060E-01	3.46	5.480E+03
$C_7H_{16} + C_3H_5 \longrightarrow C_3H_6 + 3C_2H_4 + CH_3$	2.350E+02	3.30	1.980E+04
$C_7H_{16} + H \longrightarrow H_2 + C_3H_6 + C_2H_4 + C_2H_5$	2.600E+06	2.40	4.470E+03
$C_7H_{16} + O \longrightarrow OH + C_3H_6 + C_2H_4 + C_2H_5$	2.760E+05	2.60	1.910E+03
$C_7H_{16} + OH \longrightarrow H_2O + C_3H_6 + C_2H_4 + C_2H_5$	3.800E+06	2.00	-5.960E+02
$C_7H_{16} + O_2 \longrightarrow HO_2 + C_3H_6 + C_2H_4 + C_2H_5$	7.920E+13	0.00	4.759E+04
$C_7H_{16} + HO_2 \longrightarrow H_2O_2 + C_3H_6 + C_2H_4 + C_2H_5$	1.930E+04	2.60	1.390E+04
$C_7H_{16} + CH_3 \longrightarrow CH_4 + C_3H_6 + C_2H_4 + C_2H_5$	4.270E+11	0.00	1.050E+04
$C_7H_{16} + C_3H_5 \longrightarrow C_3H_6 + C_3H_6 + C_2H_4 + C_2H_5$	1.566E+02	3.30	1.820E+04
$C_7H_{16} + H \longrightarrow H_2 + C_4H_8 + C_2H_4 + CH_3$	2.080E+06	2.40	4.470E+03
$C_7H_{16} + H \longrightarrow H_2 + C_6H_{12} + CH_3$	5.200E+05	2.40	4.470E+03
$C_7H_{16} + O \longrightarrow OH + C_4H_8 + C_2H_4 + CH_3$	2.210E+05	2.60	1.910E+03
$C_7H_{16} + O \longrightarrow OH + C_6H_{12} + CH_3$	0.550E+05	2.60	1.910E+03
$C_7H_{16} + OH \longrightarrow H_2O + C_4H_8 + C_2H_4 + CH_3$	3.496E+06	2.00	-1.312E+03
$C_7H_{16} + OH \longrightarrow H_2O + C_6H_{12} + CH_3$	0.874E+06	2.00	-1.312E+03
$C_7H_{16} + O_2 \longrightarrow HO_2 + C_4H_8 + C_2H_4 + CH_3$	6.340E+13	0.00	4.760E+04
$C_7H_{16} + O_2 \longrightarrow HO_2 + C_6H_{12} + CH_3$	1.580E+13	0.00	4.760E+04
$C_7H_{16} + HO_2 \longrightarrow H_2O_2 + C_4H_8 + C_2H_4 + CH_3$	1.540E+04	2.60	1.390E+04
$C_7H_{16} + HO_2 \longrightarrow H_2O_2 + C_6H_{12} + CH_3$	3.860E+03	2.60	1.390E+04
$C_7H_{16} + CH_3 \longrightarrow CH_4 + C_4H_8 + C_2H_4 + CH_3$	2.410E+00	3.46	5.480E+03
$C_7H_{16} + CH_3 \longrightarrow CH_4 + C_6H_{12} + CH_3$	6.020E-01	3.46	5.480E+03
$C_7H_{16} + C_3H_5 \longrightarrow C_3H_6 + C_4H_8 + C_2H_4 + CH_3$	1.250E+02	3.30	1.820E+04
$C_7H_{16} + C_3H_5 \longrightarrow C_3H_6 + C_6H_{12} + CH_3$	3.130E+01	3.30	1.820E+04
$C_7H_{16} + H \longrightarrow H_2 + C_5H_{10} + C_2H_5$	1.300E+06	2.40	4.470E+03
$C_7H_{16} + O \longrightarrow OH + C_5H_{10} + C_2H_5$	1.380E+05	2.60	1.910E+03
$C_7H_{16} + OH \longrightarrow H_2O + C_5H_{10} + C_2H_5$	4.370E+06	2.00	-1.312E+03
$C_7H_{16} + O_2 \longrightarrow HO_2 + C_5H_{10} + C_2H_5$	3.960E+13	0.00	4.760E+04
$C_7H_{16} + HO_2 \longrightarrow H_2O_2 + C_5H_{10} + C_2H_5$	9.640E+03	2.60	1.390E+04
$C_7H_{16} + CH_3 \longrightarrow CH_4 + C_5H_{10} + C_2H_5$	1.510E+00	3.46	5.480E+03

Reaction	A (cm-moles-sec-K)	n	E (cal/mole)
$C_7H_{16} + C_3H_5 \longrightarrow C_3H_6 + C_5H_{10} + C_2H_5$	7.820E+01	3.30	1.820E+04
$CH_3 + C_2H_5(+M) \rightleftharpoons C_3H_8(+M)$	.9430E+13	.000	.00
Low pressure limit	2.710E+74	-16.82	13065.0
Troe parameters: a=.1527, T***=291.0, T*=2742.0, T**=7748.0			
Enhanced Collision Efficiencies:			
H_2=2.00, H_2O=6.00, CH_4=2.00, CO=1.50, CO_2=2.00, C_2H_6=3.00, AR=.70			
$O + C_3H_8 \rightleftharpoons OH + C_3H_7$	1.930E+05	2.680	3716.00
$H + C_3H_8 \rightleftharpoons C_3H_7 + H_2$	1.320E+06	2.540	6756.00
$OH + C_3H_8 \rightleftharpoons C_3H_7 + H_2O$	3.160E+07	1.800	934.00
$C_3H_7 + H_2O_2 \rightleftharpoons HO_2 + C_3H_8$	3.780E+02	2.720	1500.00
$CH_3 + C_3H_8 \rightleftharpoons C_3H_7 + CH_4$	0.903E+00	3.650	7154.00
$CH_3 + C_2H_4(+M) \rightleftharpoons C_3H_7(+M)$	2.550E+06	1.600	5700.00
Low pressure limit	3.00E+63	-14.6	18170.
Troe parameters: a=.1894, T***=277.0, T*=8748.0, T**=7891.0			
Enhanced Collision Efficiencies:			
H_2=2.00, H_2O=6.00, CH_4=2.00, CO=1.50, CO_2=2.00, C_2H_6=3.00, AR=.70			
$O + C_3H_7 \rightleftharpoons C_2H_5 + CH_2O$	9.640E+13	.000	.00
$H + C_3H_7(+M) \rightleftharpoons C_3H_8(+M)$	3.613E+13	.000	.00
Low pressure limit	4.420E+61	-13.545	11357.0
Troe parameters: a=.315, T***=369.0, T*=3285.0, T**=6667.0			
Enhanced Collision Efficiencies:			
H_2=2.00, H_2O=6.00, CH_4=2.00, CO=1.50, CO_2=2.00, C_2H_6=3.00, AR=.70			
$H + C_3H_7 \rightleftharpoons CH_3 + C_2H_5$	4.060E+06	2.190	890.00
$HO_2 + C_3H_7 \rightleftharpoons O_2 + C_3H_8$	2.550E+10	0.255	-943.00
$HO_2 + C_3H_7 \longrightarrow OH + C_2H_5 + CH_2O$	2.410E+13	.000	.00
$CH_3 + C_3H_7 \rightleftharpoons 2\,C_2H_5$	1.927E+13	-0.320	.00
$C_3H_7 \longrightarrow C_3H_6 + H$	1.250E+14	0.000	37045.00
$C_3H_6 + H \longrightarrow C_3H_7$	3.713E+13	0.000	3346.00
$C_4H_7 \longrightarrow C_4H_6 + H$	1.200E+14	0.000	49235.00
$C_4H_6 + H \longrightarrow C_4H_7$	1.343E+14	0.000	7242.00
$C_4H_7 + O_2 \rightleftharpoons C_4H_6 + HO_2$	1.000E+11	0.000	.00
$C_4H_8 \longrightarrow C_3H_5 + CH_3$	8.000E+16	0.000	73374.00
Duplicate Reaction			
$C_3H_5 + CH_3 \longrightarrow C_4H_8$	2.070E+14	0.000	7218.00
Duplicate Reaction			
$C_4H_8 \longrightarrow C_4H_7 + H$	4.110E+18	-1.000	97514.00
$C_4H_7 + H \longrightarrow C_4H_8$	1.494E+17	-1.000	1083.00
$C_4H_8 + H \rightleftharpoons C_4H_7 + H_2$	5.000E+13	0.000	3896.00
$C_4H_8 + OH \rightleftharpoons C_4H_7 + H_2O$	1.750E+13	0.000	6955.00
$C_4H_8 + OH \rightleftharpoons C_3H_7 + CH_2O$	6.500E+12	0.000	.00
$C_6H_{11} \rightleftharpoons C_3H_5 + C_3H_6$	2.500E+13	0.000	30115.00
$C_7H_{13} \rightleftharpoons C_3H_5 + C_4H_8$	2.500E+13	0.000	30115.00
$C_4H_7(I) \longrightarrow C_3H_4 + CH_3$	1.000E+13	0.000	51147.00
$C_3H_4 + CH_3 \longrightarrow C_4H_7(I)$	2.000E+11	0.000	7505.00
$C_4H_8(I) \longrightarrow C_3H_5 + CH_3$	5.000E+18	-1.000	73374.00
$C_3H_5 + CH_3 \longrightarrow C_4H_8(I)$	2.000E+13	0.000	.00
$C_4H_8(I) \longrightarrow C_4H_7(I) + H$	1.000E+17	0.000	87954.00
$C_4H_7(I) + H \longrightarrow C_4H_8(I)$	2.000E+13	0.000	.00
$C_4H_8(I) + H \longrightarrow C_4H_7(I) + H_2$	1.000E+13	0.000	3800.00
$C_4H_7(I) + H_2 \longrightarrow C_4H_8(I) + H$	3.000E+13	0.000	25096.00
$C_4H_8(I) + O \rightleftharpoons C_4H_7(I) + OH$	2.500E+05	2.600	-1123.00
$C_4H_8(I) + O \rightleftharpoons C_3H_7 + HCO$	7.230E+05	2.30	-1052.00
$C_4H_8(I) + OH \rightleftharpoons C_4H_7(I) + H_2O$	9.600E+12	0.000	1243.00
$C_4H_8(I) + OH \rightleftharpoons C_3H_7 + CH_2O$	1.500E+12	0.000	.00

Reaction	A (cm-moles-sec-K)	n	E (cal/mole)
$C_4H_9(I) \rightleftharpoons C_3H_6 + CH_3$	1.000E+14	0.000	32744.00
$C_4H_9(I) \longrightarrow C_4H_8(I) + H$	2.000E+13	0.000	36090.00
$C_4H_8(I) + H \longrightarrow C_4H_9(I)$	1.000E+13	0.000	1195.00
$C_4H_9(I) + O_2 \rightleftharpoons C_4H_8(I) + HO_2$	2.340E+10	0.000	.00
$C_4H_9(T) \longrightarrow C_4H_8(I) + H$	3.160E+15	0.000	43738.00
$C_4H_8(I) + H \longrightarrow C_4H_9(T)$	3.100E+13	0.000	1506.00
$C_4H_9(T) \rightleftharpoons C_3H_6 + CH_3$	1.585E+15	0.000	46367.00
$C_4H_9(T) + O_2 \rightleftharpoons C_4H_8(I) + HO_2$	1.170E+11	0.000	.00
$C_5H_{11} \rightleftharpoons C_4H_8(I) + CH_3$	1.000E+11	0.000	26052.00
$C_6H_{10} \longrightarrow C_3H_5 + C_3H_5$ Duplicate Reaction	2.512E+14	0.000	59512.00
$C_3H_5 + C_3H_5 \longrightarrow C_6H_{10}$ Duplicate Reaction	1.020E+13	0.000	-263.00
$C_7H_{13} \rightleftharpoons C_4H_8(I) + C_3H_5$	2.500E+13	0.000	6118.00
$C_7H_{13} \rightleftharpoons C_3H_6 + C_4H_7(I)$	2.500E+13	0.000	6118.00
$C_7H_{13} \longrightarrow C_6H_{10} + CH_3$	1.000E+14	0.000	8939.00
$C_6H_{10} + CH_3 \longrightarrow C_7H_{13}$	3.200E+11	0.000	9106.00
$AC_7H_{14} \rightleftharpoons C_4H_7(I) + C_3H_7$	2.500E+16	0.000	70985.00
$AC_7H_{14} \rightleftharpoons C_3H_5 + C_4H_9(T)$	2.500E+16	0.000	70985.00
$AC_7H_{14} + O \rightleftharpoons C_7H_{13} + OH$	2.540E+05	2.600	-1099.00
$AC_7H_{14} + OH \rightleftharpoons C_7H_{13} + H_2O$	6.800E+13	0.000	3107.00
$SC_7H_{14} \rightleftharpoons C_6H_{11} + CH_3$	2.500E+16	0.000	70985.00
$SC_7H_{14} + H \rightleftharpoons C_7H_{13} + H_2$	2.800E+13	0.000	4015.00
$SC_7H_{14} + O \rightleftharpoons C_7H_{13} + OH$	2.540E+05	2.600	-1099.00
$SC_7H_{14} + OH \rightleftharpoons C_7H_{13} + H_2O$	6.800E+13	0.000	3107.00
$IC_8H_{16} \rightleftharpoons C_4H_7(I) + C_4H_9(T)$	2.500E+16	0.000	70985.00
$IC_8H_{16} \rightleftharpoons C_7H_{13} + CH_3$	2.500E+16	0.000	70985.00
$IC_8H_{16} + OH \rightleftharpoons C_4H_8(I) + C_4H_7(I) + H_2O$	1.300E+09	1.300	693.00
$AC_8H_{17} \longrightarrow DC_8H_{17}$	6.000E+11	0.000	14101.00
$DC_8H_{17} \longrightarrow AC_8H_{17}$	9.000E+11	0.000	14101.00
$AC_8H_{17} \longrightarrow SC_8H_{17}$	1.000E+11	0.000	16109.00
$SC_8H_{17} \longrightarrow AC_8H_{17}$	9.000E+11	0.000	21128.00
$AC_8H_{17} \rightleftharpoons AC_7H_{14} + CH_3$	1.000E+11	0.000	26051.00
$AC_8H_{17} \rightleftharpoons C_4H_8(I) + C_4H_9(I)$	1.300E+13	0.000	29636.00
$BC_8H_{17} \rightleftharpoons SC_7H_{14} + CH_3$	1.000E+13	0.000	26051.00
$SC_8H_{17} \rightleftharpoons C_4H_8(I) + C_4H_9(T)$	5.000E+12	0.000	28920.00
$DC_8H_{17} \rightleftharpoons AC_7H_{14} + CH_3$	1.250E+13	0.000	32744.00
$DC_8H_{17} \rightleftharpoons C_5H_{11} + C_3H_6$	1.300E+13	0.000	29637.00
$DC_8H_{17} \rightleftharpoons IC_8H_{16} + H$	3.300E+14	0.000	36090.00
$C_8H_{18} \rightleftharpoons C_4H_9(T) + C_4H_9(I)$	4.000E+16	0.000	78155.00
$C_8H_{18} \rightleftharpoons C_5H_{11} + C_3H_7$	2.000E+16	0.000	78155.00
$C_8H_{18} + H \rightleftharpoons AC_8H_{17} + H_2$	8.440E+07	2.000	7696.00
$C_8H_{18} + H \rightleftharpoons BC_8H_{17} + H_2$	9.000E+06	2.000	4995.00
$C_8H_{18} + H \rightleftharpoons SC_8H_{17} + H_2$	1.260E+14	0.000	7314.00
$C_8H_{18} + H \rightleftharpoons DC_8H_{17} + H_2$	5.628E+07	2.000	7696.00
$C_8H_{18} + O \rightleftharpoons AC_8H_{17} + OH$	1.500E+14	0.000	7863.00
$C_8H_{18} + O \rightleftharpoons BC_8H_{17} + OH$	2.800E+13	0.000	5210.00
$C_8H_{18} + O \rightleftharpoons SC_8H_{17} + OH$	1.000E+13	0.000	3274.00
$C_8H_{18} + O \rightleftharpoons DC_8H_{17} + OH$	1.000E+14	0.000	7863.00
$C_8H_{18} + OH \rightleftharpoons AC_8H_{17} + H_2O$	1.290E+10	1.100	1816.00

Reaction	A (cm-moles-sec-K)	n	E (cal/mole)
$C_8H_{18} + OH \rightleftharpoons BC_8H_{17} + H_2O$	1.300E+09	1.300	693.00
$C_8H_{18} + OH \rightleftharpoons SC_8H_{17} + H_2O$	1.960E+12	0.000	454.00
$C_8H_{18} + OH \rightleftharpoons DC_8H_{17} + H_2O$	8.610E+09	1.100	1816.00
$C_8H_{18} + HO_2 \rightleftharpoons AC_8H_{17} + H_2O_2$	1.680E+13	0.000	19407.00
$C_8H_{18} + HO_2 \rightleftharpoons BC_8H_{17} + H_2O_2$	3.350E+12	0.000	17017.00
$C_8H_{18} + HO_2 \rightleftharpoons SC_8H_{17} + H_2O_2$	3.000E+12	0.000	14412.00
$C_8H_{18} + HO_2 \rightleftharpoons DC_8H_{17} + H_2O_2$	1.120E+13	0.000	19407.00
$C_8H_{18} + CH_3 \rightleftharpoons AC_8H_{17} + CH_4$	5.850E+12	0.000	11616.00
$C_8H_{18} + CH_3 \rightleftharpoons BC_8H_{17} + CH_4$	1.200E+12	0.000	9512.00
$C_8H_{18} + CH_3 \rightleftharpoons SC_8H_{17} + CH_4$	1.000E+11	0.000	7911.00
$C_8H_{18} + CH_3 \rightleftharpoons DC_8H_{17} + CH_4$	3.900E+12	0.000	11616.00
$C_8H_{18} + O_2 \rightleftharpoons AC_8H_{17} + HO_2$	3.750E+13	0.000	48996.00
$C_8H_{18} + O_2 \rightleftharpoons BC_8H_{17} + HO_2$	2.000E+13	0.000	48040.00
$C_8H_{18} + O_2 \rightleftharpoons SC_8H_{17} + HO_2$	2.000E+12	0.000	46128.00
$C_8H_{18} + O_2 \rightleftharpoons DC_8H_{17} + HO_2$	2.500E+13	0.000	48996.00
Mechanism of NOx chemistry			
$N + NO \rightleftharpoons N_2 + O$	2.700E+13	.000	355.00
$N + O_2 \rightleftharpoons NO + O$	9.000E+09	1.000	6500.00
$N + OH \rightleftharpoons NO + H$	3.360E+13	.000	385.00
$N_2O + O \rightleftharpoons N_2 + O_2$	1.400E+12	.000	10810.00
$N_2O + O \rightleftharpoons 2\,NO$	2.900E+13	.000	23150.00
$N_2O + H \rightleftharpoons N_2 + OH$	3.870E+14	.000	18880.00
$N_2O + OH \rightleftharpoons N_2 + HO_2$	2.000E+12	.000	21060.00
$N_2O(+M) \rightleftharpoons N_2 + O(+M)$	7.910E+10	.000	56020.00
Low pressure limit	6.370E+14	.000	56640.00
Enhanced Collision Efficiencies: H_2=2.00, H_2O=6.00, CH_4=2.00, CO=1.50, CO_2=2.00, C_2H_6=3.00, AR=.625			
$HO_2 + NO \rightleftharpoons NO_2 + OH$	2.110E+12	.000	-480.00
$NO + O + M \rightleftharpoons NO_2 + M$	1.060E+20	-1.410	.00
Enhanced Collision Efficiencies: H_2=2.00, H_2O=6.00, CH_4=2.00, CO=1.50, CO_2=2.00, C_2H_6=3.00, AR=.70			
$NO_2 + O \rightleftharpoons NO + O_2$	3.900E+12	.000	-240.00
$NO_2 + H \rightleftharpoons NO + OH$	1.320E+14	.000	360.00
$NH + O \rightleftharpoons NO + H$	4.000E+13	.000	.00
$NH + H \rightleftharpoons N + H_2$	3.200E+13	.000	330.00
$NH + OH \rightleftharpoons HNO + H$	2.000E+13	.000	.00
$NH + OH \rightleftharpoons N + H_2O$	2.000E+09	1.200	.00
$NH + O_2 \rightleftharpoons HNO + O$	4.610E+05	2.000	6500.00
$NH + O_2 \rightleftharpoons NO + OH$	1.280E+06	1.500	100.00
$NH + N \rightleftharpoons N_2 + H$	1.500E+13	.000	.00
$NH + H_2O \rightleftharpoons HNO + H_2$	2.000E+13	.000	13850.00
$NH + NO \rightleftharpoons N_2 + OH$	2.160E+13	-.230	.00
$NH + NO \rightleftharpoons N_2O + H$	3.650E+14	-.450	.00
$NH_2 + O \rightleftharpoons OH + NH$	3.000E+12	.000	.00
$NH_2 + O \rightleftharpoons H + HNO$	3.900E+13	.000	.00
$NH_2 + H \rightleftharpoons NH + H_2$	4.000E+13	.000	3650.00
$NH_2 + OH \rightleftharpoons NH + H_2O$	9.000E+07	1.500	-460.00
$H + NO + M \rightleftharpoons HNO + M$	4.480E+19	-1.320	740.00
Enhanced Collision Efficiencies:			

Reaction	A (cm-moles-sec-K)	n	E (cal/mole)
H_2=2.00, H_2O=6.00, CH_4=2.00, CO=1.50, CO_2=2.00, C_2H_6=3.00, AR=.70			
$HNO + O \rightleftharpoons NO + OH$	2.500E+13	.000	.00
$HNO + H \rightleftharpoons H_2 + NO$	9.000E+11	.720	660.00
$HNO + OH \rightleftharpoons NO + H_2O$	1.300E+07	1.900	-950.00
$HNO + O_2 \rightleftharpoons HO_2 + NO$	1.000E+13	.000	13000.00
$CN + O \rightleftharpoons CO + N$	7.700E+13	.000	.00
$CN + OH \rightleftharpoons NCO + H$	4.000E+13	.000	.00
$CN + H_2O \rightleftharpoons HCN + OH$	8.000E+12	.000	7460.00
$CN + O_2 \rightleftharpoons NCO + O$	6.140E+12	.000	-440.00
$CN + H_2 \rightleftharpoons HCN + H$	2.950E+05	2.450	2240.00
$NCO + O \rightleftharpoons NO + CO$	2.350E+13	.000	.00
$NCO + H \rightleftharpoons NH + CO$	5.400E+13	.000	.00
$NCO + OH \rightleftharpoons NO + H + CO$	0.250E+13	.000	.00
$NCO + N \rightleftharpoons N_2 + CO$	2.000E+13	.000	.00
$NCO + O_2 \rightleftharpoons NO + CO_2$	2.000E+12	.000	20000.00
$NCO + M \rightleftharpoons N + CO + M$	3.100E+14	.000	54050.00
Enhanced Collision Efficiencies:			
H_2=2.00, H_2O=6.00, CH_4=2.00, CO=1.50, CO_2=2.00, C_2H_6=3.00, AR=.70			
$NCO + NO \rightleftharpoons N_2O + CO$	1.900E+17	-1.520	740.00
$NCO + NO \rightleftharpoons N_2 + CO_2$	3.800E+18	-2.000	800.00
$HCN + M \rightleftharpoons H + CN + M$	1.040E+29	-3.300	126600.00
Enhanced Collision Efficiencies:			
H_2=2.00, H_2O=6.00, CH_4=2.00, CO=1.50, CO_2=2.00, C_2H_6=3.00, AR=.70			
$HCN + O \rightleftharpoons NCO + H$	2.030E+04	2.640	4980.00
$HCN + O \rightleftharpoons NH + CO$	5.070E+03	2.640	4980.00
$HCN + O \rightleftharpoons CN + OH$	3.910E+09	1.580	26600.00
$HCN + OH \rightleftharpoons HOCN + H$	1.100E+06	2.030	13370.00
$HCN + OH \rightleftharpoons HNCO + H$	4.400E+03	2.260	6400.00
$HCN + OH \rightleftharpoons NH_2 + CO$	1.600E+02	2.560	9000.00
$H + HCN(+M) \rightleftharpoons H_2CN(+M)$	3.300E+13	.000	.00
Low pressure limit	1.400E+26	-3.400	1900.00
Enhanced Collision Efficiencies:			
H_2=2.00, H_2O=6.00, CH_4=2.00, CO=1.50, CO_2=2.00, C_2H_6=3.00, AR=.70			
$H_2CN + N \rightleftharpoons N_2 + CH_2$	6.000E+13	.000	400.00
$CH + N_2 \rightleftharpoons HCN + N$	3.120E+09	0.880	20130.00
$CH + N_2(+M) \rightleftharpoons HCNN(+M)$	3.100E+12	.150	.00
Low pressure limit	1.300E+25	-3.160	740.00
Troe parameters: a=.6670, T***=235.00, T*=2117.00, T**=4536.00			
Enhanced Collision Efficiencies:			
H_2=2.00, H_2O=6.00, CH_4=2.00, CO=1.50, CO_2=2.00, C_2H_6=3.00, AR=1.0			
$CH_2 + N_2 \rightleftharpoons HCN + NH$	1.000E+13	.000	74000.00
$CH + NO \rightleftharpoons HCN + O$	4.100E+13	.000	.00
$CH + NO \rightleftharpoons H + NCO$	1.620E+13	.000	.00
$CH + NO \rightleftharpoons N + HCO$	2.460E+13	.000	.00
$CH_2 + NO \rightleftharpoons H + HNCO$	3.100E+17	-1.380	1270.00
$CH_2 + NO \rightleftharpoons OH + HCN$	2.900E+14	-.690	760.00
$CH_2 + NO \rightleftharpoons H + HCNO$	3.800E+13	-.360	580.00
$CH_3 + NO \rightleftharpoons HCN + H_2O$	9.600E+13	.000	28800.00
$CH_3 + NO \rightleftharpoons H_2CN + OH$	1.000E+12	.000	21750.00
$HCNN + O \rightleftharpoons CO + H + N_2$	2.200E+13	.000	.00

Reaction	A (cm-moles-sec-K)	n	E (cal/mole)
$HCNN + O \rightleftharpoons HCN + NO$	2.000E+12	.000	.00
$HCNN + O_2 \rightleftharpoons O + HCO + N_2$	1.200E+13	.000	.00
$HCNN + OH \rightleftharpoons H + HCO + N_2$	1.200E+13	.000	.00
$HCNN + H \rightleftharpoons CH_2 + N_2$	1.000E+14	.000	.00
$HNCO + O \rightleftharpoons NH + CO_2$	9.800E+07	1.410	8500.00
$HNCO + O \rightleftharpoons HNO + CO$	1.500E+08	1.570	44000.00
$HNCO + O \rightleftharpoons NCO + OH$	2.200E+06	2.110	11400.00
$HNCO + H \rightleftharpoons NH_2 + CO$	2.250E+07	1.700	3800.00
$HNCO + H \rightleftharpoons H_2 + NCO$	1.050E+05	2.500	13300.00
$HNCO + OH \rightleftharpoons NCO + H_2O$	3.300E+07	1.500	3600.00
$HNCO + OH \rightleftharpoons NH_2 + CO_2$	3.300E+06	1.500	3600.00
$HNCO + M \rightleftharpoons NH + CO + M$	1.180E+16	.000	84720.00
Enhanced Collision Efficiencies: H_2=2.00, H_2O=6.00, CH_4=2.00, CO=1.50, CO_2=2.00, C_2H_6=3.00, AR=.70			
$HCNO + H \rightleftharpoons H + HNCO$	2.100E+15	-.690	2850.00
$HCNO + H \rightleftharpoons OH + HCN$	2.700E+11	.180	2120.00
$HCNO + H \rightleftharpoons NH_2 + CO$	1.700E+14	-.750	2890.00
$HOCN + H \rightleftharpoons H + HNCO$	2.000E+07	2.000	2000.00
$HCCO + NO \rightleftharpoons HCNO + CO$	0.900E+13	.000	.00
$CH_3 + N \rightleftharpoons H_2CN + H$	6.100E+14	-.310	290.00
$CH_3 + N \rightleftharpoons HCN + H_2$	3.700E+12	.150	-90.00
$NH_3 + H \rightleftharpoons NH_2 + H_2$	5.400E+05	2.400	9915.00
$NH_3 + OH \rightleftharpoons NH_2 + H_2O$	5.000E+07	1.600	955.00
$NH_3 + O \rightleftharpoons NH_2 + OH$	9.400E+06	1.940	6460.00
$NH + CO_2 \rightleftharpoons HNO + CO$	1.000E+13	.000	14350.00
$CN + NO_2 \rightleftharpoons NCO + NO$	6.160E+15	-0.752	345.00
$NCO + NO_2 \rightleftharpoons N_2O + CO_2$	3.250E+12	.000	-705.00
$N + CO_2 \rightleftharpoons NO + CO$	3.000E+12	.000	11300.00
$NNH \rightleftharpoons N_2 + H$	3.300E+08	.000	.00
$NNH + M \rightleftharpoons N_2 + H + M$	1.300E+14	-.110	4980.00
Enhanced Collision Efficiencies: H_2=2.00, H_2O=6.00, CH_4=2.00, CO=1.50, CO_2=2.00, C_2H_6=3.00, AR=.70			
$NNH + O_2 \rightleftharpoons HO_2 + N_2$	5.000E+12	.000	.00
$NNH + O \rightleftharpoons OH + N_2$	2.500E+13	.000	.00
$NNH + O \rightleftharpoons NH + NO$	7.000E+13	.000	.00
$NNH + H \rightleftharpoons H_2 + N_2$	5.000E+13	.000	.00
$NNH + OH \rightleftharpoons H_2O + N_2$	2.000E+13	.000	.00
$NNH + CH_3 \rightleftharpoons CH_4 + N_2$	2.500E+13	.000	.00

C

A comparison between a turbulent and laminar propane flame

The obtained results from chapter 4 have been further analysed. A comparison has been made between the turbulent flame simulation and the laminar flame. First the temperatures obtained from the measurements and the simulation are compared as a function of the axial distance and the radius in the combustion chamber. This is shown in figure C.1. Clearly the influence of heat loss is seen in the measurements. This is not taken into account by the model, explaining the overprediction of temperature at the exit of the combustor. Nevertheless the development from a cold mixture at the inlet towards a reacted state is modelled correctly according to the comparison between the experimental data and the model results.

Secondly, from the turbulent simulation, points have been sampled from the iso-volume where the reaction progress variable develops from 0 to 1. This

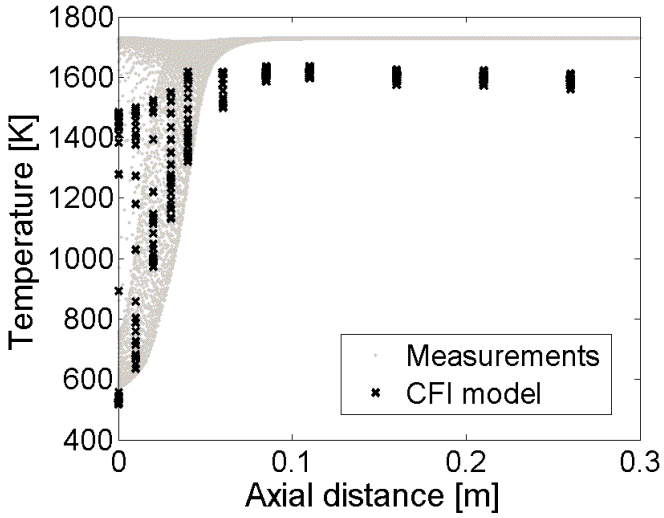

Figure C.1: Scatter-plot of the measured and modelled temperatures

generates interesting results when a comparison is made as a function of temperature, as is done in figures C.2–C.6. Despite the inherent different nature of the flows, the concentration of the species almost follows the same trajectory for the major species C_3H_8, CO_2 and H_2O. In the plots, the influence of turbulence is seen: there is a clear variation around the laminar values when going to higher temperatures. The flame front marker molecule OH has the same maximum concentrations in the turbulent situations as in the laminar situation, but the peak concentration is shifted slightly towards higher a temperature. For low temperatures the comparison is not really accurate, as was explained already in chapters 3 and 4.

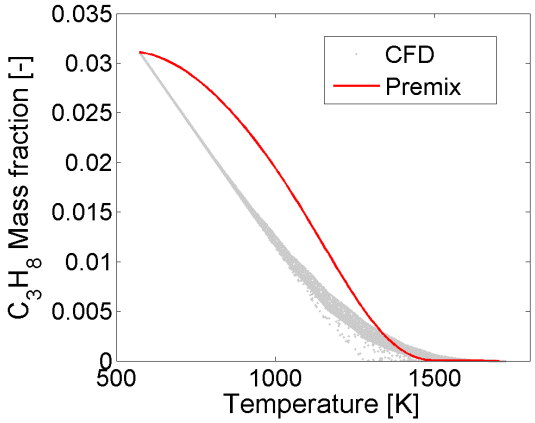

Figure C.2: The concentration of C_3H_8

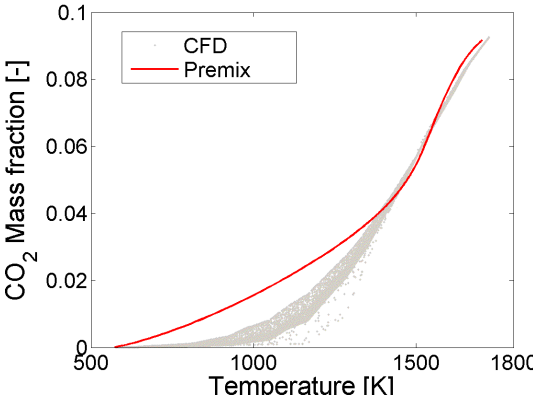

Figure C.3: The concentration of CO_2

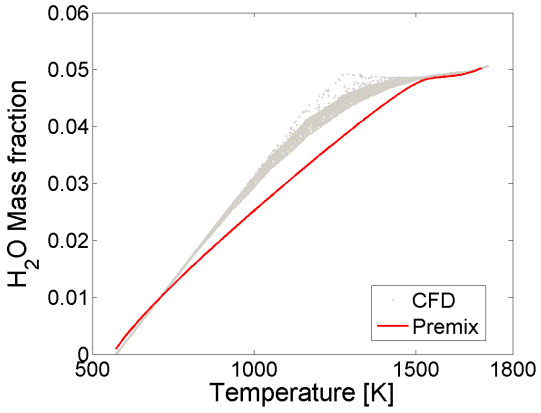

Figure C.4: The concentration of H_2O

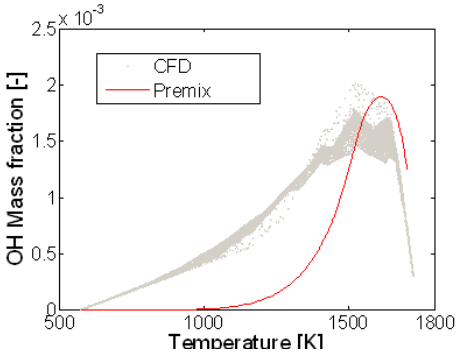

Figure C.5: The concentration of the flame front marker OH

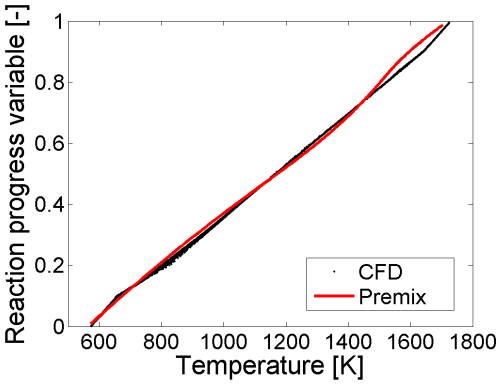

Figure C.6: The concentration of the flame front marker OH

D

Simulation of a jet spray

D.1 Setup

The implementation of the two-phase model as described in chapter 6 has been tested by applying the model to a setup that has been extensively investigated by the Maarten Luther University in Halle. The setup consists of a vertical channel with a spray injector at the bottom of this channel. By using a grid at the air inlet turbulence is induced. The liquid, glycerol, is injected in a coflow of air.

D.2 Numerical issues and boundary conditions

All the equations are solved on an unstructured grid using a hybrid discretisation method that switches between a 2^{nd} accurate scheme and 1^{st} order accurate scheme, depending on the Peclet number of the cell. It is found that an isotropic grid is needed in order to diminish the effect of numerical diffusion on the spray properties.

Grid 1	
No. of cells	118315 (2 mm edge length)
Grid 2	
No. of cells	1576922 (1.5 mm edge length)
Inlet conditions	
Mass flows	
Air	5.6 10^{-3} kg/s
Glycerol	2.0 10^{-5}kg/s, SMR = 20 x 10^{-5}m
Turbulence	
Velocity fluctuation	44%
Eddy length scale	15 mm
Temperature	
Air	500 K
Glycerol	300 K

Table D.1: Grid & inlet conditions

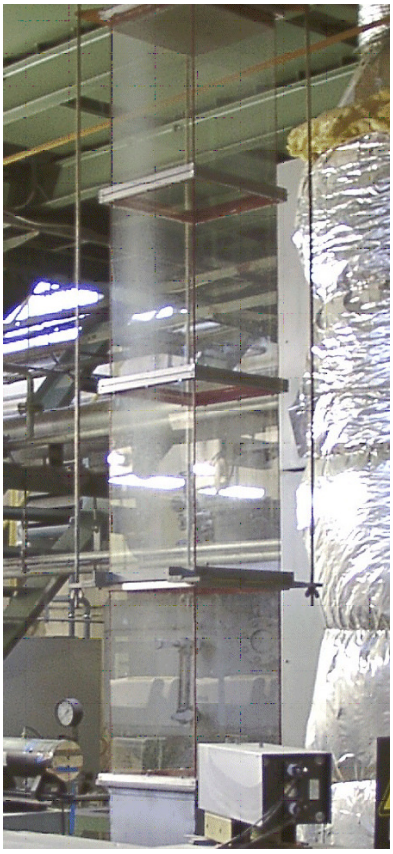

Figure D.1: Photograph of Halle experimental setup

In table D.2 inlet conditions for the simulations are given. For calculations the model described in this thesis and a standard Lagrangian parcel tracking model have been used.

In order to have a fine, isotropic grid with a reasonable number of grid-points, the flow is assumed to be symmetrical and a slice of the domain is chosen for discretisation. This symmetry has been taken into account by using translational periodic boundary conditions.

D.3 Results

Using the 1^{st} grid and inlet data as specified in table D.2 simulations have been performed that look at the development of the spray cloud without mass and heat transfer. Both the Lagrangian model and the Beck & Watkins model (Eulerian) model have been used in the simulations. In this paragraph results are compared.

When looking at the liquid velocity through the center line of the geometry in figure D.2(a) it is seen that the velocities for both models are comparable and that differences are negligible. Figure D.2(b) shows that the element aver-

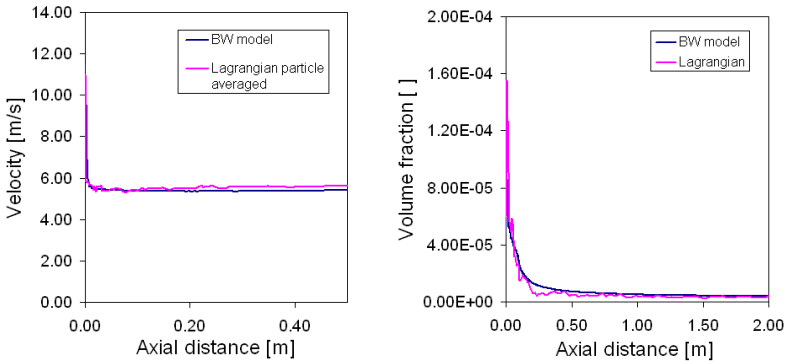

(a) Axial spray velocity (b) Volume fraction of spray

Figure D.2: Comparison between Eulerian solution and Lagrangian solution

aged Lagrangian volume fraction is equal to the volume fraction of the liquid phase in the BW model. As both the axial velocities and volume fractions are comparable it can be argued that equal behaviour of the liquid phase is found, and that this does not depend on the applied model.

Comparing the Lagrangian particle tracks from figure D.3(a) with the liquid volume fraction obtained with the BW model in figure D.3(b) it is seen that an almost equal spread of the spray presence in horizontal (y-axis) direction is found.

Next to the obtained volume fractions, also a comparison has been made of the axial velocity of the air stream surrounding the droplets. Some results can be found in figure D.4 It is seen that the development of the air velocity is almost equal. However, near the spray nozzle, there is a difference between the La-grang-ian model and the Eulerian model. It seems that the La-grang-

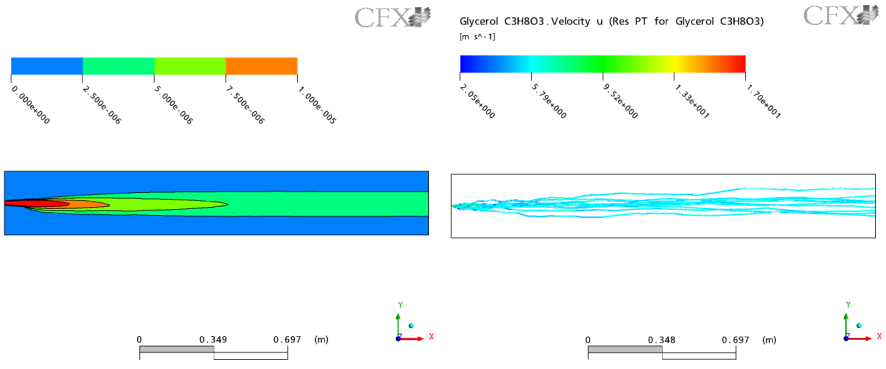

(a) Volume fraction of spray (b) Particle tracks

Figure D.3: Flow field of the spray according to the Eulerian and Lagrangian solution

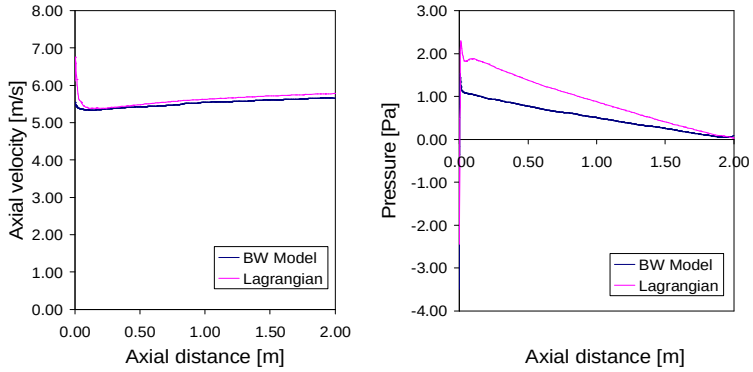

Figure D.4: Axial air velocity and relative static pressure

Grid 1		
	Lagrangian (1000 particles)	Eulerian ('full spray')
Solution time (CPUs)	41,350	39,420
Time / iteration (CPUs)	103.4	166.1

Table D.2: Comparison of computational times for the two grids and models

ian model has a larger impact on the air velocity compared to the Eulerian model at in this area. Although the mass load of the droplets on the air is equal for both cases, apparently momentum transfer from spray droplets to air is higher for the Lagrangian particle model than for the spray model. A reason for this could be the fact that implementation of the Lagrangian momentum sources is differing from the implementation of the Eulerian phase transfer source terms. The higher velocity for the Lagrangian model near the spray nozzle corresponds with the higher relative pressure.

The BW model also gives insight in the development of the spray properties, by looking at the Sauter mean diameter (see equation). This can be seen in Figures 4-8 where lineplots of the SMR are plotted. It is seen that the SMR does not keep the value as specified on the inlet, the reference SMR. Although the surface (Q_2) and volume fraction (Q_3) have diminished, they did not do so proportional. Next to that there is an interpolation error of the surface (Q_2) at the inlet of the spray. It might be worth investigating whether a correction for this interpolation error is needed. This will depend on the grid properties.

For the second grid, the spray development looks much different. The SMR is increasing along the direction of the upward flow axis. Next to that it is noted the spray has dispersed less in horizontal direction compared to the SMR obtained on at grid 1. This indicates that numerical diffusion has a rather large influence on the spray development. One extra reason could be

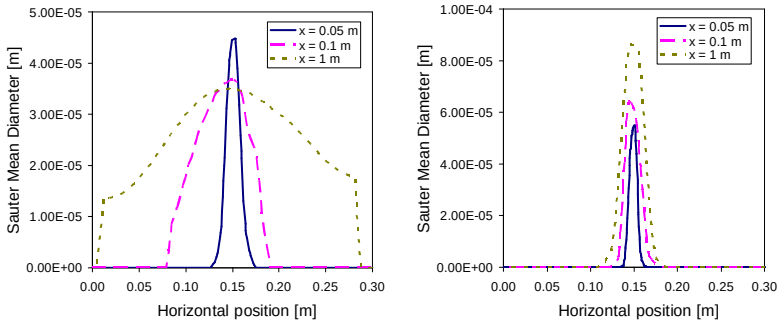

(a) Grid 1 (b) Grid 2

Figure D.5: SMD at several horizontal positions

the small spray inlet volume fraction, that might be of equal order of numerical diffusion effects. To check whether the solution goes to a grid independent solution, a finer grid should be applied.

When looking at the volume fraction at several horizontal positions in the geometry, again there is a clear difference between the results obtained for both grids. Mass conservation should ensure that at both grids the total volume fraction of the spray should be equal

D.4 Conclusions

The statistical Euler-Euler spray model from chapter 6 has been implemented in ANSYS-CFX. The Euler-Euler model compares well to Lagrange-Euler simulations of a glycerol jet spray. The Eulerian spray model is numerically more efficient as it does not need to solve for individual particle tracks. A liquid fuel spray can now be modeled based on a continuum assumption for the statistical moments of the droplet number distribution function of the liquid spray.

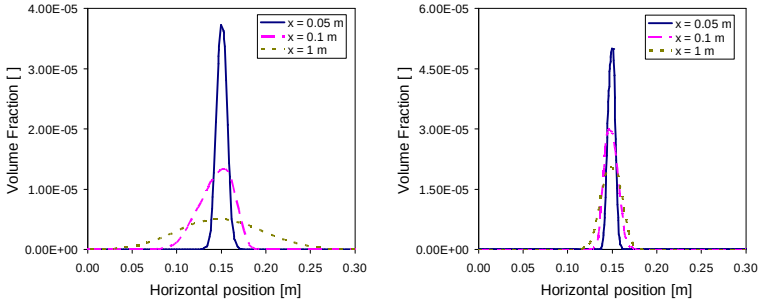

(a) Grid 1 (b) Grid 2

Figure D.6: Volume fraction of the spray on several horizontal positions

The results of the numerical study show that finding a grid independent solution for the Euler-Euler model will involve millions of finite volumes. It is expected that this number of cells will increase more in the case of a combusting spray.

E

Methanol database

Some output of the laminar database creation for methanol-air combustion is given in this appendix. As the variables of this database are a function of c, f and i, the plots are all conditionally plotted to i as a function of c and f.

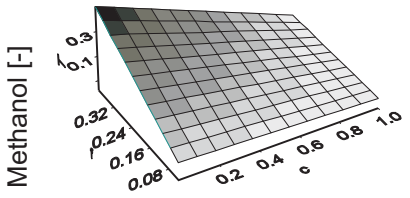

(a) Conditional to 0 < i < 0.1

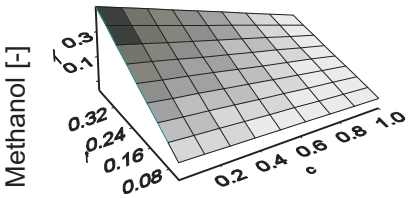

(b) Conditional to 0.1 < i < 0.2

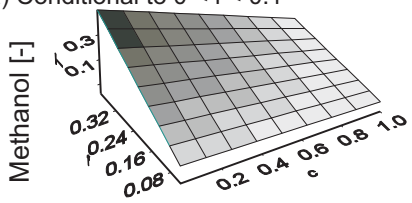

(c) Conditional to 0.2 < i < 0.3

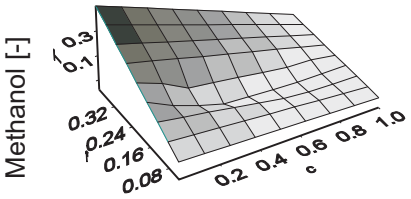

(d) Conditional to 0.3 < i < 0.4

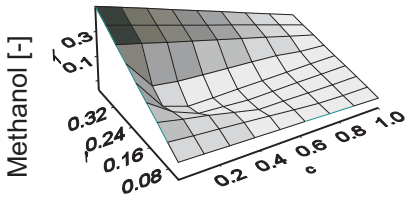

(e) Conditional to 0.4 < i < 0.5

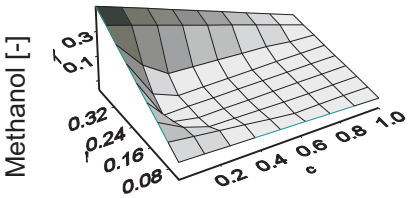

(f) Conditional to 0.5 < i < 0.6

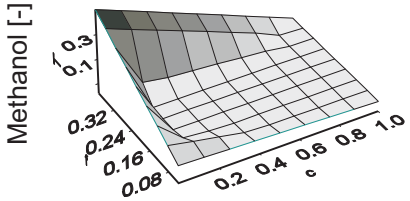

(g) Conditional to 0.6 < i < 0.7

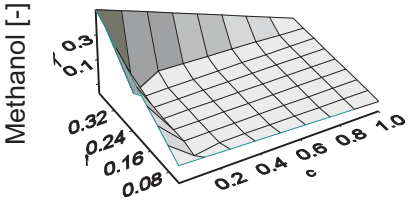

(h) Conditional to 0.7 < i < 0.8

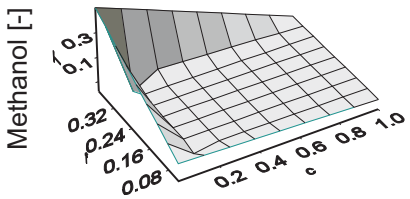

(i) Conditional to 0.8 < i < 0.9

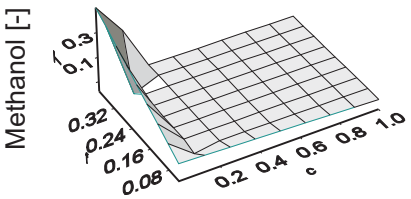

(j) Conditional to 0.9 < i < 1

Figure E.1: Concentration of CH_3OH conditional to i

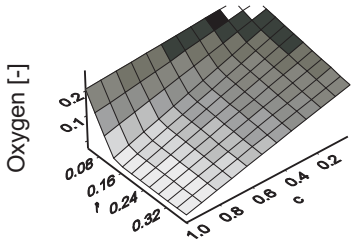

(a) Conditional to 0 < i < 0.1

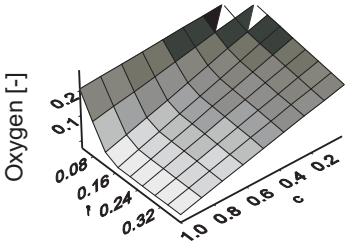

(b) Conditional to 0.1 < i < 0.2

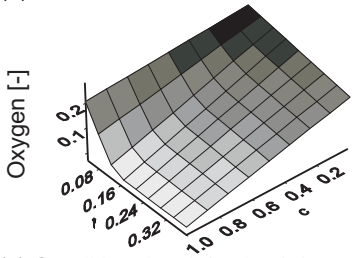

(c) Conditional to 0.2 < i < 0.3

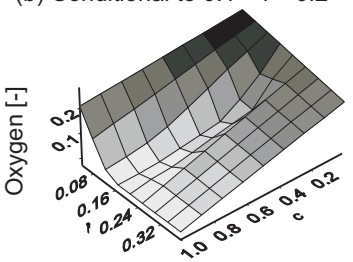

(d) Conditional to 0.3 < i < 0.4

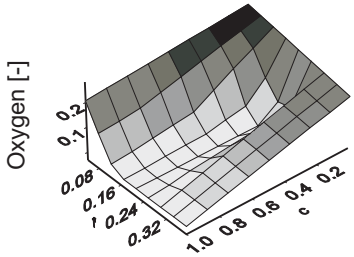

(e) Conditional to 0.4 < i < 0.5

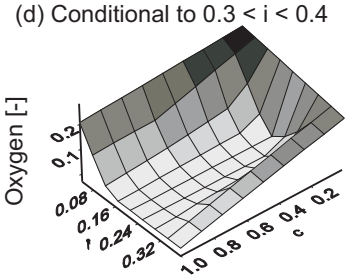

(f) Conditional to 0.5 < i < 0.6

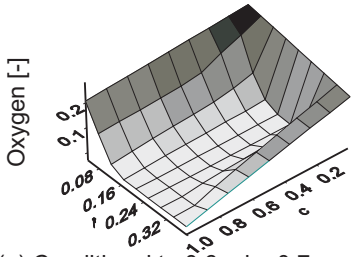

(g) Conditional to 0.6 < i < 0.7

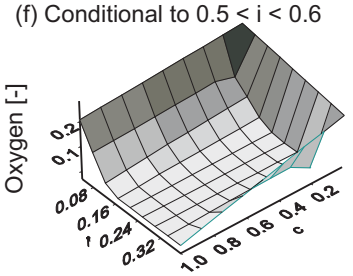

(h) Conditional to 0.7 < i < 0.8

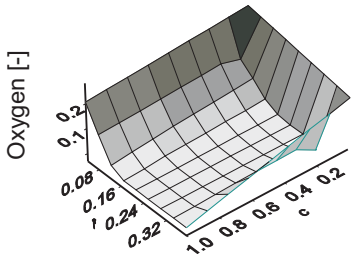

(i) Conditional to 0.8 < i < 0.9

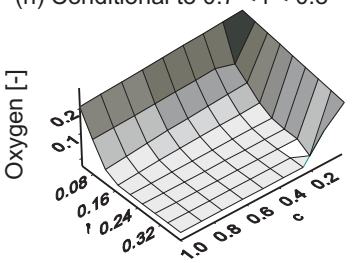

(j) Conditional to 0.9 < i < 1

Figure E.2: Concentration of O_2 conditional to i

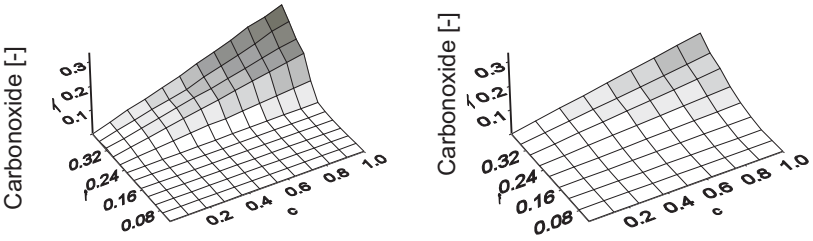

(a) Conditional to 0 < i < 0.1

(b) Conditional to 0.1 < i < 0.2

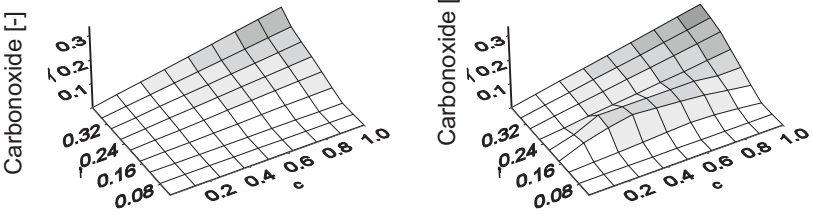

(c) Conditional to 0.2 < i < 0.3

(d) Conditional to 0.3 < i < 0.4

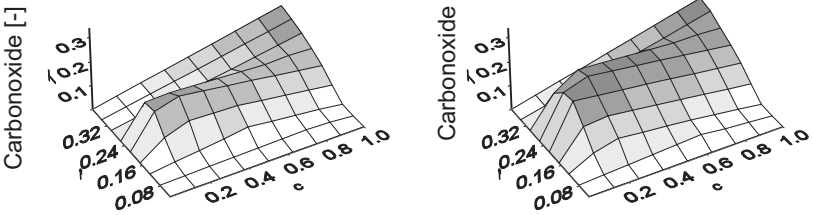

(e) Conditional to 0.4 < i < 0.5

(f) Conditional to 0.5 < i < 0.6

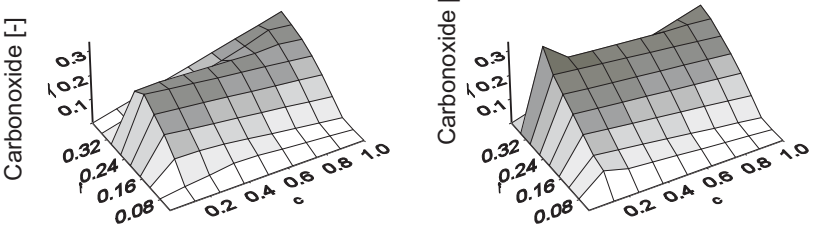

(g) Conditional to 0.6 < i < 0.7

(h) Conditional to 0.7 < i < 0.8

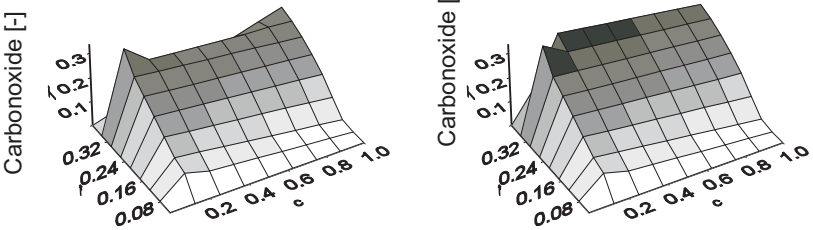

(i) Conditional to 0.8 < i < 0.9

(j) Conditional to 0.9 < i < 1

Figure E.3: Concentration of CO conditional to i

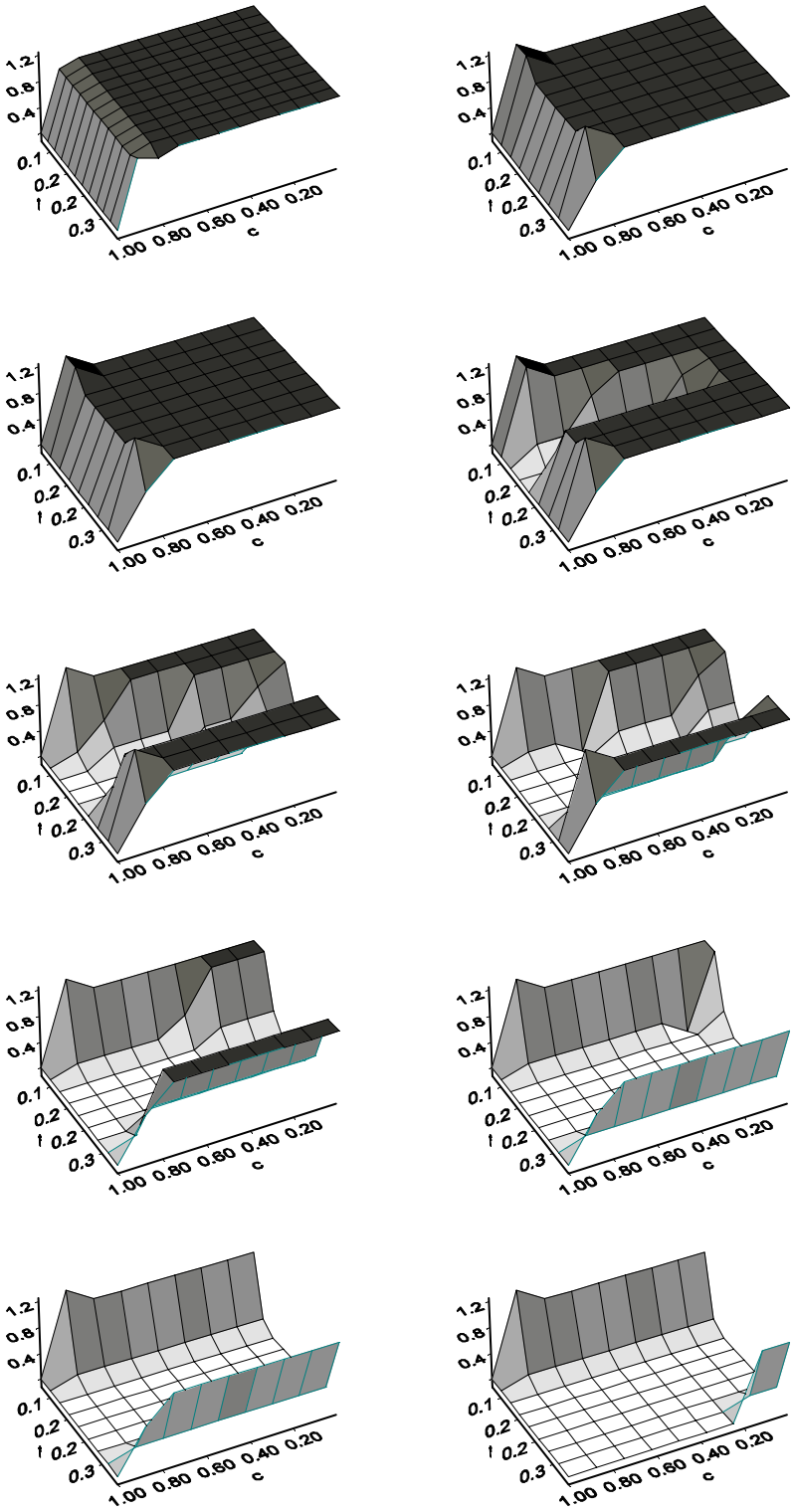

Figure E.4: Interpolation scalar conditional to i

F

Grid independence for the Eulerian model

F.1 Widmann [1, 2] spray simulations

A grid independent solution is necessary to ensure that conclusions are only based on modelling and discretisation schemes. The effect of the mesh should not influence the solution of CFD calculation. To ensure that the spray model results of chapter 7 can be assessed on intrinsic properties and are not depending on the numerical grid, a simple grid independence study has been carried out. The axial velocity of the gas phase is compared for 4 different meshes with an increasing number of elements. All meshes are constructed from hexahedral elements, of which the actual number can be found in table F.1.

The simulations of chapter 7 are carried out on grid no. 3.

	No. of elements
Mesh 1	15,431
Mesh 2	390,816
Mesh 3	938,851
Mesh 4	2,193,804

Table F.1: Overview of the number of elements.

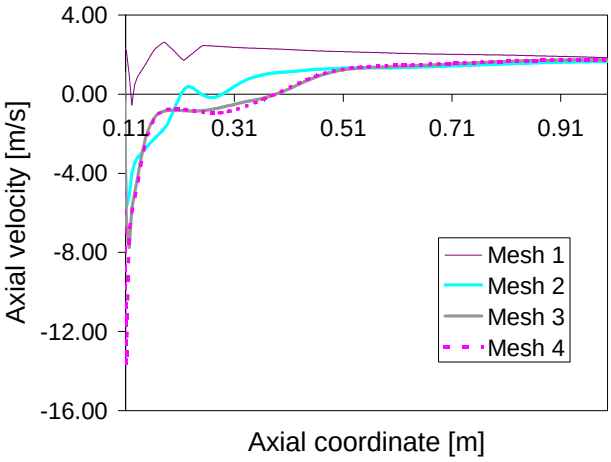

Figure F.1: Axial velocities along the centerline of the combustor for grids 1–4

G

Derivation of CFI equations

In this appendix the modifications to the CFI transport equations for a two-phase flow system are discussed by treating the derivation for the reaction progress variable c.

Derksen [15] provides a generalized framework for the formulation of the CFI transport equations. The laminar transport equation for the reaction progress variable is derived from the laminar conservation of species equation 2.3 and the definition of the reaction progress variable 2.27. Derksen then gives the following relation:

$$
\begin{aligned}
&\eta^{s,u}\underbrace{\left(\frac{\partial \rho}{\partial t}+\nabla\cdot(\rho\boldsymbol{U})\right)}_{1}+\\
&\left(cW_f+\eta_f^{s,u}\right)\underbrace{\left\{\rho\frac{\partial f}{\partial t}+\rho\boldsymbol{U}\nabla f-\nabla\cdot(\rho D\nabla f)\right\}}_{2}+\\
&cW_i\underbrace{\left\{\rho\frac{\partial i}{\partial t}+\rho\boldsymbol{U}\nabla i-\nabla\cdot(\rho D\nabla i)\right\}}_{3}+\\
&W\underbrace{\left\{\frac{\partial \rho c}{\partial t}+\nabla\cdot(\rho\boldsymbol{U})-\nabla\cdot(\rho D\nabla c)\right\}}_{4}=\\
&\rho Dc(\nabla f)^2W_{ff}+\rho Dc\nabla f\nabla iW_{fi}+\rho D\nabla f\nabla cW_f+\\
&\rho Dc(\nabla i)^2W_{ii}+\rho Dc\nabla i\nabla fW_{ff}+2W_i\rho D\nabla i\nabla c+\\
&\rho D\nabla c\nabla fW_f+\rho D(\nabla f)^2\eta_{ff}^{s,u}+\omega^c
\end{aligned}
\tag{G.1}
$$

In this equation the LHS contains both the first and the second are not equal to zero, in contrast to gaseous combustion.

1. From the first line of the LHS the bracketed part corresponds to the mass conservation equation that should equal the amount of mass introduced in the gas phase due to evaporation of the spray.

2. In the second line, the bracketed part represents the transport equation for the mixture fraction variable. That part should equal the mass production from evaporation and the appropriate value of mixture fraction corresponding to the evaporated mass.

3. The third line of the LHS should equate with the complete RHS of the enthalpy scalar transport equation.

Bringing terms to the RHS and multiplying with W, this yields the following equation for a reaction progress variable in a two-phase flow:

$$\begin{aligned} \frac{\partial \rho c}{\partial t} + \nabla \cdot (\rho \boldsymbol{U}) - \nabla \cdot (\rho D \nabla c) = \\ \frac{1}{W}(\rho D c (\nabla f)^2 W_{ff} + \rho D c \nabla f \nabla i W_{fi} + \\ \rho D \nabla f \nabla c W_f + \rho D c (\nabla i)^2 W_{ii} + \\ \rho D c \nabla i \nabla f W_{ff} + 2 W_i \rho D \nabla i \nabla c + \rho D \nabla c \nabla f W_f + \\ \rho D (\nabla f)^2 \eta_{ff}^{s,u} + \omega^c - \\ S_m \eta^{s,u} - \left(c W_f + \eta_f^{s,u} \right) S_f - c W_i S_i) \end{aligned} \tag{G.2}$$

The term containing $\eta_{ff}^{s,u}$ cancels out as this derivative equals zero, η being a linear function of mixture fraction. Treating this equation in the same manner as done by Derksen* allows to write the Favre averaged transport equation for c as follows:

$$\begin{aligned} \nabla . \left(\bar{\rho} \tilde{\boldsymbol{U}} \tilde{c} \right) - \nabla . (\bar{\rho} D_T \nabla \tilde{c}) = \\ \tilde{S}_c - \overline{\left(\frac{W_i}{W} \right) c S_i} - \overline{\left(c \frac{W_f}{W} + \frac{\eta_f^u}{W} \right) S_f} + \\ \overline{\left(\frac{W_{ff}}{W} \right)} \tilde{c} \frac{1}{2} \bar{\rho} R_T \frac{\varepsilon}{k} \overline{f''^2} + \\ \widetilde{S_m c} \end{aligned} \tag{G.3}$$

*In his thesis a thorough derivation can be found resulting in an expression equal to the expression in this thesis, apart from the phase transfer terms.

Nawoord

Zo. De hoge woorden zijn eruit. Het proefschrift is geschreven. Na vier jaren van onderzoek is dit het resultaat. Met een significante hoeveelheid plezier heb ik de afgelopen vier jaren mogen werken aan beschreven zaken. In eerste instantie aangenomen als 'assistent in opleiding' en na ongeveer een jaar 'bevorderd' tot 'promovendus'. Niet dat dit veel verandering bracht in de dagelijkse praktijk, maar goed.

Dit nawoord is een zeer geschikte plek om diegenen te bedanken die in de afgelopen periode met raad en daad ondergetekende hebben bijgestaan. Als eerste wil ik m'n begeleider en co-promoter, Jim Kok, bedanken: voor de mogelijkheid die vier jaar geleden door jou werd aangeboden om in dit onderzoek te stappen, voor de vrijheid van handelen binnen het onderzoeksproject en voor de nuttige, aanscherpende inhoudelijke discussies over de thema's van dit proefschrift.

Theo van der Meer wil ik bedanken voor zijn actieve rol als promotor. Zijn vragen en opmerkingen heb ik als opbouwend ervaren. Bovendien is zijn passie voor goed onderwijs *en* goede wetenschap bijzonder inspirerend. Daarnaast waren de lunch en borrel discussies over compleet andere onderwerpen ook altijd onderhoudend.

Uiteraard mogen de voormalige collega's van de vakgroep Thermische Werktuigbouwkunde niet ontbreken. Sjoerd Pater, Genie Stoffels: dank voor jullie waardevolle, kritische bijdragen aan het manuscript. De service van Sally en de ict-support van Eise wil ik ook nadrukkelijk noemen, bedankt! En als Chris Bakker er niet was geweest, had schrijver dezens nu nog met logistieke problemen gekampt. Bedankt voor je lassen aan onze tweelingkinderwagen. Daarnaast was het optimisme van Eddy zeer zeker ondersteunend!

Marco Derksen, Sjoerd Pater en Bogdan Albrecht hebben danwel met heldere uiteenzetting danwel met zeer relevante vragen ook zeker hun steen bijgedragen aan de wording van dit proefschrift, hartelijk dank daarvoor! De generieke CFI database code van Marco Derksen vormt een belangrijke pijler voor een aantal hoofdstukken van dit proefschrift. Hiervoor dank!

De samenwerking met de partners binnen het Europese kaderproject MAST-B-LIQUID heeft ook bijgedragen tot de totstandkoming van dit proefschrift. Dimitris Goussis en George Skevis hebben zeer waardevolle bijdragen geleverd aan dit proefschrift en de begripsvorming van de auteur op het gebied van chemie en CSP. Verder is de samenwerking met Alex Taylor, John Simmie en Stefan Horender erg nuttig gebleken.

In dit nawoord wil ook Fernando Biagioli en Khawar Syed noemen, mede door hun begeleiding en enthousiasme gedurende mijn stage en afstuderen bij toendertijd Alstom Power is de interesse voor het verbrandingsonderzoek ontstaan.

M'n vroegere kamergenoten Bogdan Albrecht en Ziad Abu El Rub hebben hier ook een plek verdiend. Het was altijd buitengewoon interessant om met jullie te discussiëren en te spreken. Erg verlichtend voor mijn kijk op ons polderlandje. Mensen zoals jullie maken een Nederlandse samenleving een stuk interessanter.

Hannah, je bent echt een rots in de branding geweest, dankzij jou was het erg gemakkelijk om de beslommeringen van het dagelijks ploeteren te vergeten.

Bram de Jager

Julianadorp, februari 2007